Lawrence Berkeley National Laboratory
LBL Dissertations

Title

ANALYSIS OF PUMPING TEST DATA OF A LEAKY AND LAYERED AQUIFER WITH PARTIALLY PENETRATING WELLS

Permalink

https://escholarship.org/uc/item/0r23p2fk

Author

Yates, C.C.

Publication Date

1988-12-01

Thesis/dissertation

eScholarship.org Powered by the California Digital Library
University of California

LBL-26542

Lawrence Berkeley Laboratory

UNIVERSITY OF CALIFORNIA

EARTH SCIENCES DIVISION

RECEIVED
LAWRENCE
BERKELEY LABORATORY

MAR 27 1989

LIBRARY AND
DOCUMENTS SECTION

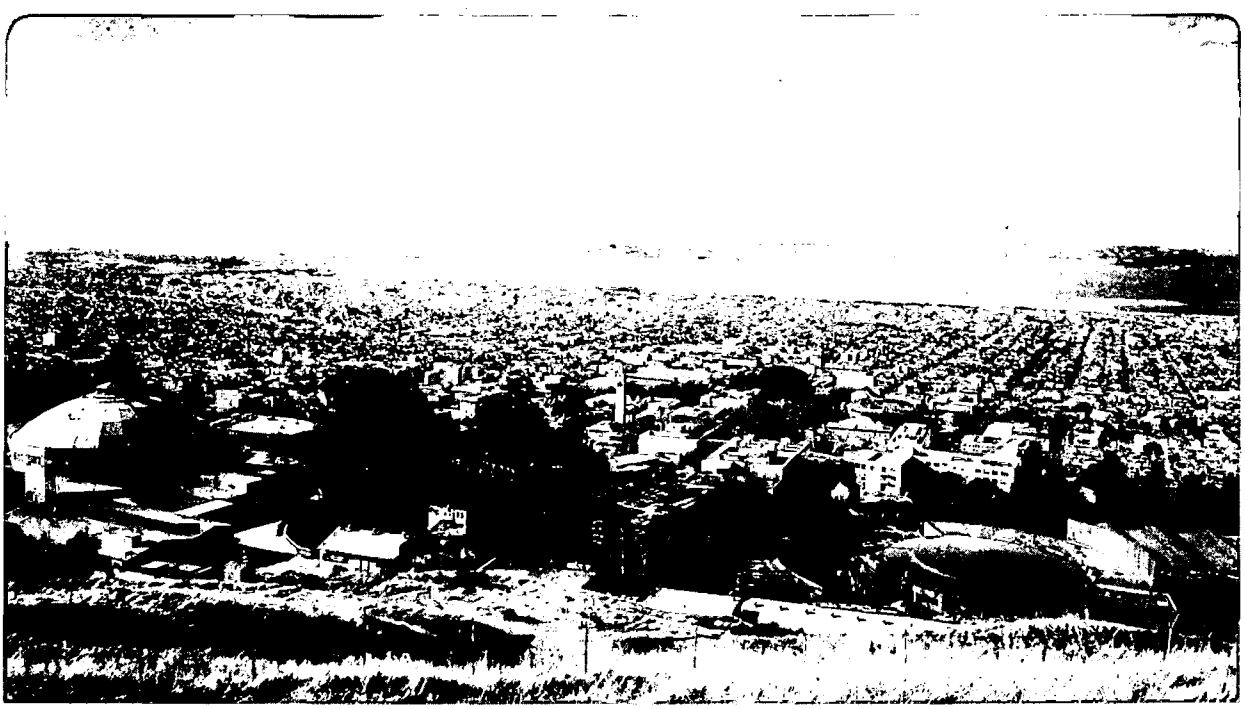
Analysis of Pumping Test Data of a Leaky and Layered Aquifer with Partially Penetrating Wells

C.C. Yates
(M.S. Thesis)

December 1988

TWO-WEEK LOAN COPY

This is a Library Circulating Copy which may be borrowed for two weeks.



Prepared for the U.S. Department of Energy under Contract Number DE-AC03-76SF00098.

LBL-26542
c.2

DISCLAIMER

This document was prepared as an account of work sponsored by the United States Government. While this document is believed to contain correct information, neither the United States Government nor any agency thereof, nor the Regents of the University of California, nor any of their employees, makes any warranty, express or implied, or assumes any legal responsibility for the accuracy, completeness, or usefulness of any information, apparatus, product, or process disclosed, or represents that its use would not infringe privately owned rights. Reference herein to any specific commercial product, process, or service by its trade name, trademark, manufacturer, or otherwise, does not necessarily constitute or imply its endorsement, recommendation, or favoring by the United States Government or any agency thereof, or the Regents of the University of California. The views and opinions of authors expressed herein do not necessarily state or reflect those of the United States Government or any agency thereof or the Regents of the University of California.

LBL-26542

ANALYSIS OF PUMPING TEST DATA OF A LEAKY AND LAYERED AQUIFER WITH PARTIALLY PENETRATING WELLS

Cynthia C. Yates

M.S. Thesis

Earth Sciences Division
Lawrence Berkeley Laboratory
1 Cyclotron Road
Berkeley, California 94720

December 1988

This work was supported by the U.S. Bureau of Reclamation, under U.S. Department of Interior Interagency Agreement 8-AA-20-06330, through U.S. Department of Energy Contract DE-AC03-76SF00098.

Table of Contents

LIST OF FIGURES iv

LIST OF TABLES viii

NOMENCLATURE x

ACKNOWLEDGMENTS xii

1.0 INTRODUCTION 1

2.0 KESTERSON RESERVOIR 3

2.1 LOCATION AND TOPOGRAPHY 3

2.2 HISTORICAL BACKGROUND 3

2.3 GEOLOGY 8

2.3.1 Regional Geologic Setting 8

2.3.2 Local Geologic Setting 10

2.4 HYDROLOGY 13

2.4.1 Regional Hydrologic Setting 13

2.4.2 Local Hydrologic Setting 14

2.5 EXTENT OF CONTAMINATION 17

3.0 THEORY 19

3.1 PHYSICS OF GROUNDWATER FLOW 19

3.2 AQUIFER RESPONSE TO PUMPING 23

3.2.1 Ideal Aquifer 24

3.2.2 Leaky Aquifer 26

3.2.3 Effects due to Partial Penetration 30

3.2.4 Layered Aquifer 35

4.0 FIELD PROCEDURES 38

4.1 SINGLE-WELL STEADY-STATE TESTS 42

4.2 SINGLE-WELL AND MULTIPLE-WELL TRANSIENT TESTS 43

4.2.1 Instrumentation 43
4.2.2 Single-well and Interference Transient Test Procedure 49
4.2.3 Pulse Test Procedure 55

5.0 METHODS OF ANALYSIS 64
5.1 NUMERICAL METHODS 65
5.1.1 Numerical Code 65
5.1.2 Computation Grid 67
5.1.3 Curve Matching Technique 70
5.2 ANALYTICAL METHODS 75
5.2.1 Single-Well Steady-State Pump Tests 76
5.2.2 Single-Well and Interference Pressure Transient Tests 77
5.2.3 Pulse Pressure Transient Tests 79

6.0 NUMERICAL SIMULATIONS 83
6.1 SINGLE-WELL STEADY-STATE RESULTS 83
6.2 NUMERICAL RESULTS 85
6.2.1 Results from Single-Well Transient Tests 97
6.2.2 Results from Interference Tests 97
6.2.3 Results from Pulse Tests 102

7.0 COMPARISON OF NUMERICAL AND ANALYTICAL RESULTS 105
7.1 RESULTS OF THE ANALYTICAL ANALYSES 105
7.1.1 Single-Well Transient and Interference Test Results 105
7.1.2 Pulse Test Results 123
7.2 DISCUSSION OF RESULTS 125

8.0 CONCLUSION 130

REFERENCES 132

APPENDIX 135

LIST OF FIGURES

Figure 2.1	Location map of Kesterson Reservoir (Taken from Mandle, 1986).	4
Figure 2.2	Map showing the San Luis Drain in relation to Kesterson Reservoir.	5
Figure 2.3	Location map showing the 12 regulating and evaporation ponds of Kesterson Reservoir.	6
Figure 2.4	Location map showing test sites from which geophysical and lithological logs were obtained and cross-sections A-A' and B-B'.	11
Figure 2.5	Cross-section A-A' showing general stratigraphy at Kesterson Reservoir.	12
Figure 2.6	Schematic hydrologic cross-section of the San Joaquin Valley.	15
Figure 3.1	Schematic diagram of an ideal aquifer responding to pumping.	25
Figure 3.2	Theoretical log-log type-curve for an ideal aquifer (Theis, 1935).	27
Figure 3.3	Schematic diagram of a leaky aquifer responding to pumping.	29
Figure 3.4	Theoretical log-log type-curve for a leaky aquifer (Hantush and Jacob, 1955).	31
Figure 3.5	Schematic diagram of an aquifer responding to pumping with partially penetrating wells.	32
Figure 3.6	Schematic diagram of an aquifer with partially penetrating wells showing the definitions of Z and h.	34
Figure 3.7	Theoretical log-log type-curve for an aquifer with partially penetrating wells (Hantush, 1957).	36
Figure 4.1	Location map showing the LBL hydrologic tests sites.	39
Figure 4.2	Plan view of the LBLI/HO Site and the 12 wells used for pump tests.	40
Figure 4.3	Schematic cross-sectional view of the 12 wells at the LBLI/HO Site used for pump tests.	41
Figure 4.4	Schematic diagram showing the placement of a transducer and inflatable packer in an observation well.	44

Figure 4.5	Pressure vs. time plots recorded during Interference Test 2 showing a) the atmospheric pressure measured and b) the pressure response recorded at Observation Well I9 before and after P_{atm} was subtracted.	46
Figure 4.6	Schematic diagram showing the data aquisition computer system housed in a delivery-type van.	48
Figure 4.7	Single-well transient test pressure responses recorded at Production Wells I1, HO60, and HO80.	51
Figure 4.8	Interference test pressure response recorded at Observation Wells I2-I9 while pumping Production Well I1.	52
Figure 4.9	Interference test pressure response recorded at Observation Wells I2-I9 while pumping Production Well HO60.	53
Figure 4.10	Interference test pressure response recorded at Observation Wells I2-I9 while pumping Production Well HO80.	54
Figure 4.11	Schematic diagram showing the major difference between interference and pulse testing.	56
Figure 4.12	Pulse test pressure response recorded at Observation Wells I2 and I6 while pumping Production Well I1.	59
Figure 4.13	Pulse test pressure response recorded at Observation Well I2 while pumping Production Well I1.	60
Figure 4.14	Pulse test pressure response recorded at Observation Well I3 while pumping Production Well I1.	61
Figure 4.15	Pulse test pressure response recorded at Observation Well I5 while pumping Production Well I1.	62
Figure 4.16	Pulse test pressure response recorded at Observation Well I3 while pumping Production Well HO60.	63
Figure 5.1	The computational grid used to divide the aquifer system at the LBLI/HO Site into volume elements. Water is withdrawn from the system through Node 555. The grid is finer in the vicinity of the observation wells.	68
Figure 5.2	Verification of the computational grid with the Theis type-curve.	71
Figure 5.3	Verification of the computational grid with the leaky aquifer type-curve.	72
Figure 5.4	Plot showing a match of simulated data and field data from Interference Test 1 and Observation Well I2.	73
Figure 5.5	Pseudo-skin factor S_p as a function of b and h/r_w (Taken from Brons and Marting, 1961).	78

Figure 5.6	Schematic diagram describing the method used at the LBLI/HO Site in order to conduct pulse tests. The frequency of the pulses was not held constant.	80
Figure 5.7	Schematic diagram showing that when the pressure change is equal to ΔP_{max}, Δt is then equal to t_{lag}.	81
Figure 6.1	Schematic diagram of the initial aquifer model used in numerical simulations of the aquifer system at the LBLI/HO Site at Kesterson Reservoir.	86
Figure 6.2	Field and simulated pressure responses of Interference Test 1 recorded at Observation Well I2 and I3 using the initial aquifer model.	88
Figure 6.3	Field and simulated pressure responses of Interference Test 1 recorded at Observation Well I6 and I7 using the initial aquifer model.	89
Figure 6.4	Schematic diagram of the second aquifer model used in numerical simulations of the aquifer system at the LBLI/HO Site at Kesterson Reservoir.	90
Figure 6.5	Field and simulated pressure responses of Single-Well Transient Test 1 recorded at Production Well I1 using the second aquifer model.	91
Figure 6.6	Field and simulated pressure responses of Interference Test 1 recorded at Observation Well I2 and I3 using the second aquifer model.	92
Figure 6.7	Field and simulated pressure responses of Interference Test 3 recorded at Observation Well I2 using a) the second aquifer model without a clay layer included and b) the final aquifer model including a clay layer with a permeability of 9×10^{-14} m^2.	93
Figure 6.8	Schematic diagram of the final aquifer model used in numerical simulations of the aquifer system at the LBLI/HO Site at Kesterson Reservoir.	95
Figure 6.9	Schematic plan view of Layer 2 showing approximate location of the two permeable regions, 21 and 22.	101
Figure 7.1	Match of Single-Well Transient Test 1 field data to leaky aquifer type-curve showing "match points" P_D, t_D, ΔP, and t/r^2.	107
Figure 7.2	Match of Single-Well Transient Test 2 field data to leaky aquifer type-curve showing "match points" P_D, t_D, ΔP, and t/r^2.	108

Figure 7.3	Match of Single-Well Transient Test 3 field data to leaky aquifer type-curve showing "match points" P_D, t_D, ΔP, and t/r^2.	109
Figure 7.4	Match of Interference Test 1 field data to leaky aquifer type-curve showing "match points" P_D, t_D, ΔP, and t/r^2.	112
Figure 7.5	Match of Interference Test 2 field data from Observation Wells I2, I3, I5, I7, and I9 to leaky aquifer type-curve showing "match points" P_D, t_D, ΔP, and t/r^2.	113
Figure 7.6	Match of Interference Test 2 field data from Observation Wells I4, I6, and I8 to leaky aquifer type-curve showing "match points" P_D, t_D, ΔP, and t/r^2.	114
Figure 7.7	Match of Interference Test 3 field data from Observation Well I2 to leaky aquifer type-curve showing "match points" P_D, t_D, ΔP, and t/r^2.	115
Figure 7.8	Match of Interference Test 3 field data from Observation Well I3 to leaky aquifer type-curve showing "match points" P_D, t_D, ΔP, and t/r^2.	116
Figure 7.9	Match of Interference Test 3 field data from Observation Well I4 to leaky aquifer type-curve showing "match points" P_D, t_D, ΔP, and t/r^2.	117
Figure 7.10	Match of Interference Test 3 field data from Observation Well I5 to leaky aquifer type-curve showing "match points" P_D, t_D, ΔP, and t/r^2.	118
Figure 7.11	Match of Interference Test 3 field data from Observation Well I6 to leaky aquifer type-curve showing "match points" P_D, t_D, ΔP, and t/r^2.	119
Figure 7.12	Match of Interference Test 3 field data from Observation Well I7 to leaky aquifer type-curve showing "match points" P_D, t_D, ΔP, and t/r^2.	120
Figure 7.13	Match of Interference Test 3 field data from Observation Well I8 to leaky aquifer type-curve showing "match points" P_D, t_D, ΔP, and t/r^2.	121
Figure 7.14	Match of Interference Test 3 field data from Observation Well I9 to leaky aquifer type-curve showing "match points" P_D, t_D, ΔP, and t/r^2.	122

LIST OF TABLES

Table 2.1	Chronological order of events involving the detection of selenium poisoning at Kesterson Reservoir.	7
Table 4.1	Single-well and interference transient tests conducted at Site LBLI/HO.	49
Table 4.2	Pulse tests conducted at Site LBLI/HO.	57
Table 6.1	Hydrologic parameters obtained from the analytical analysis of the single-well steady-state pump tests.	84
Table 6.2	Permeability values obtained from the numerical analysis of the single-well transient and interference test data using the second aquifer model.	94
Table 6.3	Geometric factors, physical properties, and initial and boundary conditions used for the final aquifer model.	96
Table 6.4	Individual well permeability values obtained from the numerical analysis of the single-well transient and interference test data using the final aquifer model.	98
Table 6.5	Permeability results from the numerical analysis of the single-well test data.	99
Table 6.6	Permeability results from the numerical analysis of the interference test data.	100
Table 6.7	Permeability results from the numerical analysis of the pulse test data.	103
Table 6.8	Summary of the numerical permeability results of pulse tests.	104
Table 6.9	Summary of the permeability results obtained from the numerical analysis of the transient test data.	104
Table 7.1	Analytical results of the single-well transient test data.	106
Table 7.2	Analytical permeability results of the interference test data.	110
Table 7.3	Analytical permeability results of pulse tests.	124

Table 7.4	Summary of permeability values obtained from pumping tests.	126
Table 7.5	Permeability results obtained from analytical and numerical methods of analysis showing radial zoning of aquifer.	129

Nomenclature

A	-	cross-sectional area (m^2)
b	-	penetration ratio of a partially penetrating well
D	-	distance between two nodal points (m)
g	-	acceleration due to gravity (m/s^2)
g_w	-	volumetric rate of fluid generation per unit bulk volume ($kg/m^3 \cdot s$)
G_w	-	volumetric rate of fluid generation (kg/s)
h	-	thickness of the total productive interval of a partially penetrating well (m)
H	-	aquifer thickness (m)
H′	-	leaky aquitard thickness (m)
k	-	absolute or intrinsic permeability (m^2)
k_{eff}	-	effective permeability (m^2)
k_r	-	radial component of permeability (m^2)
k_{rel}	-	relative permeability
k_z	-	vertical component of permeability (m^2)
k′	-	aquitard permeability (m^2)
K	-	hydraulic conductivity (m/s)
K_s	-	saturated hydraulic conductivity (m/s)
K′	-	aquitard hydraulic conductivity (m/s)
l	-	distance between hydraulic measurement points (m)
l	-	arbitrary volume element
L	-	length of screened interval in a pumping well (m)
m	-	surface segment of *l*
m	-	(number of pulse periods)/2
m_c	-	specific fluid mass capacity (kg/m^4)
M	-	total number of surface segments
M_c	-	fluid mass capcity (kg/m)
n	-	porosity
P	-	pressure (Pa)
P_{abs}	-	absolute pressure(Pa)
P_{atm}	-	barometric or atmospheric pressure (Pa)
P_D	-	dimensionless pressure
P_{gage}	-	gage pressure (Pa)
ΔP_{max}	-	maximun pressure change (Pa)
q	-	Darcy's velocity (m/s)
Q	-	flow rate (m^3/s)

$Q/\Delta\phi$	-	specific capacity ($m^3/s/m$)
r	-	radial distance (m)
r_D	-	dimensionless radius
r_e	-	effective radius (m)
r_w	-	well radius (m)
r/B	-	leakage factor
S	-	storativity
S_p	-	pseudo-skin factor
S_s	-	specific storativity (m^{-1})
S'	-	aquitard storativity
t	-	time (s)
t_D	-	dimensionless time
t_{lag}	-	time lag of a pulse (s)
t_p	-	time interval of one pulse (s)
T	-	transmissivity (m^2/s)
T_P	-	period of one pulse cycle (s)
V_B	-	bulk volume (m^3)
V_w	-	volume of water (m^3)
$W(u)$	-	well function
$W(u,r/B)$	-	leaky well function
z	-	elevation head (m)
Z	-	distnace from the top boundary of an aquifer to the middle of a screened interval in a pumping well (m)
α	-	matrix compressibility (Pa^{-1})
β	-	compressibility of water (Pa^{-1})
Γ	-	surface area of l (m^2)
η	-	diffusivity (m^2/s)
μ	-	fluid viscosity (kg/m·s)
ρ	-	fluid density (kg/m^3)
ϕ	-	hydraulic head (m)
Φ	-	fluid potential (m^2/s^2)
ψ	-	pressure head (m)

ACKNOWLEDGMENTS

I would like to thank Dr. Paul A. Witherspoon for accepting me into U. C. Berkeley as one of his students, for his support and guidance during my years of graduate studies, and for his review of this work as a committee member. My deepest gratitude goes to Dr. Sally M. Benson for her expertise, hours and hours of patience, guidance, and support. Her encouragement and enthusiasm were very much appreciated and will not be forgotten.

I am grateful to the other members of my committee, Dr. T. Narasimhan and Dr. J. Hunt, for critically reviewing this work and I would also like to thank Dr. G. Bodvarsson for the use of the numerical code PT.

I am very grateful to Scott Gaulke for making most of the tables in this report and for his help and encouragement during these last three years. Last but not least, I would like to thank my family for being supportive and for being properly surprised and happy that I made it through graduate school.

1.0 INTRODUCTION

Between the years 1981 and 1986, agricultural drainage water containing high concentrations of selenium, boron, and other salts was transported to the storage and evaporation ponds of Kesterson Reservoir, located in Merced County, California. Due to selenium poisoning of fish and migratory birds at the Reservoir, intensive scientific investigations of the surface water, groundwater, soils, sediments, and ecology were initiated. The preliminary groundwater investigations revealed that due to the leakage of the agricultural drainage water from the storage ponds down to the underlying shallow aquifer, a saline and boron-rich contaminant plume had been created in the aquifer and was slowly migrating to the northeast. The primary purpose of this report is to determine the hydrologic properties of this underlying aquifer system. The field work was carried out at the LBLI/HO Site at Kesterson Reservoir.

Initial hydrological pump test data and data from geophysical and lithological logs show that the shallow aquifer system (above the valley-wide Corcoran Clay Member of the Tulare Formation) is approximately 61 m (200 ft) thick and consists of a complex sequence of interbedded sands, silts, and clays bounded on the top by a leaky aquitard. Complicating the hydrologic setting even more is the fact that the hydrologic test wells only partially penetrate the aquifer. Because of the complexity of this leaky and layered aquifer system with partially penetrating wells, fluid flow towards a production well will deviate from that of an ideal system. Choosing a pump test that will reveal these deviations in fluid flow is important in obtaining a complete data set for analysis. Four types of pump tests were conducted at the LBLI/HO Site: 1) single-well steady-state tests, 2) single-well transient tests, 3) multiple-well standard interference tests, and 3) multiple-well pulse tests.

Analyzing the pumping test data obtained from the LBLI/HO Site involves making simplifying assumptions about the aquifer system. Since the aquifer system studied in this report is very complex, different methods of analysis using different

simplifying assumptions can result in several interpretations of the hydrologic properties. One of the objectives of this report is to find which method of analysis would result in the most acceptable and detailed hydrologic model of the aquifer system.

The best method of analysis is defined as the one that results in a hydrological model that can incorporate the data from the four pump tests and consistently yield a unique interpretation. Once the best method of analyzing the hydrologic data of the shallow aquifer system underlying the LBLI/HO Site has been determined, this same method can be applied to future hydrologic testing at Kesterson Reservoir or to other locations within the San Joaquin Valley which have similar hydrogeological conditions.

Complications arising in the analysis of the pump test data obtained from the aquifer system at the LBLI/HO Site consisted of 1) leakage from the storage and evaporation ponds down into the aquifer, 2) the vertical heterogeneity of the aquifer, and 3) the partial penetration of the pump test wells. The pump test data were analyzed using primarily numerical methods because the aquifer system was too complex to conform to many of the simplifying assumptions used to develop analytical solutions. However, results from the analytical and numerical methods will be compared in order to determine the applicability of some commonly used analytical solutions.

2.0 KESTERSON RESERVOIR

2.1 LOCATION AND TOPOGRAPHY

Kesterson Reservoir, which is within Kesterson National Wildlife Refuge, is located in Merced County, California, approximately five miles east of the town of Gustine (see Figure 2.1). The Reservoir is situated in the northwestern part of the San Joaquin Valley and west of the San Joaquin River. The San Joaquin Valley and the Sacramento Valley make up the Central Valley of California.

The topography at Kesterson Reservoir is very flat with slopes of only 0-2% (USBR, 1986). The Reservoir is 19.8-24.4 m (65-80 ft) above sea level.

2.2 HISTORICAL BACKGROUND

Kesterson Reservoir and the San Luis Drain were constructed between the years 1968 and 1975 by the U. S. Bureau of Reclamation (USBR) with the intent of transporting and regulating mineral-laden, agricultural drainage water from farmlands in the central San Joaquin Valley (see Figure 2.2). The drainage water originally was meant to empty into the Sacramento-San Joaquin Delta but, due to lack of funds and disagreement over the environmental impact of discharging agricultural drainage water into the Delta, this plan was revised. Kesterson Reservoir consists of 12 unlined ponds (see Figure 2.3) separated by earth berms and was intended to be used as a regulating reservoir for the drainage water. The Reservoir became, instead, the disposal facility.

In 1970, the USBR and the U. S. Fish and Wildlife Service (USRWS) established the 5.19 km^2 (1283 acres) Kesterson Reservoir, along with surrounding land, to form the 23.9 km^2 (5900 acres) Kesterson National Wildlife Refuge. From 1972 to 1981, the San Luis Drain delivered mainly surface runoff to Kesterson Reservoir. By

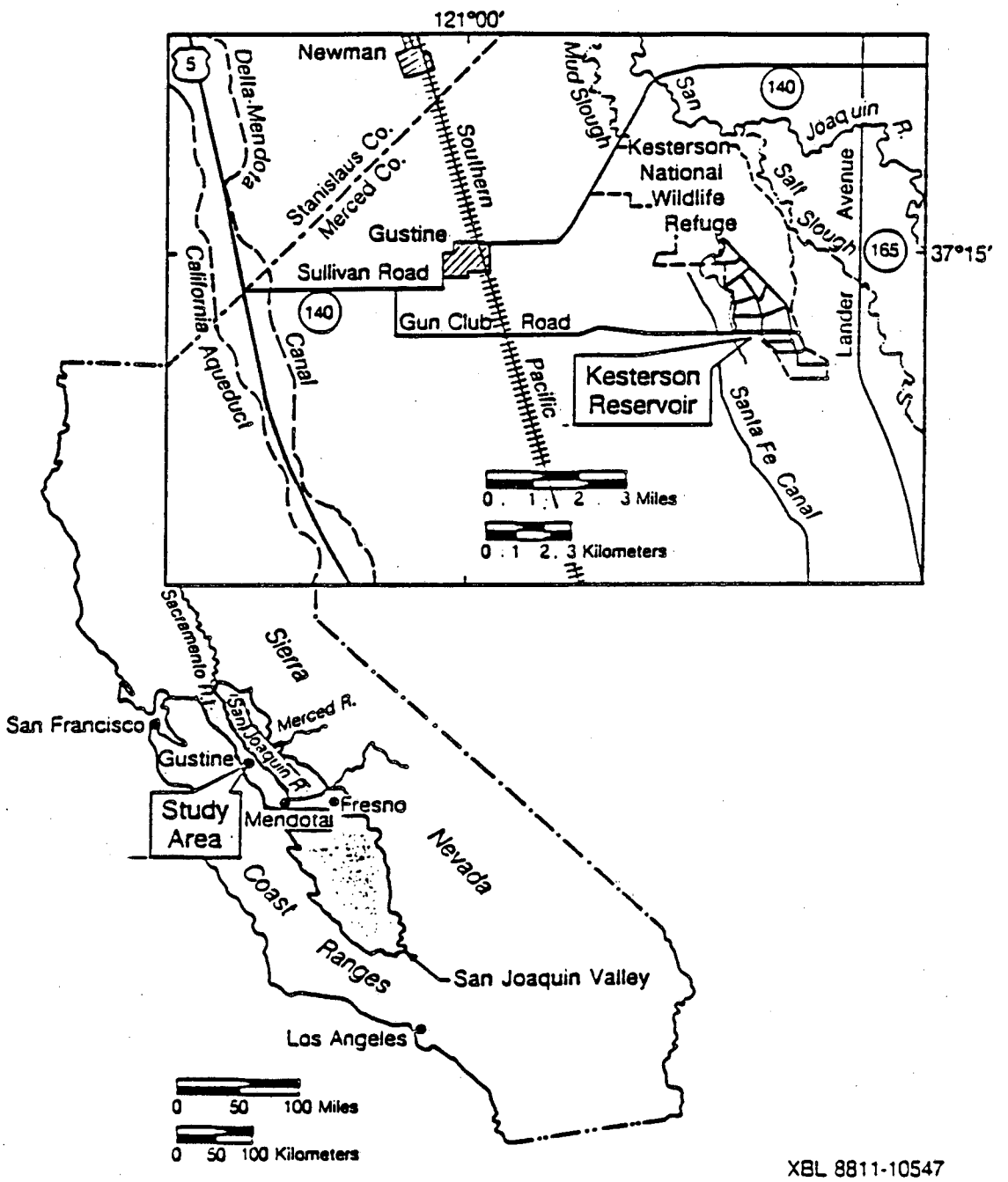


Figure 2.1 Location map of Kesterson Reservoir (Taken from Mandle, 1986).

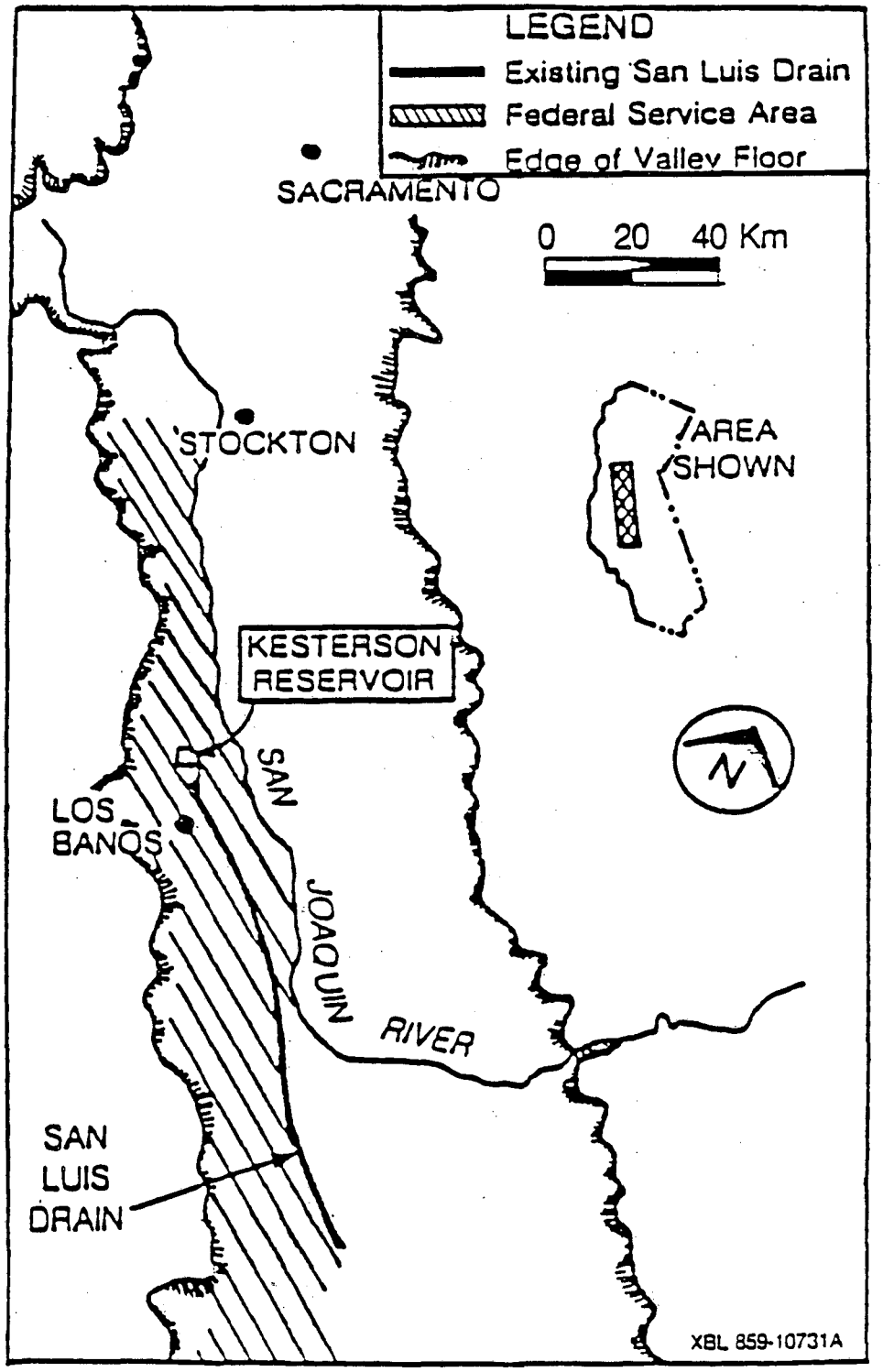


Figure 2.2 Map showing the San Luis Drain in relation to Kesterson Reservoir.

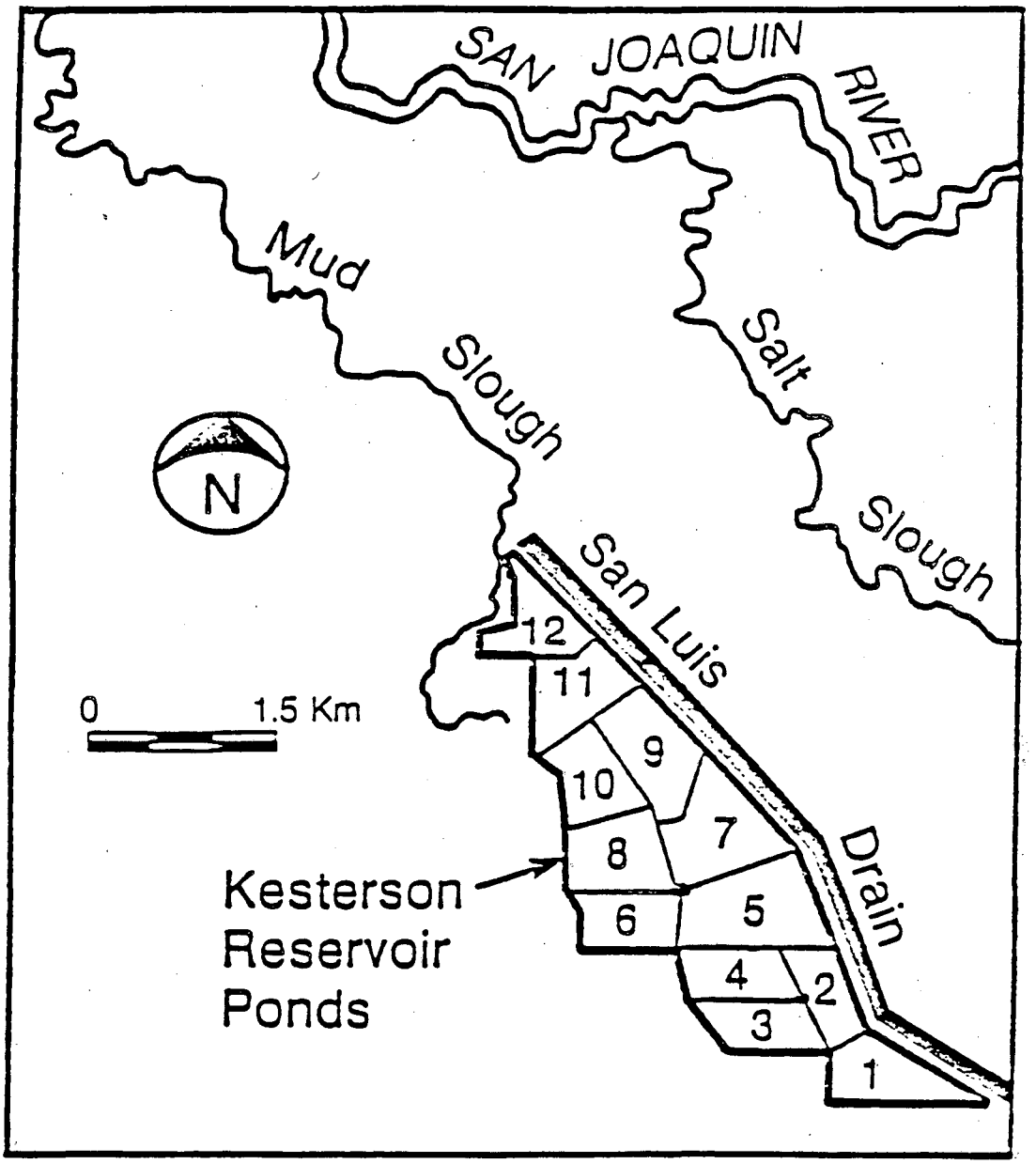


Figure 2.3 Location map showing the 12 regulating and evaporation ponds of Kester -son Reservoir.

1981, the San Luis Drain was delivering mostly contaminated subsurface drainage water.

High levels of selenium were found in fish at Kesterson Reservoir in 1982 (DOI, 1984) and deaths and deformities of migratory birds were noticed in 1983 (see Table 2.1). Test results showed that selenium poisoning was the cause and that selenium could be traced to the farmlands where it occurs naturally in the irrigated soils and had been transported to Kesterson Reservoir by way of the subsurface drainage water. The subsurface drainage water had originated as irrigation water which had percolated through the soils of the farmlands and then had been carried, by way of subsurface tile drains, into the San Luis Drain. The concentration of selenium in the drainage water ranged from 200-300 parts per billion (ppb). The Environmental Protection Agency's (EPA) current drinking water standard for selenium is 10 ppb (Weres et al., 1985). Disposal of drainage water to Kesterson Reservoir ceased in 1986.

Table 2.1. Chronological order of events involving the detection of selenium poisoning at Kesterson Reservoir.

1968-1975	-	Kesterson Reservoir and the San Luis Drain were constructed.
1972-1981	-	Uncontaminated surface water runoff began flowing to Kesterson Reservoir.
1981	-	Contaminated subsurface drainage water began flowing to Kesterson Reservoir.
1982	-	Three species of game fish died off.
1983	-	Death adn deformities were noticed in migratory birds.
		Selenium poisoning was determined to be the cause and was traced to naturally occuring selenium in the farmland soils.
1986	-	Disposal of drainage water to Kesterson Reservoir ceased.

Approximately 10 million m^3/yr (8097 acre-ft/yr) of drainage water was delivered to Kesterson Reservoir between 1981 and 1986. An estimated 9000 kg (19,841 lb) of selenium was discharged into the ponds during these years. Along with the selenium, high amounts of total dissolved solids (TDS) were also transported. Of the drainage water delivered to Kesterson Reservoir, approximately 50% seeped into

the underlying aquifer (USBR, 1986) and 50% evaporated. Evaporation tended to concentrate salts and selenium in the ponds and in the sediments.

Since 1986, the effects of the selenium contamination at Kesterson Reservoir have been investigated by scientists at Lawrence Berkeley Laboratory (LBL) and at the Sanitary Engineering and Environmental Health Research Laboratory (SEEHRL). The primary goal of the research program (LBL, 1988) is to assess the extent of contamination in surface waters and groundwater, to characterize the behavior of selenium in this wetlands environment, and to suggests methods of eliminating the impact of the contamination on wildlife.

2.3 GEOLOGY

2.3.1 Regional Geologic Setting

Kesterson Reservoir is located in the northwestern part of the San Joaquin Valley. The San Joaquin Valley comprises the southern two-thirds of the Central Valley of California with the Sacramento Valley making up the other one-third to the north. The San Joaquin Valley is a major structural feature of California and is approximately 81-97 km (50-60 miles) wide and about 400 km (250 miles) long.

The valley is a topographic trough bounded on the east by the pre-Tertiary, igneous and metamorphic rock of the Sierra Nevada Mountains and on the west by the Jurassic, Cretaceous, and Tertiary, folded and faulted sedimentary rocks of the Coast Ranges. The Sierra Nevada batholith slopes southwestward and makes up the basement complex of the valley floor (Smith, 1964).

During the Jurassic time period, before the formation of the Coast Ranges, the area existed as a low region of subsidence (Hoots et al, 1954). Marine sediments were deposited almost continuously in seas that covered this low region from Jurassic to late Tertiary time. From this period of sedimentation, the Great Valley Sequence and the Laguna Seca Formation were deposited. The Cretaceous age Great Valley

Sequence is made up of marine sandstones and siltstones in the central part of the low region with alluvial conglomerates along the eastern margin of the basin (Manning, 1972). Lying conformably on top of the Great Valley Sequence is the Laguna Seca Formation of Paleocene age (Herd, 1979). This unit consists of a fine grained sandstone. The marine sediments of the Great Valley Sequence and the Laguna Seca Formation, containing large amounts of organic matter, became the raw material for the petroleum found in the San Joaquin Valley.

Folding and faulting occurred during middle Quaternary time, deforming all the previously deposited units. The Coast Ranges and much of the present topography was formed at this time. Normal faulting occurred along the eastern margin of the basin and folding occurred in the central and western parts of the basin. The Coast Ranges dip eastward and overlie the basement complex of the Sierra Nevada batholith under the valley.

Unconsolidated sediments were deposited over the consolidated rocks of the Coast Ranges and the Sierra Nevada batholith in the valley during late Pliocene to Holocene time. These deposits make up the bulk of the material underlying the San Joaquin Valley and comprise a maximum stratigraphic thickness of greater than 670.6 m (2200 ft) in the western San Joaquin Valley. The unconsolidated deposits can be divided into the Tulare Formation of Pliocene and Pleistocene age and the younger terrace, alluvial, and flood-basin deposits of Pleistocene and Holocene age (Hotchkiss and Balding, 1971).

The Tulare Formation can be subdivided into three units, the lower section, the Corcoran Clay Member, and the upper section. The lower and upper sections are composed of highly to variably permeable, poorly- to well-sorted lenticular deposits of gravels, sands, silts, and clays. These deposits are derived from both the Coast Ranges and the Sierra Nevada Mountains. The Corcoran Clay Member is composed of a low permeable, lacustrine and marsh, sandy to silty clay deposit and is equivalent to what has been mapped as the E-Clay by Mitten et al. (1969). The Corcoran Clay

Member lies in the upper half of the Tulare Formation between the lower and upper sections and is the principle hydrologic confining layer for the aquifer system of the San Joaquin Valley.

The terrace deposits are composed of highly permeable gravels, sands, and silts in a clay matrix. The alluvium deposits are composed of interbedded, poorly- to well-sorted, permeable to moderately permeable gravels, sands, silts, and clays and were mapped in terms of recent or older alluvial fans by Hotchkiss and Balding (1971). The flood-basin deposits are composed of sands, silts, clays, and organic material with locally high concentrations of salts and alkali. Stream channel deposits of sands and gravels are also included in the flood-basin deposits.

2.3.2 Local Geologic Setting

Kesterson Reservoir is underlain, for the most part, by what has been mapped as the Dos Palos alluvium by Lettis (1982). The Dos Palos alluvium consists of sediments of mid-Pleistocene to Holocene age and are equivalent to the flood-basin deposits described by Hotchkiss and Balding (1971) above.

Geophysical and lithological logs were obtained from a total of 18 wells, both LBL test wells and USBR KR-200 series wells (see Figure 2.4), from which the subsurface geology of Kesterson Reservoir can be assembled. The general stratigraphy is shown in cross-section A-A' (see Figure 2.5). The top 3.05-6.1 m (10-20 ft) is characterized as a sandy loam (C1) with the top portion consisting of the surficial clay layer. The surficial clay layer thickness varies over the Reservoir from 0-12.2 m (0-40 ft). Below this depth is approximately 8.29 m (60 ft) of highly permeable sand (S1). An interpretation of shallow core samples of the sediments underlying Kesterson Reservoir (Flexser, 1988) relates C1 and possibly the upper portion of S1 to Lettis' Dos Palos alluvium.

Underlying S1 is approximately 3.05 m (10 ft) of a fine-grained, relatively low permeable clay layer (C2). This unit is underlain by approximately 36.58 m (120 ft)

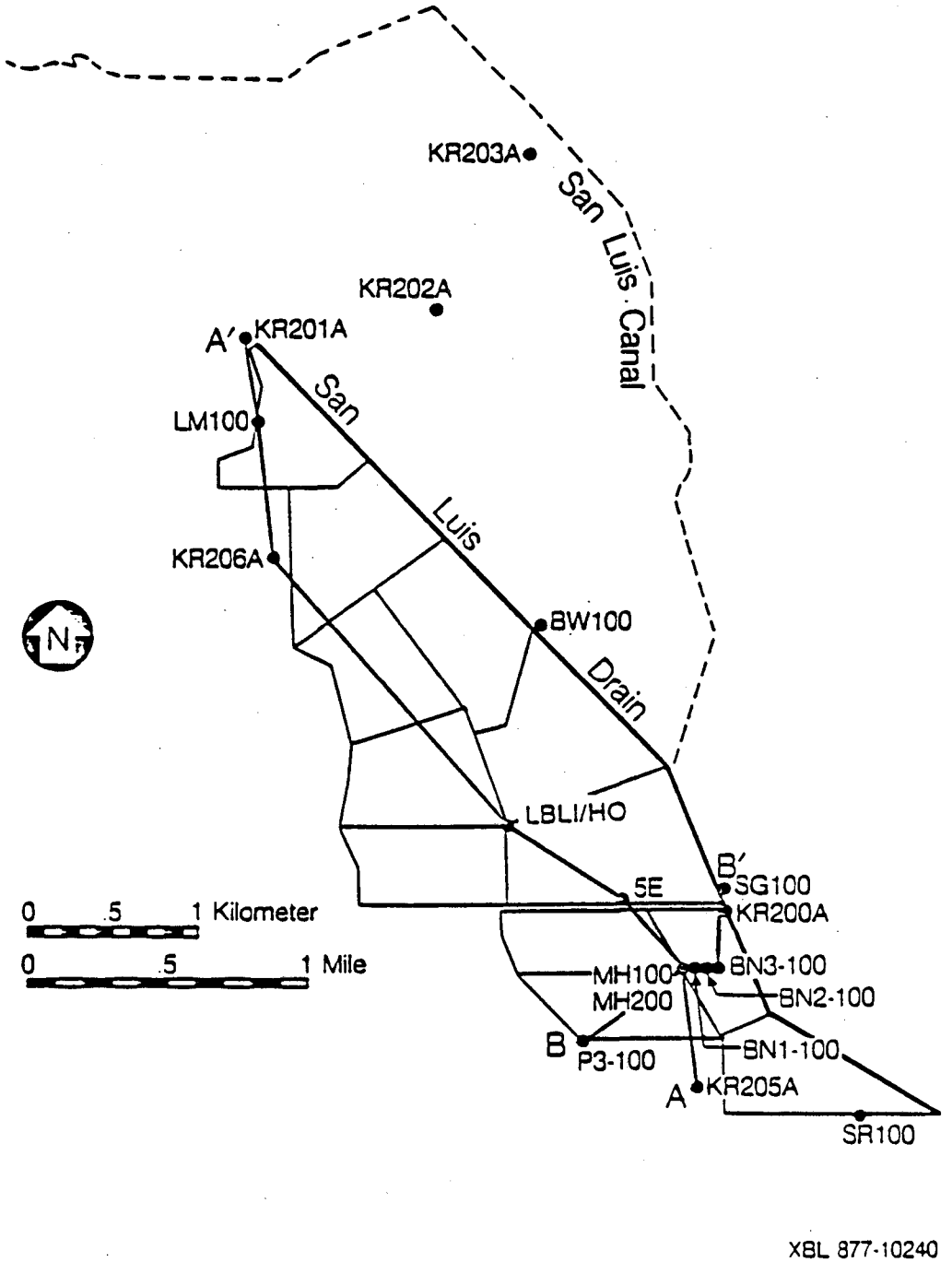


Figure 2.4 Location map showing test sites from which geophysical and lithological logs were obtained and cross-sections A-A' and B-B'.

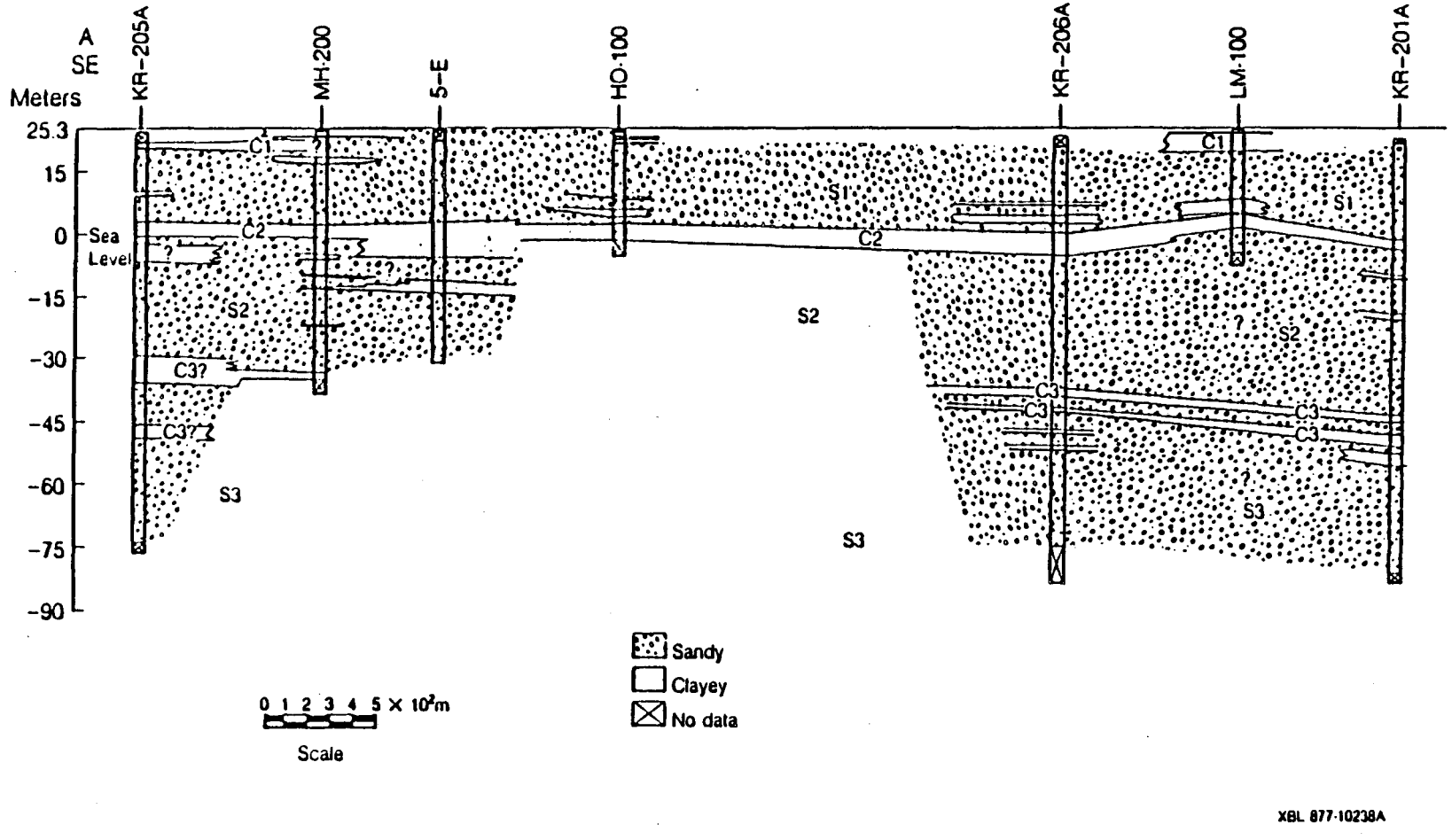


Figure 2.5 Cross-section A-A' showing general stratigraphy at Kesterson Reservoir.

of another high permeable sand unit (S2) which reaches to the top of the Corcoran Clay (C3) of the Tulare Formation. The Corcoran Clay is about 3.05-9.14 m (10-30 ft) thick and is typically encountered at depths of greater than 60.96 m (200 ft). At least 30.48 m (100 ft) of sand (S3) underlies the Corcoran clay. Below this depth the local stratigraphy is not known.

This interpretation of the geology at Kesterson Reservoir is very idealized. In actuality, the system is more complex with both horizontally and vertically heterogeneous and anisotropic sediments. Clay lenses and interfingering of sands and clays occur throughout the subsurface deposits.

2.4 HYDROLOGY

2.4.1 Regional Hydrologic Setting

In the past, precipitation along the Sierra Nevada Mountain front was the major source of water for agriculture in the San Joaquin Valley. At present, irrigation water exceeds precipitation as the major source. In the valley itself, there is an average annual rainfall of less than 15.24 cm (six inches), whereas, the potential evaporation rate is 165.1 cm (65 inches) a year (Davis et al., 1959). Regionally, groundwater along the western margin of the San Joaquin Valley moves northeastward towards the valley's trough and then northwestward towards the Sacramento-San Joaquin Delta. Both surface water and ground water are used for irrigation. With the increasing use of groundwater throughout the last few decades, the water level in the San Joaquin Valley has declined over 121.9 m (400 ft) in places and has resulted in the largest known volume of land subsidence due to fluid withdrawal in the world (Williamson et al., 1985).

The unconsolidated deposits of late Tertiary and Quaternary age contain most of the usable groundwater in the San Joaquin Valley. The Corcoran Clay Member of the Tulare Formation is the hydrologic confining layer for the aquifer system in the valley

(see Figure 2.6). Above the Corcoran Clay Member is a semi-confined aquifer (the Upper Aquifer) which ranges in thickness throughout the valley from approximately 61 m (200 ft), as seen in the lithological and geophysical logs of Kesterson Reservoir, to approximately 243.8 m (800 ft), as reported by Croft (1972). The aquifer beneath the Corcoran Clay Member (the Lower Aquifer) is a confined system and extends down to the consolidated rocks of the Coast Ranges and the Sierra Nevada batholith. The Upper Aquifer is used for irrigation and livestock watering, whereas, the Lower Aquifer is used mainly as a drinking water supply but does contain some saline water.

2.4.2 Local Hydrologic Setting

Prior to development of Kesterson Reservoir, the depth to the water table ranged from 0-3.66 m (0-12 ft) below the ground surface (Jackson, 1967). The direction of groundwater flow was from the south and west of the Reservoir towards the Salt Slough and the San Joaquin River. The hydraulic gradient ranged from 1×10^{-4} to 10×10^{-4} meters of water/meters of distance (State of California, 1967). After Kesterson Reservoir was constructed and proceeded to operate as a storage facility for agricultural drainage water, the Reservoir acted as a groundwater recharge mound superimposed on the regional groundwater system (Mandle and Kontis, 1986). During operations, groundwater flowed vertically and horizontally away from the Reservoir in all directions.

The water table fluctuates seasonally due to recharge from precipitation in the Sierra Nevada Mountains and due to changes in water use such as flooding of duck ponds in the vicinity of the Reservoir. The nearby duck ponds are flooded in early fall to attract migratory birds and then are drained in the spring. The water table at the Reservoir is generally highest during the months of December and January and is lowest from June through October. Potential evapotranspiration rates are highest in the dry summer months.

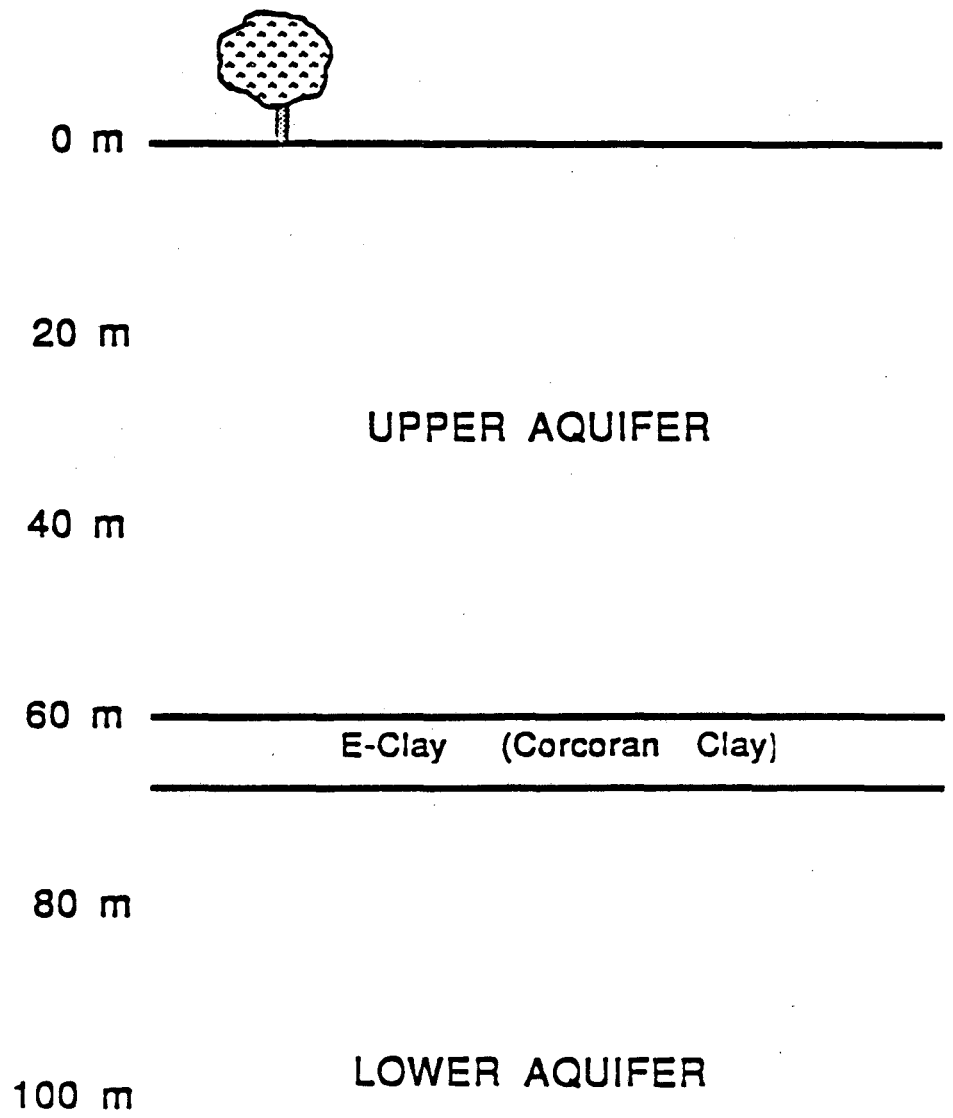


Figure 2.6 Schematic hydrologic cross-section of the San Joaquin Valley.

Since the agricultural drainage water that was stored at Kesterson Reservoir contained high amounts of TDS, selenium, boron, and other trace metals, the relationship between the ponds and the underlying aquifers is important in determining the possible extent of contamination. Extensive groundwater monitoring has shown that the Lower Aquifer (beneath the Corcoran Clay Member) is not influenced by the operations at the Reservoir, therefore, only the Upper Aquifer is of real concern (LBL, 1987). Beneficial uses of the Upper Aquifer include providing water for irrigation and livestock.

The ponds at Kesterson Reservoir are underlain by a fine-grained soil through which drainage water needs to pass in order to get to the Upper Aquifer. During operation of the Reservoir, these soils served as a barrier to the rapid seepage of the contaminated drainage water. Infiltration studies of these soils were carried out prior to the construction of the Reservoir by Luthin (1966) and a value for saturated hydraulic conductivity K_s of 3.5×10^{-7} m/s (1.2×10^{-6} ft/s) was reported. LBL also conducted infiltration tests (LBL, 1987) at several locations, yielding field measurements of a very high K_s for the uppermost 0.3 m (1 ft) of soil, sometimes exceeding 3.2×10^{-6} m/s (1.0×10^{-5} ft/s). The predominance of macropores in the soil was thought to be one possible explanation for the high K_s values in this depth range. Below this depth, K_s gradually decreased until values ranging from 3.2×10^{-8} to 3.2×10^{-7} m/s (1.0×10^{-7} to 1.0×10^{-6} ft/s) were reached. LBL (1987) determined that the permeability increases again below a depth ranging from 2 m to 12 m (6.6-39.4 ft) indicating that the top of the low-permeable soil causing the impediment to fluid flow was located at about 0.3 m (1 ft) and the bottom of the layer was found as deep as 12 m (39.4 ft).

In order to determine the hydrologic properties and the subsurface geology of the Upper Aquifer, several sites at Kesterson Reservoir were chosen by LBL for intensive investigation. Each site consists of a nest of boreholes drilled to various depths. These boreholes were used to obtain geophysical and lithological logs, to perform

steady-state and pressure transient pumping tests, and to perform tracer tests (LBL, 1987). The pumping tests were performed in order to determine the hydraulic conductivity as a function of depth. From these tests, the arithmetic mean horizontal K of the Upper Aquifer was determined to be equal to 1.9×10^{-4} m/s and the geometric mean was equal to 1.1×10^{-4} m/s (Benson, 1988).

The second clay unit (C2), mentioned previously in Section 2.3.2, is believed to be continuous throughout the area and may be important as an aquitard in impeding the vertical flux of drainage water. Because of this, one of the objectives of this report was to determine the permeability of this layer. C2 is found at a depth of about 24 m (80 ft) and is approximately 3 m (10 ft) thick.

Because of the strong possibility that C2 acts as an aquitard and because most of the contaminant plume extends to depths of 25 m (82 ft) or less, most of the work conducted at Kesterson Reservoir by LBL and all of the work conducted for this report focused on the sediments above C2. For the remainder of this report, the uppermost 30.5 m (100 ft) of sand, silts, and clays will be referred to as "the aquifer system" and consists of the sand unit S1 bounded on the top by C1 and on the bottom by C2.

2.5 EXTENT OF CONTAMINATION

The agricultural drainage water that was delivered to the storage and evaporation ponds of Kesterson Reservoir from 1981 to 1986 was high in total dissolved solids (TDS), selenium, boron, and other trace metals. As the contaminated drainage water seeped from the storage ponds down into the underlying aquifer, the selenium became immobilized in the pond-bottom sediments due to biochemical activity (Weres et al., 1985). The contaminant plume that did develop in the underlying aquifer, however, was still high in TDS, boron, and other trace metals and was two to three times more saline than the original groundwater of the aquifer.

In some isolated areas, specifically under the junction of Ponds 2, 3, 4, and 5, selenium did seep down through the pond-bottom sediments into the shallow aquifer system. Seepage through the pond-bottom sediments into these isolated areas has been determined to be caused by elevated concentrations of nitrate, a decreased supply of organic matter, and an increased downward seepage rate (LBL, 1987). Other factors that could have contributed to these isolated areas of selenium are the method of constructing the berms surrounding the ponds and local variations of permeability and lithology within the aquifer. These factors are thoroughly discussed in the Kesterson Reservoir Annual Report (LBL, 1987).

Studies carried out by LBL have indicated that the contaminant plume has migrated to depths ranging from about 6.1-25 m (20-82 ft) (LBL, 1987). Geophysical tracking of the plume indicates that horizontal migration is limited to a thin band that extends a maximum of 350 m (1148.3 ft) to the east of the San Luis Drain (Goldstein, Alumbaugh, and Benson, 1988).

3.0 THEORY

3.1 PHYSICS OF GROUNDWATER FLOW

The study of groundwater flow is important in many fields of science and engineering such as geology, hydrology, soil science, geotechnical engineering, and ecology, just to name a few. Historically, the study of groundwater has been mainly concerned with the development of water supplies and groundwater as a resource. These aspects are still important today. But in order to continue using groundwater as a resource, it needs to be protected from contamination. Due to population growth and an increase in industrial and agricultural production since the second world war, man is creating more waste than the environment can absorb with an end result of environmental contamination (Freeze and Cherry, 1979).

In 1856, Darcy was the first to describe groundwater hydrology as a quantitative science (Wang and Anderson, 1982). By experimentation, Darcy determined that the flow rate Q of water, through a given type of sand, was directly proportional to the cross-sectional area A of a cylinder and to the drop in hydraulic head ($\phi_2-\phi_1$) over the distance between the measurement points (l_2-l_1). Letting K be the constant of proportionality, Darcy's Law can be written as

$$Q = -KA\frac{d\phi}{dl} \tag{3.1}$$

where K is the hydraulic conductivity and $d\phi/dl$ is the hydraulic gradient. The negative sign signifies that the flow is in the direction of head loss. Darcy's Law can also be expressed in terms of Darcy's velocity q by dividing Eq. 3.1 through by the cross-sectional area A.

$$q = -K\frac{d\phi}{dl} \tag{3.2}$$

The hydraulic conductivity K is a function of both the fluid and the porous medium. Experiments were carried out to find a parameter that was a function of only the porous medium. K was found to be directly proportional to the fluid density ρ and the acceleration due to gravity g but inversely proportional to the viscosity of the fluid μ. The constant of proportionality k was then defined as the absolute or intrinsic permeability and is a function of the porous medium only.

$$K = \frac{k\rho g}{\mu} \tag{3.3}$$

Darcy's Law had been developed for a *saturated* porous medium, but soils near the ground surface are not always fully saturated. In 1907, Buckingham proposed some ideas about the flow of fluid through *unsaturated* porous medium independently of Darcy. Darcy's Law was found applicable to both saturated and unsaturated conditions and is sometimes referred to as the Darcy-Buckingham Law. To take into account the decrease in permeability due to unsaturated conditions in which the air (or any other fluid) in the pore spaces competes with the water for available flow paths, the absolute permeability k is multiplied by a relative permeability k_{rel} to yield the effective permeability k_{eff}.

$$kk_{rel} = k_{eff} \qquad \text{where} \quad 0 \le k_{rel} \le 1.0 \tag{3.4}$$

The hydraulic conductivity can now be written as

$$K = \frac{kk_{rel}\rho g}{\mu} \qquad \text{or} \qquad K = \frac{k_{eff}\rho g}{\mu} \tag{3.5}$$

Hubbert (1940) first clarified the use of both elevation and pressure with the concept of groundwater potential. Both pressure and elevation act on a unit mass of groundwater. The work per unit mass required to raise water from an initial pressure of P_o to a pressure P (if the water is assumed to be slightly compressible) is

$$\frac{\text{work}}{\text{unit mass}} = \int_{P_o}^{P} \frac{dP}{\rho} \tag{3.6}$$

The work per unit mass required to raise water from an initial elevation z_o to an elevation z is

$$\frac{\text{work}}{\text{unit mass}} = g(z - z_o) \tag{3.7}$$

The fluid potential Φ is then

$$\Phi = g(z - z_o) + \int_{P_o}^{P} \frac{dP}{\rho} \tag{3.8}$$

Groundwater flows from a point of high potential to a point of low potential.

To express pressure P in terms of pressure head ψ, divide both sides of Eq. 3.8 by the acceleration due to gravity g and assume that P_o and z_o are equal to zero.

$$\frac{\Phi}{g} = z + \frac{1}{g}\int_{\psi_o}^{\psi} d\psi \tag{3.9}$$

Darcy's hydraulic head ϕ can be related to fluid potential Φ by

$$\phi = \frac{\Phi}{g} = z + \psi \tag{3.10}$$

$P/\rho g$ is equal to ψ (the length of the liquid column) and is called the pressure head. The hydraulic head is equal to the pressure head plus the elevation head.

The Law of Mass Conservation states that mass can be neither created nor destroyed. If the mass of fluid entering a volume element of a porous medium is not equal to the mass of fluid coming out, then the excess mass is being stored in the volume element.

Inflow – Outflow = Change in Storage

This is called the continuity equation. The rate at which mass is entering and leaving the volume element is controlled by Darcy's Law, the equation of motion. By combining Darcy's Law with the continuity equation, a partial differential equation describing transient flow can be obtained. A transient problem is one in which the unknown variable, in this case ϕ, changes with time. The mass of water flowing into

a volume element is not equal to the mass of water flowing out.

By letting the volume element become vanishingly small so that the hydraulic head is defined and continuous at a point and then incorporating Darcy's Law, the continuity equation for saturated or unsaturated conditions in a homogeneous aquifer can be written as

$$\nabla \cdot \rho K \nabla \phi = m_c \frac{\partial \phi}{\partial t} \tag{3.11}$$

where $\partial\phi/\partial t$ is the change in hydraulic head per change in time and m_c is the specific fluid mass capacity and is equal to the change in fluid mass dM_f per change in pressure head $d\psi$ per unit bulk volume V_B. For a system which is fully saturated, $m_c = \rho S_s$, Eq. 3.11 can be written as

$$\nabla^2 \phi = \frac{S_s}{K} \frac{\partial \phi}{\partial t} \tag{3.12}$$

where S_s is the specific storage and is defined in groundwater terms as:

$$S_s = \rho g n(\alpha + \beta) \tag{3.13}$$

n is the porosity of the matrix, α is the pore compressibility of the matrix, and β is the compressibility of water. If Eq. 3.12 is multiplied on both sides by H, the thickness of the aquifer, it then can be written in terms of storativity and transmissivity since $S = S_s H$ and $T = KH$.

$$\nabla^2 \phi = \frac{S}{T} \frac{\partial \phi}{\partial t} \tag{3.14}$$

Any addition of fluid to a groundwater system is considered a source, any depletion, such as pumping a well, is a sink. If we include the change in storage due to a source or a sink, the complete continuity equation can be written as

$$\nabla \cdot \rho K \nabla \phi = m_c \frac{\partial \phi}{\partial t} - \rho g_w \tag{3.15}$$

where g_w is defined as the source or sink volumetric rate of water per unit bulk volume.

If the groundwater system is at steady-state, which means that the mass of water flowing into a volume element is equal to the mass of water flowing out, then the change in storage is equal to zero. Eq. 3.15 can then be written as

$$\nabla \cdot K \nabla \phi = -g_w \tag{3.16}$$

and is known as Poisson's equation. If the system is at steady-state but does not have a source nor sink, Eq. 3.15 is written as

$$\nabla \cdot \rho K \nabla \phi = 0 \tag{3.17}$$

and is known as Laplace's equation.

A governing equation, such as Laplace's or Poisson's equation, and boundary conditions form a mathematical model of groundwater flow at steady-state conditions. A transient system not only needs the governing equation and boundary conditions, but also needs initial conditions in order to form a model of groundwater flow at transient conditions. The transient equation represents an initial-boundary value problem.

3.2 AQUIFER RESPONSE TO PUMPING

The aquifer system at Kesterson Reservoir is a leaky and layered system with partially penetrating wells. Each of these characteristics (ie. leakage, layering, and partial penetration) individually effect the flow of fluid to a pumping well in an aquifer in different ways. A description here of how each characteristic effects the flow field in an otherwise ideal aquifer is necessary before describing the aquifer system at Kesterson Reservoir. The types of aquifers that will be examined are 1) an ideal, confined aquifer, 2) a leaky aquifer, 3) an aquifer in which the well screen only partial penetrates the aquifer, and 4) a layered aquifer. This section of the report is to familiarize the reader as to what exactly constitutes an ideal aquifer, a leaky aquifer, a layered aquifer, and an aquifer with partial penetration.

3.2.1 Ideal Aquifer

For the most ideal case describing flow to a well in an aquifer, the aquifer is assumed to be confined, horizontal, homogeneous, and isotropic with a constant thickness and infinite in areal extent. The pumping rate is constant with time, the pumping well diameter is infinitesimally small, the initial hydraulic head is uniform throughout, and the screened interval of the well fully penetrates the aquifer (see Figure 3.1). Transient flow analysis involves measurement of hydraulic head decline or pressure decline in the pumping well or an observation well throughout pumping. For a fully saturated system, Eq. 3.14 can be rewritten in radial coordinates as

$$\frac{\partial^2\phi}{\partial r^2} + \frac{1}{r}\frac{\partial\phi}{\partial r} = \frac{S}{T}\frac{\partial\phi}{\partial t} \tag{3.18}$$

when subjected to the following initial and boundary conditions.

Initial Condition:

$$\phi(r,0) = \phi_o$$

Boundary Conditions:

$$\phi(\infty,t) = \phi_o$$

$$Q = \lim_{r\to 0}\left[2\pi r T\frac{\partial\phi}{\partial r}\right]$$

The solution (Theis, 1935) is

$$s = \frac{Q}{4\pi T}\int_u^\infty \frac{e^{-u}}{u}du = \frac{Q}{4\pi T}W(u) \tag{3.19}$$

where $s = (\phi_o - \phi)$. In terms of pressure change ΔP, the solution is written as

$$\Delta P = \frac{Q\rho g}{4\pi T}\int_u^\infty \frac{e^{-u}}{u}du = \frac{Q\rho g}{4\pi T}W(u) \tag{3.20}$$

The exponential integral, also called the *well function* W(u), can be expressed as an evaluated infinite series:

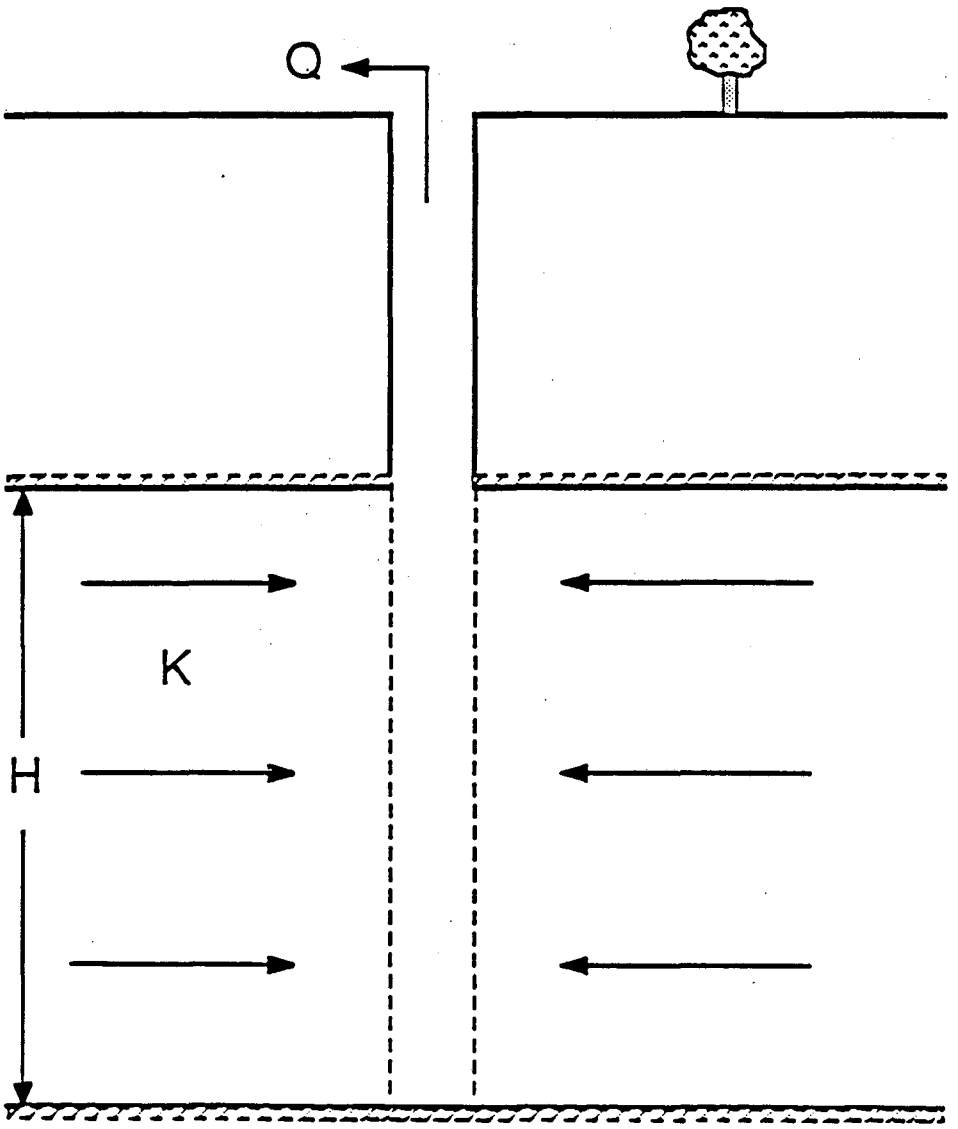


Figure 3.1 Schematic diagram of an ideal aquifer responding to pumping.

$$W(u) = -0.5772 - \ln u + u - \frac{u^2}{2\cdot 2!} + \frac{u^3}{3\cdot 3!} - \frac{u^4}{4\cdot 4!} + ... \qquad (3.21)$$

In order to simplify analysis by using graphical solutions, the dimensionless parameters

$$u = \frac{r^2 S}{4Tt} \qquad \text{and} \qquad W(u) = \frac{4\pi Ts}{Q} \qquad (3.22)$$

have been introduced. In petroleum and in some groundwater literature, dimensionless pressure P_D and dimensionless time t_D are used instead of W(u) and u where

$$t_D = \frac{1}{4u} \qquad \text{and} \qquad P_D = \frac{W(u)}{2} \qquad (3.23)$$

The theoretical pressure response of an ideal aquifer, once production begins, can be plotted as log P_D versus log t_D as shown in Figure 3.2. The early part of the ideal aquifer type-curve (also called the Theis curve) shows the steep initial change of pressure in the aquifer due to production at a well. At a later time, pressure drawdown is much more gradual and the curve starts to level off. The curve, however, never completely levels off because steady-state condition can not be reached in a horizontally infinite aquifer.

3.2.2 Leaky Aquifer

An aquifer is considered leaky if it is recharged with fluid from a top or a bottom confining layer as the aquifer is being pumped. The assumption made for the ideal aquifer situation in which the confining layers are impermeable is seldom satisfied in nature. The theory of fluid flow in a leaky aquifer was developed by Hantush and Jacob (1955) who provided the partial differential equation relating the theoretical Theis response of an ideal aquifer to that of a leaky aquifer. The aquifer system used for the development of this theory consists of a homogeneous and isotropic aquifer, infinite in areal extent and of constant thickness, overlain by an aquitard and underlain by an aquiclude. The wells fully penetrate the aquifer and have

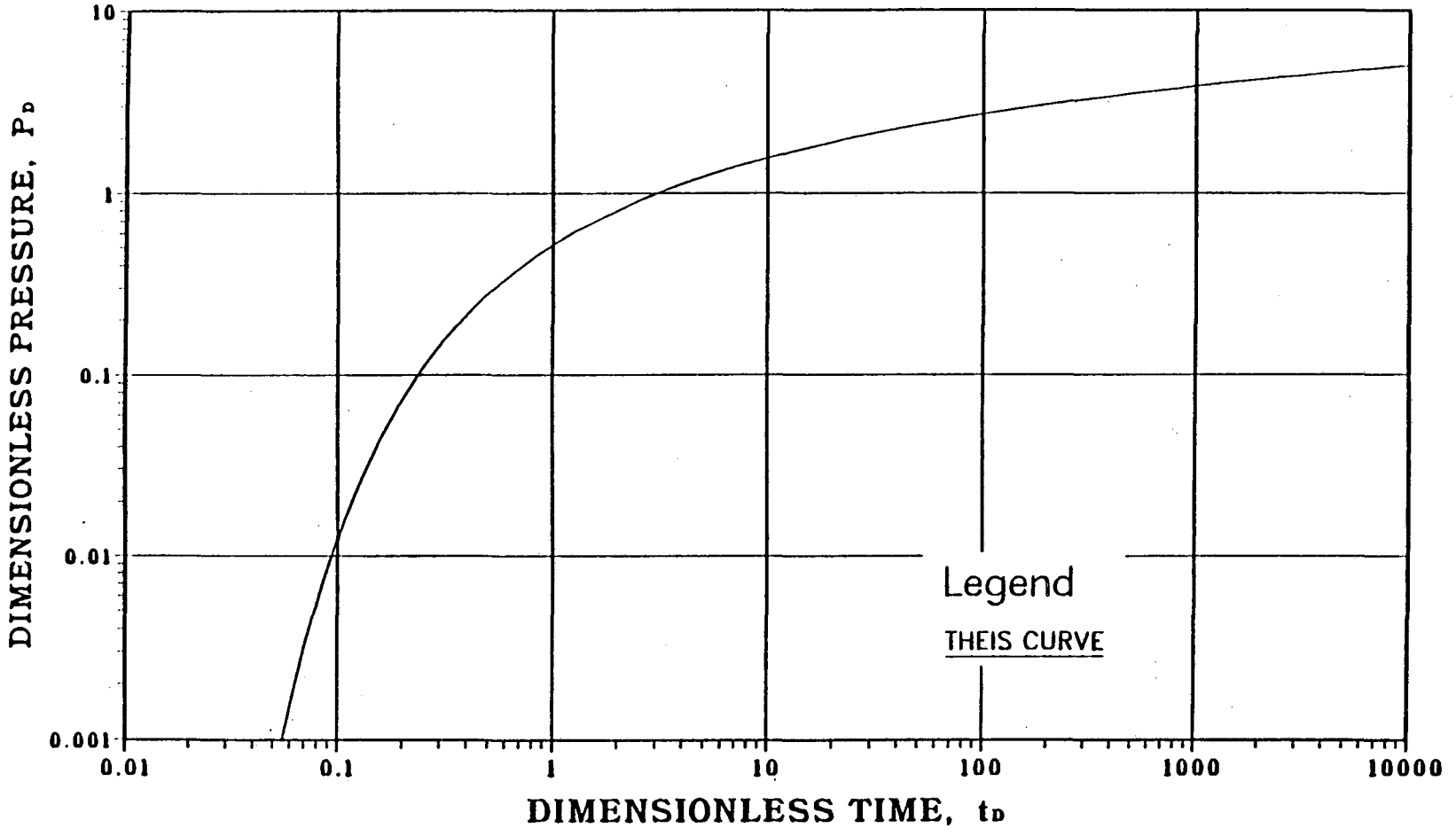


Figure 3.2 Theoretical log-log type-curve for an ideal aquifer (Theis, 1935).

infinitesimal diameters. Overlying the aquitard is a source layer providing water to the system (see Figure 3.3).

One method of simplifying the mathematics involved in solving the problem of a leaky aquifer is to assume that the flow is vertical through the aquitard and horizontal in the aquifer. The errors due to this assumption are less than 5% (Neuman and Witherspoon, 1969) if the hydraulic conductivity of the aquifer is two orders of magnitude greater than the hydraulic conductivity of the aquitard.

In developing this solution, restrictive basic assumptions were made. The upper boundary of the aquitard was assumed to be at a constant hydraulic potential and the rate of leakage into the aquifer from the aquitard was assumed to be proportional to the drawdown that occurs in the aquifer. The first assumption implies that drawdown in the source layer is equal to zero during pumping of the aquifer. The second assumption neglects the effects due to compressibility in the aquitard.

Neglecting drawdown in the source layer and the compressibility of the aquitard, the governing equation for a leaky aquifer system is similar to Eq. 3.18 but with a non-linear source term, ϕ/B^2.

$$\frac{\partial^2\phi}{\partial r^2} + \frac{1}{r}\frac{\partial\phi}{\partial r} - \frac{\phi}{B^2} = \frac{S}{T}\frac{\partial\phi}{\partial t} \tag{3.24}$$

where

$$B = \sqrt{\frac{kHH'}{k'}} \tag{3.25}$$

where H' is the thickness of the aquitard and k' is the permeability of the aquitard. The same initial and boundary conditions apply.

When pumping commences at a well, a cone of pressure depression forms and keeps expanding until steady-state is reached. Because of this, the potential gradient is greater near the pumping well and, therefore, the rate of leakage from the aquitard to the aquifer is also greater near the pumping well. The solution to Eq. 3.24 is similar to Theis' solution of Eq. 3.19 except that the well function W(u) is now also a

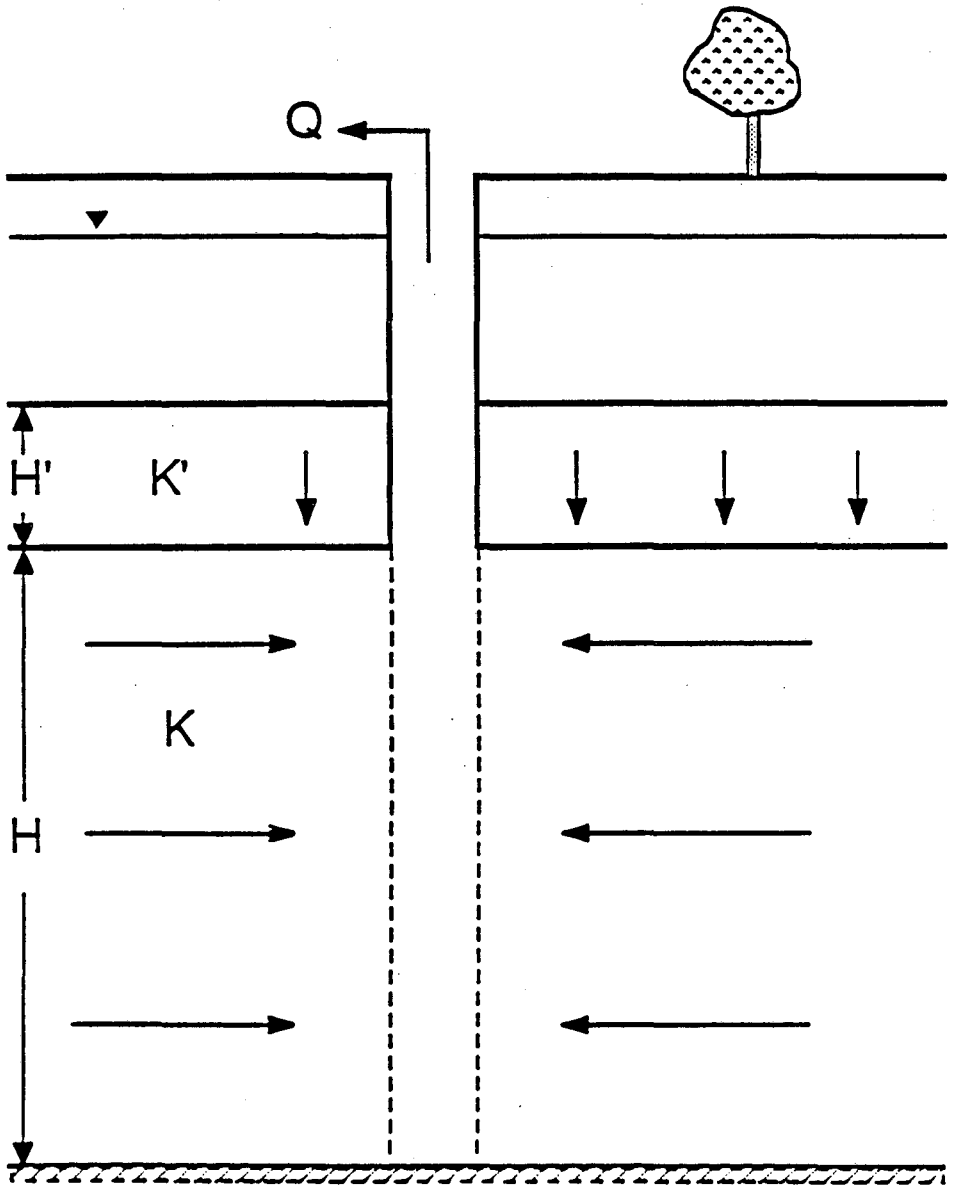


Figure 3.3 Schematic diagram of a leaky aquifer responding to pumping.

function of r the radial distance from the well and B, which incorporates the hydraulic conductivity K′ and the thickness H′ of the aquitard. The solution is written as

$$s = \frac{Q}{4\pi T}\int_{u}^{\infty}\exp\left[-u - \frac{r^2}{4B^2u}\right]\frac{du}{u} = \frac{Q}{4\pi T}W(u,r/B) \qquad (3.26)$$

W(u,r/B) is called the *leaky well function* (Hantush, 1964).

The theoretical pressure response of a leaky aquifer, once production begins, can be plotted as log P_D versus log t_D for different values of r/B as shown in Figure 3.4. The early-time pressure response is the same as that of an ideal aquifer. However, the later-time pressure response of the leaky aquifer levels off completely, due to recharge from the aquitard, to a constant value of ΔP as the aquifer reaches steady-state conditions. The stabilized value of ΔP is smaller for wells that are farthest from the production well. The more leaky the aquitard is, the faster the pressure response equilibrates. For the case of an impermeable confining layer, when r/B goes to zero, the leaky aquifer type-curve reduces to the Theis curve.

3.2.3 Effects Due To Partial Penetration

When a well is not screened over the entire thickness of an aquifer, it is said to only partial penetrate the aquifer. This condition is also referred to as *limited entry*. The effects on well productivity due to partial penetration and the procedures used in the analysis of pumping test data have been studied by many authors starting with Muskat (1949), Van Everdingen (1953), and Hurst (1953).

At early-time, fluid flow around the vicinity of the screened interval is essentially radial. As time progresses, however, and a larger volume of the aquifer responds to pumping, the flow to the screened interval becomes spherical. At an even later-time, flow to the well again becomes radial, but the entire aquifer is now affected (see Figure 3.5). A new term is added to the solution of the ideal aquifer case which takes into account the effects due to partial penetration:

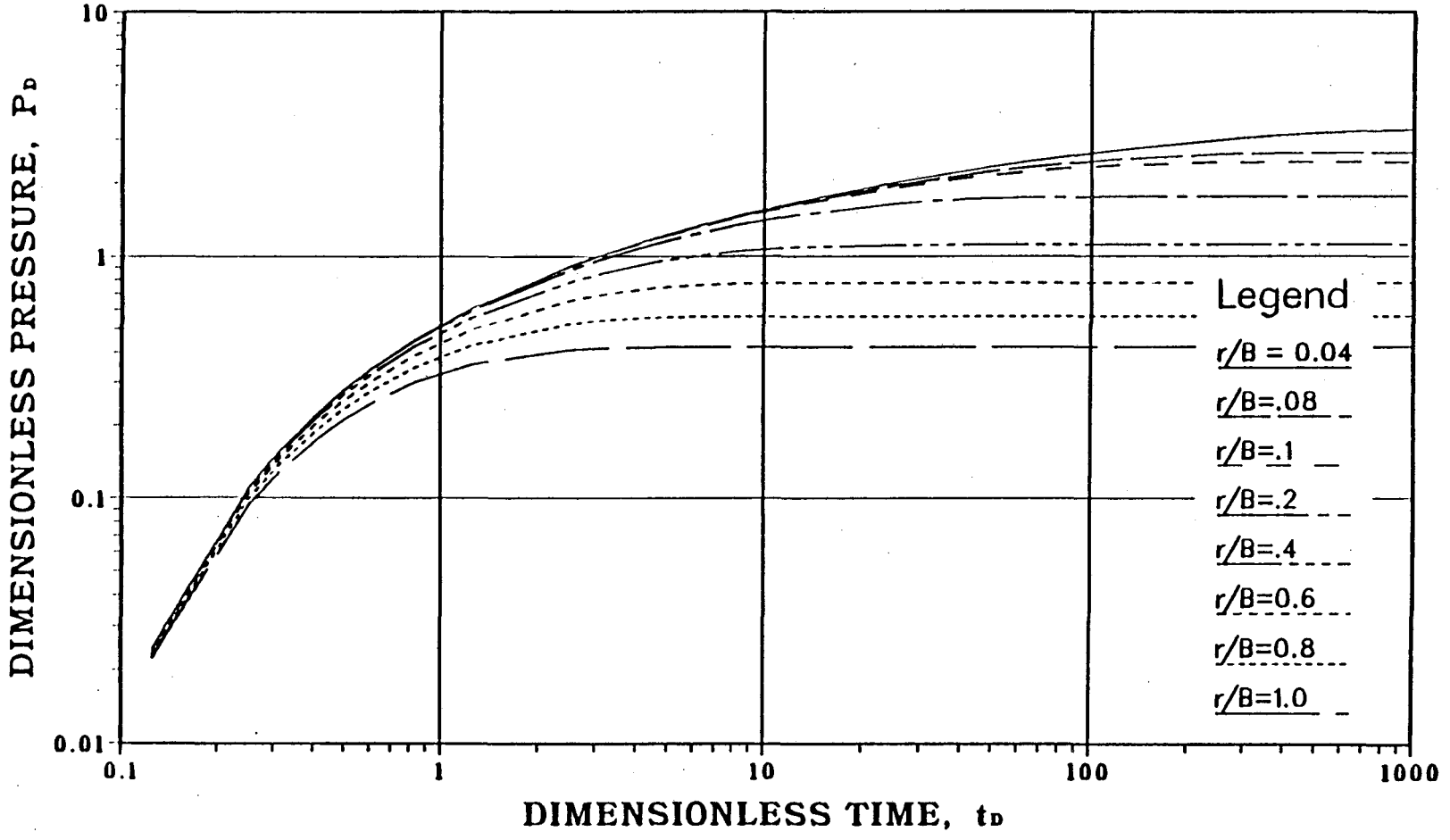


Figure 3.4 Theoretical log-log type-curve for a leaky aquifer (Hantush and Jacob, 1955).

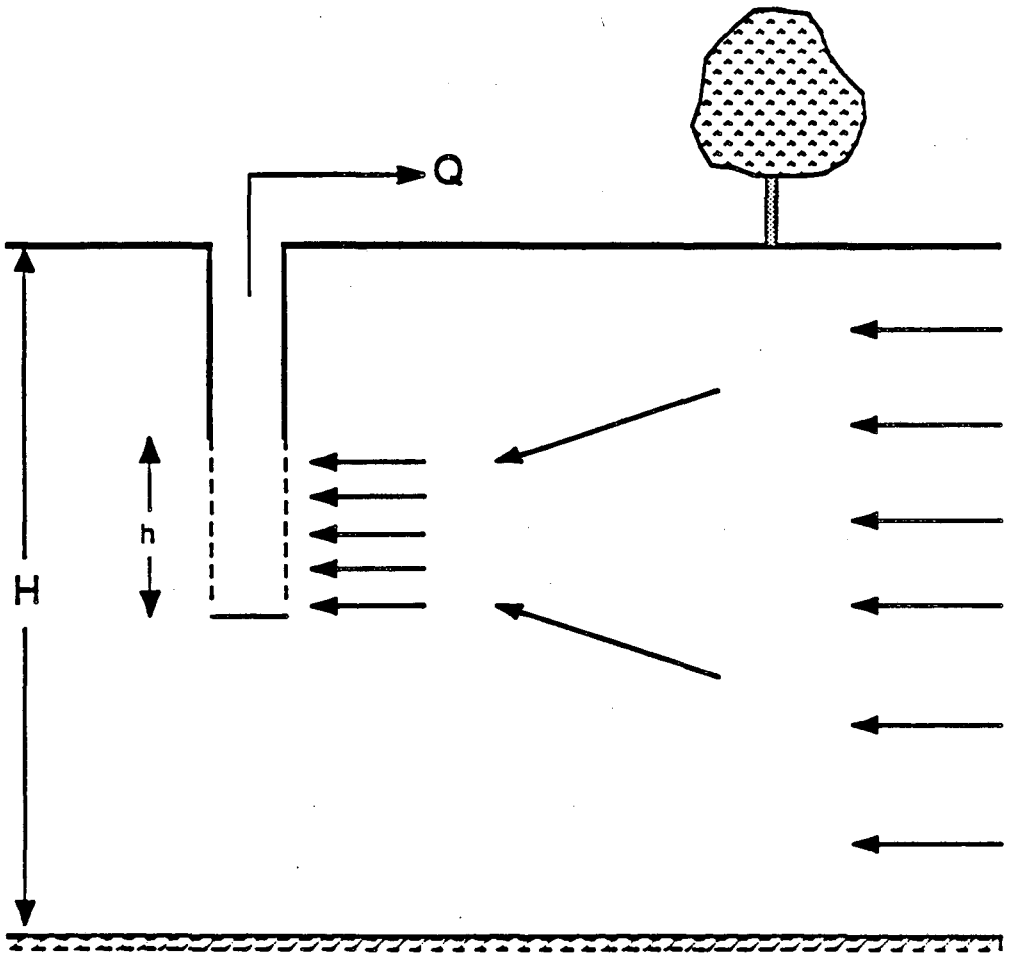


Figure 3.5 Schematic diagram of an aquifer responding to pumping with partially penetrating wells.

$$\frac{\partial^2\phi}{\partial r^2} + \frac{1}{r}\frac{\partial\phi}{\partial r} + \frac{\partial^2\phi}{\partial z^2} = \frac{S}{T}\frac{\partial\phi}{\partial t} \tag{3.27}$$

z is the distance from the upper boundary of the aquifer to any point in the aquifer. Since the hydraulic head is now a function of r, z, and t, the initial and boundary conditions are as follows.

Initial Condition:

$$\phi(r,z,0) = \phi_o$$

Boundary Conditions:

$$\phi(\infty,z,t) = \phi_o$$

$$\frac{\partial\phi}{\partial z}(r,0,t) = 0$$

$$\frac{\partial\phi}{\partial z}(r,H,t) = 0$$

$$Q = \lim_{r\to 0}\left[2\pi K \int_0^H r\frac{\partial\phi}{\partial r}dz\right]$$

The solution is simplified to

$$W(u) = \int_u^\infty \frac{e^{-u}}{u}\,du + f(Z,h,r) \tag{3.28}$$

where Z is the distance from the top boundary of the aquifer to the middle of the screened interval in the observation well and h is the length of the screened interval in the pumping well (see Figure 3.6).

$$f(Z,L,r) = \frac{2H}{\pi L}\sum_{n=1}^{\infty}\frac{1}{n}\cos\frac{n\pi Z}{H}\sin\frac{n\pi h}{H}\int_u^\infty \exp\left[-u - \frac{k_z(n\pi r)^2}{4k_r H^2 u}\right]\frac{du}{u} \tag{3.29}$$

$$n = 1,2,3,\ldots$$

where in this case

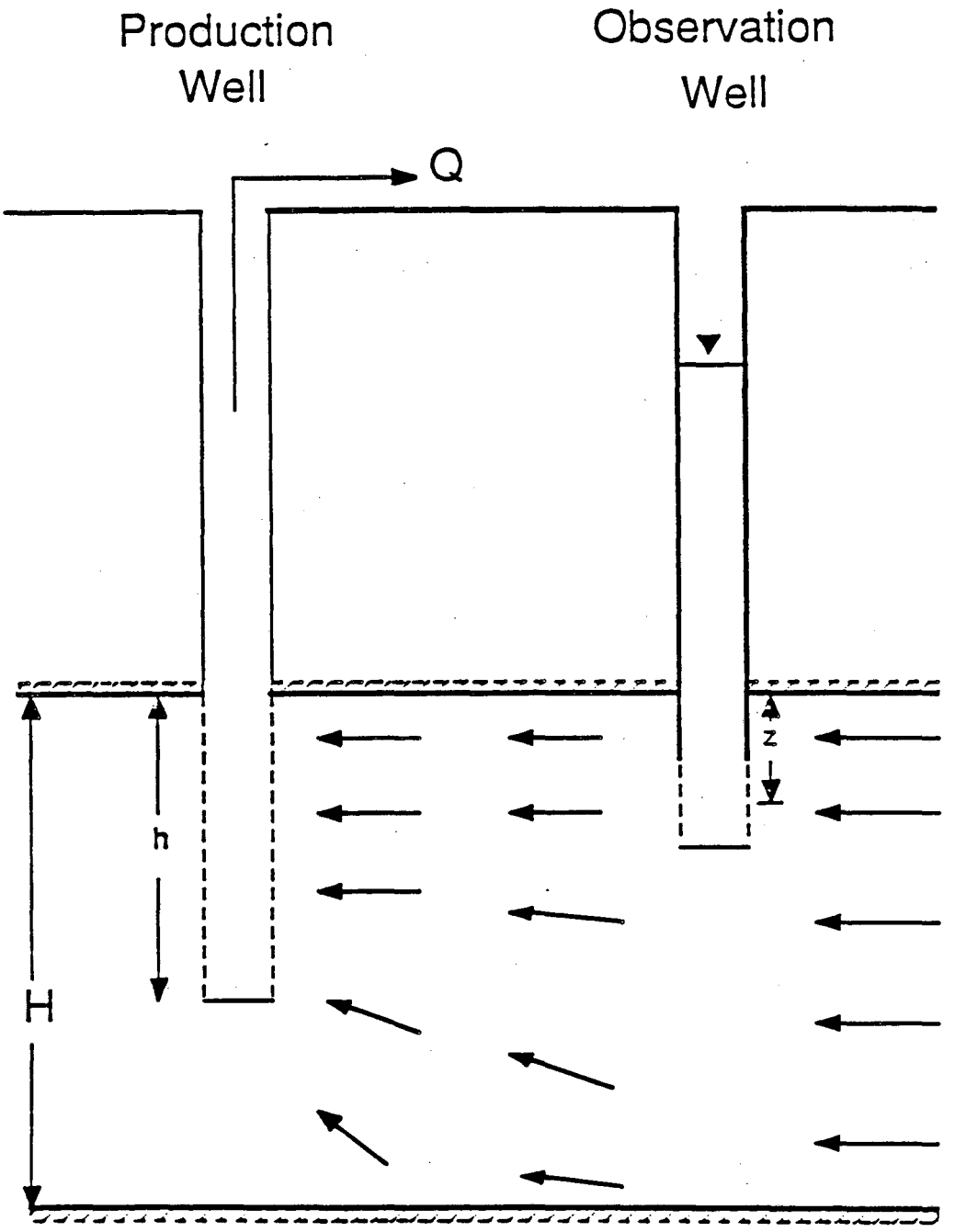


Figure 3.6 Schematic diagram of an aquifer with partially penetrating wells showing the definitions of Z and h.

$$u = \frac{r^2 S \mu}{4 k_r \rho g H t} \tag{3.30}$$

k_r is the radial component of permeability and k_z is the vertical component of permeability to account for the possibility of anisotropic conditions.

The effects of partial penetration can be ignored if the distance from the production well to the observation well r is

$$r \geq 1.5H\sqrt{\frac{k_r}{k_z}} \tag{3.31}$$

Beyond this distance, the flow was determined to be essentially radial and, therefore, the well could be assumed to be fully penetrating (Witherspoon et al., 1967). The solution for an ideal aquifer, Eq. 3.19, can then be used to solve any problems.

The theoretical pressure response of an aquifer with partially penetrating wells, once production begins, can be plotted as log P_D versus t_D for different values of h/H, r/H and Z/H. Figure 3.7 shows the case of h/H = 0.1, Z/H = 0.0 and 0.5, and values of r/H ranging from 0.05 to 1.0. It can be seen from Figure 3.7 that as the distance from the production well to the observation well increases, the curves reduce to the Theis curve.

3.2.4 Layered Aquifer

In nature, it is common to find geological formations that are vertically heterogeneous due to stratification upon deposition. All natural formations are heterogeneous to some degree or another and it is common to find layers of sand interbedded with silts and clays (Streltsova, 1988). Once production begins in a well, the water in the different layers of a stratified formation will respond to the pressure change at different rates depending on the hydrologic properties of each layer. This differential pressure depletion causes the water in the aquifer to flow in a non-radial fashion towards the production well.

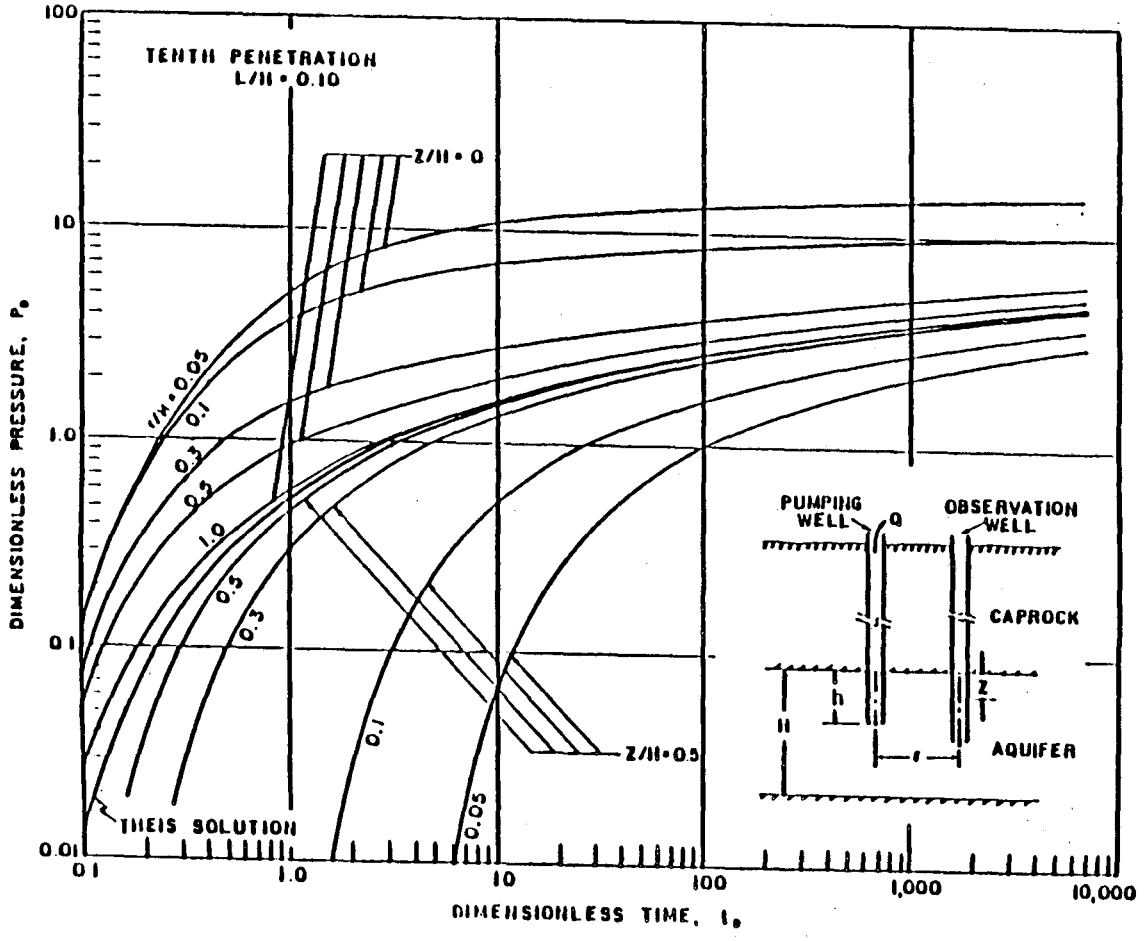


Figure 3.7 Theoretical log-log type-curve for an aquifer with partially penetrating wells (Hantush, 1957).

Many of the studies of stratified aquifers involve permeability contrasts between layers of two or more orders of magnitude. For these cases, the aquifer system is similar to that of a leaky aquifer system as described earlier in this report. However, as the permeability contrast between layers decreases, a layered aquifer starts behaving more and more like a uniform single-layered aquifer. Russel and Prats (1962) concluded that in a layered aquifer with a fully penetrating well, the pressure behavior acts the same as a homogeneous, single-layered aquifer with the same dimensions and an arithmetic total permeability-thickness $(kH)_t$ product equal to the layered system.

$$(kH)_t = \sum_{j=1}^{J} (kH)_j \qquad j = 1,2,3,...,J \qquad (3.32)$$

where J is the total number of layers in the system.

4.0 FIELD PROCEDURES

All of the work for this report was conducted at the LBLI/HO Site which is located at the intersections of Ponds 5, 6, 7, and 8 (see Figure 4.1). The aquifer system at this site consists of a layered aquifer of interbedded sands, silts, and clays bounded on the top by a leaky aquitard. The storage and evaporation ponds overlying the aquifer system were full of agricultural drainage water at the time pumping tests were conducted, creating a constant potential boundary.

In the last chapter, the individual characteristics of leakage, partial penetration, and layering in an otherwise ideal aquifer were discussed. The pressure responses, due to pumping, in aquifers with these characteristics were described. In this chapter, the pumping tests used in obtaining pressure data from the aquifer system at the LBLI/HO Site will be discussed and the pressure responses from each of the pump tests will be described.

Twelve wells were drilled at the LBLI/HO Site for the purpose of conducting pumping tests (see Figure 4.2). The boreholes were drilled with a rotary drilling rig using polymer mud to carry drill cuttings to the surface and to maintain borehole stability during drilling. Wells were completed using 10.2 cm (4 in) diameter casings and were screened and gravel packed over the bottom 6.1 m (20 ft) interval of each. A 6.1 m (20 ft) bentonite pellet seal was placed above the gravel pack. Nine of the wells, I1-I9, were each drilled to a depth of 12.2 m (40 ft). Wells HO60, HO80, and HO100 were drilled respectively to 18.3 m (60 ft), 24.4 m (80 ft), and 30.5 m (100 ft) (see Figure 4.3).

Four different types of pumping tests were conducted at the LBLI/HO Site, single-well steady-state tests, single-well transient tests, multiple-well transient interference and pulse tests. Pump tests provide *in situ* measurements of the hydrologic parameters of an aquifer, information on the hydraulic conductivity, storativity,

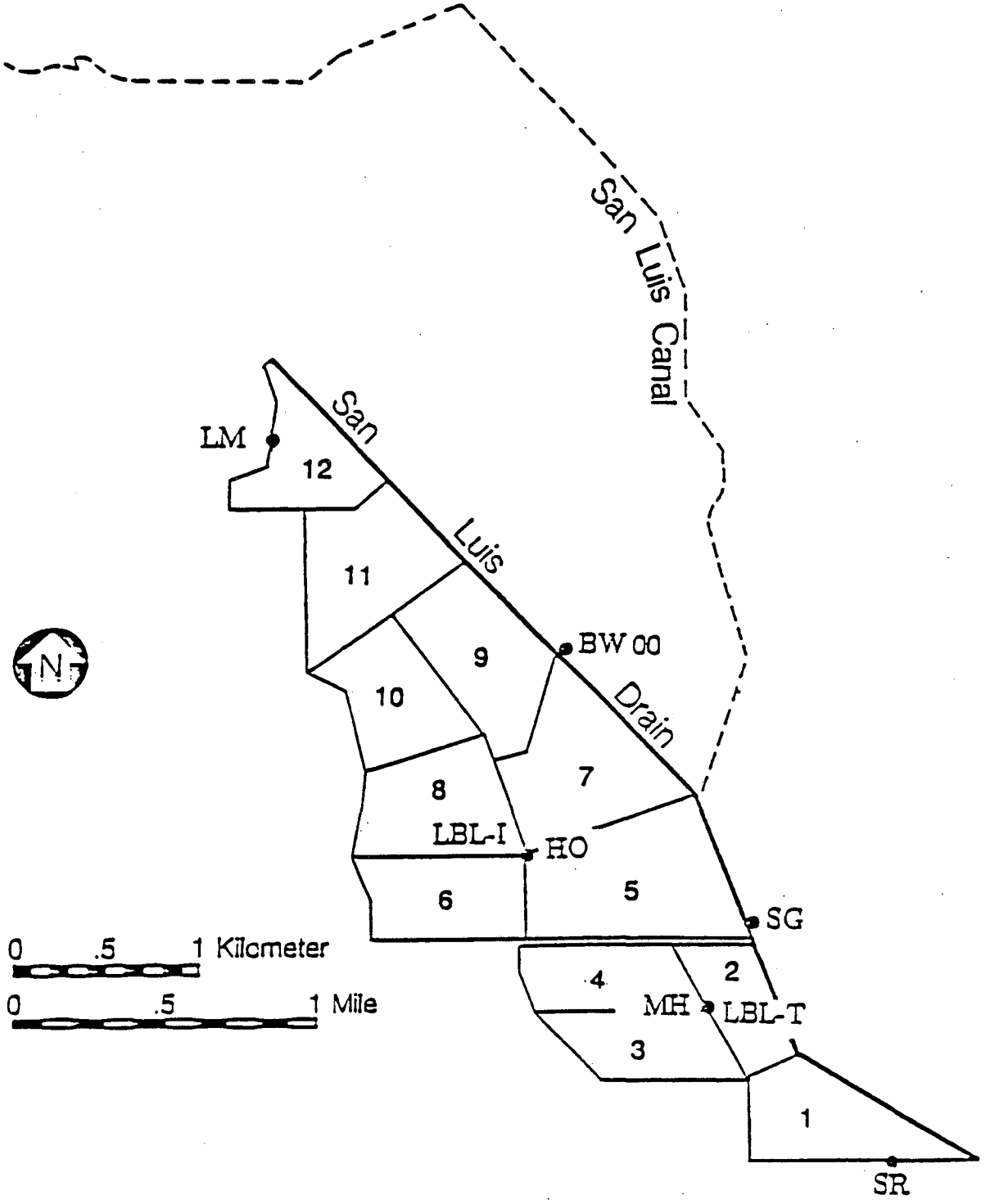


Figure 4.1 Location map showing the LBL hydrologic tests sites.

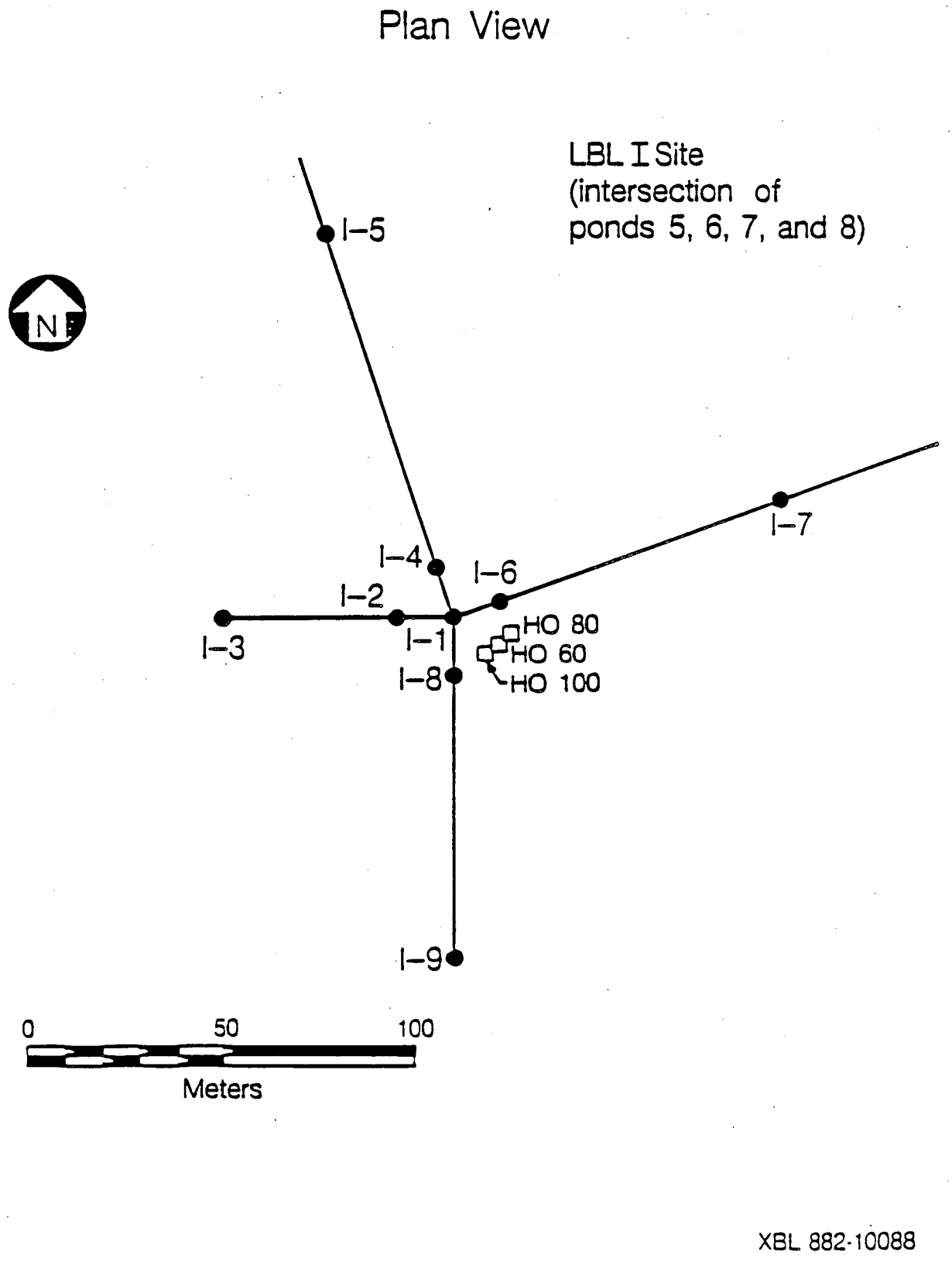


Figure 4.2 Plan view of the LBLI/HO Site and the 12 wells used for pump tests.

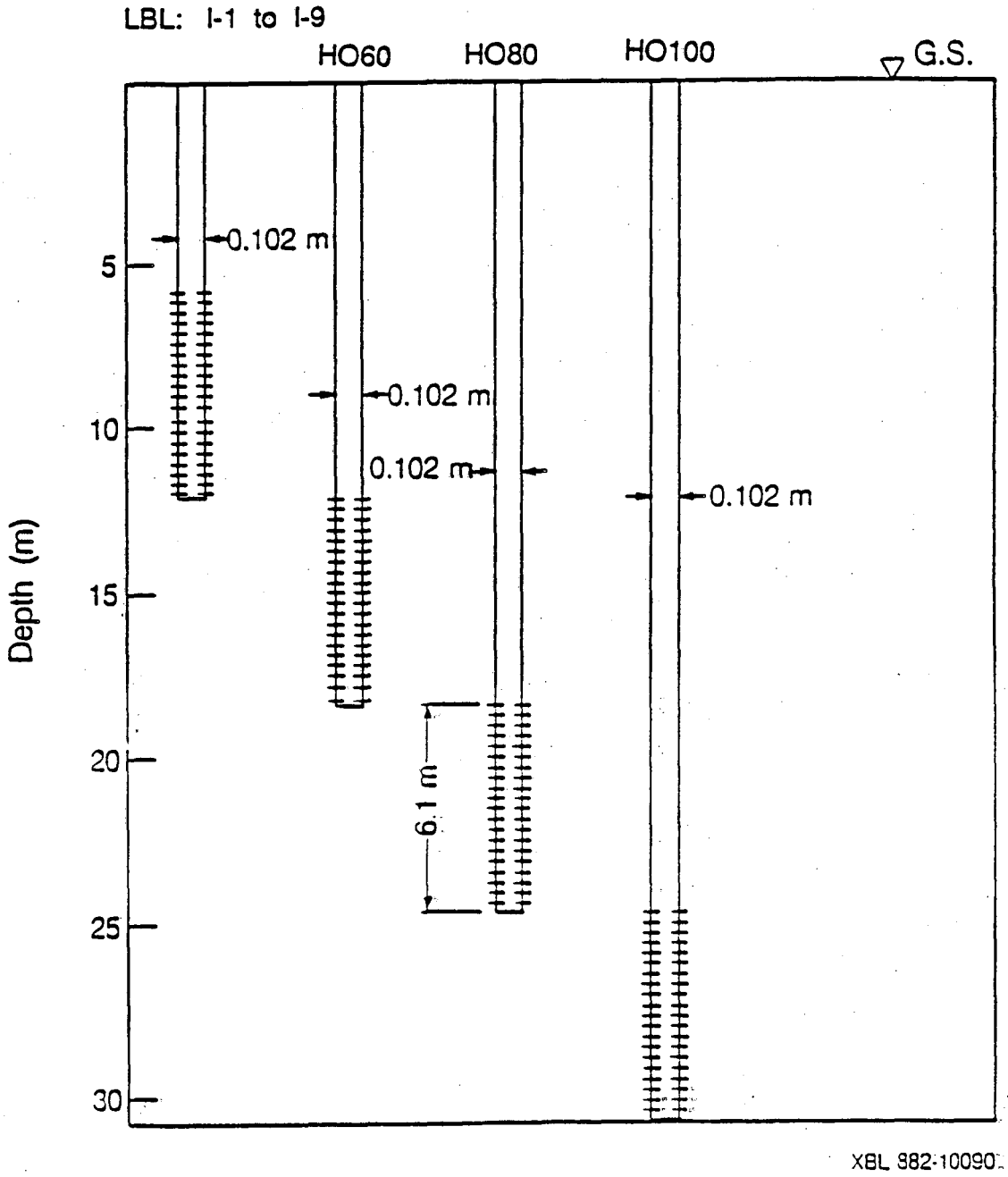


Figure 4.3 Schematic cross-sectional view of the 12 wells at the LBLI/HO Site used for pump tests.

and variability of the medium. Single-well steady-state tests were the first to be conducted and were performed in all 12 wells. After the single-well steady-state tests were completed, the wells were then instrumentated for the pressure transient tests. The single-well transient test data were collected simultaneously as the interference transient test data by measuring the pressure response in a producing well (I1, HO60, or HO80) at the same time as measuring pressure responses in the observation wells (I2-I9). The pressure transient pulse tests were conducted by producing I1, HO60, or HO80 and measuring the pressure responses in first the four inner region observation wells (I2, I4, I6, and I8) and then the four outer region observation wells (I3, I5, I7, and I9).

4.1 SINGLE-WELL STEADY-STATE TESTS

The single-well steady-state pump tests conducted at the LBLI/HO Site were performed in order to determine the specific capacity of each borehole. Specific capacity is defined as discharge per unit drawdown. The specific capacity gives a first approximation of the aquifer's permeability which can then be used to design additional tests.

The tests were conducted by lowering a 5.1 cm (2 in) diameter suction line, connected to a centrifugal pump at the surface, to the bottom of a well. The well was then pumped at a constant rate, while the hydraulic head drawdown was measured with respect to time, until steady-state conditions were reached. The criterion for determining steady-state conditions, in this case, was when drawdown in the well became negligible. Drawdown was measured by lowering a conductivity water-level detector down into the observation wells. As the water-level detector comes into contact with the water, an electrical circuit is completed and a signal is sent to the surface. The distance down to the detector is measured and is equivalent to the hydraulic head drawdown plus the distance down to the initial water level. The hydraulic head drawdowns measured for the single-well tests ranged from 0.5-6.4 m

(1.7-21 ft).

The pumping rate was measured using both a Doppler meter and a bucket and stop-watch method. The error in pumping rate accuracy was determined to be ±15%. The water-level detector was determined to be accurate to within 2.5 cm. These tests usually took about 30 minutes to complete.

4.2 SINGLE-WELL AND MULTIPLE-WELL TRANSIENT TESTS

4.2.1 Instrumentation

A computerized data acquisition system was used at the LBLI/HO Site to collect and process data from the single-well and multiple-well pressure transient pump tests. The instrumentation involved in the computerized system included pressure transducers, packers, pump, flow meter, and computer hardware and software.

Pressure Transducers

In order to determine the hydrologic parameters of an aquifer from single-well and multiple-well transient tests, changes in hydraulic head $\Delta\phi$ or changes in pressure ΔP with respect to time need to be measured accurately. For the transient pumping tests at the LBLI/HO Site, ΔP was measured using high resolution Paroscientific Digiquartz pressure transducers. The pressure transducers were placed approximately 3.05 m (10 ft) below the potentiometric surface (the static water level) in the wells (see Figure 4.4). They operate by using quartz crystals, which oscillate at different frequencies depending upon the pressure, to measure the changing pressure. The transducers convert the pressure into a digital signal and send it to the recorder. Transducers with three different pressure ranges, 0.3, 2.8, and 6.2 MPa (45, 400, and 900 psi), were used to measure the transient pressure changes with resolutions of 6.9, 34.5, and 69.0 Pa (0.001, 0.005, and 0.01 psi) respectively. A change in pressure of 1000 Pa (0.15 psi) corresponds to a change of water level in a well of approximately 10 cm (3.9 in). For the duration of the transient tests, barometric pressure changes were

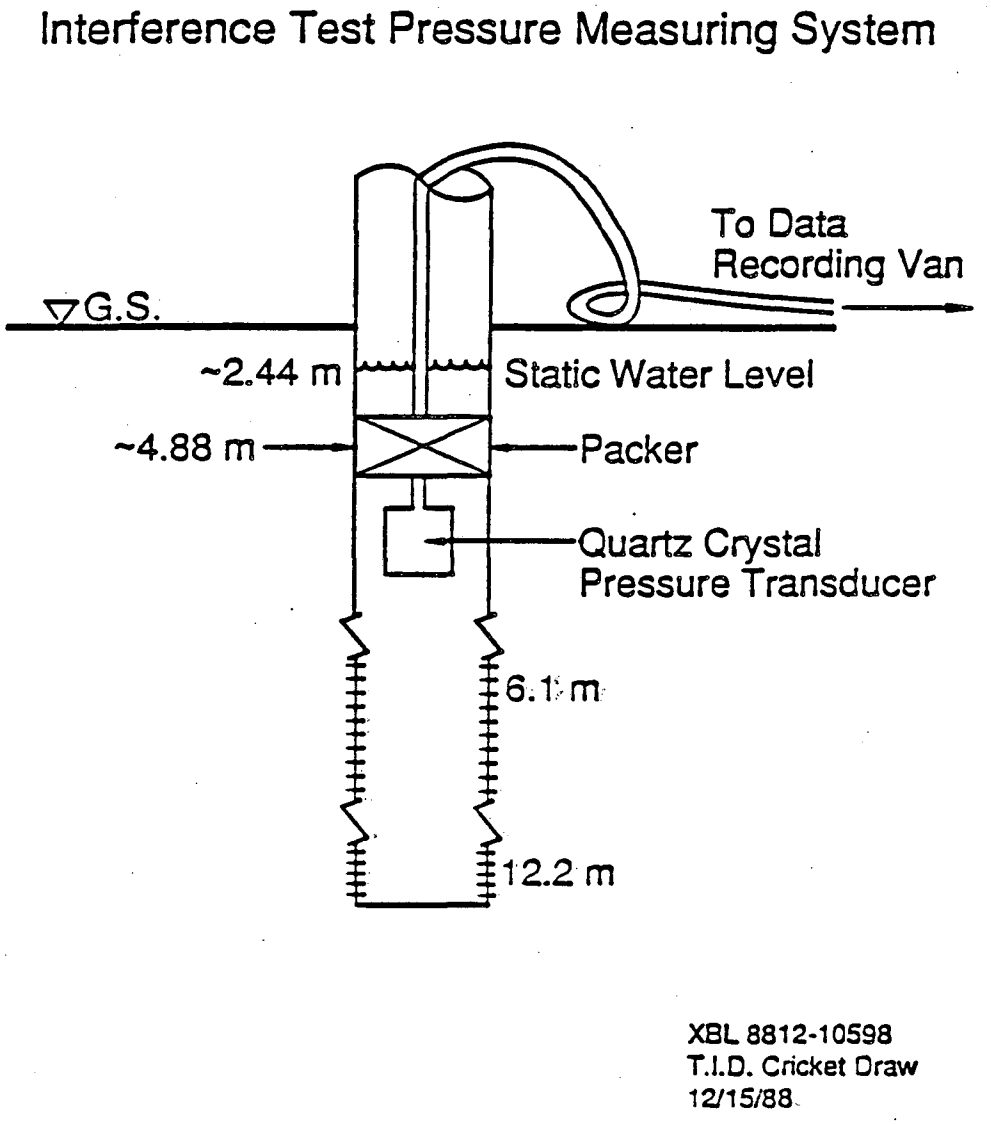


Figure 4.4 Schematic diagram showing the placement of a transducer and inflatable packer in an observation well.

measured using a transducer with a pressure range of 0.1 MPa (14.5 psi).

Packers

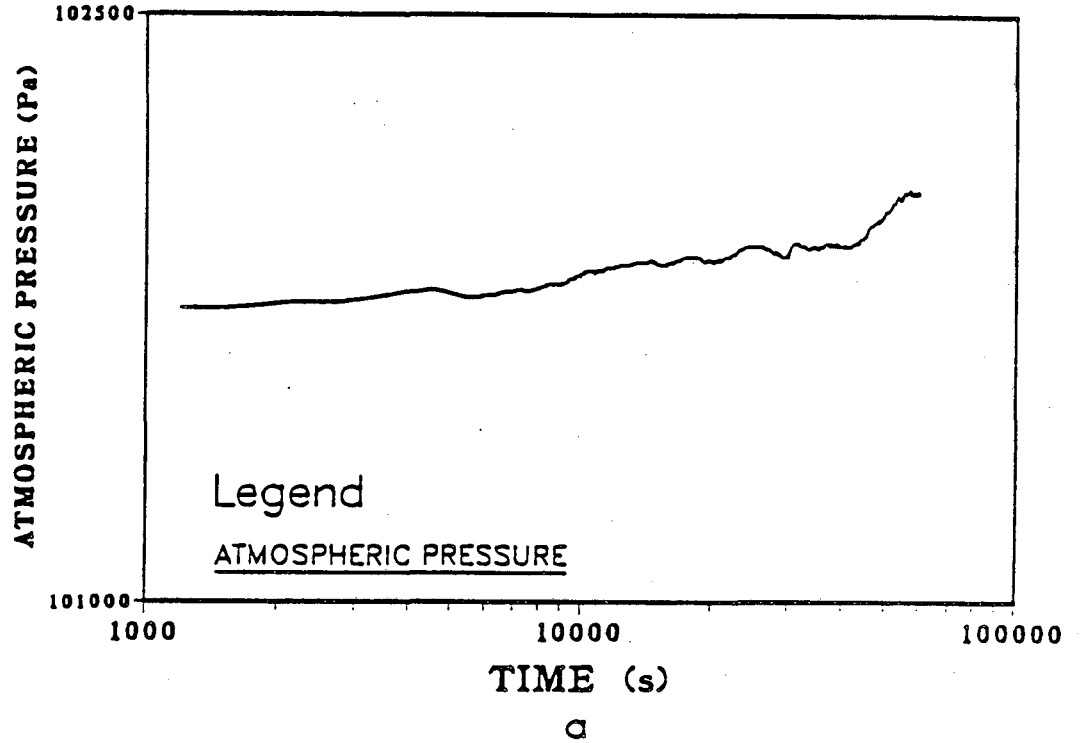
Inflatable packers were installed above the pressure transducers in the observation wells in order to minimize the effects of wellbore storage and to isolate the wells from barometric pressure changes. Wellbore storage effects, however, were found to be negligible. Packers were not installed in the production wells.

Barometric pressure changes do not effect pressure responses measured in wells which are completed in an unconfined aquifer because the water table and the water-level in the wells both respond to the barometric pressure changes with very little time lag. However, in a confined aquifer, barometric pressure changes can produce sizable pressure changes in the wells depending on barometric efficiency. Barometric efficiency is defined as the ratio of the hydrologic pressure change in a well due to a barometric pressure change over the barometric pressure change. The barometric efficiency value usually ranges from 20% to 75% (Todd, 1959).

By placing packers above the pressure transducers in the wells at the LBLI/HO Site, the effect of barometric pressure changes on the water-level in the wells was eliminated. Unfortunately, barometric pressure changes were noticed in the pressure response data of the pressure transient tests indicating that the aquifer was only semi-confined and was being affected by barometric pressure changes and, therefore, installing packers in the wells was unnecessary. In order to correct for the barometric pressure changes effecting the aquifer, but not effecting the water-levels in the wells, the actual pressure response due to pumping P_{gage} can be calculated by:

$$P_{gage} = P_{abs} - P_{atm} \tag{4.1}$$

where P_{abs} is the measured pressure response with the packers installed and P_{atm} is the barometric or atmospheric pressure. Figure 4.5 shows the results of subtracting the barometric pressure changes P_{atm} measured for Interference Test 2 from the measured pressure response P_{abs} from Observation Well I9 yielding P_{gage}.



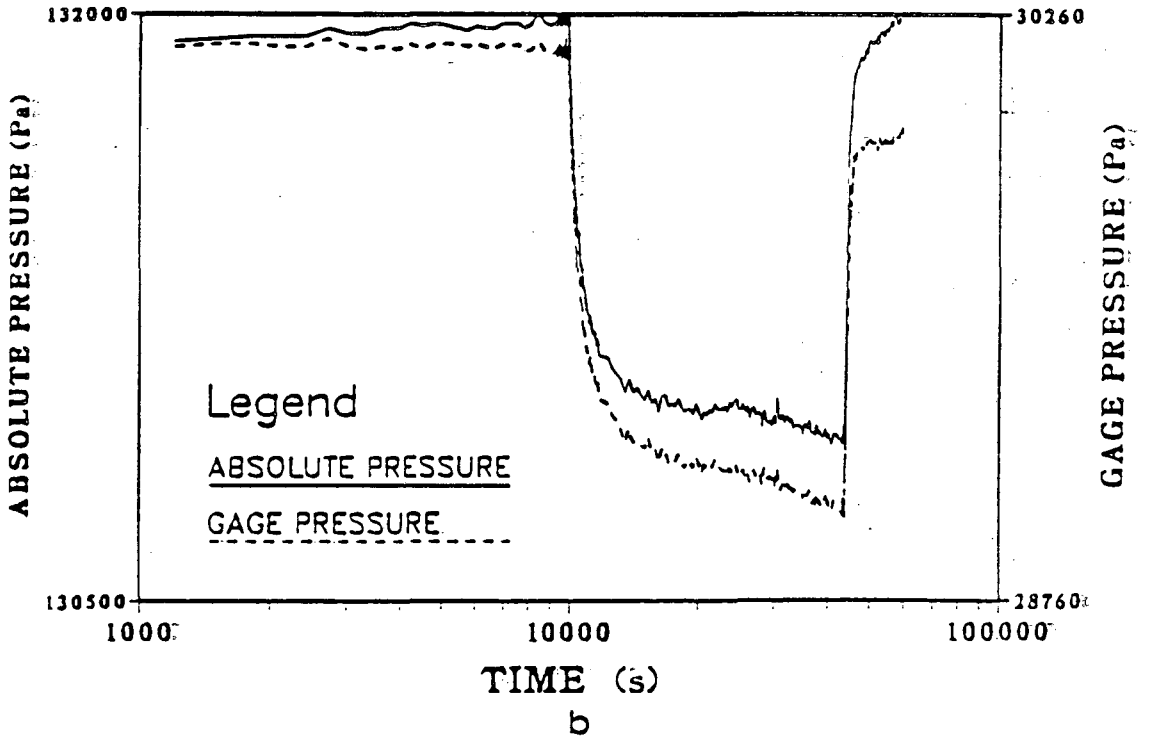


Figure 4.5 Pressure vs. time plots recorded during Interference Test 2 showing a) the atmospheric pressure measured and b) the pressure response recorded at Observation Well I9 before and after P_{atm} was subtracted.

Pump

The pump used for the transient single-well and multiple-well tests is a 3.73 kW (5 hp) downhole submersible pump. It has a 6.3 L/s (100 gpm) capacity and was positioned in the production wells approximately 9.1 m (30 ft) below the ground surface.

Flow Meter

The water pumped from the production wells was carried up the wellbore and through a manifold before being discharged to an area away from the production well. Two total-flow turbine meters were installed in the manifold in order to measure and double-check the flow. The meters agreed with each other to within 2% (LBL, 1986).

Computer System

The transient pressure response data of the pump tests were collected and processed by a computer-based system (Benson, 1986). The system is housed in a delivery-type van (see Figure 4.6) which can be moved easily to different field sites. In its current configuration, the computer system can make up to 10 pressure readings per second and is equipped for 20 different pressure transducer input signals.

The pressure transducers, installed in each observation well, send a digital signal by way of a connector panel to a Hewlett Packard (HP) Model 3497A Data Acquisition and Control Unit which is used to multiplex the signal to a HP Model 5334A 100 MHz Universal frequency counter. The Data Acquisition and Control Unit also provides a real-time clock and synchronizes the frequency counter with the HP 9000 Series 200 Modular Computer.

The computer code is written in Basic 3.0 and is used primarily for data acquisition such as recording, displaying, storing, and printing the measured data. The program can be interrupted at any time to perform other functions such as graphing and printing previously stored data. The actual pressure response in the observation wells can be displayed on the terminal screen as it is being collected.

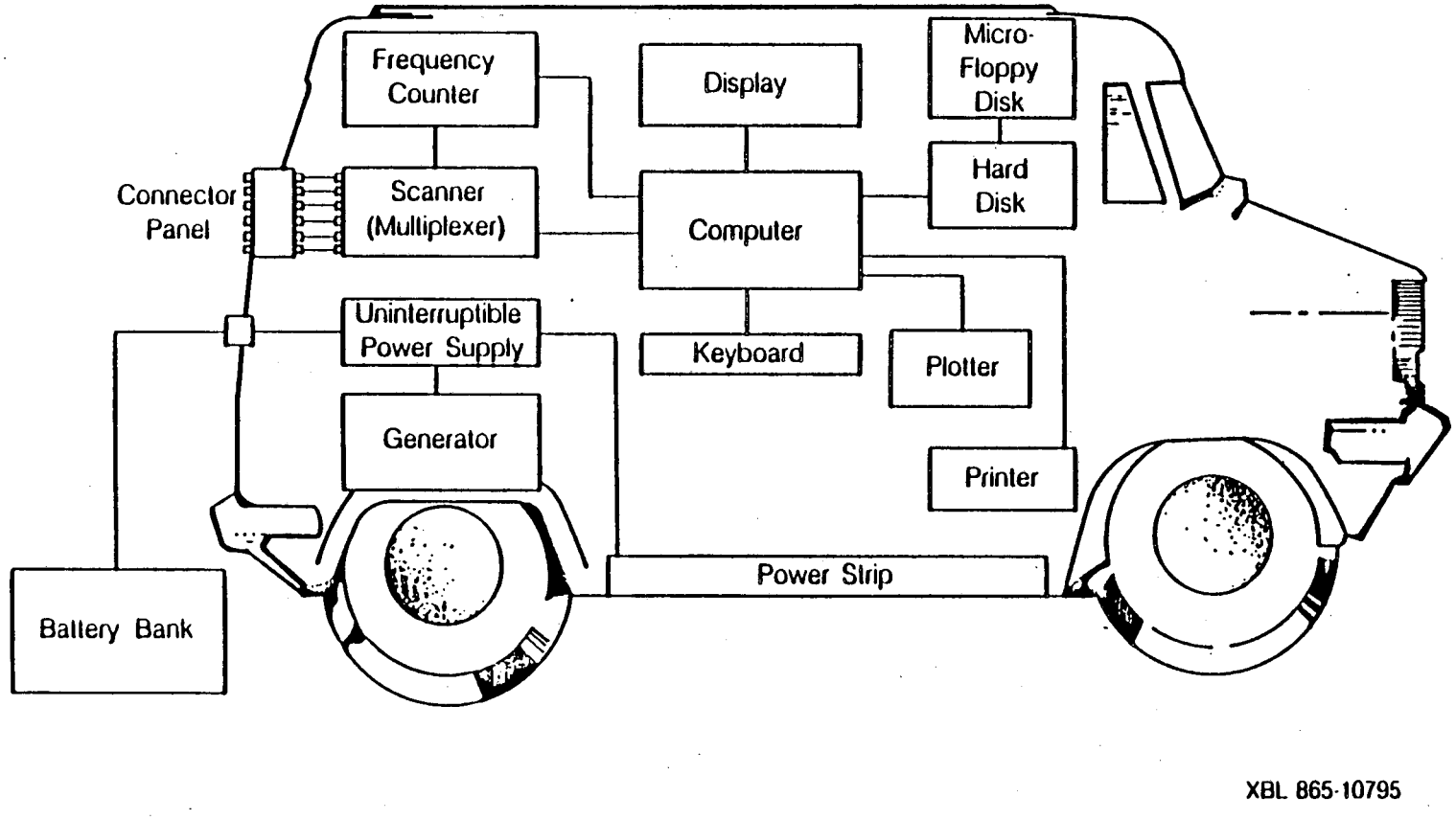


Figure 4.6 Schematic diagram showing the data aquisition computer system housed in a delivery-type van.

4.2.2 Single–Well and Interference Transient Test Procedure

Single-well transient tests involve measuring the pressure response in the same well which is being produced, whereas, interference transient tests involve pumping one well and measuring the pressure response in one or more observation wells. The pressure responses are then analyzed to determine the hydrologic properties of the aquifer.

The single-well and interference transient tests were conducted simultaneously at the LBLI/HO Site. A total of three tests were conducted using I1, HO60, and HO80 consecutively as the production wells. Due to low-permeable sediments adjacent to the screened interval of Well HO100, HO100 was impossible to pump with the large-capacity pump used for the transient tests. Therefore, HO100 was not used for any of the pressure transient tests. Wells I2-I9, which are all screened from 6.1-12.2 (20-40 ft), were used as observation wells for the interference tests.

Pressure data were collected before each test to record the background pressure trend. Background pressure data were collected for approximately 17 hrs for Test 1 and for approximately 3 hrs for Tests 2 and 3 (see Table 4.1). The pump was then

Table 4.1. Single-well and interference transient tests conducted at Site LBLI/HO.

Test	Production Well	Screened Interval (m)	Observation Wells	Background Pre-Test Data (hrs)	Test Time (hrs)	Background Post-Test Data (hrs)	Flow Rate Q (m^3/s)	Date and Time of Pumping
1	I1	6.1-12.2	I2-I9	~17	5.13	~1	6.0×10^{-3}	2/13/86 13:11:00
2	HO60	12.2-18.3	I1-I9	~3	9.45	~4	5.0×10^{-3}	2/24/86 21:03:30
3	HO80	18.3-24.4	I2-I9	~3	12.48	~6	5.5×10^{-3}	2/25/86 18:40:00

turned on and the pressure response at each observation well was recorded. An example of how often data would have been collected for a typical test is as follows:

every 5 s for the first 100 s after pumping had began, every 10 s for the next 1000 s, and then every 600 s for the duration of the test. The production well was pumped for 5.13 hrs for Test 1, 9.45 hrs for Test 2, and 12.48 hrs for Test 3. After the production wells were shut-in, pressure build-up measurements were recorded for several hours.

The pressure response data from the three single-well transient tests conducted at the LBLI/HO Site are shown in Figure 4.7. Well I1 was produced at a rate of 6×10^{-3} m^3/s (95 gpm) and a maximum pressure change of approximately 25,000 Pa (3.62 psi) was recorded. This is equivalent to a water-level drawdown in the well of 2.55 m (8.37 ft). HO60 and HO80 were produced at rates of 5×10^{-3} m^3/s and 5.5×10^{-3} $m^{3/s}$ (79 gpm and 87 gpm) respectively. The maximum pressure changes recorded for these two wells (HO60 and HO80) were both approximately 50,000 Pa (7.25 psi) which is equivalent to about 5 m (16.4 ft) of water-level drawdown in the wells.

The pressure response curves from all three tests show a rapid initial drawdown similar to the pressure response of an ideal aquifer with a finite radius well, however, the curves level off after about six hours indicating that recharge is occurring such as for a leaky aquifer. The radius for each well as indicated in Figure 4.7 refers to the radius of the well casing.

The pressure responses from Observation Wells I2-I9 for Interference Tests 1, 2, and 3 are shown in Figures 4.8, 4.9, and 4.10 respectively. The pressure changes for Test 1 ranged from 813 Pa to 4350 Pa (0.1-0.6 psi) which corresponds to water-level drawdowns of 0.08 to 0.4 m (0.3-1.4 ft). The pressure changes for Test 2 ranged in value from 470 Pa to 3090 Pa (0.07-0.4 psi) which corresponds to drawdowns of 0.04m to 0.3 m (0.15-1.0 ft). Test 3 had the lowest pressure changes of 620 Pa to 1990 Pa (0.09-0.29 psi) which correspond to drawdowns of 0.06 m to 0.2 m (0.2-0.7 ft).

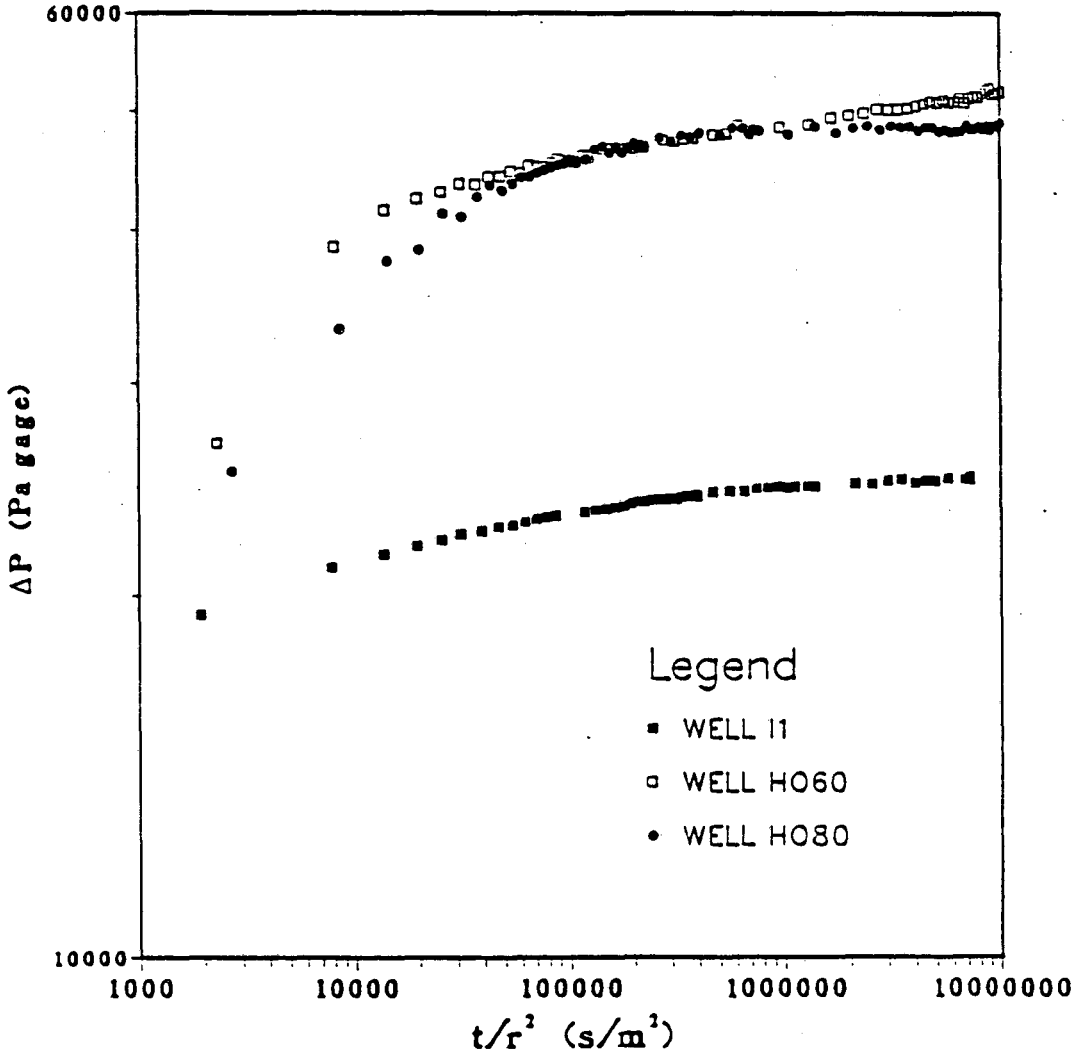


Figure 4.7 Single-well transient test pressure responses recorded at Production Wells I1, HO60, and HO80.

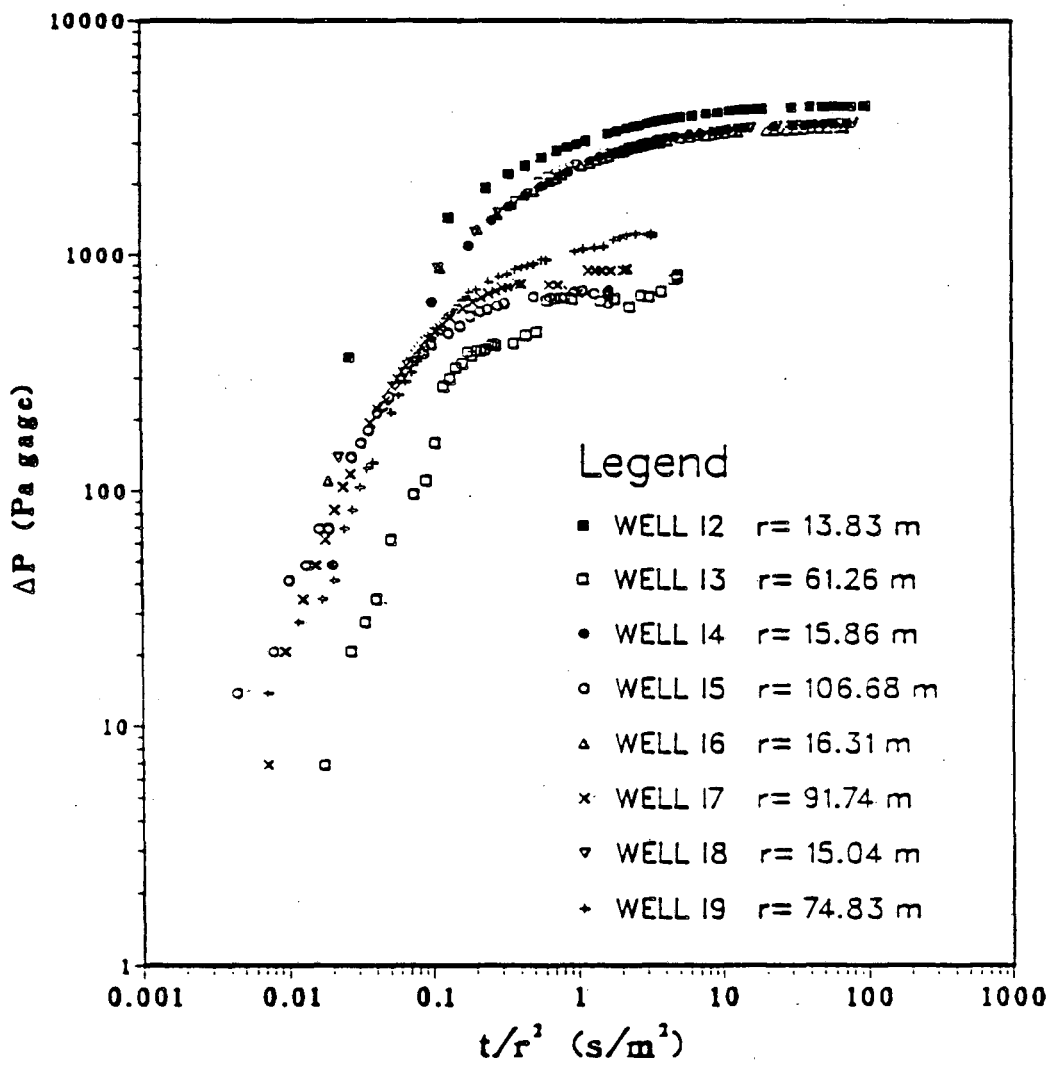


Figure 4.8 Interference test pressure response recorded at Observation Wells I2-I9 while pumping Production Well I1.

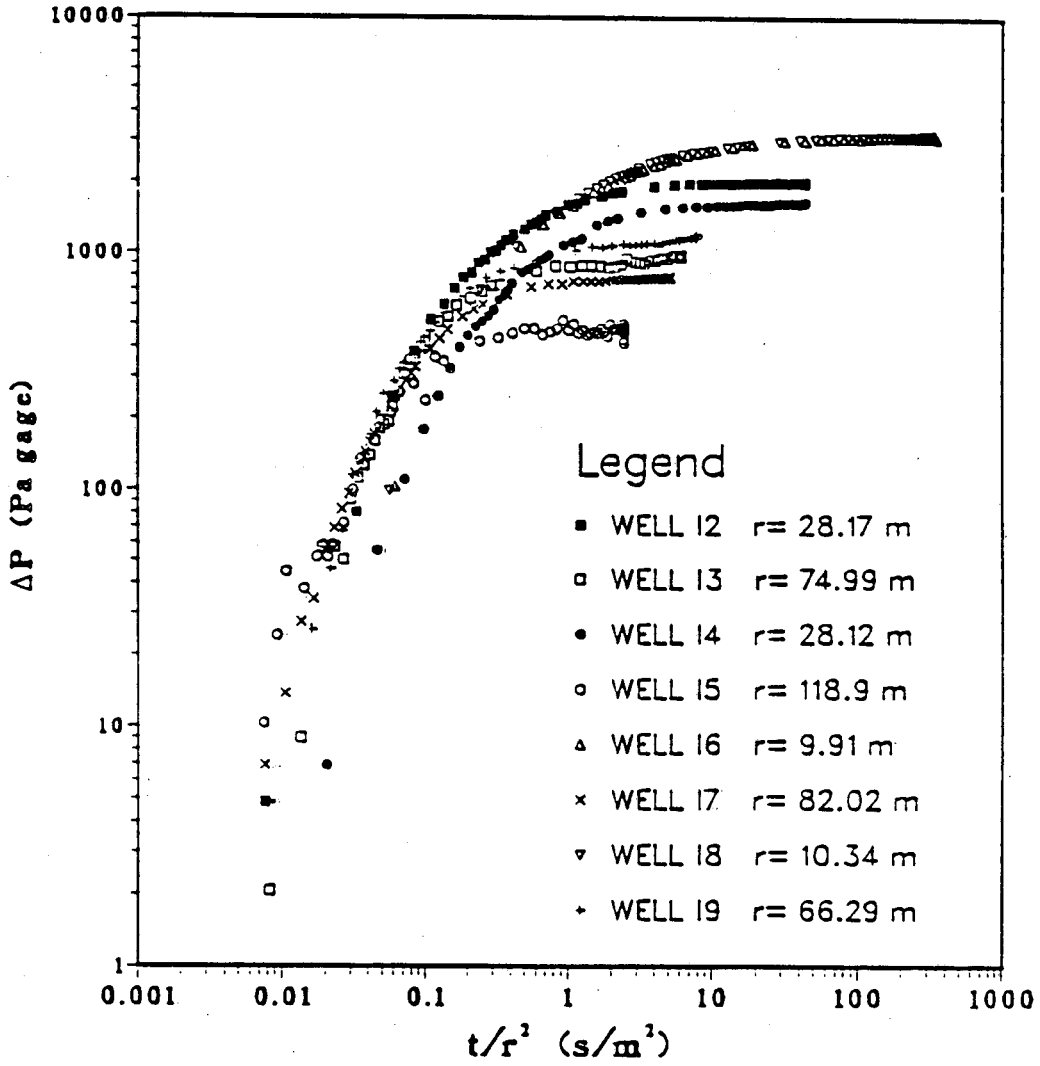


Figure 4.9 Interference test pressure response recorded at Observation Wells I2-I9 while pumping Production Well HO60.

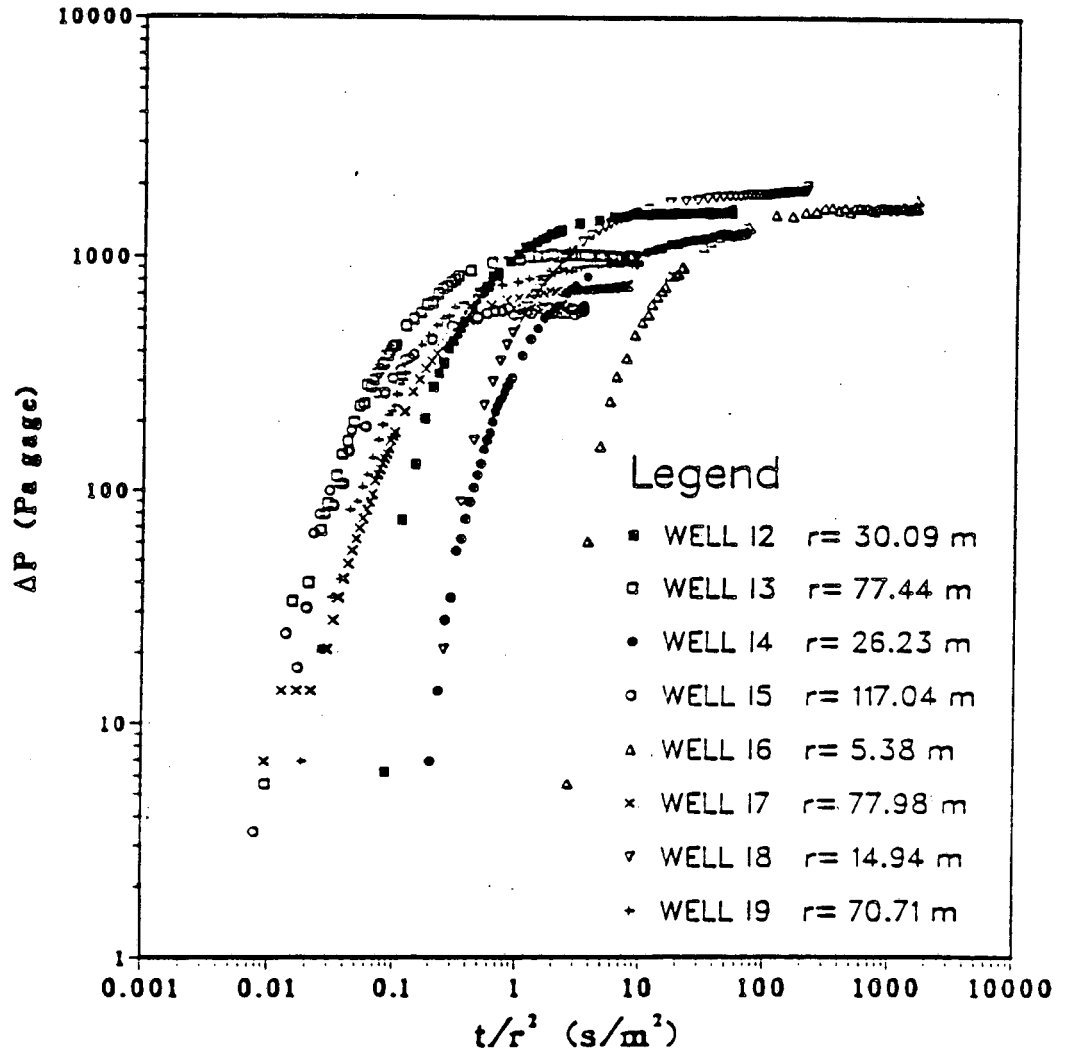


Figure 4.10 Interference test pressure response recorded at Observation Wells I2-I9 while pumping Production Well HO80.

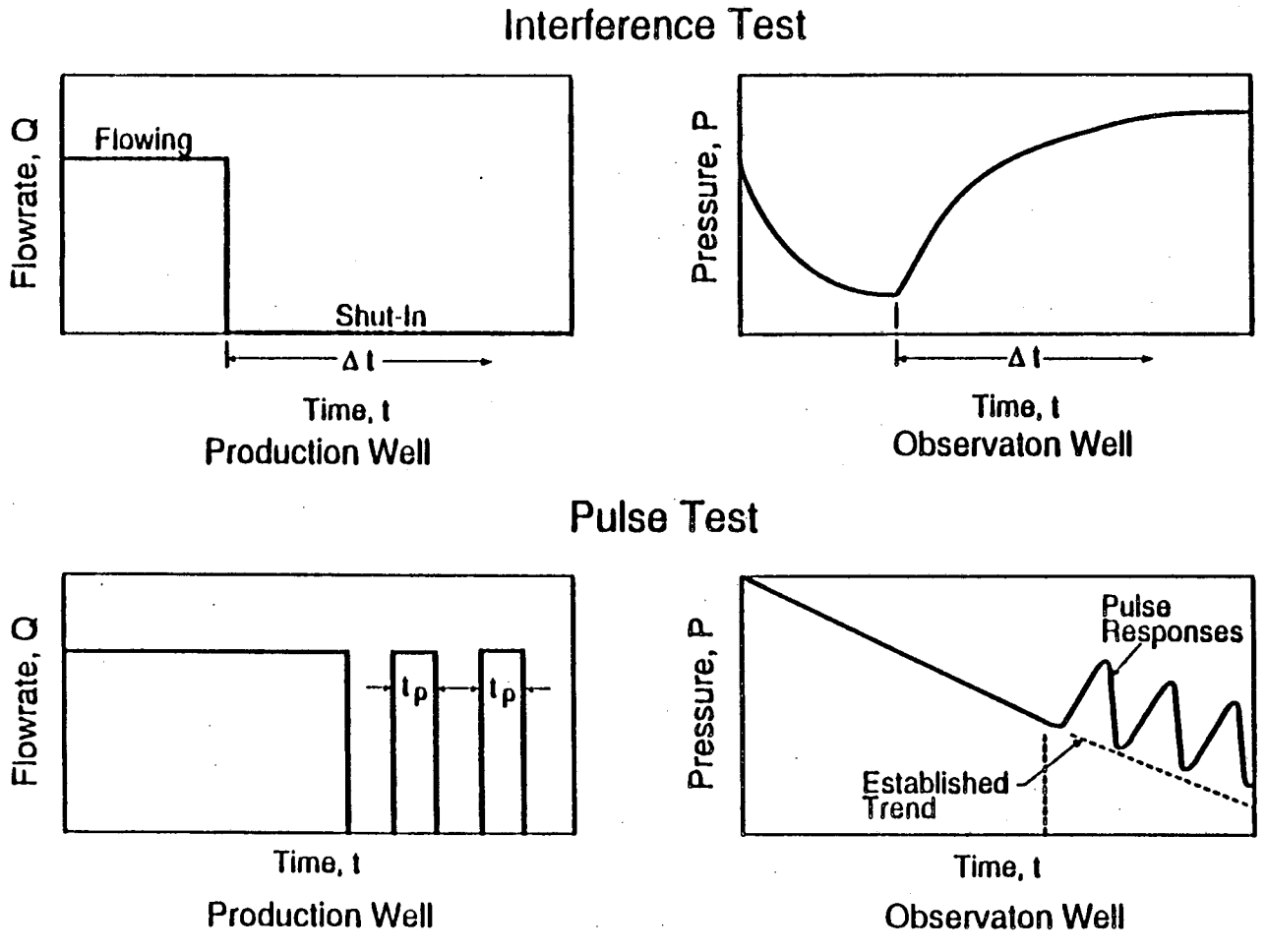
All the pressure responses follow the same pattern of an initial rapid drawdown and then gradually leveling off within approximately six hours. Because the curves are plotted ΔP versus t/r^2, the pressure responses from every observation well should collapse down to the same curve if the aquifer and aquitard were homogeneous and isotopic. The pressure responses from Tests 1 and 2 could possible fall on one leaky aquifer type-curve but the pressure responses of Test 3 could not.

4.2.3 Pulse Test Procedure

Pulse testing is another form of interference testing and was first described by Johnson, Greenkorn, and Woods (1966) and Brigham (1970). The major difference between pulse testing and interference testing is that the production well is pumped for very short periods, called pulses (see Figure 4.11). Some of the advantages of pulse testing over interference testings are 1) the testing time is much shorter, 2) because of the cyclic nature of the pulse periods, the pressure response at the observation well can be easily distinguished from background pressure trends, 3) if the frequency and amplitude of the pulses are constant, several pulses can be added together to filter out background noise, and 4) the permeability k and the specific storage S_s can be easily solved for without using type-curve matching techniques. The disadvantage is in trying to measure very small pressure responses. Highly sensitive pressure transducers are usually required.

When the pulse arrives at the observation well after a certain time lag t_{lag}, the pressure amplitude ΔP_{max} will be smaller than the original pulse produced at the production well. The pulse will also arrive at the observation well after a certain time lag t_{lag}. The amplitude and the time lag are the two variables that are obtained from the pressure response data in order to determine the hydrologic parameters of the aquifer.

Numerous pulse tests were conducted at the LBLI/HO Site, four tests were conducted while using I1 as the production well, two tests using HO60, and three tests



XBL 8812-10599
Adobe 88
12/15/88

Figure 4.11 Schematic diagram showing the major difference between interference and pulse testing.

using HO80 (see Table 4.2). With the exception of the tests using I1 as the production well, the pulse tests were performed within 2 hrs after the completion of the interference test for each production well. This was possible because of the cyclic nature of pulse tests, the pulses can easily be distinguished from the background pressure trend, making long hours of background data collecting unnecessary.

Table 4.2. Pulse tests conducted at Site LBLI/HO

Test	Production Well	Screened Interval (m)	Observation Wells	Number of Pulses	Length of Pulse (s)	Flow Rate Q (m^3/s)	Date and Time of Pumping
1-3	I1	6.1-12.2	I2,I4,I6,I8	8	15,30,60,120	6.0×10^{-3}	2/24/86 12:02:00
4	I1	6.1-12.2	I3,I5,I7,I9	2	120,300	6.0×10^{-3}	2/24/86 13:20:00
5	HO60	12.2-18.3	I2,I4,I6,I8	7	15,30,60	5.0×10^{-3}	2/25/86 11:56:00
6	HO60	12.2-18.3	I3,I5,I7,I9	1	300	5.0×10^{-3}	2/25/86 12:48:30
7a	HO80	18.3-24.4	I2,I4,I6,I8	1	60	5.5×10^{-3}	2/26/86 14:08:30
7b	HO80	18.3-24.4	I2,I4,I6,I8	3	60	5.2×10^{-3}	2/26/86 14:17:00
8	HO80	18.3-24.4	I3,I5,I7,I9	1	300	6.0×10^{-3}	2/26/86 16:10:30

Because the pulse tests are for such a short duration, pressure measurements were recorded every second instead of every five seconds or greater such as for an interference test. At this rate of measurement, the computerized data acquisition system was able to record the pressure responses from only four transducers instead of the nine used in interference testing. Therefore, only four observation wells at a time could be used for pulse testing.

A total of ten pulses, Tests 1-4, were generated at the I1 production well, eight pulse responses were recorded at the inner observation wells (I2, I4, I6, and I8) and two pulse responses were recorded at the outer observation wells (I3, I5, I7, and I9).

The time interval of the pulses generated at the production well ranged from 15-300 s. A total of eight pulses were generated from the HO60 production well with seven pulse responses measured at the inner wells (Test 5) and 1 pulse response measured at the outer wells (Test 6). Five pulses were generated at Production Well HO80. The inner observation wells were used to record the pressure response of the first four pulses, Tests 7a and 7b, and the outer observation wells were used to record the pressure response of the last pulse. Test 7 was broken up into two parts because Test 7b used a slightly lower pumping rate and, therefore, had to be analyzed separately.

A typical pressure drop for the inner region observation wells (I2, I4, I6, and I8) (see Figures 4.12 and 4.13) and for the outer region observation wells (I3, I5, I7, and I9) (see Figure 4.14) while pumping I1 was about 1500 Pa (0.2 psi) and 100 Pa (0.01 psi) respectively. Time lags measured ranged from 1-10 s for the inner region observation wells and from 36-162 s for the outer region wells. The first pulse response recorded at Observation Well I5 for Test 4 (see Figure 4.15) was very noisy and, therefore, was not used.

Pressure changes ranging from 137 Pa to 1185 Pa (0.02-0.17 psi) were recorded for the seven pulses generated at Production Well HO60 for Test 5. Time lags ranged from 2 to 24 s. The data from Observation Well I4 was determined to be inaccurate and were not used.

Pressure changes recorded at the outer region wells while pumping HO60 for Test 6 (see Figure 4.16) ranged from 200 Pa to 310 Pa (0.03-0.04 psi) with time lags ranging from 45 to 100 s. The data from Observation Well I5 was too noisy to determine an accurate time lag or pressure change and, therefore, was not used.

Pressure changes recorded at the inner region observation wells while pumping HO80 for Test 7 ranged from 27 Pa to 227 Pa (0.004-0.03 psi). Time lags ranged from 38 to 215 s. Pressure changes recorded at the outer region observation wells while pumping HO80 for Test 8 ranged from 69 Pa to 340 Pa (0.01 to 0.05 psi) and time lags ranged from 114 to 305 s.

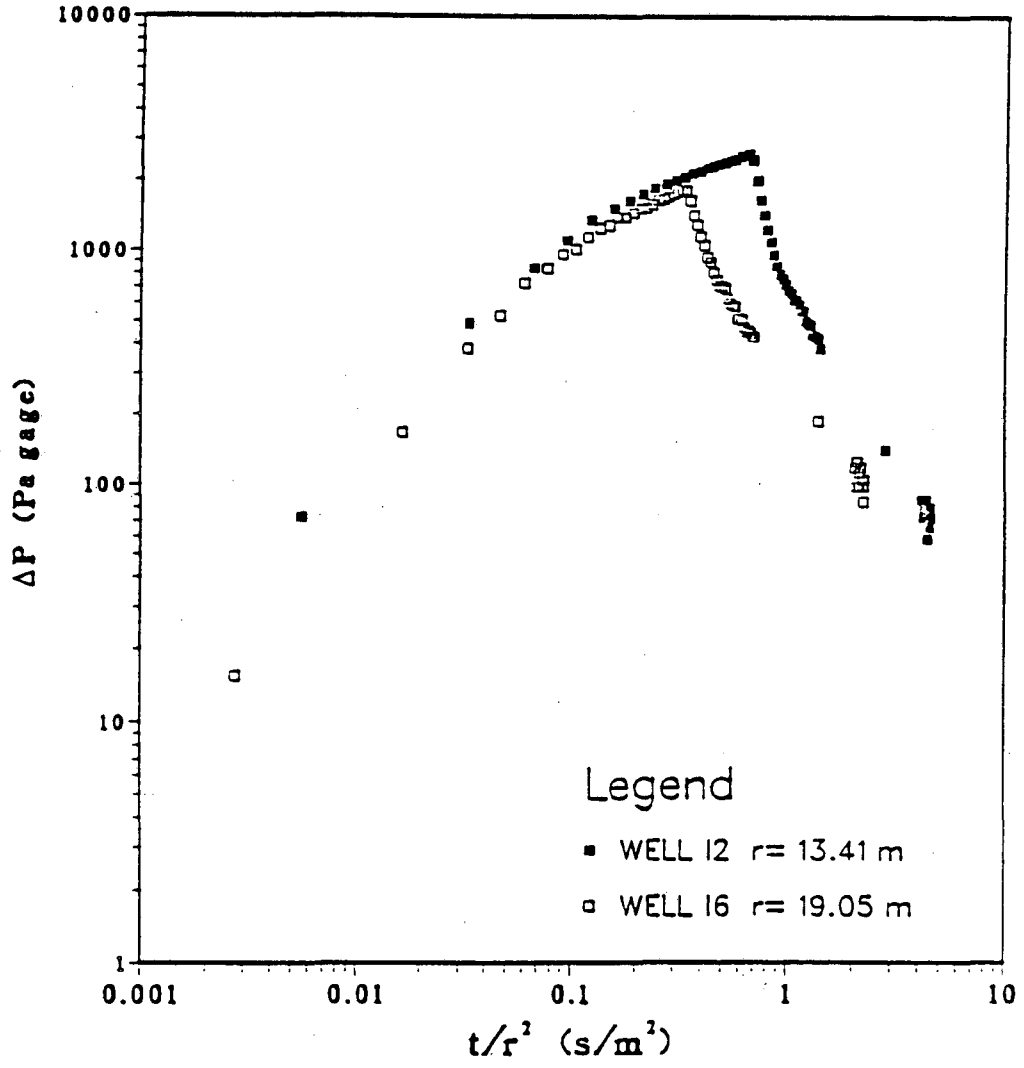


Figure 4.12 Pulse test pressure response recorded at Observation Wells I2 and I6 while pumping Production Well I1.

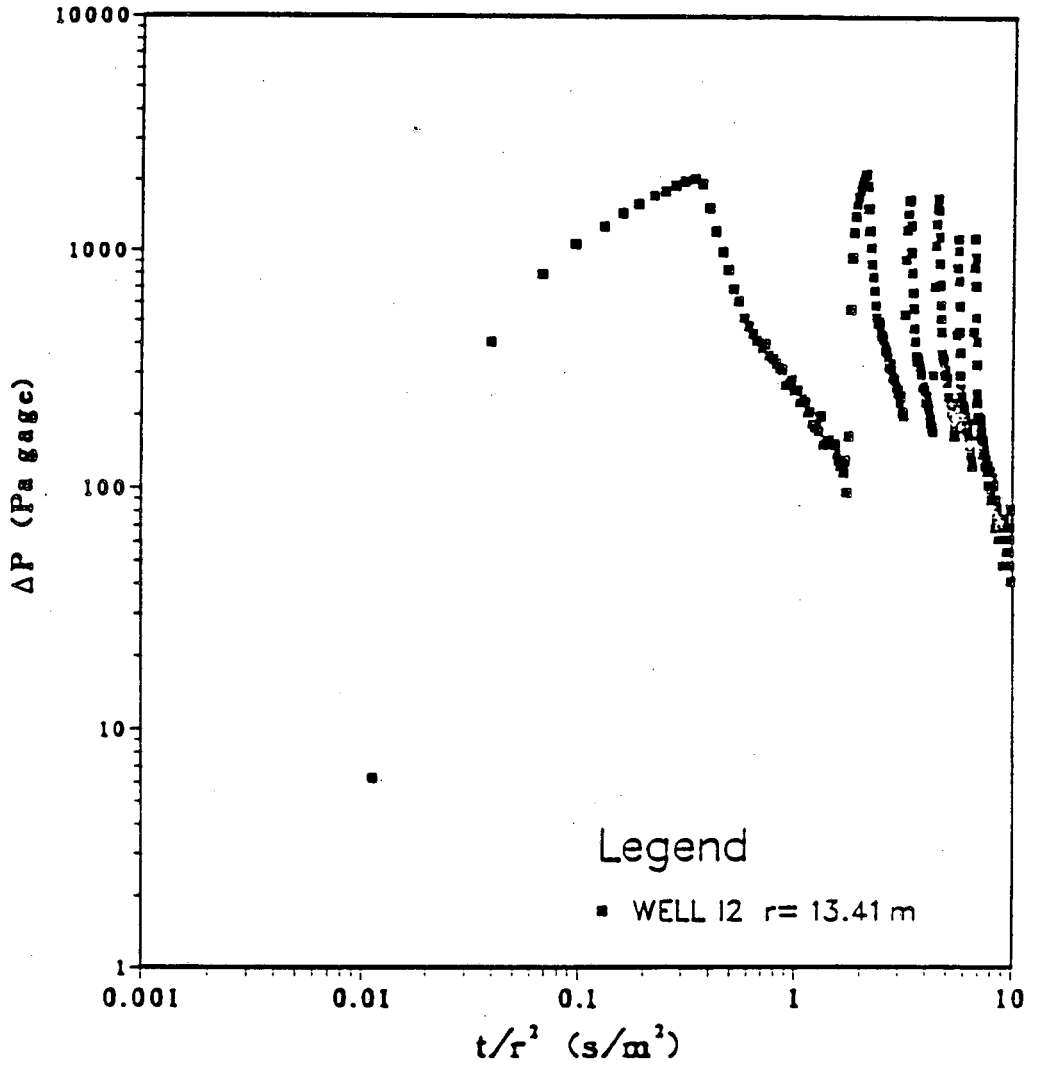


Figure 4.13 Pulse test pressure response recorded at Observation Well I2 while pumping Production Well I1.

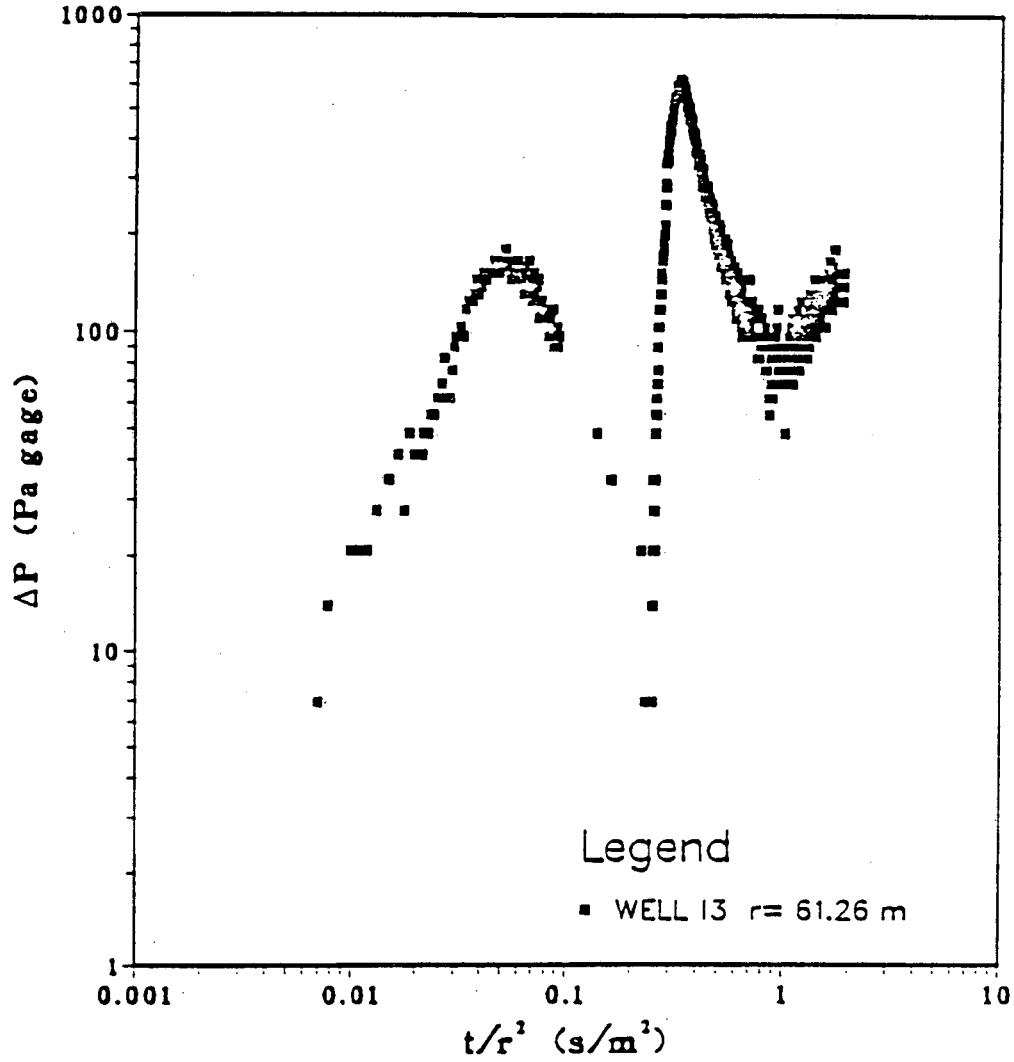


Figure 4.14 Pulse test pressure response recorded at Observation Well I3 while pumping Production Well I1.

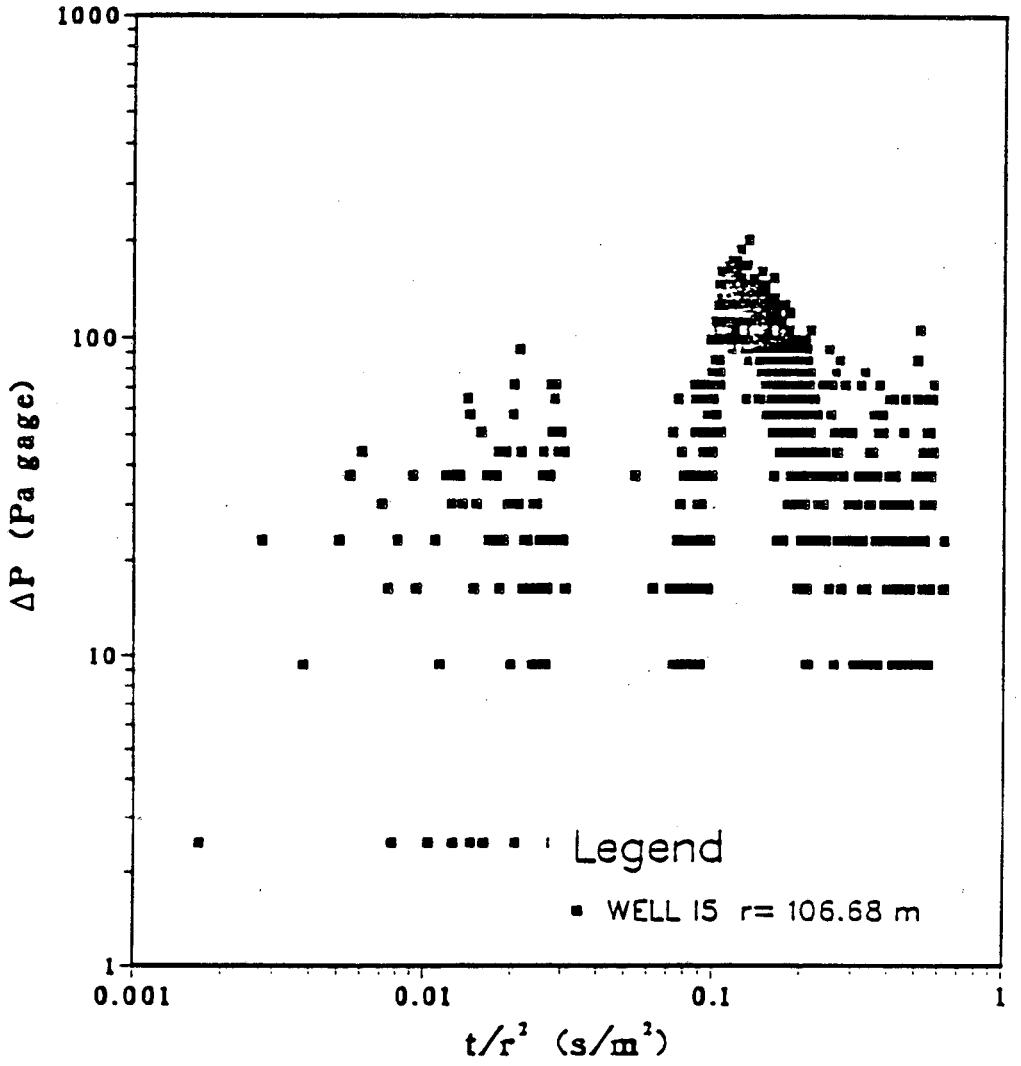


Figure 4.15 Pulse test pressure response recorded at Observation Well I5 while pumping Production Well I1.

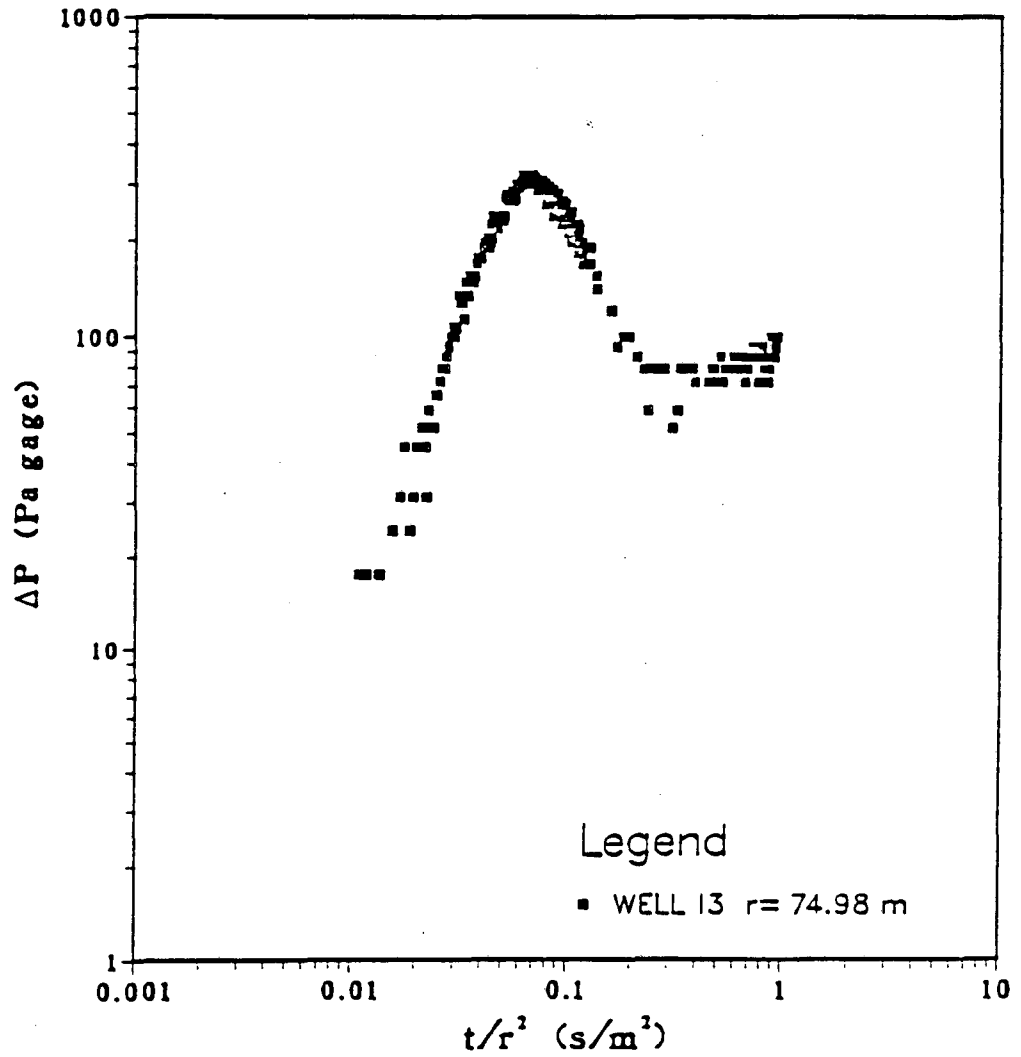


Figure 4.16 Pulse test pressure response recorded at Observation Well I3 while pumping Production Well HO60.

5.0 METHODS OF ANALYSIS

A mathematical model of a groundwater system consists of a set of differential equations which describe the flow of fluid through the system. The accuracy of the model depends on how closely the model represents the actual groundwater system. The actual system is usually far too complex to be simulated exactly, therefore, simplifying assumptions must be made.

Analytical methods are used widely for solving groundwater problems, although the simplifying assumptions used in analytical methods are usually too restrictive to describe most realistic situations accurately. An alternative to using analytical methods is to approximate the groundwater system using numerical techniques. Numerical methods were the primary method used in this report to determine the hydrologic properties of the aquifer system at the LBLI/HO Site at Kesterson Reservoir. However, it is uncommon to have as much pumping test information available about an aquifer system as was available for this report and, therefore, numerically simulating aquifer pumping tests is usually not done. Benson (1988) used numerical methods to evaluated single-well pressure transient tests and this report is thought to be one of the first to use numerical methods to simulate interference and pulse pressure transient pumping tests.

The aquifer system at the LBLI/HO Site consists of a complex system of layered sedimentary units bounded on the top by a leaky semi-confining layer and on the bottom by a relatively impermeable layer. Storage and evaporation ponds overlie the aquifer system creating a constant potential boundary. The wells that were drilled in order to conduct hydrologic pumping tests only partially penetrated the aquifer, making analysis of the pressure response data even more difficult. Numerical methods of analyzing the data were considered the more accurate method because of the complex nature of the system, but analytical methods were also used in order to make a comparison between the two methods and determine the uniqueness of the results. In this

study, the single-well steady-state tests were analyzed analytically, whereas, the pressure transient tests were analyzed both analytically and numerically.

5.1 NUMERICAL METHODS

Numerical methods were the primary method of evaluating the hydrologic properties of the aquifer system at the LBLI/HO Site because of the complex nature of the system and the amount of information available about the system. The basic problem consisted of modeling radial flow towards a partially penetrating production well in a layered and leaky aquifer. A constant potential boundary exists along the top of the aquifer system (due to the storage and evaporation ponds) and along the outer boundary (to simulate an aquifer of infinite areal extent). The lower boundary is assumed to be impermeable.

Numerical modeling involves dividing up the flow region into a convenient number of volume elements of finite size and then applying the integral form of the continuity equation to each volume element. Three different numerical methods are available: the Finite Difference Method, the Integrated Finite Difference Method, and the Finite Element Method. The difference between these methods is the manner in which the shape of the volume element is chosen and the method in which the hydraulic gradients are defined and evaluated.

5.1.1 Numerical Code

The numerical code PT (Pressure-Temperature) was used to simulated the transient pressure pumping tests that were conducted at the LBLI/HO Site. PT was developed by Bodvarsson (1982) for studies of geothermal fields under natural and exploitative conditions.

The numerical code is capable of solving one-, two-, and three-dimensional mass and/or energy transport problems and can also solve one-dimensional consolidation

problems using a theory developed by Terzaghi (1925). The code allows for pressure and/or temperature dependent rock and fluid properties. The numerical method used by PT is the Integrated Finite Difference Method (Edwards, 1972; Narasimhan and Witherspoon, 1976). The IFDM divides the groundwater flow region into a convenient number of arbitrarily shaped polyhedrons of finite size constructed by drawing perpendicular bisectors to lines connecting nodal points. The integral form of the governing groundwater equation is then applied to each of the volume elements. Each volume element can have its own hydrogeologic properties.

PT uses the basic governing equations for the conservation of mass and energy. In simulating the aquifer system at the LBLI/HO Site, only the mass balance equation was utilized. This was because the system is essential isothermal and, therefore, the energy balance equation was not used and will not be discussed in this report.

The mass balance equation expressed in differential form is the same as the complete continuity equation, Eq. 3.13 found in Chapter 3, and is stated again here.

$$\nabla\cdot\rho K\nabla\phi = m_c\frac{\partial\phi}{\partial t} - \rho g_w \tag{3.13}$$

This equation can also be expressed in the integral form by considering a single, finite, arbitrary volume element l with a surface area Γ. If Eq. 3.13 is multiplied on both sides by the bulk volume $V_{B,l}$ of the element l and if Γ is divided into a large number of surface segments with areas of $\Delta\Gamma$, then the rate of fluid flow across a surface segment m is

$$\vec{Q}_m = \vec{q}_m \Delta\Gamma_m \qquad m = 1,2,3,\ldots,M \tag{5.1}$$

where M is the total number of surface segments, $\vec{q}_m$ is the average Darcy's velocity in the direction perpendicular to the surface segment m, and $\Delta\Gamma_m$ is the area of the surface segment m. If the number of surface segments goes to infinity ($M \rightarrow \infty$) and $\vec{q}_m = -\vec{q}\cdot\vec{n}_m$, the continuity equation can then be written in integral form as

$$\int_\Gamma \rho K\vec{\nabla}\phi\cdot\vec{n}\, d\Gamma = M_{c,l}\frac{\partial\phi_l}{\partial t} - \rho G_{w,l} \tag{5.2}$$

$M_{c,l}$ is the fluid mass capacity of element l and $G_{w,l}$ is the volumetric rate of fluid generated from element l where

$$M_{c,l} = m_{c,l} V_{B,l} \qquad G_{w,l} = g_{w,l} V_{B,l} \tag{5.3}$$

In order to set up one mass balance equation for each volume element in the flow region, Eq. 5.2 needs to be discretized. The discretized numerical equation using the IFDM for an isotropic, homogeneous, three-dimensional flow region takes the form

$$\sum_i \frac{\rho K \Delta\Gamma_{l,i}}{D_{l,i}}(\phi_i - \phi_l) + \sum_b \frac{\rho K \Delta\Gamma_{l,b}}{D_{l,b}}(\phi_b - \phi_l) = M_{c,l}\frac{\Delta\phi}{\Delta t} - \rho G_{w,l} \tag{5.4}$$

where i and b denote all interior and boundary nodal points of the flow region communicating with node l. $D_{l,i}$ and $D_{l,b}$ are the distances from the nodal point l to the interface between the nodal points i and b respectively.

PT solves Eq. 5.4 for each node in the flow region and calculates the change in pressure ΔP at each node for a series of time steps. The pressure value assigned to the nodal point represents an average over the entire volume of the element. The inverse problem of obtaining the hydrologic parameters of the aquifer from known pressure changes can be achieved by matching the simulated pressure response curve.

5.1.2 Computation Grid

The flow region at the LBLI/HO Site was divided up into volume elements by a computational grid (see Figure 5.1) which was calculated using a logarithmic function to define the distance from the production well to the boundary of each node. The grid is radially centered around the production well and is finer in the vicinity of the observation wells in order to reduce any error in calculating the pressure due to averaging over the volume of the node.

The radial distance from the production well to the outer boundary is 3,048 m (10,000 ft). The outer boundary is kept at a constant potential in order to simulate an

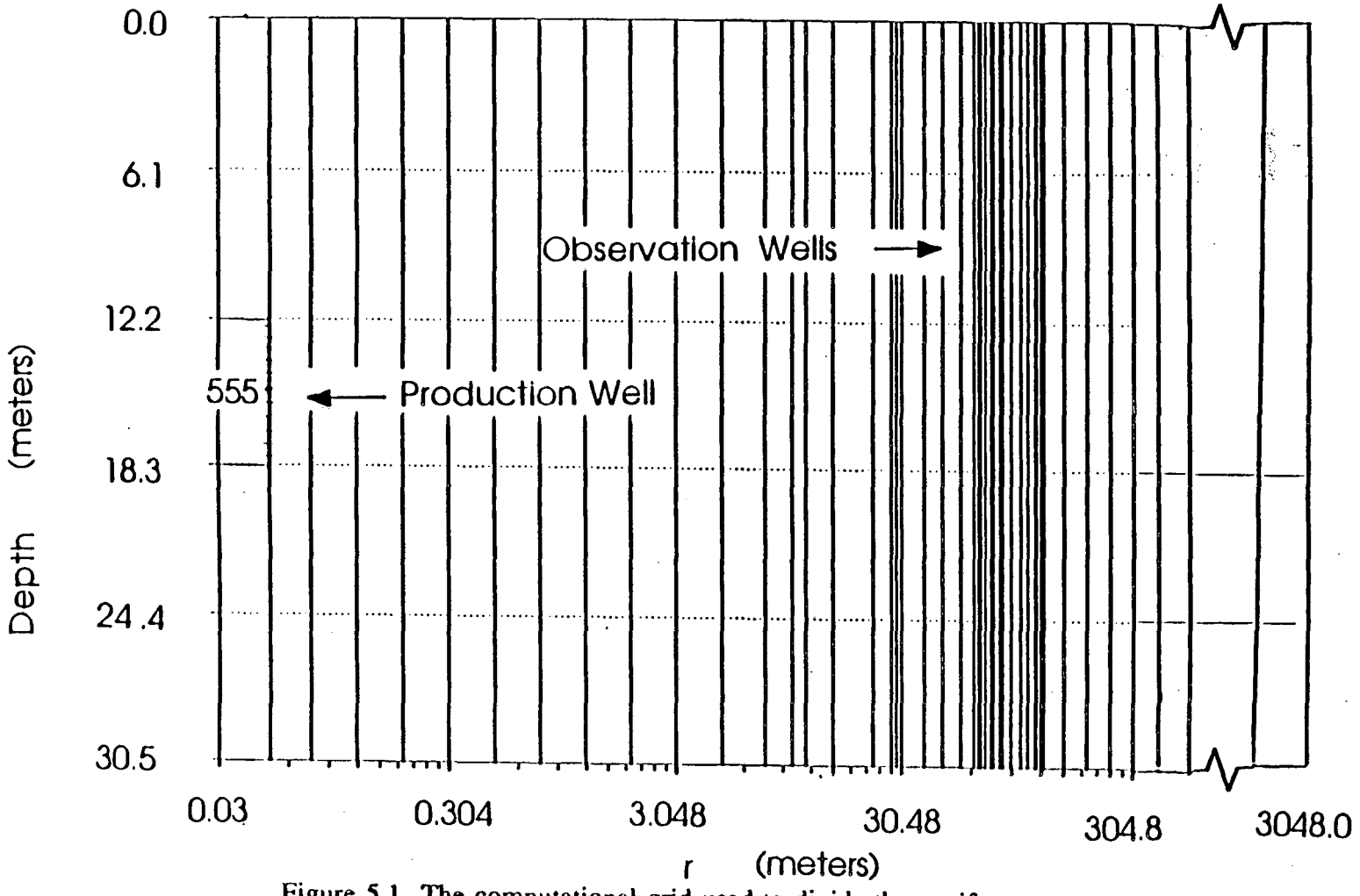


Figure 5.1 The computational grid used to divide the aquifer system at the LBLI/HO Site into volume elements. Water is withdrawn from the system through Node 555. The grid is finer in the vicinity of the observation wells.

aquifer of infinite horizontal extent. The top boundary is also kept at a constant pressure in order to simulate the effects due to the fully flooded ponds above the aquifer system at the LBLI/HO Site. The bottom boundary is considered impermeable since field observations have shown that there isn't any communication between the low-permeable clay layer C2 and the next aquifer system below.

Water is withdrawn from the system directly from Node 555, which represents the screened interval of the production wells and can be connected to any layer or set of layers depending upon which production well is being simulated. Node 555 has a volume equivalent to the volume of a production well screen interval, $V_{555} = \pi r_w^2 h$, where r_w is 0.05 m and h is 6.1 m. The specific capacity M_c of Node 555 is calculated in the computer code as

$$M_c = V_{555} n \rho (\alpha + \beta) \tag{5.5}$$

where n is the porosity of Node 555 and is set equal to 0.99, ρ is the fluid density, α is the matrix compressibility of Node 555, and β is the compressibility of water. Since the wellbore, which Node 555 represents, does not contain any matrix but only contains fluid, the matrix compressibility is used as an adjustable variable in order to mimic the actual field pressure response. This pseudo-compressibility takes into account the time lag in the pressure response due to wellbore storage and due to any timing errors involved with recording the moment that the pump was turned on. The pseudo-compressibility is discussed further in Section 5.1.3.

The initial temperature for all nodes was set to 20°C and the initial fluid density was set equal to 1000 kg/m^3, the density of water at 20°C. The initial pressure for all nodes was set to 5.91×10^5 Pa (85.8 psi) which is a little over the maximum hydrostatic pressure of any point in the flow region. Since the important aspect used in calculating the hydrologic parameters is the change in pressure ΔP and not the actual pressure, the system can be set to any initial pressure as long as the affects due to gravity are negligible.

The computation grid and numerical solution algorithm were verified against the Theis curve and the leaky aquifer type-curve as shown in Figures 5.2 and 5.3. This was conducted by simulating the pressure response of a 18.3 m thick, homogeneous aquifer with a permeability k equal to 4.0×10^{-11} m^2, a matrix compressibility α equal to 1.0×10^{-8} Pa^{-1}, a flowrate Q equal to 5.5×10^{-3} m^3/s, and a porosity n equal to 0.4. The pressure response was then plotted log-log and matched against the Theis curve. The calculated values of k and S_s obtained from the Theis type-curve agreed with the values used in the simulation. The same procedure was then used to simulate the pressure response of a leaky aquifer. A permeability k′ of 4.66×10^{-13} m^2 and a thickness of 6.1 m were used for the aquitard. Again, the calculated values determined from the leaky aquifer type-curves (k, k′, and S_s) agreed with the values used in the simulations.

5.1.3 Curve Matching Technique

After each numerical simulation using PT, the curve matching technique was applied to the simulated and field pressure data to determine if any adjustments were needed to the hydrologic values of the aquifer model. The aquifer model represents the different sedimentary units of the aquifer system at the LBLI/HO Site. Each sedimentary unit has its own hydrologic properties which can be individually adjusted. The curve matching technique involves comparing simulated pressure response curves with field measured pressure response curves and iteratively adjusting the hydrologic parameters of the aquifer model, usually the permeabilities of each sedimentary unit, until the two curves match. An example of a good match between simulated and field data is shown in Figure 5.4. The curve matching technique was used on the pressure responses of each individual production and observation well for the three single-well and interference transient tests and the series of pulse tests that were performed at the LBLI/HO Site. The technique was used on a total of 51 field pressure response curves.

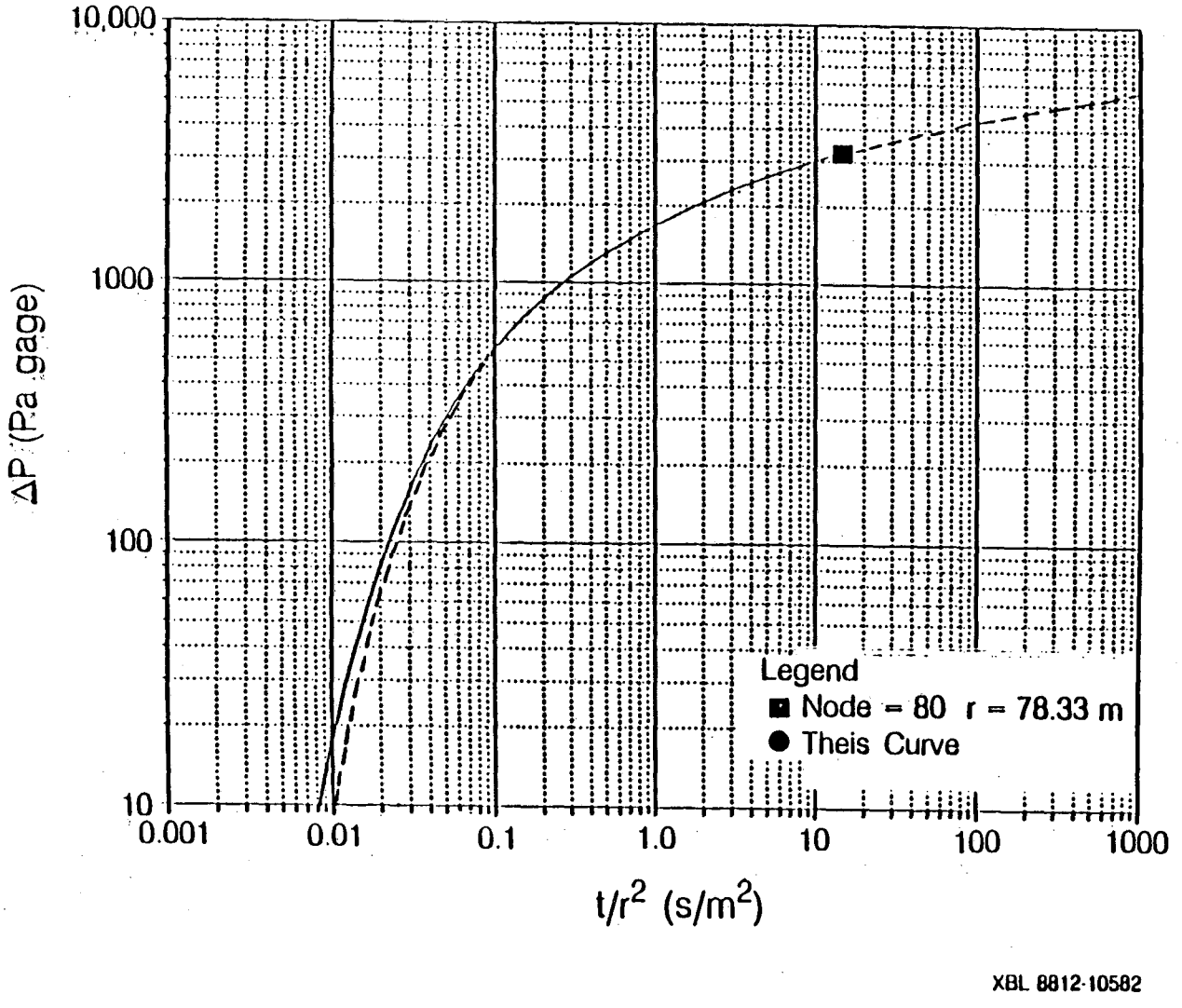


Figure 5.2 Verification of the computational grid with the Theis type-curve.

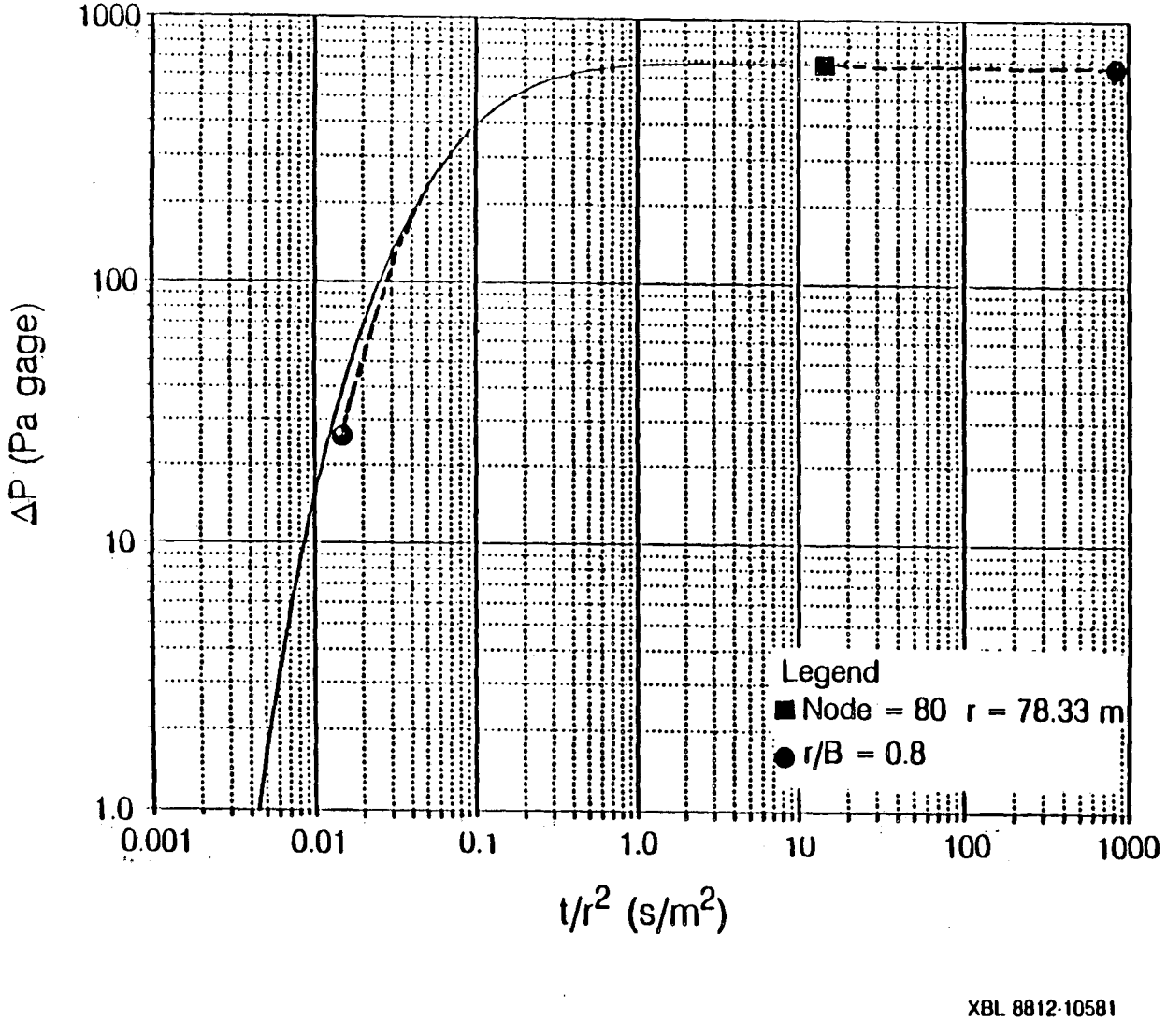


Figure 5.3 Verification of the computational grid with the leaky aquifer type-curve.

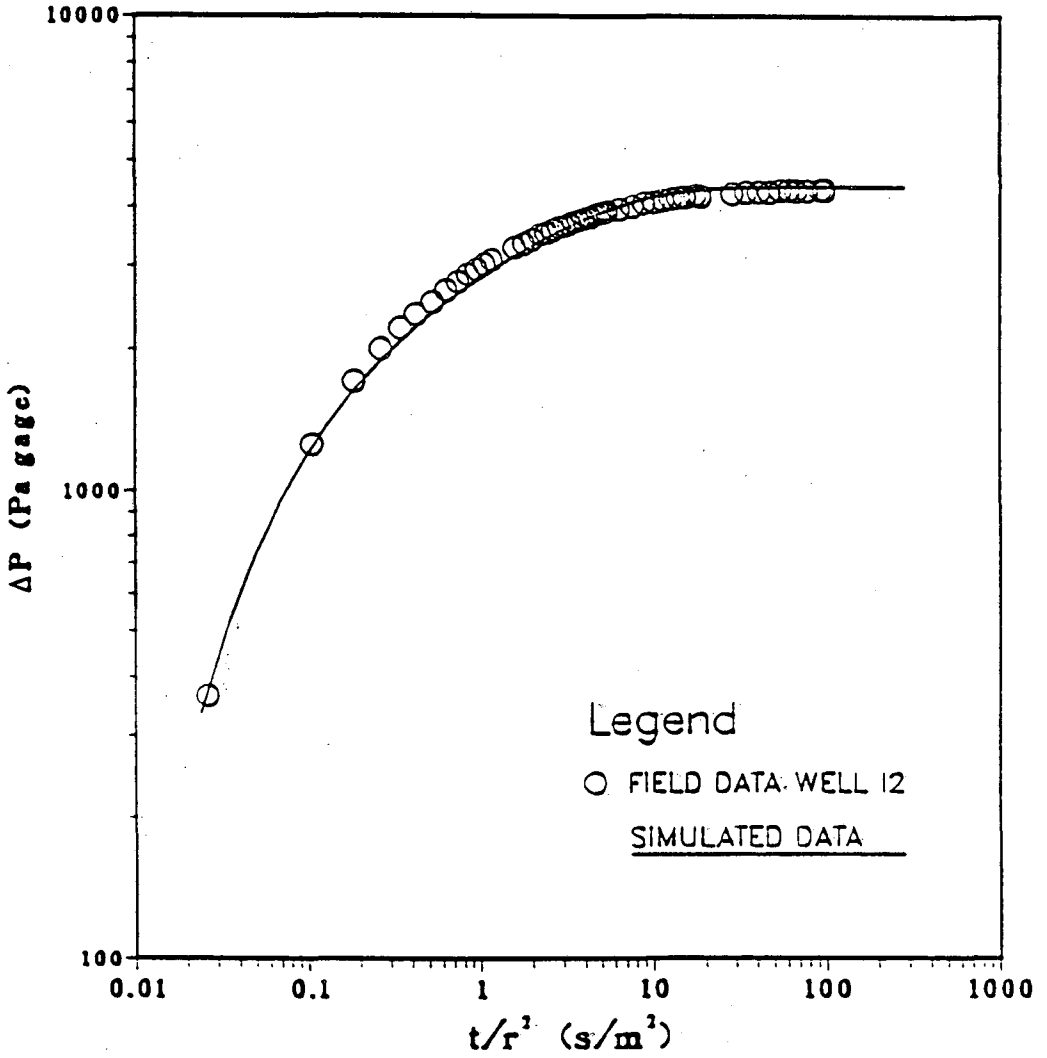


Figure 5.4 Plot showing a match of simulated data and field data from Interference Test 1 and Observation Well I2.

The parameter that was adjusted most often was the permeabilities of the sedimentary units of the aquifer model. Starting with the permeability values from the single-well steady-state tests, the values never needed to be adjusted by more than 2×10^{-11} m^2 (2.2×10^{-10} ft^2) but just needed to be refined. Depending upon which production well was pumped, the 12.2, the 18.3, or the 24.4 meter (40, 60, or 80 ft) deep well, determined for which units in the aquifer model that the pressure response was most sensitive too.

A pseudo matrix compressibility was used as an adjustable parameter for the analysis of the single-well transient pump tests. This was required because of wellbore storage effects (Earlougher, 1977) and timing errors involved with turning on the pump. The wellbore storage coefficient is defined as the change in fluid volume in the wellbore per unit change in bottom-hole pressure:

$$C = \frac{\Delta V_w}{\Delta P} \tag{5.6}$$

where V_w is the volume of water. Wellbore storage effects occur because each production well has a finite volume which is initially filled with water. Once production begins, the pump takes water not only from the aquifer formation but also from the storage water already in the wellbore. This causes a time lag to occur before the flowrate from the aquifer into the wellbore equals the flowrate out of the well at the surface.

If the wellbore storage coefficient is expressed as the well mass capacity in terms of mass per unit pressure change, then

$$\text{capacity} = \frac{\rho\pi r_w^{\,2}}{\rho g} = 8.0\times10^{-4}\ \text{kg/Pa} \tag{5.7}$$

However, the computer code PT calculates the specific mass capacity of Node 555 (the node which represents the screened interval of the wellbore), described earlier in Eq. 5.5, as

$$M_c = V_{555}n\rho(\alpha + \beta) \tag{5.5}$$

Solving for α and substituting in the well capacity from Eq. 5.7 for the specific fluid mass capacity:

$$\alpha = \frac{M_c}{V_{555} n \rho} - \beta = 1.7 \times 10^{-5} \text{ Pa}^{-1} \tag{5.8}$$

where $V_{555} = 0.048$ m^3, $n = 0.99$, $\rho = 1000$ kg/m^3, and β is the compressibility of water and is equal to 4.4×10^{-10} Pa^{-1} at 20°C (Freeze and Cherry, 1979). The value of α is the value used by the pseudo-compressibility in order to mimic the field pressure response and was adjusted slightly to take into account any timing errors. The final pseudo-compressibility values used in the aquifer model were 2×10^{-6} Pa^{-1} for Production Well I1, 2.9×10^{-6} Pa^{-1} for Production Well HO60, and 5×10^{-6} Pa^{-1} for Production Well HO80.

Most of the work involved in adjusting the parameters of each sedimentary unit focused on 1) individually matching simulated pressure responses to all 51 field measured pressure responses and then 2) finding one set of common values which would reasonably match all 51 field measured pressure responses. This was achieved after many numerical simulations and the results will be discussed in Chapter 6.

5.2 ANALYTICAL METHODS

Analytical methods of analyzing the data from the pump tests at the LBLI/HO Site were conducted in order to compare the analytical results with the numerical results. The basic assumptions used for analytical analysis of the pumping test data at the LBLI/HO Site are as follows. The aquifer and leaky aquitard are assumed to be homogeneous and isotropic with a constant thickness and infinite in areal extent. The pumping rate is assumed to be constant and the initial pressure of the aquifer system is uniform throughout. The flow in the aquitard is assumed to be vertical and the flow in the aquifer, except for the single-well steady-state analysis, is assumed to be radial. The single-well steady-state analysis takes into account the effects due to

partial penetration, whereas, the other two analytical methods assume fully penetrating wells.

5.2.1 Single–Well Steady–State Pump Tests

Single-well steady-state pump tests at the LBLI/HO Site consisted of pumping a well at a constant rate until steady-state conditions were achieved. The pumping rate Q and the change in hydraulic head $\Delta\phi$ were used to calculate the specific capacity $Q/\Delta\phi$. The specific capacity is useful as a first approximation of the aquifer's permeability and permeability variations and is useful in designing multiple-well interference and pulse tests. The specific capacity is substituted into Theim's equation which is an equation that describes steady-state flow to a well in a confined, homogeneous aquifer (Theim, 1906). Modifying Theim's equation to take into account the pseudo-skin factor due to partial penetration, the equation can then be solved for the permeability:

$$k = \left[\frac{-Q}{\Delta\phi}\right]\frac{\mu}{2\pi H\rho g}\left[\ln\left[\frac{r_e}{r_w}\right] + S_p\right] \tag{5.9}$$

where r_w is the radius of the well and r_e is defined as the effective radius. The effective radius (also called the radius of influence or the radius of investigation) is the distance beyond which the pressure drawdown is negligible. The effective radius for a single-well test is not exactly known but can be estimated by the effective radius known for a pulse test (Vela and McKinley, 1970) which is, in units of meters

$$r_{eff} = 1.774\sqrt{\frac{kt}{n\mu(\alpha+\beta)}} \tag{5.10}$$

where t is time, n is the porosity of the matrix, μ is the fluid viscosity in units of [kg/m·s], α is the matrix compressibility in units of [Pa^{-1}], and β is the compressibility of water in unit of [Pa^{-1}].

The pseudo-skin factor S_p takes into account the increase in pressure drop due to the partial penetration of the production well. The pseudo-skin factor is a function of the penetration ratio b and of the ratio h/r_w (Brons and Marting, 1961) where b is

defined as the total interval open to fluid entry divided by the total thickness of the aquifer H, h is defined as the thickness of the total productive interval, and r_w is the well radius. Brons and Marting calculated pseudo-skin factors for a range of h/r_w and b values as shown in Figure 5.5. The pseudo-skin factor is smaller for a well that is screened in the middle of an aquifer than for a well in which the screened interval is located at the top or at the bottom of an aquifer, therefore, the pseudo-skin factor will be less for Well HO60 in which the screen is located in the middle of the aquifer from 12.2-18.3 m (40-60 ft) than for all the other wells in which the screens are located either at the top of the aquifer at 6.1-12.2 m (20-40 ft) or at the bottom of the aquifer at 18.3-24.4 m (60-80 ft).

5.2.2 Single–Well and Interference Pressure Transient Tests

The analytical analysis of the single-well and interference pressure transient test data assumes that the aquifer system at the LBLI/HO Site behaves as a leaky aquifer as described in Chapter 3, Section 3.2.2. In order to simplify analysis, a graphical method of analysis was developed (Theis, 1935). The graphical method utilizes a type-curve matching procedure by plotting observed field data on log-log paper as change in pressure ΔP versus t/r^2. This field data curve is then matched to the theoretical pressure response log-log curve of P_D versus t_D and convenient "match points" are picked. The curves should be the same shape but just shifted along the X and/or Y axis by a constant. The values at the "match point" on both curves are recorded providing values for ΔP, t/r^2, P_D, and t_D. The permeability and specific storage can then be solved for by using the expressions:

$$k = \frac{Q\mu P_D}{2\pi H \Delta P} \qquad S_s = \frac{k\rho g}{\mu t_D}\left[\frac{t}{r^2}\right] \tag{5.11}$$

The value for r/B is taken off of the leaky aquifer type-curve so that the permeability k' of the leaky aquitard can be solved for by using Eq. 3.23.

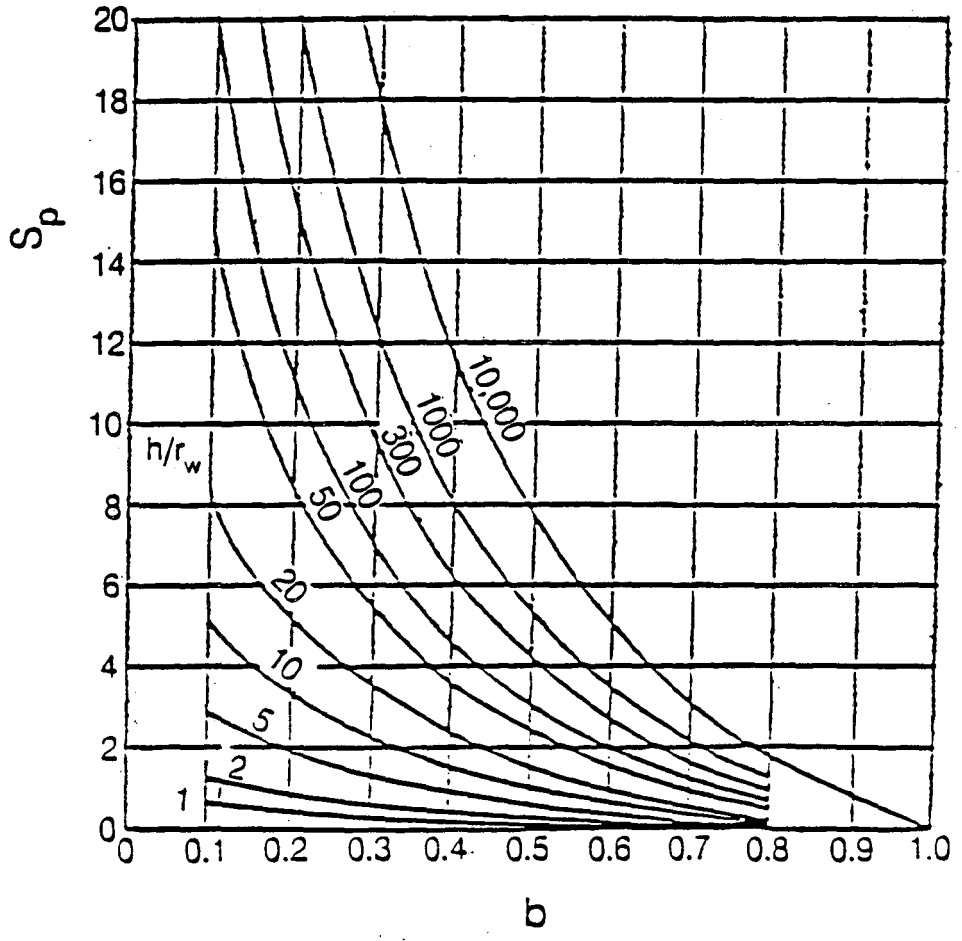


Figure 5.5 Pseudo-skin factor S_p as a function of b and h/r_w (Taken from Brons and Marting, 1961).

$$k' = \frac{kHH'}{B^2} \tag{3.23}$$

For the case of an impermeable confining layer, the leaky aquifer type-curves reduce to the Theis type-curve of an ideal aquifer.

5.2.3 Pulse Pressure Transient Tests

The method used at the LBLI/HO Site to conduct pulse tests consisted of pumping the production well at a constant rate for a short duration of time (called a pulse) and measuring the resulting pressure response at an observation well. The time in which the pressure response took to reach the observation well is called the time lag t_{lag} and the magnitude of the pressure response recorded at the observation well is called the pressure amplitude ΔP_{max}. The frequency of the pulses generated at the production well was not constant (see Figure 5.6) and, therefore, each pulse response recorded at an observation well needed to be analyzed independently because of varying values of t_{lag} and ΔP_{max}. The solution for one pulse can be written as

$$\Delta P = \frac{Q\rho g}{4\pi T}\left[W\left(\frac{r^2 S}{4T(t_p + \Delta t)}\right) - W\left(\frac{r^2 S}{4T\Delta t}\right)\right] \tag{5.12}$$

where t_p is the time interval of the pulse generated at the production well and Δt is the time from when the production well was shut-in. When the pressure change ΔP is equal to ΔP_{max}, the derivative is equal to zero and Δt is equal to the time lag (see Figure 5.7)

$$\frac{d\,\Delta P_{max}}{dt} = 0 \qquad \text{and} \qquad \Delta t = t_{lag} \tag{5.13}$$

Using the chain rule to obtain the derivative of Eq. 5.12 and then setting the derivative equal to zero

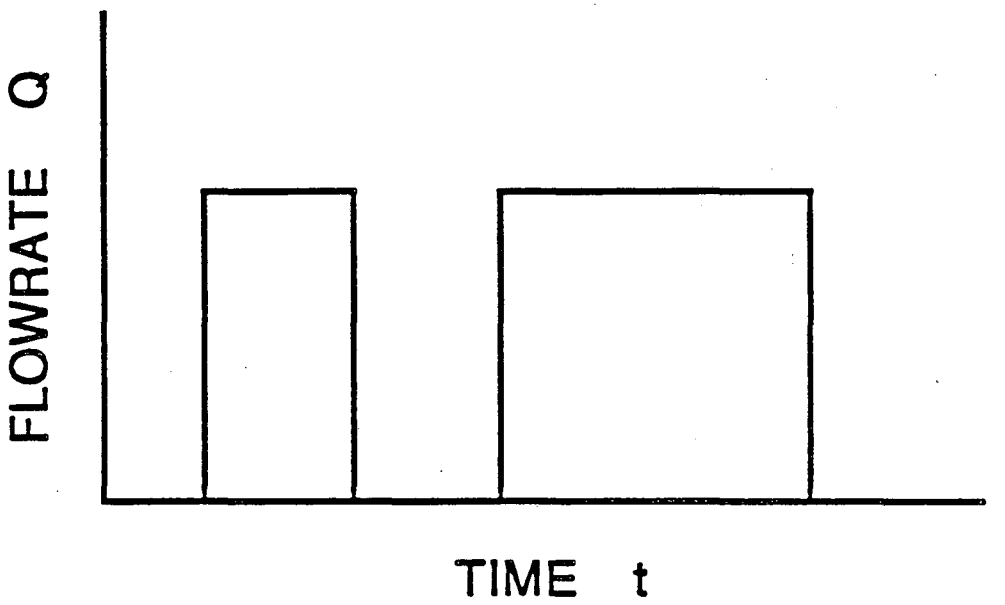
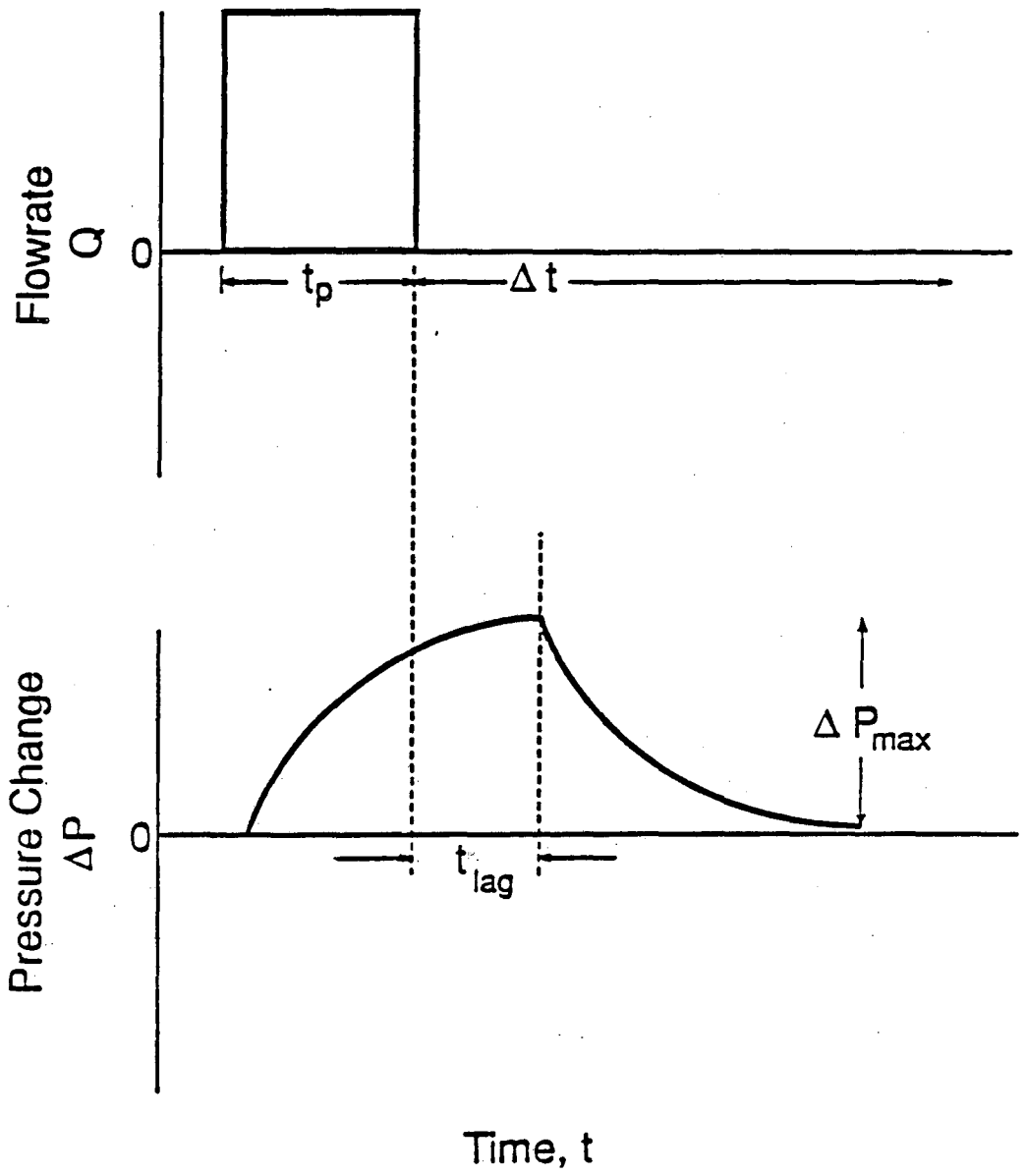


Figure 5.6 Schematic diagram describing the method used at the LBLI/HO Site in order to conduct pulse tests. The frequency of the pulses was not held constant.



XBL 8812-10597
T.I.D. Adobe 88
12/14/88

Figure 5.7 Schematic diagram showing that when the pressure change is equal to ΔP_{max}, Δt is then equal to t_{lag}.

$$\frac{d\Delta P}{dt} = \frac{\partial \Delta P}{\partial u}\frac{\partial u}{\partial t} = 0 = \frac{Q\rho g}{4\pi T}\left[\frac{-\exp\left[\frac{-r^2 S}{4T(t_p + t_{lag})}\right]}{t_p + t_{lag}} + \frac{\exp\left[\frac{-r^2 S}{4T t_{lag}}\right]}{t_{lag}}\right] \quad (5.14)$$

$$\frac{\exp\left[\frac{-r^2 S}{4T(t_p + t_{lag})}\right]}{t_p + t_{lag}} = \frac{\exp\left[\frac{-r^2 S}{4T t_{lag}}\right]}{t_{lag}} \quad (5.15)$$

Solving for the diffusivity η where $\eta = T/S$

$$\eta = \frac{T}{S} = \left[\frac{r^2 t_p}{4t_{lag}(t_p + t_{lag})}\right]\left[\frac{1}{\ln\left[\frac{t_p + t_{lag}}{t_{lag}}\right]}\right] \quad (5.16)$$

In order to calculate η, only the time lag t_{lag} and the time interval of the pulse t_p need to be known. η is then substituted into Eq. 5.12 for when $\Delta P = \Delta P_{max}$.

$$\Delta P_{max} = \frac{Q\rho g}{4\pi T}\left[W\left[\frac{r^2}{4\eta(t_p + t_{lag})}\right] - W\left[\frac{r^2}{4\eta t_{lag}}\right]\right] \quad (5.17)$$

Solving for T:

$$T = \frac{Q\rho g}{4\pi \Delta P_{max}}\left[W\left[\frac{r^2}{4\eta(t_p + t_{lag})}\right] - W\left[\frac{r^2}{4\eta t_{lag}}\right]\right] \quad (5.18)$$

or for the permeability k:

$$k = \frac{Q\mu}{4\pi H \Delta P_{max}}\left[W\left[\frac{r^2}{4\eta(t_p + t_{lag})}\right] - W\left[\frac{r^2}{4\eta t_{lag}}\right]\right] \quad (5.19)$$

The storativity and the specific storage values are then easily solved for from the expressions

$$S = \frac{T}{\eta} = \frac{k\rho g H}{\mu\eta} \qquad S_s = \frac{k\rho g}{\mu\eta} \quad (5.20)$$

The time lag t_{lag} and the amplitude ΔP_{max} can be measured either from a plot of ΔP vs t or directly from the recorded values of ΔP and t.

6.0 NUMERICAL SIMULATIONS

The primary purpose of this report was to determine the hydrologic properties of the leaky and layered aquifer system at the LBLI/HO Site at Kesterson Reservoir. Because of the complexity of the aquifer system, numerical methods were used to simulate the pressure transient pumping tests that were conducted at the site. The results obtained from the analytical analysis of the single-well steady-state pump tests were used in designing an initial aquifer model. In this chapter, the procedures involved in refining an initial aquifer model into the final model which best represents the aquifer system are discussed and the hydrologic results are presented.

6.1 SINGLE-WELL STEADY-STATE RESULTS

The hydrologic parameters obtained from the single-well steady-state tests conducted at the LBLI/HO Site are listed in Table 6.1. The analytical method used in analyzing the single-well pump test data was discussed earlier in Chapter 5, Section 5.2.1. The specific capacity $Q/\Delta\phi$ is substituted into Eq. 5.6 which is then solved for the permeability k. The permeability of the sediments adjacent to each well and the average permeability of the aquifer can then be determined.

$$k = \left[\frac{Q}{\Delta\phi}\right] \frac{\mu}{2\pi H\rho g} \left[\ln\left[\frac{r_e}{r_w}\right] + S_p\right] \qquad (5.6)$$

The well radius r_w of all the wells is equal to 0.05 m (2.0 in) and the aquifer thickness is assumed to be 18.3 m (60 ft). The pseudo-skin factor S_p for Production Well HO60 is equal to 7.0 while the pseudo-skin factor for all the other wells at the LBLI/HO Site is equal to 8.46. The effective radius r_e of the LBLI/HO Site was estimated, using Eq. 5.7, as 233 m (764 ft).

Table 6.1. Hydrologic parameters obtained from the analytical analysis of the single-well steady-state pump tests.

Test	Well	S_p	$(Q/\Delta\phi) \times 10^{-3}$ ($m^3/s \cdot m$)	$k \times 10^{-11}$ (m^2)
1	I1	8.46	3.5	5.25
2	I2	8.46	2.1	3.15
3	I3	8.46	0.32	0.48
4	I4	8.46	4.3	6.45
5	I5	8.46	0.3	0.59
6	I6	8.46	1.4	2.10
7	I7	8.46	0.36	0.54
8	I8	8.46	3.0	4.50
9	I9	8.46	2.6	3.90
10	HO60	7.00	0.93	1.27
11	HO80	8.46	1.1	1.65
12	HO100	8.46	0.049	0.073

The single-well steady-state pump tests were conducted in wells which were screened over the bottom 6.1 m (20 ft) of each and, therefore, the permeability values obtained from these tests are averaged over 6.1 meters. Nine of the twelve wells were screened from 6.1-12.2 m (20-40 ft), therefore, most of the hydrologic information obtained from the single-well steady-state pump tests pertain to this depth interval. These nine wells, however, cover an area of approximately 44,400 m^2 (447,836 ft^2) and, therefore, can provide a good indication of the areal heterogeneity of the site.

The results from the single-well steady-state tests indicate that the sedimentary layer located at a depth interval of 6.1-12.2 m consists of two permeability regions. The permeability of the sediments adjacent to the inner region wells (I1, I2, I4, I6, and I8) is almost an order of magnitude higher than the permeability of the sediments adjacent to the outer region wells (I3, I5, I7, and I9) with the exception of Well I9. The inner region geometric mean permeability value of the sediments is 4.0×10^{-11} m^2 (4.3×10^{-10} ft^2), whereas, the outer region geometric mean, excluding Well I9, is 5.3×10^{-12} m^2 (5.7×10^{-11} ft^2). If Well I9 is included, the outer region value is 8.8×10^{-12} m^2 (9.5×10^{-11} ft^2). The geometric mean permeability value of the entire sedimentary layer at the depth of 6.1-12.2 m is 2.0×10^{-11} m^2 (2.2×10^{-10} ft^2).

The arithmetic mean permeability for the entire aquifer at the LBLI/HO Site, as determined from the single-well tests, is equal to 1.6×10^{-11} m^2 (1.7×10^{-10} ft^2).

The apparent zoning of the permeability can be accounted for geologically by the abundant interfingering of the sediments in the upper aquifer. The interfingering seems to create two distinct hydrological zones resembling a lens of relatively more-permeable sediments approximately centered at the production wells I1, HO60, and HO80 surrounded by less-permeable sediments. somewhere in between the inner wells and the outer wells.

The permeability value obtained from Well HO100 indicates the presence of a relatively low-permeable layer located at the bottom of the aquifer. This layer has a permeability value of 5.3×10^{-13} m^2 (5.7×10^{-12} ft^2).

6.2 NUMERICAL RESULTS

Since the aquifer system was assumed to be 30.5 m (100 ft) thick and information was available for every 6.1 m (20 ft), the initial aquifer model was a purely layered model, contained only five layers, each 6.1 m (20 ft) thick. The steps involved in refining the initial model into the final model are described below.

The initial model was divided up into five layers of constant thicknesses and differing permeabilities (see Figure 6.1). The initial permeability value used for Layer 1 (the leaky aquitard) was obtained from matching the interference pump test pressure data to a leaky aquifer type-curve. A value of 4.2×10^{-13} m^2 (4.5×10^{-10} ft^2) was obtained for the aquitard. The initial permeability values used for Layers 2-5 were those values obtained from the single-well steady-state tests for Wells I1, HO60, HO80, and HO100 respectively. The model consisted of three sand layers bounded on the top and on the bottom by relatively low-permeable confining layers.

The initial model was used to simulate the interference tests involving Production Wells I1 and HO60. Pressure response matches were obtained and examples of these

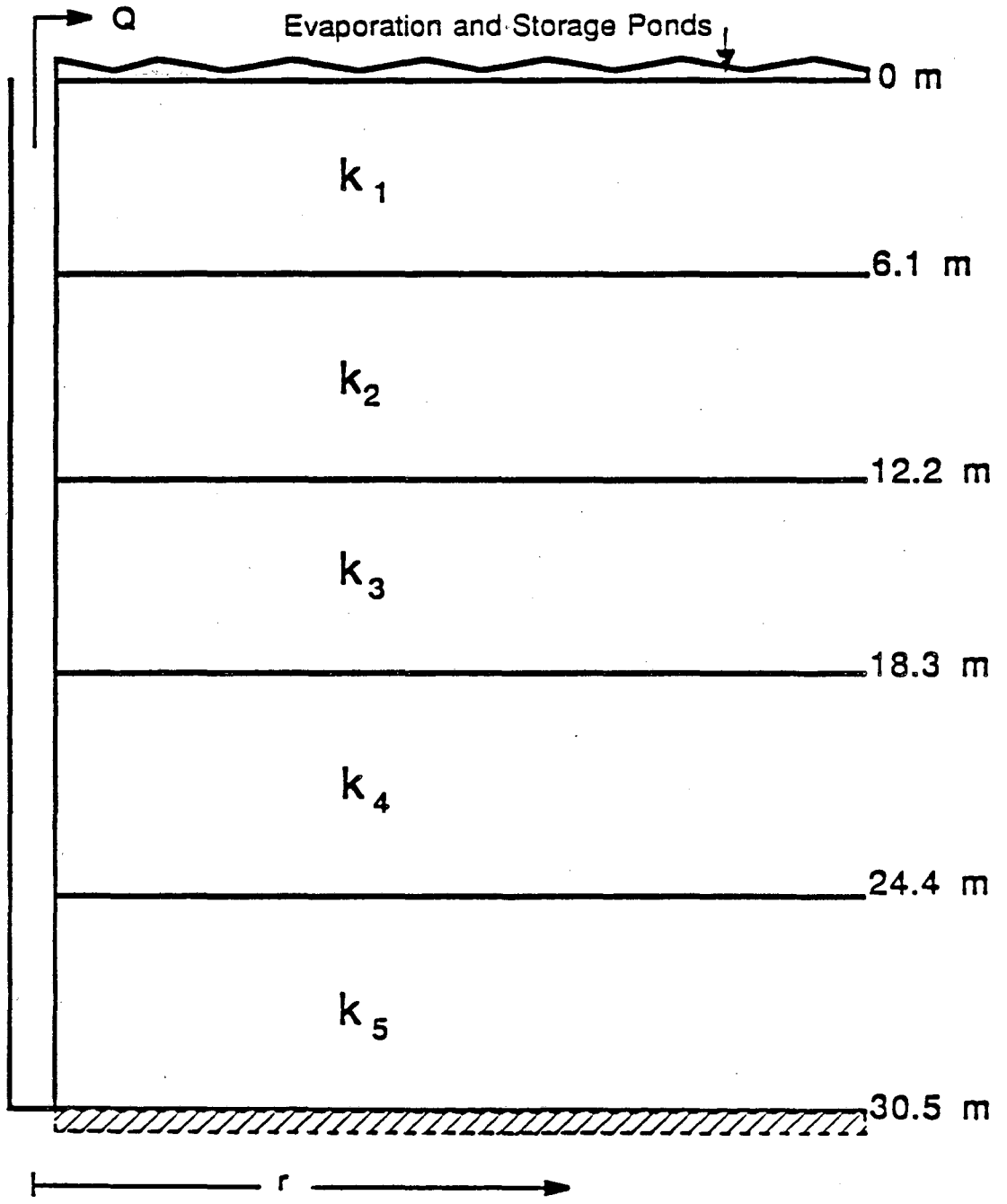


Figure 6.1 Schematic diagram of the initial aquifer model used in numerical simula -tions of the aquifer system at the LBLI/HO Site at Kesterson Reservoir.

matches are shown in Figures 6.2 and 6.3. Since most of the information obtained from the single-well pump tests pertained to Layer 2, the initial aquifer model was refined in order to take into account the two permeable regions that were mentioned earlier, an inner radius zone with relatively high permeabilities and an outer radius zone of relatively low permeabilities. After incorporating these two permeability regions into Layer 2, the aquifer model went from being purely layered to being both layered and composite (see Figure 6.4).

Numerical simulations using the second aquifer model were made for the single-well and interference transient tests with varying results. The simulations of the single-well and interference tests conducted while pumping Production Wells I1 (see Figure 6.5 and Figure 6.6) and HO60 matched the field pressure response well indicating that the permeabilities used in the second aquifer model were possible. Table 6.2 gives the results of the permeability values used to match the pressure response data for Single-Well and Interference Tests 1 and 2 using the second aquifer model. But the matches for the tests conducted while pumping Production Well HO80, however, were difficult to achieve, indicating that the aquifer model needed to be refined even more. The difficulty arose in trying to match the early-time pressure changes. Figure 6.7a shows the best match that was achieved for Observation Well I2 while pumping Production Well HO80 and is an example of the difficulty in matching the early-time pressure response.

A review of the lithological and geophysical logs from the LBLI/HO Site indicated that a very thin clay layer (0.61 m thick) existed at a depth of approximately 16.8 m (55 ft). When this clay layer was incorporated into the aquifer model and assigned a relatively low permeability ($\approx 9.0\times10^{-14}$ m^2), reasonable matches for all three interference tests were achieved. Figure 6.7b shows the pressure response for the same test as in Figure 6.7a but a much better match was achieved by incorporating the clay layer into the aquifer model.

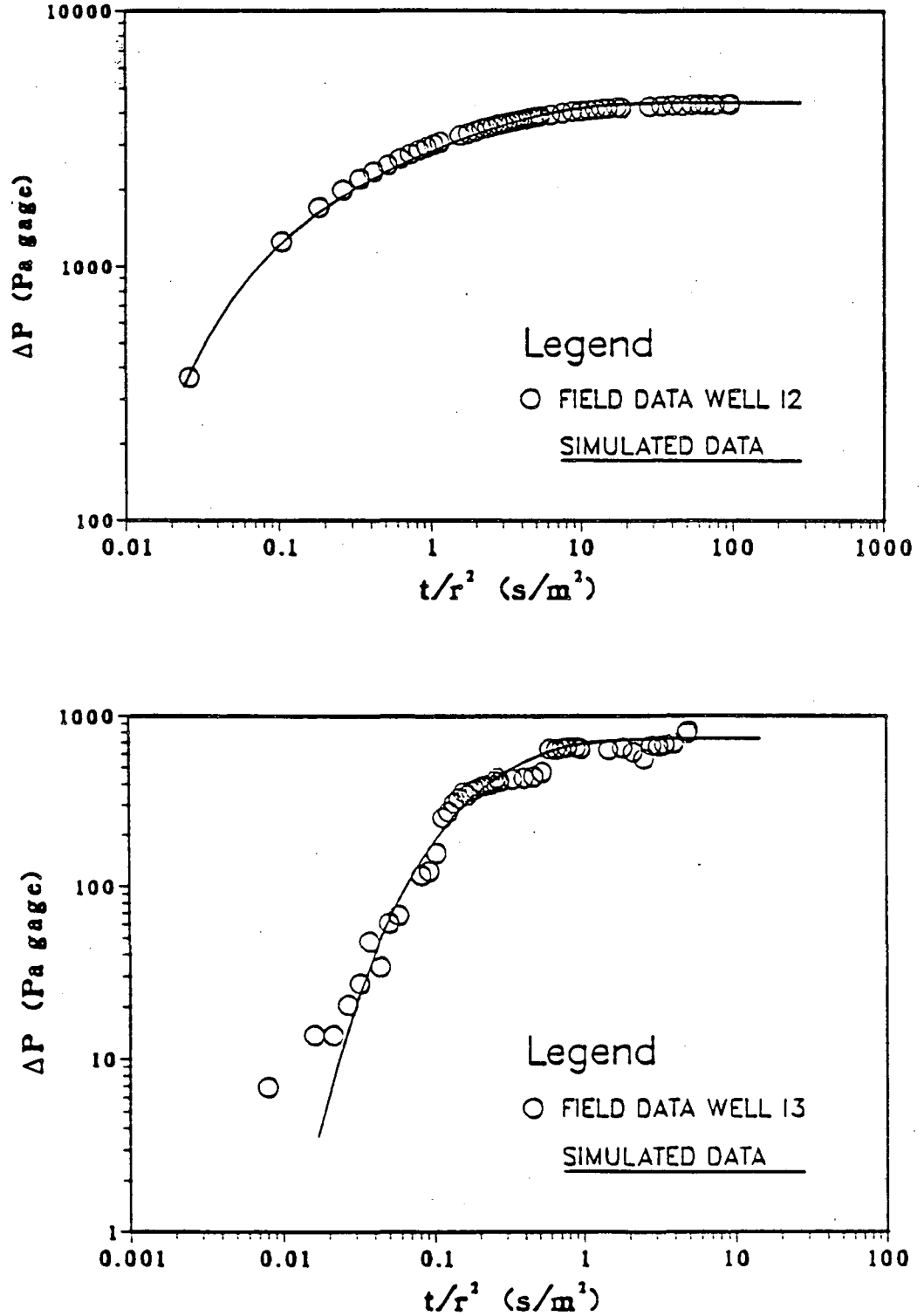


Figure 6.2 Field and simulated pressure responses of Interference Test 1 recorded at Observation Well I2 and I3 using the initial aquifer model.

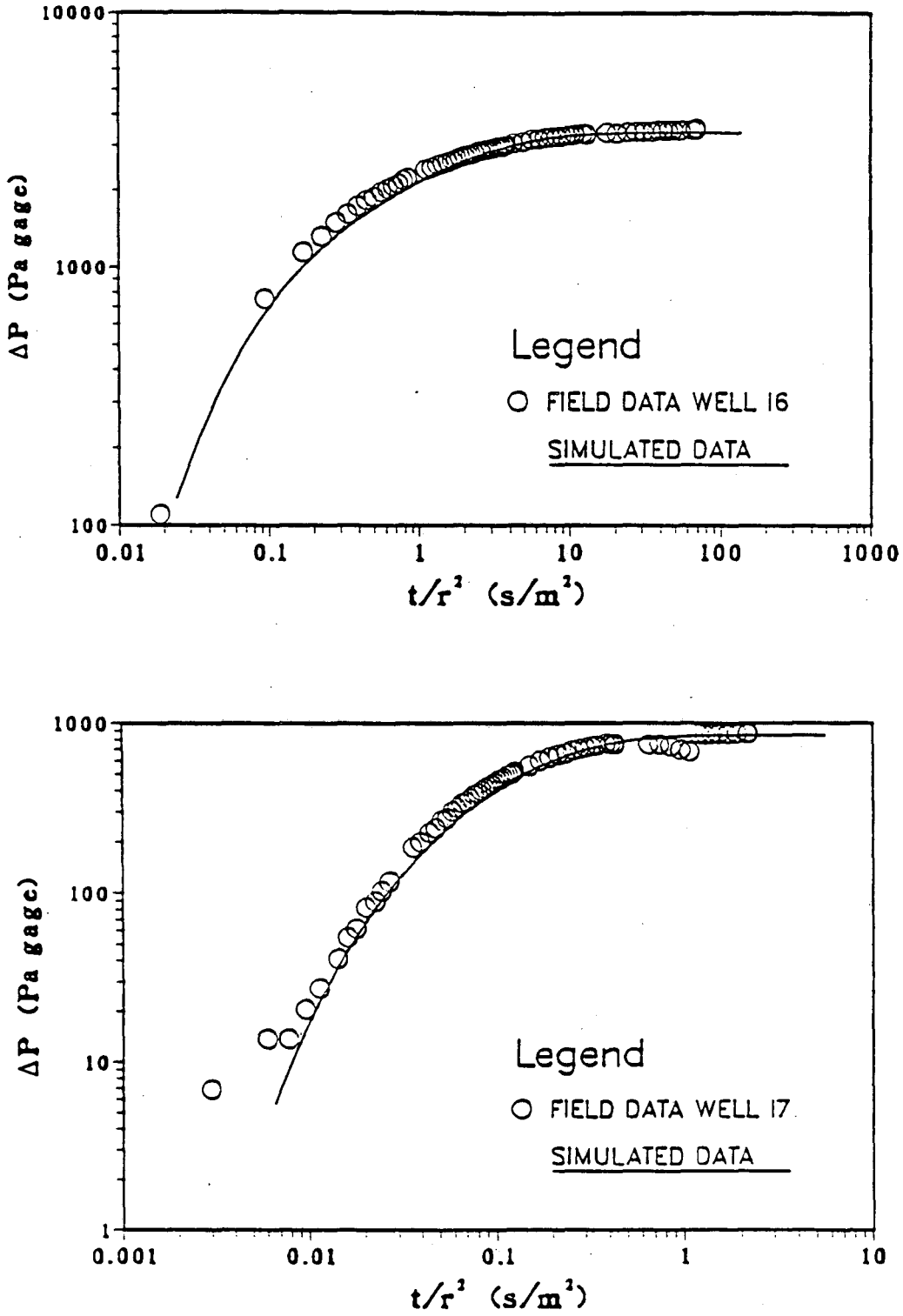


Figure 6.3 Field and simulated pressure responses of Interference Test 1 recorded at Observation Well I6 and I7 using the initial aquifer model.

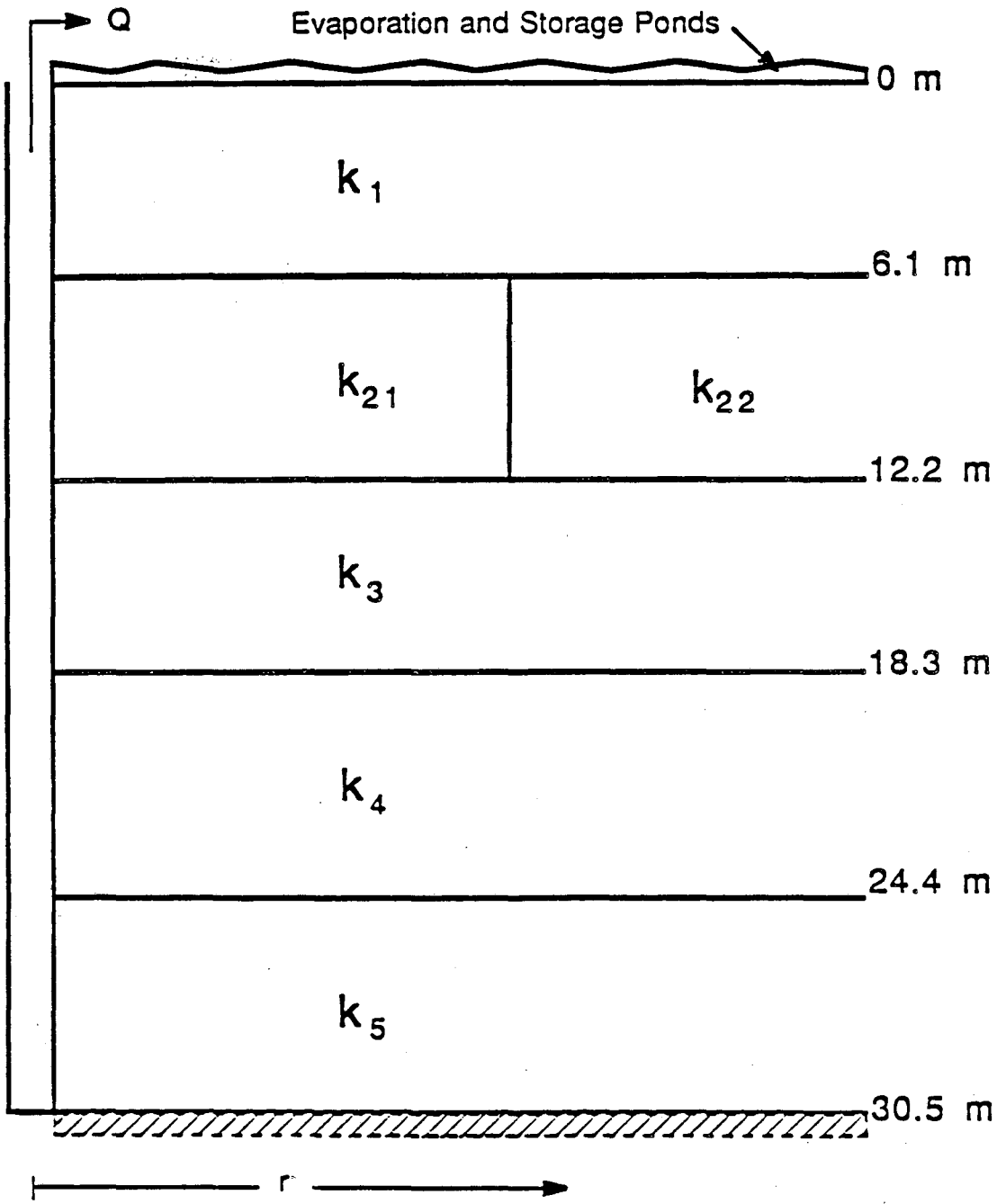


Figure 6.4 Schematic diagram of the second aquifer model used in numerical simula -tions of the aquifer system at the LBLI/HO Site at Kesterson Reservoir.

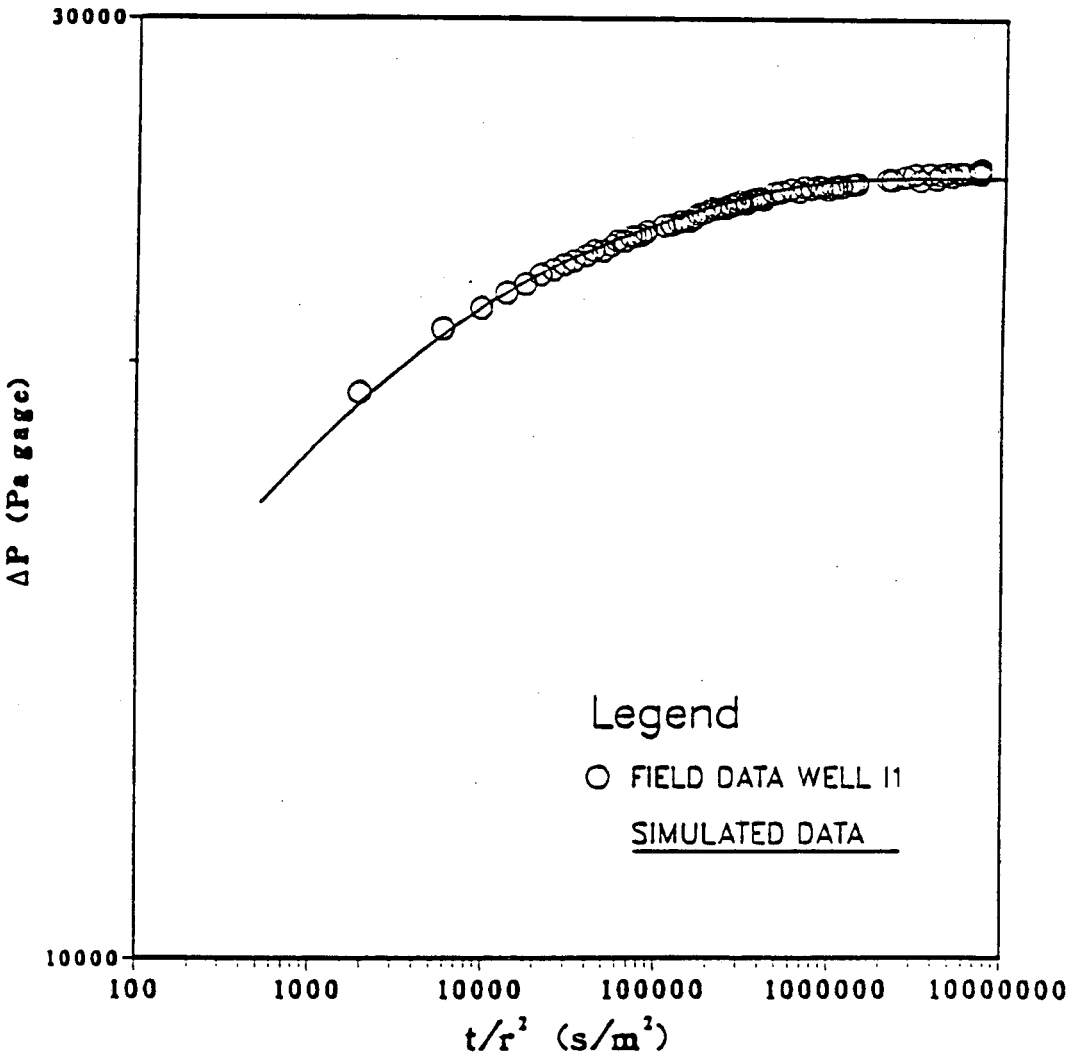
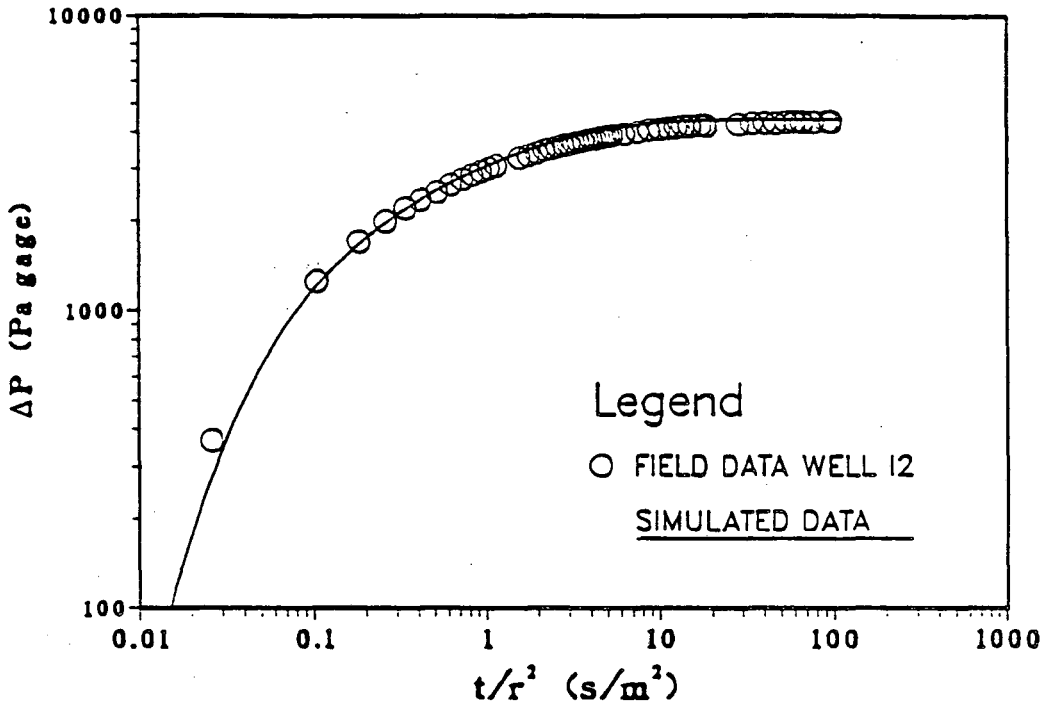


Figure 6.5 Field and simulated pressure responses of Single-Well Transient Test 1 recorded at Production Well I1 using the second aquifer model.



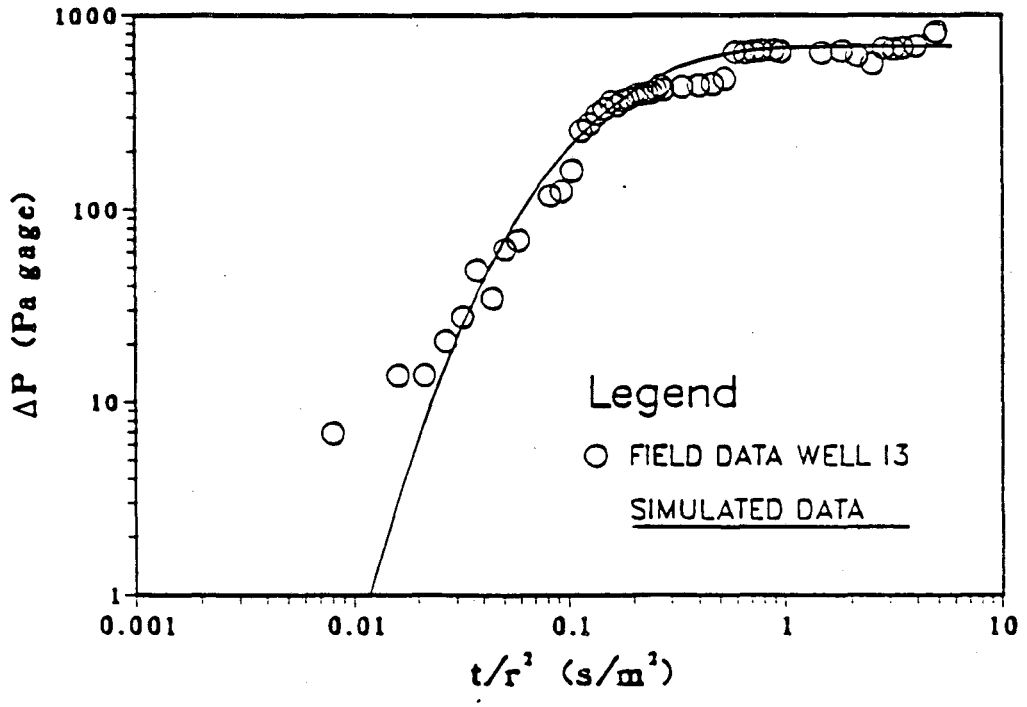
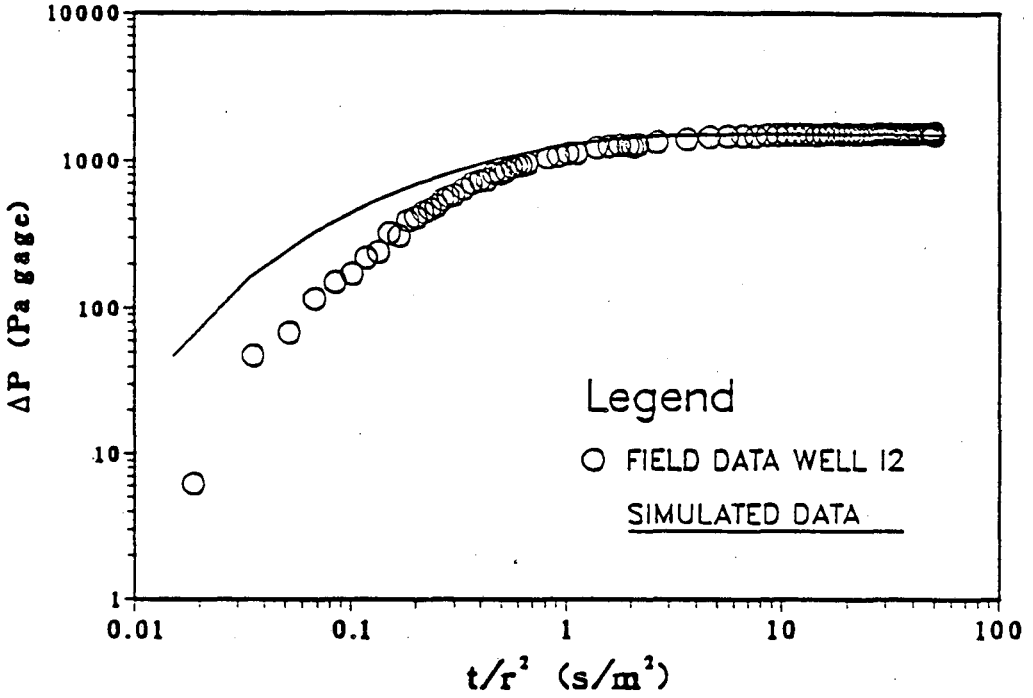
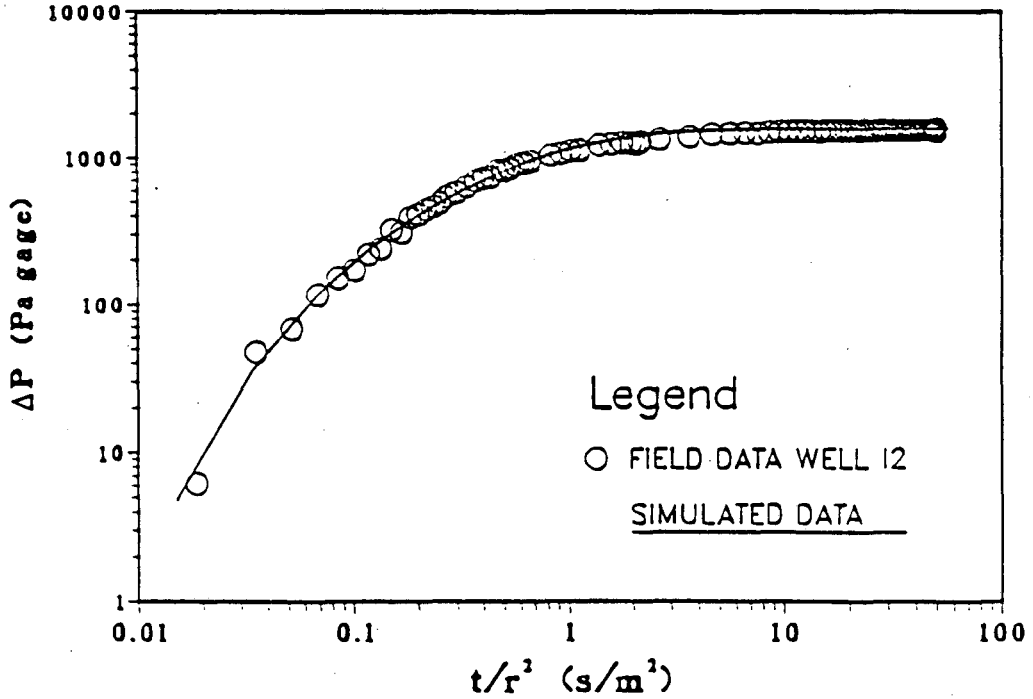


Figure 6.6 Field and simulated pressure responses of Interference Test 1 recorded at Observation Well I2 and I3 using the second aquifer model.



a



b

Figure 6.7 Field and simulated pressure responses of Interference Test 3 recorded at Observation Well I2 using a) the second aquifer model without a clay layer included and b) the final aquifer model including a clay layer with a permeability of 9×10^{-14} m^2.

Table 6.2. Permeability values obtained from the numerical analysis of the single-well transient and interference test data using the second aquifer model.

Test	Production Well	Observation Well	$k \times 10^{-11}$ (m^2)					
			Sedimentary Units					
			1	21	22	3	4	5
1	I1	I1	0.042	4.1	0.63	2.0	4.6	0.073
		I2	0.092	4.5	0.78	0.3	2.0	0.073
		I3	0.012	4.0	0.48	2.0	1.6	0.073
		I4	0.047	1.3	0.48	5.0	2.6	0.073
		I5	0.020	8.0	0.68	7.0	9.0	0.073
		I6	0.080	5.5	0.48	2.0	1.6	0.073
		I7	0.023	9.0	2.80	9.0	1.6	0.073
		I8	0.100	5.5	0.48	1.0	1.6	0.073
		I9	0.027	4.0	0.38	4.0	4.6	0.073
2	HO60	HO60	0.003	4.4	0.50	1.0	1.5	0.073
		I2	0.055	4.4	0.50	1.0	5.0	0.073
		I3	0.035	4.4	0.80	6.0	1.0	0.073
		I4	0.078	4.4	0.50	3.0	4.0	0.073
		I5	0.025	4.4	0.50	8.5	6.0	0.073
		I6	0.058	4.4	0.50	2.0	5.0	0.043
		I7	0.030	4.4	0.50	6.0	5.0	0.073
		I8	0.030	4.4	0.50	2.1	5.0	0.073
		I9	0.023	4.4	0.50	7.0	1.0	0.043

By including the clay layer in the aquifer model, the final model was completed (see Figure 6.8). Layer 2 is now divided up into two parts, 21 and 22, and Layer 3 from the initial model is divided up into three separate layers, Layer 3, Layer 4 (the clay layer), and the top portion of Layer 5. The bottom portion of Layer 5 is considered a separate layer, even though the same hydrologic values are used throughout the layer. This is because only the top portion or only the bottom portion is connected to the screened interval of the production well at any one time. Table 6.3 shows the geometric factors, initial and boundary conditions, and physical properties used in the final aquifer model.

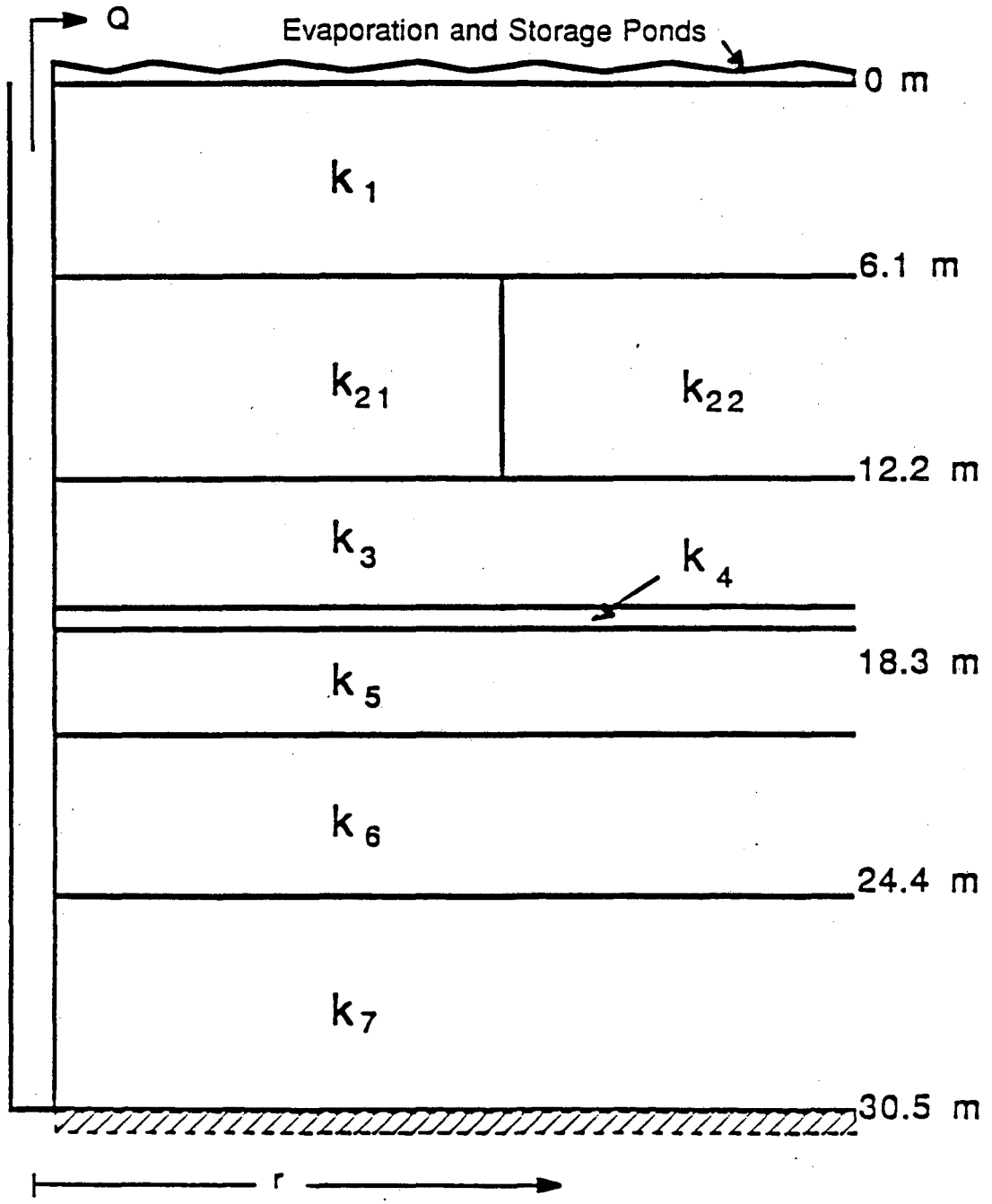


Figure 6.8 Schematic diagram of the final aquifer model used in numerical simula -tions of the aquifer system at the LBLI/HO Site at Kesterson Reservoir.

Table 6.3. Geometric factors, physical properties, and initial and boundary conditions used for the final aquifer model.

Parameter	Value	Comment
Geometric Factors		
Aquifer Thickness	30.5 m	includes top and bottom confining layers
Number of Layers	7	
Thickness of each Layer	Layer 1 - 6.10 m	leaky caprock
	Layer 2 - 6.10 m	
	Layer 3 - 4.57 m	
	Layer 4 - 0.61 m	thin clay layer
	Layer 5 - 2.44 m	
	Layer 6 - 4.57 m	
	Layer 7 - 6.10 m	bottom confining layer
Number of Sedimentary Units	8	
Radius of Aquifer	3,048 m	
Number of Elements	400	
Prodution Well Radius	5.08 cm	I1, HO60, HO80
Physical Properties		
Temperature	20°C	
Matrix Compressibility	10^{-8} Pa^{-1}	
Aquifer Anisotropy k_{horiz}/k_{vert}	1	
Aquifer Porosity	0.4	
Dynamic Viscosity	10^{-3} kg/m·s	
Fluid Compressibility	4.17×10^{-10} Pa^{-1}	
Initial and *Boundary Conditions*		
Initial Pressure of Aquifer	5.9133×10^{5} Pa	
Top Boundary	5.9133×10^{5} Pa	Constant Pressure
Outer Boundary	5.9133×10^{5} Pa	Constant Pressure
Axis Boundary		Impermeable
Bottom Boundary		Impermeable
Screened Interval of Production Well		Constant Flux

Simulating the single-well transient tests and the interference tests using the final aquifer model and individually matching pressure responses from each observation well (from each production well for the single-well tests) resulted in different permeability values for each set of well data. The permeability values are presented in Table 6.4.

Because of the non-uniqueness of the values, an attempt was made to find a single set of permeability values which would reasonably fit all the well data from all of the pump tests. Numerical simulations were once again conducted for each set of well data from all three transient pump tests, staying as close as possible to one set of permeability values while still matching simulated and field pressure response curves. The results from the best matches are presented in the next section of this report along with the arithmetic mean values of each test. The best curve matches are presented in the appendix.

6.2.1 Results from Single–Well Transient Tests

The results from the numerical analysis of the single-well transient pump tests are presented in Table 6.5. Production Well I1 is screened over the interval corresponding to Layer 2, HO60 corresponds to Layers 3, 4, and the top portion of 5, and HO80 corresponds to the bottom portion of Layer 5 and all of Layer 6.

Simulations of each test were made with a certain set of permeability values in mind until excellent matches were achieved. Taking the arithmetic mean permeability values of each sedimentary unit of the three test yields a single set of values that will more or less match all three tests.

6.2.2 Results from Interference Tests

The permeability values obtained from curve matching the simulated and field pressure response data of the interference pumping tests are presented in Table 6.6.

Table 6.4 Individual well permeability values obtained from the numerical analysis of th single-well transient and interference test data using the final aquifer model.

Test	Production Well	Observation Well	$k \times 10^{-11}$ (m^2) Sedimentary Units							
			1	21	22	3	4	5	6	7
1	I1	I1	0.060	4.4	0.5	6.0	0.008	3.0	3.0	0.073
		I2	0.070	4.0	0.5	5.0	0.008	3.0	3.0	0.073
		I3	0.090	4.0	0.5	1.0	0.008	3.0	3.0	0.073
		I4	0.070	6.0	0.5	5.0	0.008	3.0	3.0	0.073
		I5	0.030	4.0	0.5	9.0	0.001	7.0	3.0	0.073
		I6	0.030	4.0	0.5	9.0	0.001	3.0	3.0	0.073
		I7	0.027	4.0	0.5	7.0	0.005	7.0	3.0	0.073
		I8	0.060	4.0	0.5	7.0	0.005	3.0	3.0	0.073
		I9	0.035	4.0	0.5	3.0	0.005	3.0	3.0	0.073
2	HO60	HO60	0.003	4.0	0.5	1.0	0.008	3.8	1.0	0.073
		I2	0.090	4.0	0.5	1.0	0.008	7.0	1.0	0.073
		I3	0.003	4.0	0.5	5.0	0.008	7.0	1.0	0.073
		I4	0.090	4.0	0.5	1.0	0.001	5.0	5.0	0.073
		I5	0.030	4.0	0.5	8.0	0.005	3.0	3.0	0.073
		I6	0.040	4.0	0.5	8.0	0.005	3.0	3.0	0.073
		I7	0.030	4.0	0.5	8.0	0.005	3.0	3.0	0.073
		I8	0.030	4.0	0.5	8.0	0.005	3.0	3.0	0.073
		I9	0.040	4.0	0.5	5.0	0.008	5.0	1.0	0.073
3	HO80	HO80	0.050	4.4	0.5	3.7	0.005	3.0	2.7	0.073
		I2	0.050	4.4	0.5	3.7	0.09	3.0	2.7	0.073
		I3	0.030	4.4	0.5	3.7	0.04	3.0	3.0	0.073
		I4	0.050	4.4	0.5	3.7	0.04	3.0	2.7	0.073
		I5	0.035	4.4	0.5	3.7	0.02	4.0	2.7	0.073
		I6	0.050	4.4	0.5	3.7	0.008	3.0	2.7	0.073
		I7	0.050	4.4	0.5	3.7	0.004	3.0	2.7	0.073
		I8	0.070	4.4	0.5	3.7	0.01	3.0	2.7	0.073
		I9	0.050	4.4	0.5	3.7	0.009	3.0	2.7	0.073

Table 6.5 Permeability results from the numerical analysis of the single-well test data.

Test	Production Well	$k \times 10^{-11}$ (m^2)							
		Sedimentary Units							
		1	21	22	3	4	5	6	7
1	I1	.04	4.4	0.5	6.0	.009	3.0	2.7	.073
2	H060	.03	4.4	0.5	1.3	.008	3.0	1.0	.073
3	H080	.05	4.4	0.5	3.7	.005	3.0	2.7	.073
Test Average =		.04	4.4	0.5	3.7	.007	3.0	2.1	.073

The resulting permeability values of all three interference tests used in the reservoir model for Layer 1 ranged from 3.0×10^{-13} m^2 to 9.0×10^{-13} m^2 (3.2×10^{-12} ft^2 to 9.7×10^{-12} ft^2). The arithmetic mean for Layer 1 is 5.2×10^{-13} m^2 (5.6×10^{-12} ft^2). Adjusting the permeability value for Layer 1 controlled the amount of simulated leakage into the aquifer from the ponds at the surface. The late-time portion of the simulated pressure response curve was very sensitive to any changes in this value.

Constant permeability values were found for the two zones of Layer 2 in the reservoir model that would satisfy all three simulated interference tests. The permeability value found for the inner zone (part 21) is 4.4×10^{-11} m^2 (4.7×10^{-10} ft^2) and the permeability of the outer zone (part 22) is 5.0×10^{-12} m^2 (5.4×10^{-11} ft^2). The radius used in the model to the outer zone varied for every observation well and for each interference test. Some trends were noticed though, and a schematic diagram showing the approximate dimensions, obtained from the final reservoir model, of the two permeability zones of Layer is shown in Figure 6.9.

The permeability values of Layer 3 ranged from 1.0×10^{-11} m^2 to 6.0×10^{-11} m^2 (1.1×10^{-10} ft^2 to 6.5×10^{-10} ft^2) during numerical simulations with an arithmetic mean equal to 3.7×10^{-11} m^2 (4.0×10^{-10} ft^2). The permeability values for Layer 4, the 0.61 m (2 ft) thick clay layer, varied by an order of magnitude with values from 4.0×10^{-14} m^2 to 4.0×10^{-13} m^2 (4.3×10^{-12} ft^2 to 4.3×10^{-13} ft^2). The arithmetic mean

Table 6.6 Permeability results of the numerical analysis of the interference test data.

Test	Production Well	Observation Well	$k \times 10^{-11}$ (m^2) Sedimentary Units							
			1	21	22	3	4	5	6	7
1	I1	2	.065	4.4	0.5	3.7	.009	3.0	2.7	.073
		4	.08	4.4	0.5	3.7	.009	3.0	2.7	.073
		6	.035	4.4	0.5	3.7	.009	3.0	2.7	.073
		8	.06	4.4	0.5	3.7	.009	3.0	2.7	.073
		3	.09	4.4	0.5	1.0	.009	3.0	2.7	.073
		5	.03	4.4	0.5	6.5	.009	3.0	2.7	.073
		7	.035	4.4	0.5	5.0	.009	3.0	2.7	.073
		9	.035	4.4	0.5	3.7	.009	3.0	2.7	.073
2	H060	2	.07	4.4	0.5	1.0	.009	3.0	2.7	.073
		4	.08	4.4	0.5	3.7	.009	3.0	2.7	.073
		6	.05	4.4	0.5	3.7	.009	3.0	2.7	.073
		8	.05	4.4	0.5	3.7	.009	3.0	2.7	.073
		3	.04	4.4	0.5	3.7	.009	3.0	2.7	.073
		5	.04	4.4	0.5	5.0	.009	3.0	2.7	.073
		7	.05	4.4	0.5	3.7	.009	3.0	2.7	.073
		9	.04	4.4	0.5	3.7	.009	3.0	2.7	.073
3	H080	2	.05	4.4	0.5	3.7	.009	3.0	2.7	.073
		4	.05	4.4	0.5	3.7	.004	3.0	2.7	.073
		6	.05	4.4	0.5	3.7	.008	3.0	2.7	.073
		8	.07	4.4	0.5	3.7	.01	3.0	2.7	.073
		3	.03	4.4	0.5	3.7	.04	3.0	2.7	.073
		5	.035	4.4	0.5	3.7	.02	4.0	2.7	.073
		7	.05	4.4	0.5	3.7	.004	3.0	2.7	.073
		9	.05	4.4	0.5	3.7	.009	3.0	2.7	.073
Test Average k Values										
1	I1		.054	4.4	0.5	3.88	.009	3.0	2.7	.073
2	H060		.053	4.4	0.5	3.53	.009	3.0	2.7	.073
3	H080		.048	4.4	0.5	3.70	.01	3.13	2.7	.073
		Site Average	.052	4.4	0.5	3.70	.01	3.04	2.7	.073

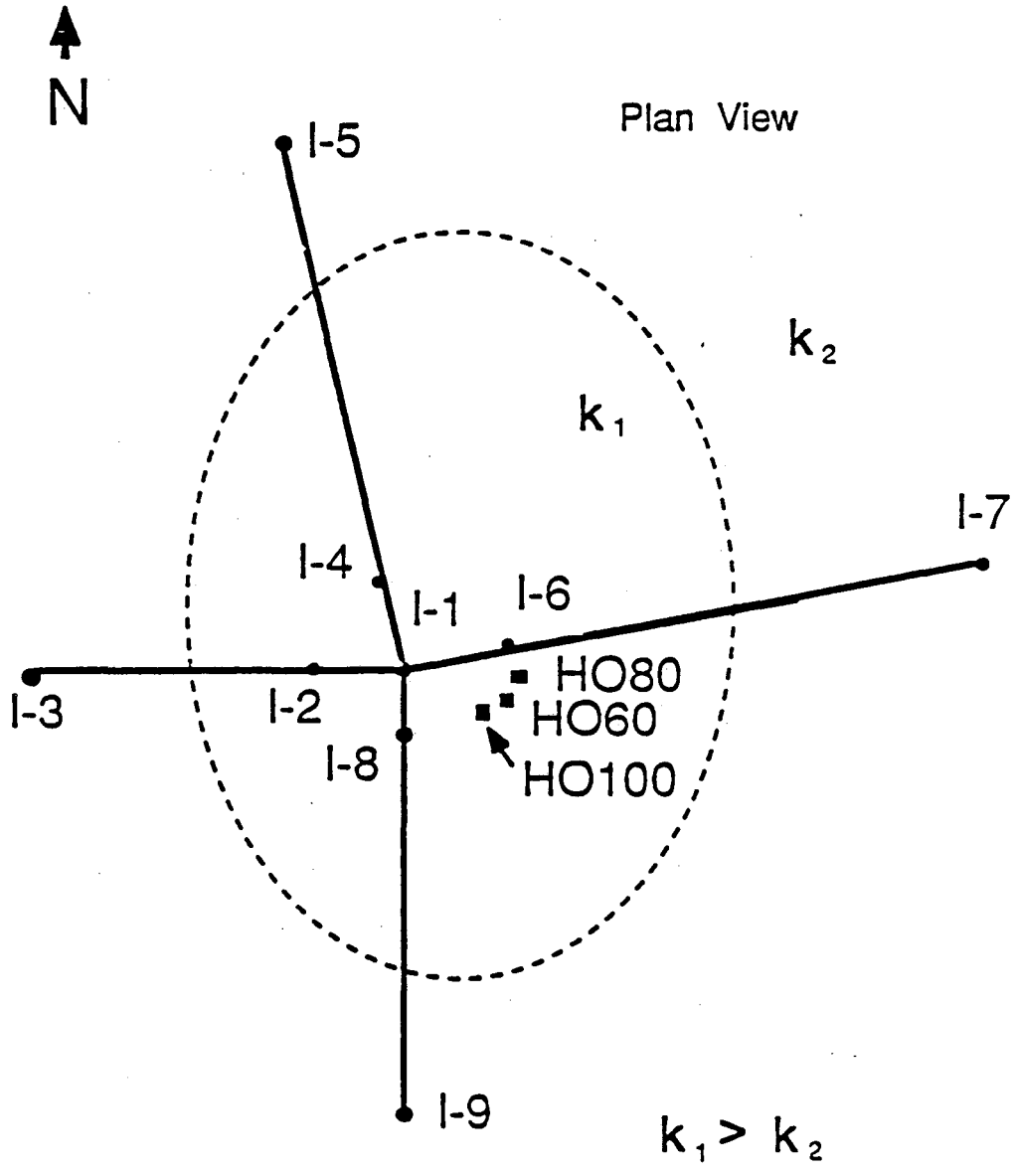


Figure 6.9 Schematic plan view of Layer 2 showing approximate location of the two permeable regions, 21 and 22.

value of this layer is 1.0×10^{-13} m^2 (1.1×10^{-12} ft^2).

Constant permeability values were found for Layers 5, 6, and 7 which would work in the reservoir model for all three interference test simulations. Layer 5 has a value of 3.0×10^{-11} m^2 (3.2×10^{-10} ft^2), Layer 6 has a value of 2.7×10^{-11} m^2 (2.9×10^{-10} ft^2), and Layer 7 has a value of 5.3×10^{-13} m^2 (5.7×10^{-12} ft^2). Layer 7 represents the bottom confining layer of the aquifer system and is considered an impermeable boundary. Adjusting the permeability of Layer 7 by plus or minus an order of magnitude does not influence the simulated pressure response curve. Therefore, the value used was the one obtained from the analysis of the single-well test for Well HO100 and was not adjusted throughout the simulations.

6.2.3 Results from Pulse Tests

Unlike the analytical method of analyzing the pulse test data, each pulse did not need to be numerically analyzed separately. A series of pulses recorded at an observation well could be analyzed together if they were generated at the same production well using a constant flow rate Q. The curve matching technique, however, did not work as well for the pulse tests as it did for the interference tests, in that the the curves did not match as well. The best matches were taken and the resulting permeability values are shown in Table 6.7. Reasonable matches for Test 7 were not found and, therefore, permeability values were not presented.

Tests 1, 2, and 3 were averaged together in Table 6.7 since these tests were all conducted from the same production well with the same flow rate. The average permeability values for each observation well are given. The results were summarized in Table 6.8 which shows the test averages and the arithmetic mean of all eight tests.

A summary of the permeability values obtained from the numerical analysis of the transient pump test data is provided in Table 6.9.

Table 6.7. Permeability results from the numerical analysis of the pulse test data.

Test	Production Well	Observation Well	Pulse Average k $\times 10^{-11}$ (m^2)							
			Sedimentary Units							
			1	21	22	3	4	5	6	7
1,2,3	I1	2	0.071	4.4	0.5	3.7	0.009	3.0	2.7	0.073
		4	0.128	4.4	0.5	3.7	0.009	3.0	2.7	0.073
		6	0.058	4.4	0.5	3.7	0.009	3.0	2.7	0.073
		8	0.065	5.1	0.5	5.4	0.009	3.0	2.7	0.073
4		3	0.150	4.4	0.5	3.7	0.009	3.0	2.7	0.073
		5	--	--	--	--	--	--	--	--
		7	0.045	4.4	0.5	3.7	0.009	3.0	2.7	0.073
		9	0.045	4.4	0.5	3.7	0.009	3.0	2.7	0.073
5	HO60	2	0.045	4.4	0.5	3.7	0.009	9.0	2.7	0.073
		4	--	--	--	--	--	--	--	--
		6	0.045	4.4	0.5	3.7	0.009	3.0	2.7	0.073
		8	0.045	4.4	0.5	3.7	0.009	3.0	2.7	0.073
6		3	0.045	4.4	0.5	3.7	0.009	1.0	2.7	0.073
		5	0.045	4.4	0.5	3.7	0.009	9.0	2.7	0.073
		7	0.045	4.4	0.5	3.7	0.009	3.0	2.7	0.073
		9	0.045	4.4	0.5	5.0	0.009	5.0	2.7	0.073
7	HO80	2	--	--	--	--	--	--	--	--
		4	--	--	--	--	--	--	--	--
		6	--	--	--	--	--	--	--	--
		8	--	--	--	--	--	--	--	--
8		3	0.030	4.4	0.5	4.0	0.009	3.0	2.7	0.073
		5	--	--	--	--	--	--	--	--
		7	0.200	4.4	0.5	3.7	0.009	3.0	2.7	0.073
		9	0.050	4.0	0.5	3.7	0.009	3.0	2.7	0.073

Table 6.8. Summary of the numerical permeability results of pulse tests.

Test	Production Well	Pulse Average $k \times 10^{-11}$ (m^2)							
		Sedimentary Units							
		1	21	22	3	4	5	6	7
1,2,3	I1	0.081	4.6	0.5	4.1	0.009	3.0	2.7	0.073
4		0.080	4.4	0.5	3.7	0.009	3.0	2.7	0.073
5	HO60	0.045	4.4	0.5	3.7	0.009	5.0	2.7	0.073
6		0.045	4.4	0.5	4.0	0.009	4.5	2.7	0.073
7	HO80	–	–	–	–	–	–	–	–
8		0.09	4.3	0.5	3.8	0.009	3.0	2.7	0.073
1-8	I1,HO60,HO80	0.068	4.4	0.5	3.9	0.009	3.7	2.7	0.073

Table 6.9 Summary of the permeability results obtained from the numerical analysis of the transient test data.

Pump Test	$k \times 10^{-11}$ (m^2) Sedimentary Units							
	1	21	22	3	4	5	6	7
Single-Well Transient	0.040	4.4	0.5	3.7	0.007	3.0	2.1	0.073
Interference	0.052	4.4	0.5	3.7	0.010	3.0	2.7	0.073
Pulse	0.068	4.4	0.5	3.9	0.009	3.7	2.7	0.073

7.0 COMPARISON OF NUMERICAL AND ANALYTICAL RESULTS

The results from the analytical analyses of the pumping test data are presented in this chapter in order to compare with the the results obtained from the numerical analysis and which were presented in the last chapter. The analytical results will include the hydrologic values obtained from the single-well transient tests, interference tests, and pulse tests. A discussion and comparison of the numerical and analytical results and an evaluation of the methods used for analysis will be presented.

7.1 RESULTS OF THE ANALYTICAL ANALYSES

Throughout the analytical analyses, certain parameters remained constant. For every analysis, the fluid viscosity μ is equal to 10^{-3} kg/m·s (1 cp), the fluid density ρ is equal to 1000 kg/m^3 (1.94 slugs/ft^3), and the acceleration due to gravity g is equal to 9.8 m/s^2 (32.2 ft/s^2).

7.1.1 Single–Well Transient and Interference Test Results

The analytical method used in analyzing the single-well transient and the interference tests is the leaky aquifer type-curve method which was explained in Chapter 5, Section 5.2.2. The permeability k and the specific storage S_s of the aquifer is solved for by using Eq. 5.8:

$$k = \frac{Q\mu P_D}{2\pi H \Delta P} \qquad S_s = \frac{k\rho g}{\mu t_D}\left[\frac{t}{r^2}\right] \tag{5.8}$$

The permeability k′ of the leaky aquitard above the aquifer is solved for by using Eq. 3.23:

$$k' = \frac{kHH'}{B^2} \qquad \text{where} \qquad B^2 = \left[\frac{r}{r/B}\right]^2 \tag{3.23}$$

The values for dimensionless pressure P_D and change in pressure ΔP are obtained from the type-curve "match points". Q is equal to 6.0×10^{-3} m^3/s (95 gpm) for Test 1, 5.0×10^{-3} m^3/s (79 gpm) for Test 2, and 5.5×10^{-3} m^3/s (87 gpm) for Test 3. The thickness of the aquifer H is assumed to be equal to 18.3 m (60 ft) and the thickness of the aquitard H′ is equal to 6.1 m (20 ft). The value for r/B is taken off of the leaky type-curves. The radius r is equal to the well radius for the single-well tests and is equal to the distance from the production well to the observation well for the interference tests.

The hydrologic parameters obtained from the single-well transient tests are presented in Table 7.1. Matching the field data to the leaky aquifer type-curves was very subjective (see Figures 7.1-7.3). The permeability values of the aquifer obtained from the leaky aquifer type-curve analysis are much smaller (as much as an order of magnitude lower) than the values obtained by numerical analysis. The specific storage S_s values are much higher (almost as much as two orders of magnitude) than the value used in numerical simulations. The value used in numerical simulations was kept at a constant value of $S_s = \rho g n(\alpha + \beta) = 3.1\times10^{-5}$ m^{-1} (9.3×10^{-6} ft^{-1}).

Table 7.1. Analytical results of the single-well transient test data.

Test	Well	$k \times10^{-11}$ (m^2)	$S_s \times10^{-5}$ (m^{-1})	r/B	B^2 (m^2)	$k' \times10^{-11}$ (m^2)
1	I1	0.83	57.0	0.01	25.0	3.7
2	HO60	0.16	950.0	0.20	0.1	290.0
3	HO80	0.34	1100.0	0.04	1.6	24.0

The worst problem with the analysis of the single-well tests using the leaky aquifer type-curve method is that the permeability values of the aquitard are higher than those obtained for the aquifer. The permeability values obtained for the aquitard were very sensitive to the value of r/B because of the small radius value used ($r = r_w = 0.05$ m). Overall, the analysis of the single-well transient data using the leaky aquifer type-curve method was unreliable.

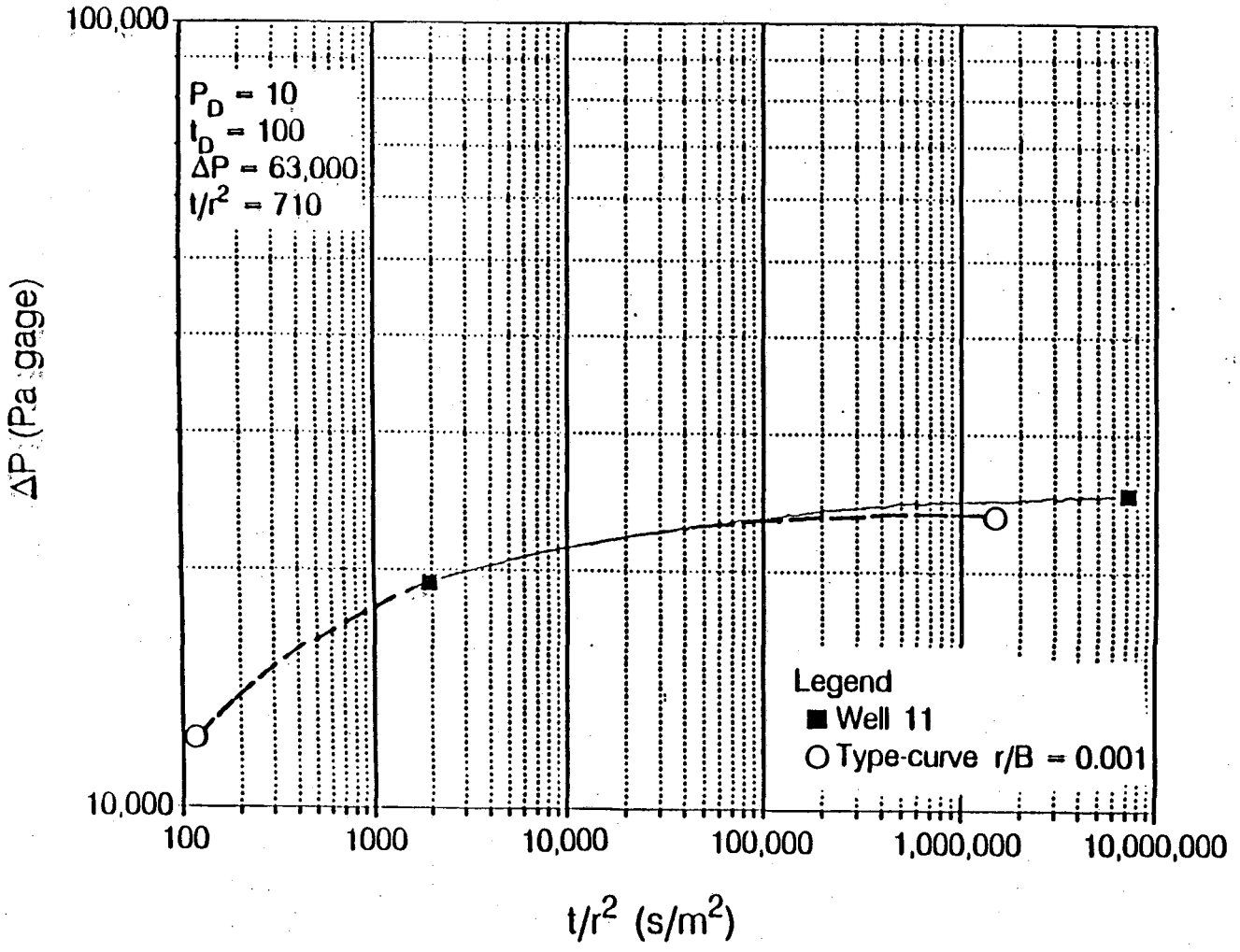


Figure 7.1 Match of Single-Well Transient Test 1 field data to leaky aquifer type -curve showing "match points" P_D, t_D, ΔP, and t/r^2.

XBL 8812-10593

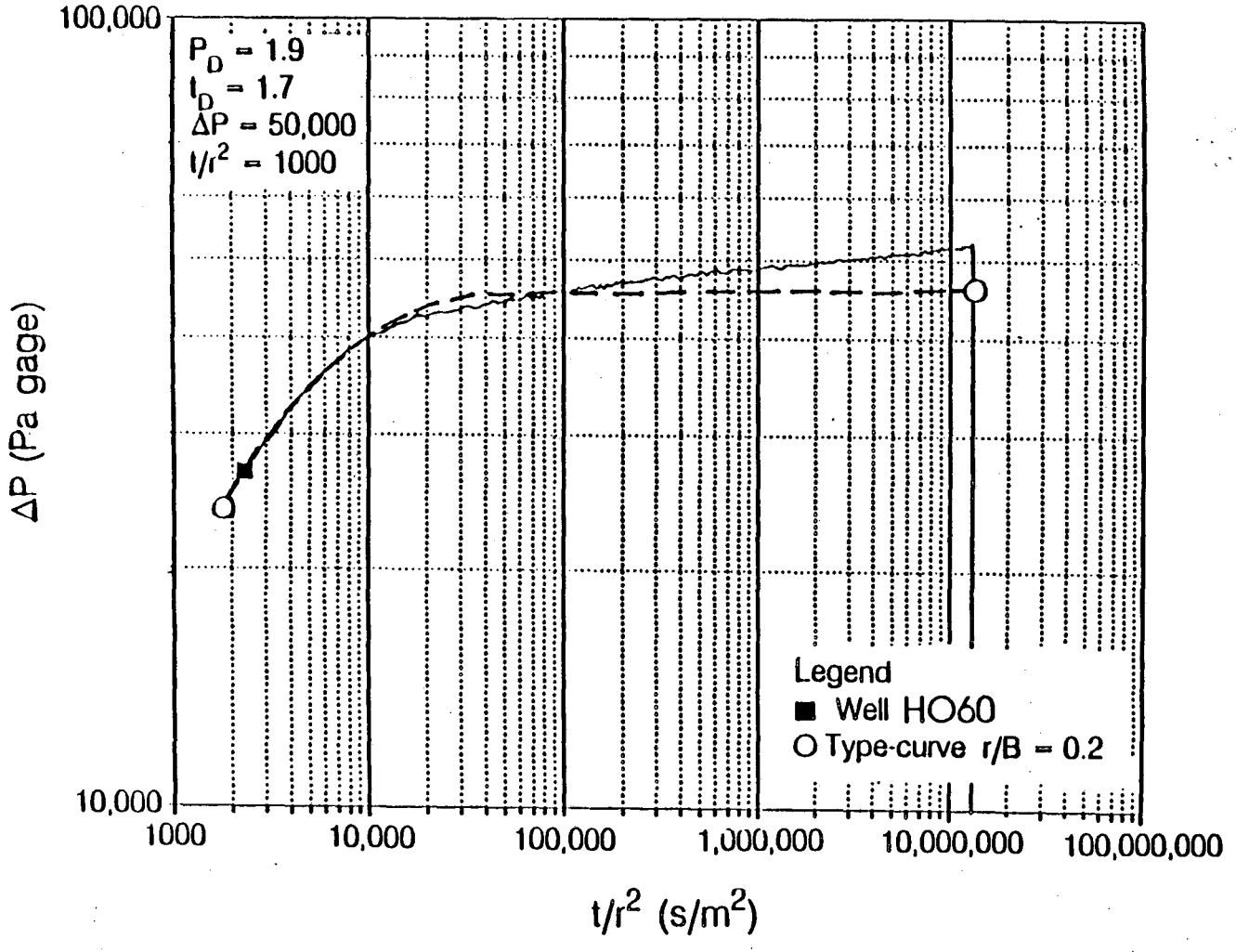
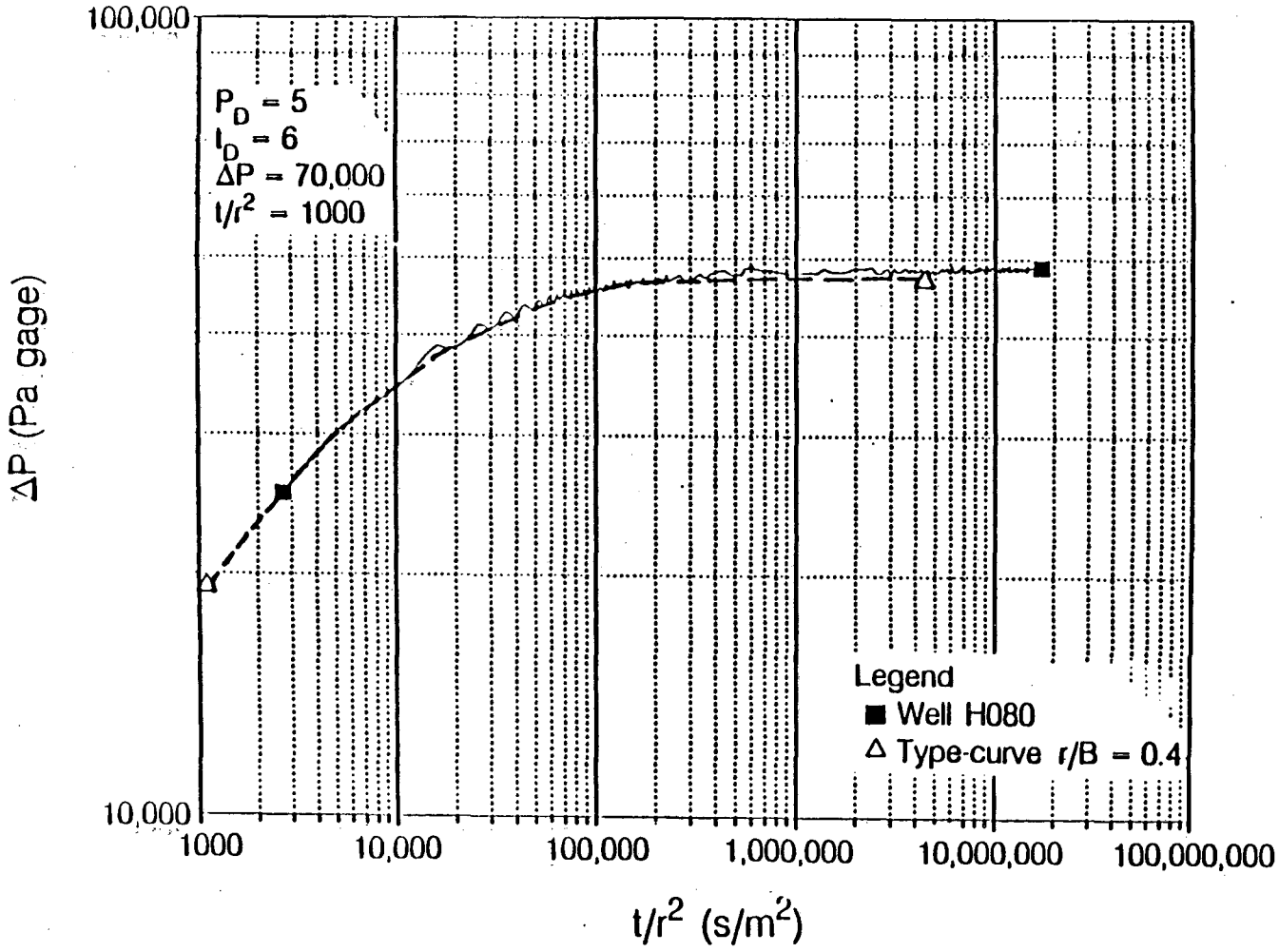


Figure 7.2 Match of Single-Well Transient Test 2 field data to leaky aquifer type-curve showing "match points" P_D, t_D, ΔP, and t/r^2.

XBL 8812-10592



XBL 8812-10591

Figure 7.3 Match of Single-Well Transient Test 3 field data to leaky aquifer type -curve showing "match points" P_D, t_D, ΔP, and t/r^2.

The hydrologic parameters obtained from the interference tests are presented in Table 7.2. The Well permeability values refers to the values obtained for each individual observation well while pumping one of the production wells. The Well permeability values were then grouped into the values obtained from the inner and outer radius regions of the LBLI/HO Site. These values are called the Region Average permeabilities and are the arithmetic mean of the Well values in that region. The Test Average then refers to the arithmetic mean permeability obtained from all eight obser-

Table 7.2. Analytical permeability results of the interference test data.

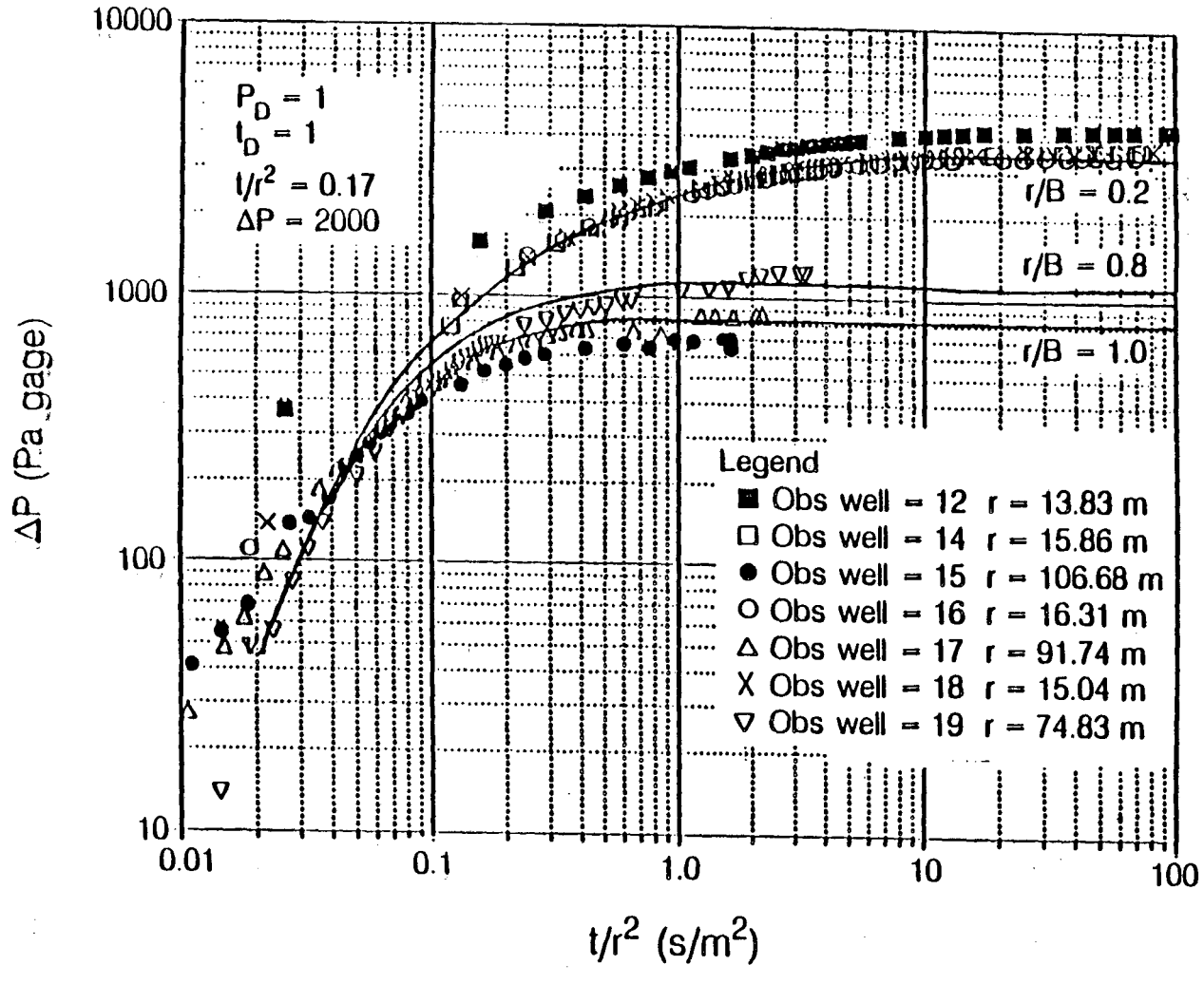
Test	Production Well	Observation Well	Well k $\times 10^{-11}$ (m^2)	Region Average k $\times 10^{-11}$ (m^2)	Test Average k $\times 10^{-11}$ (m^2)	Specific Storage (m^{-1})	r/B	B^2 (m^2)	Aquitard k $\times 10^{-11}$ (m^2)
1	I1	2	2.61	2.61	2.61	4.3×10^{-5}	0.2	4782.0	0.0609
		4	2.61			4.3×10^{-5}	0.2	6288.0	0.0463
		6	2.61			4.3×10^{-5}	0.2	6642.0	0.0439
		8	2.61			4.3×10^{-5}	0.2	5663.0	0.0514
		3	--	2.61		--	--	--	--
		5	2.61			4.3×10^{-5}	1.0	11381.0	0.0256
		7	2.61			4.3×10^{-5}	1.0	8416.0	0.0346
		9	2.61			4.3×10^{-5}	0.8	8749.0	0.0333
2	HO60	2	3.85	2.88	3.36	1.1×10^{-4}	0.2	19838.0	0.0217
		4	2.55			8.4×10^{-5}	0.5	3162.0	0.09
		6	2.55			8.4×10^{-5}	0.2	392.0	0.726
		8	2.55			8.4×10^{-5}	0.2	2672.0	0.107
		3	3.85	3.85		1.1×10^{-4}	0.6	15620.0	0.0275
		5	3.85			1.1×10^{-4}	1.0	14130.0	0.0304
		7	3.85			1.1×10^{-4}	0.7	13729.0	0.0313
		9	3.85			1.1×10^{-4}	0.5	17577.0	0.0245
3	HO80	2	1.91	2.42	3.60	1.5×10^{-4}	0.8	1415.0	0.151
		4	3.18			6.5×10^{-4}	0.6	1911.0	0.186
		6	1.59			4.2×10^{-3}	0.8	45.0	3.944
		8	2.98			4.4×10^{-4}	0.4	1395.0	0.238
		3	3.82	4.78		4.9×10^{-5}	0.6	16658.0	0.0257
		5	5.97			6.4×10^{-5}	0.6	38051.0	0.0175
		7	5.19			1.2×10^{-4}	0.6	16891.0	0.0343
		9	4.15			9.4×10^{-4}	0.6	13889.0	0.0334

vation wells (seven observation wells for Test 1 due to unreliable data from Observation Well I3) for each interference test. After the field pressure response was matched to a leaky type-curve and a value for r/B was obtained, B^2 was determined and used in solving for the permeability of the aquitard. The aquitard permeabilities are given for each set of observation well data. Figures 7.4 through 7.14 show the type-curve matches for the interference test data.

The pressure response data for Test 1 were analyzed together since the data points all more or less fall on the same base curve. The base curve mentioned here is considered to be the type-curve of the aquifer if leakage was not present. The same "match point" was used for every set of well data in Test 1 and, therefore, the same aquifer permeability values were obtained. The pressure response data of Test 2 were analyzed on two separate base curves, whereas, the pressure response data of Test 3 were each analyzed separately since not one of the pressure response curves fell on the same base curve. The arithmetic mean permeability value for the aquifer from all three interference tests is equal to 3.19×10^{-11} m^2 (3.43×10^{-10} ft^2).

The inner Region Average for each test, unlike the results from the numerical analysis, is slightly lower than the outer Region Average. Numerical simulations have shown that the interference pump test data can be matched using a composite aquifer model in which the outer region of Layer 2 has a lower permeability than the inner region. Assuming that the numerical model of the aquifer system is the most accurate, it can be seen that the values obtained from type-curve analysis of the interference tests over-estimate the permeability values of the outer region.

The permeability values of the leaky aquitard varied widely for all three tests. The values obtained for Test 1 are probably the most accurate, though, because the screened interval of Well I1 is the closest to the aquitard. The arithmetic mean permeability of the aquitard for Test 1 is 4.23×10^{-13} m^2 (4.55×10^{-12} ft^2). This value agrees well with the values obtained from numerical simulations. The arithmetic mean for k' from all three tests is 2.6×10^{-12} m^2 (2.8×10^{-11} ft^2).



XBL 8812-10595

Figure 7.4 Match of Interference Test 1 field data to leaky aquifer type-curve showing "match points" P_D, t_D, ΔP, and t/r^2.

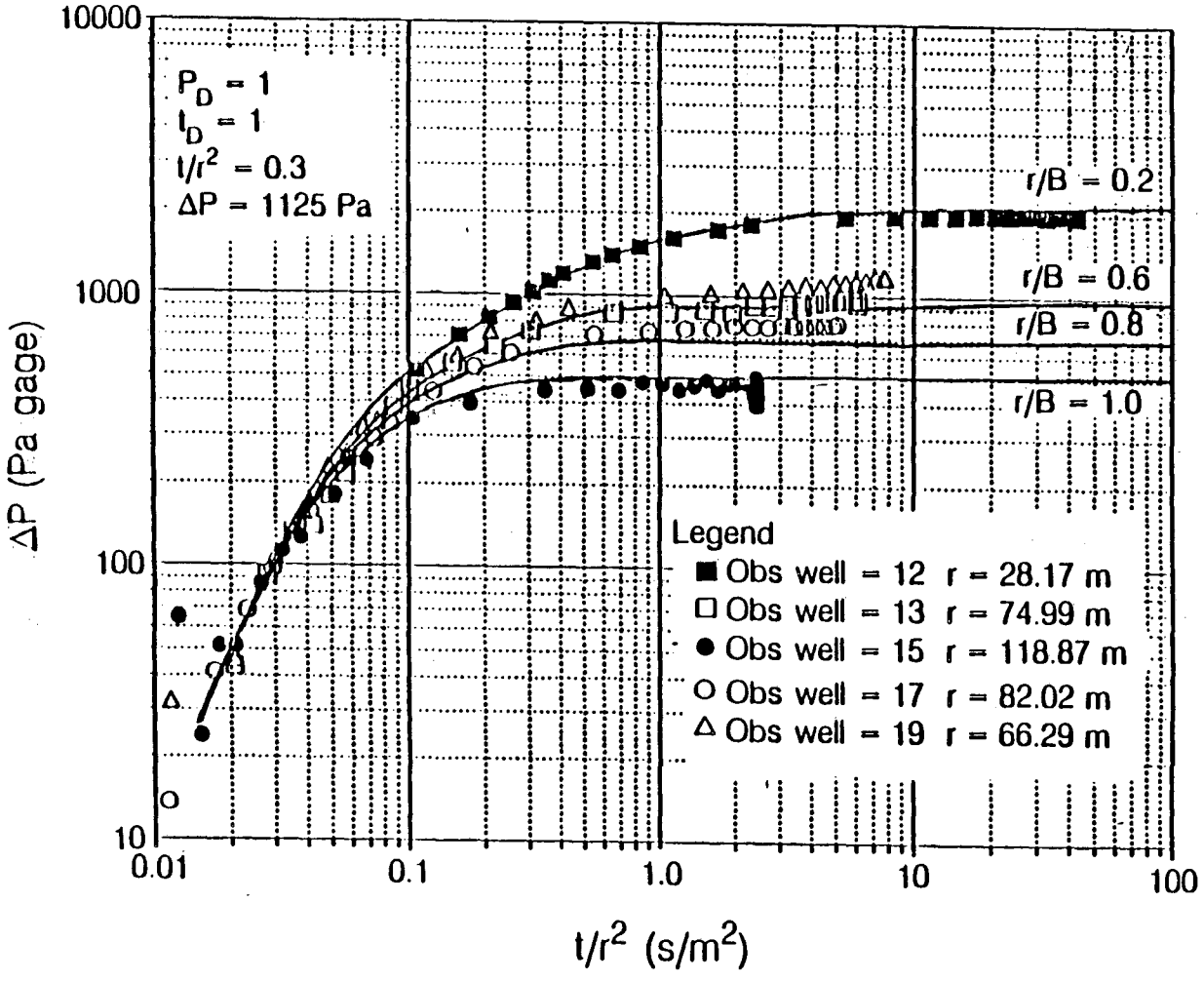


Figure 7.5 Match of Interference Test 2 field data from Observation Wells I2, I3, I5, I7, and I9 to leaky aquifer type-curve showing "match points" P_D, t_D, ΔP, and t/r^2.

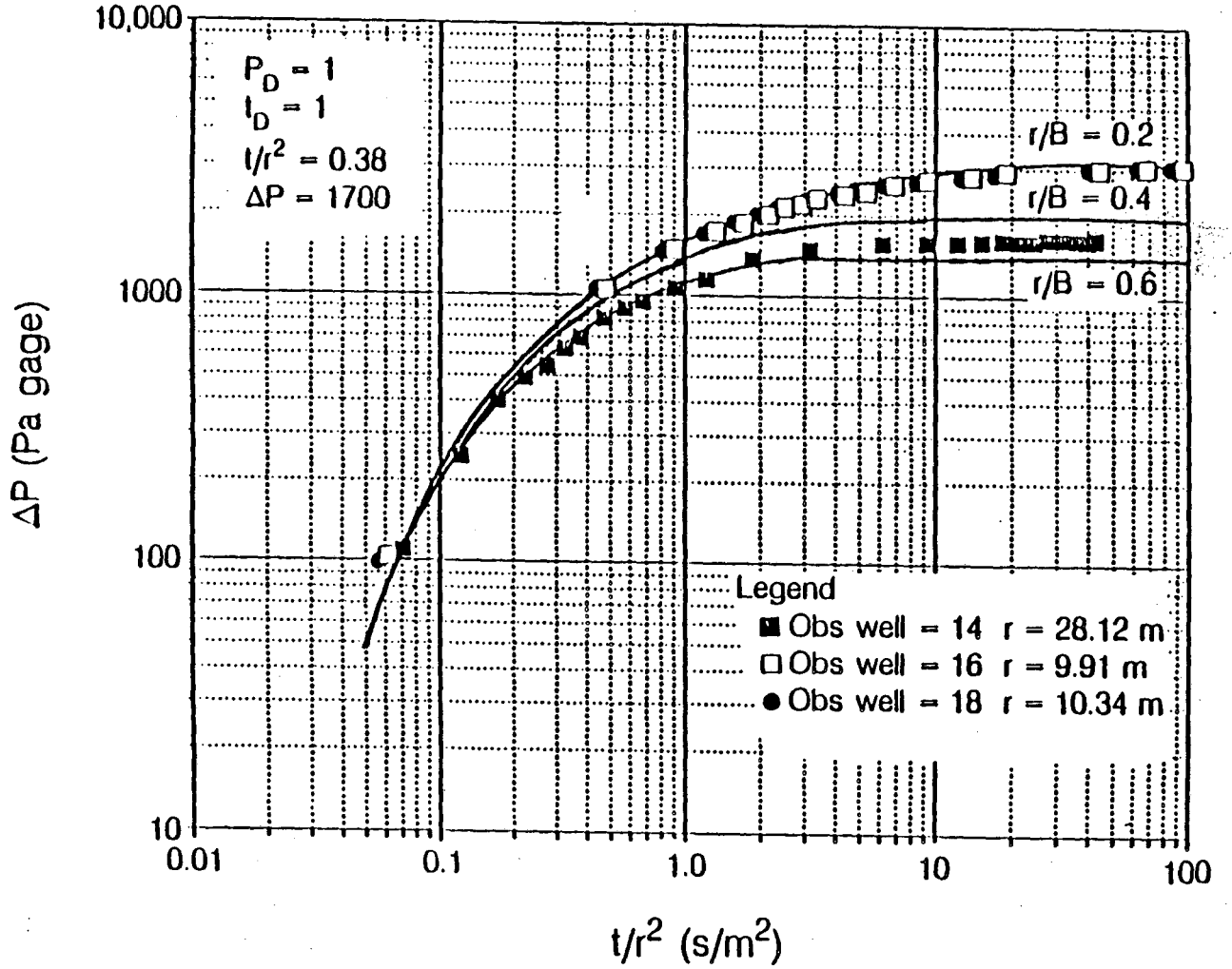


Figure 7.6 Match of Interference Test 2 field data from Observation Wells I4, I6, and I8 to leaky aquifer type-curve showing "match points" P_D, t_D, ΔP, and t/r^2. XBL 8812-10594

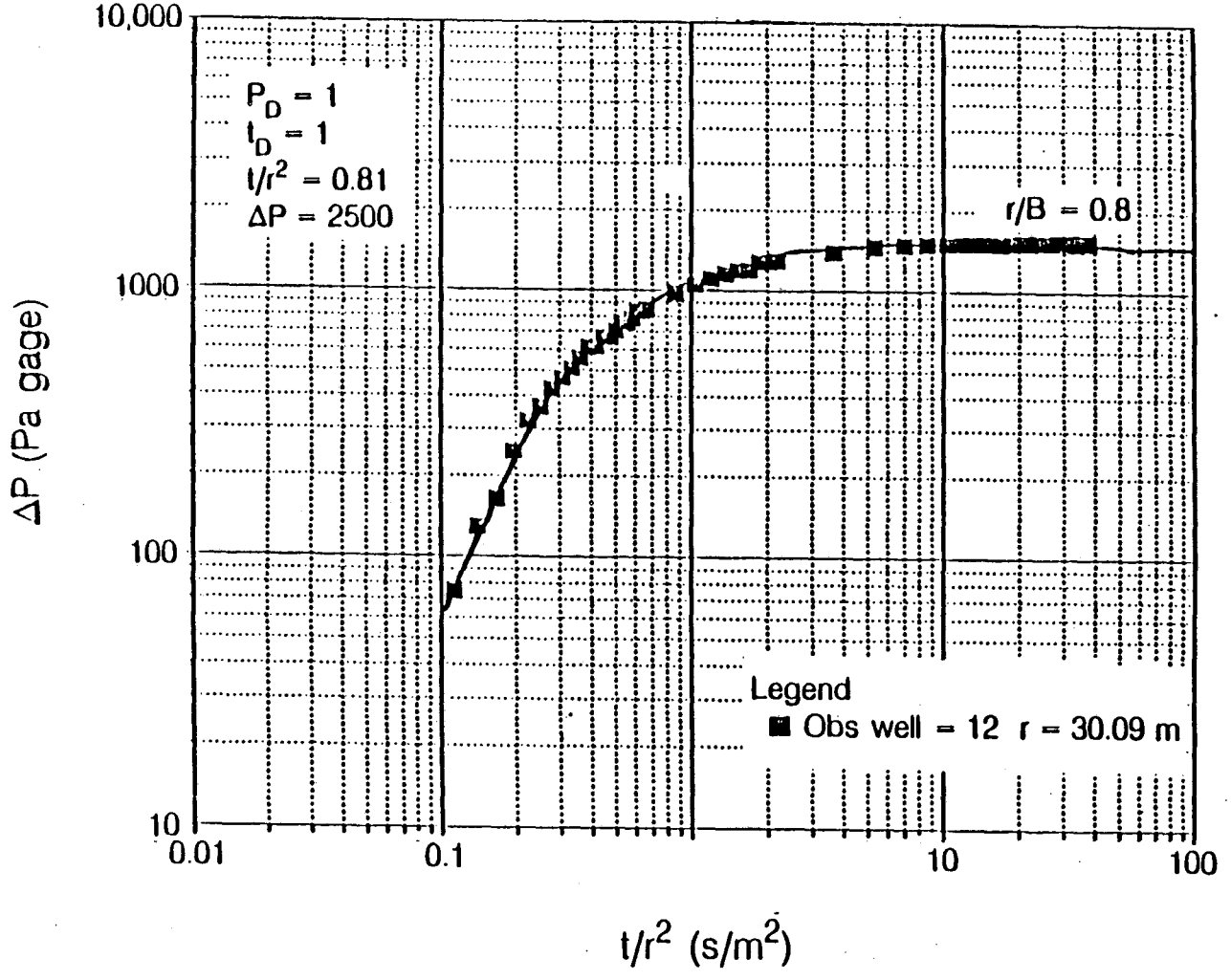
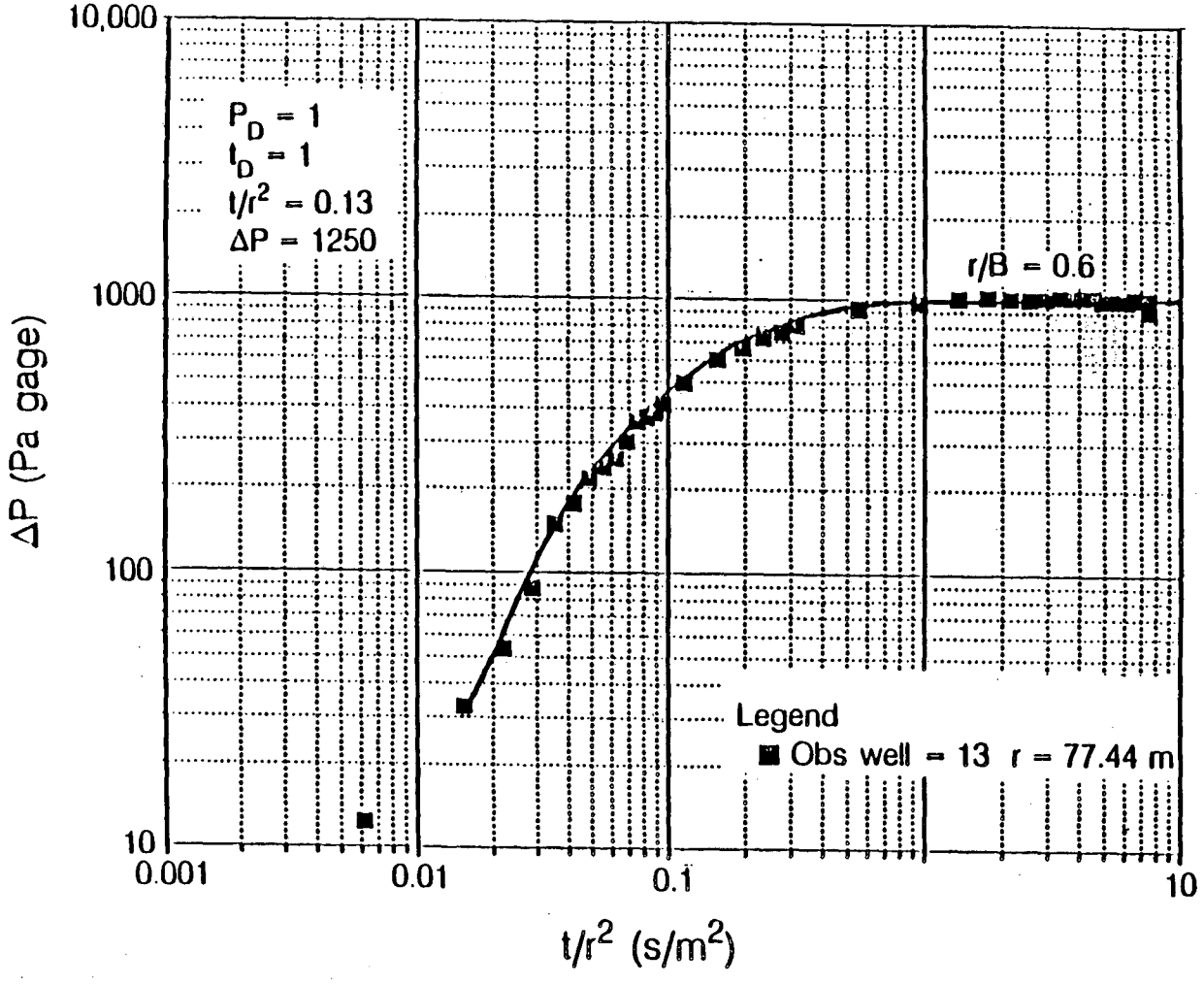


Figure 7.7 Match of Interference Test 3 field data from Observation Well I2 to leaky aquifer type-curve showing "match points" P_D, t_D, ΔP, and t/r^2.

XBL 8812-10587



XBL 8812-10586

Figure 7.8 Match of Interference Test 3 field data from Observation Well I3 to leaky aquifer type-curve showing "match points" P_D, t_D, ΔP, and t/r^2.

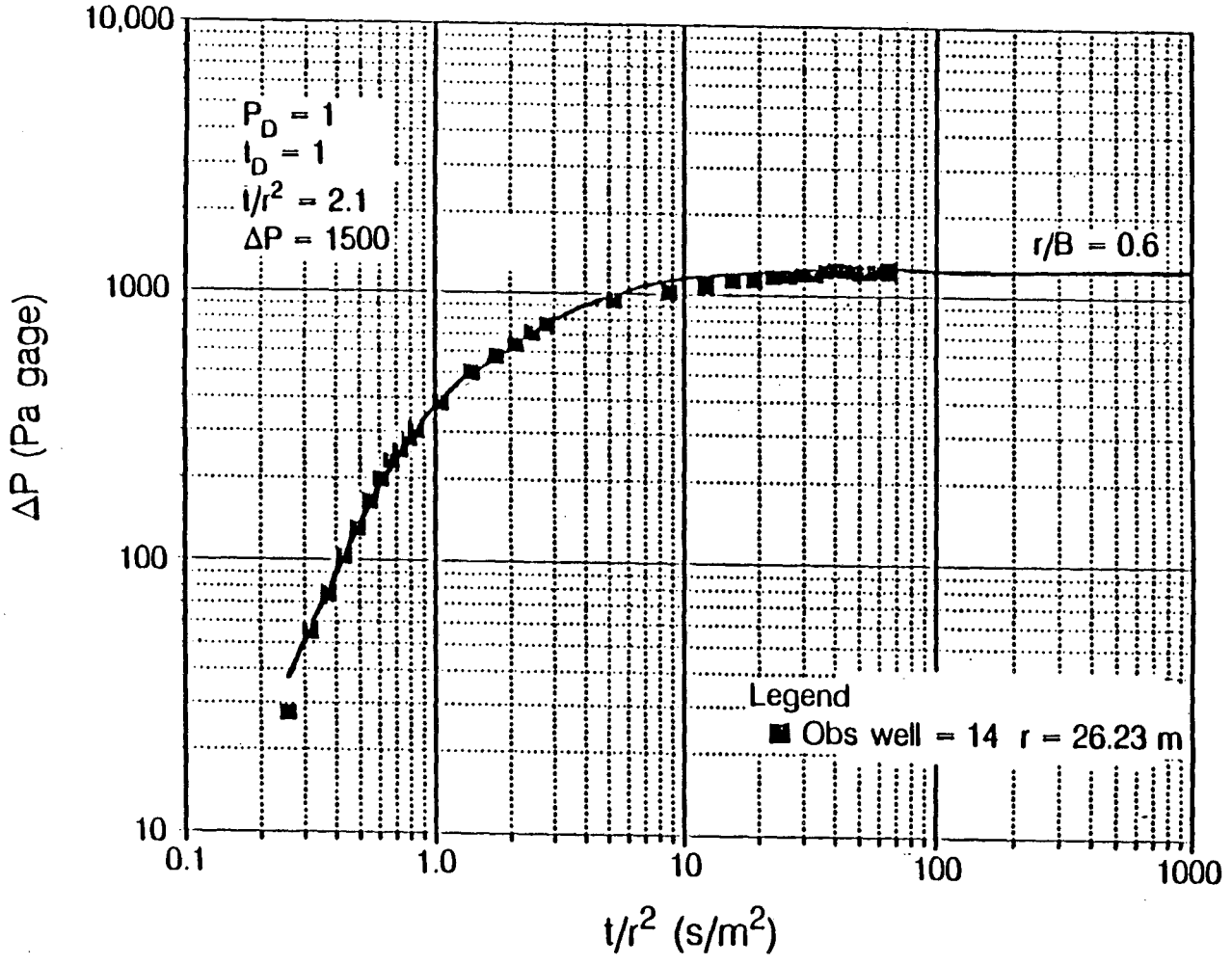
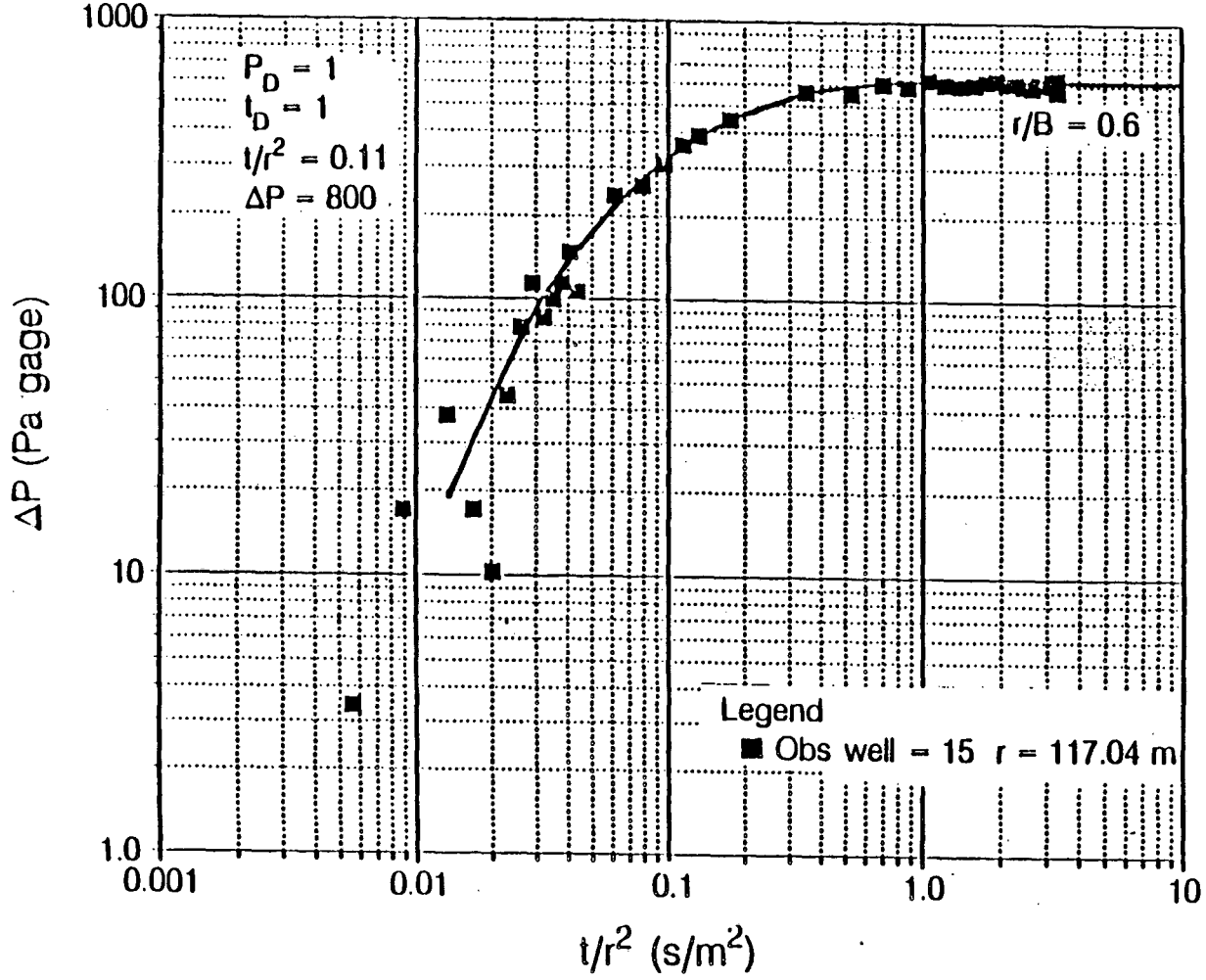


Figure 7.9 Match of Interference Test 3 field data from Observation Well I4 to leaky aquifer type-curve showing "match points" P_D, t_D, ΔP, and t/r^2.

XBL 8812-10585



XBL 8812-10584

Figure 7.10 Match of Interference Test 3 field data from Observation Well I5 to leaky aquifer type-curve showing "match points" P_D, t_D, ΔP, and t/r^2.

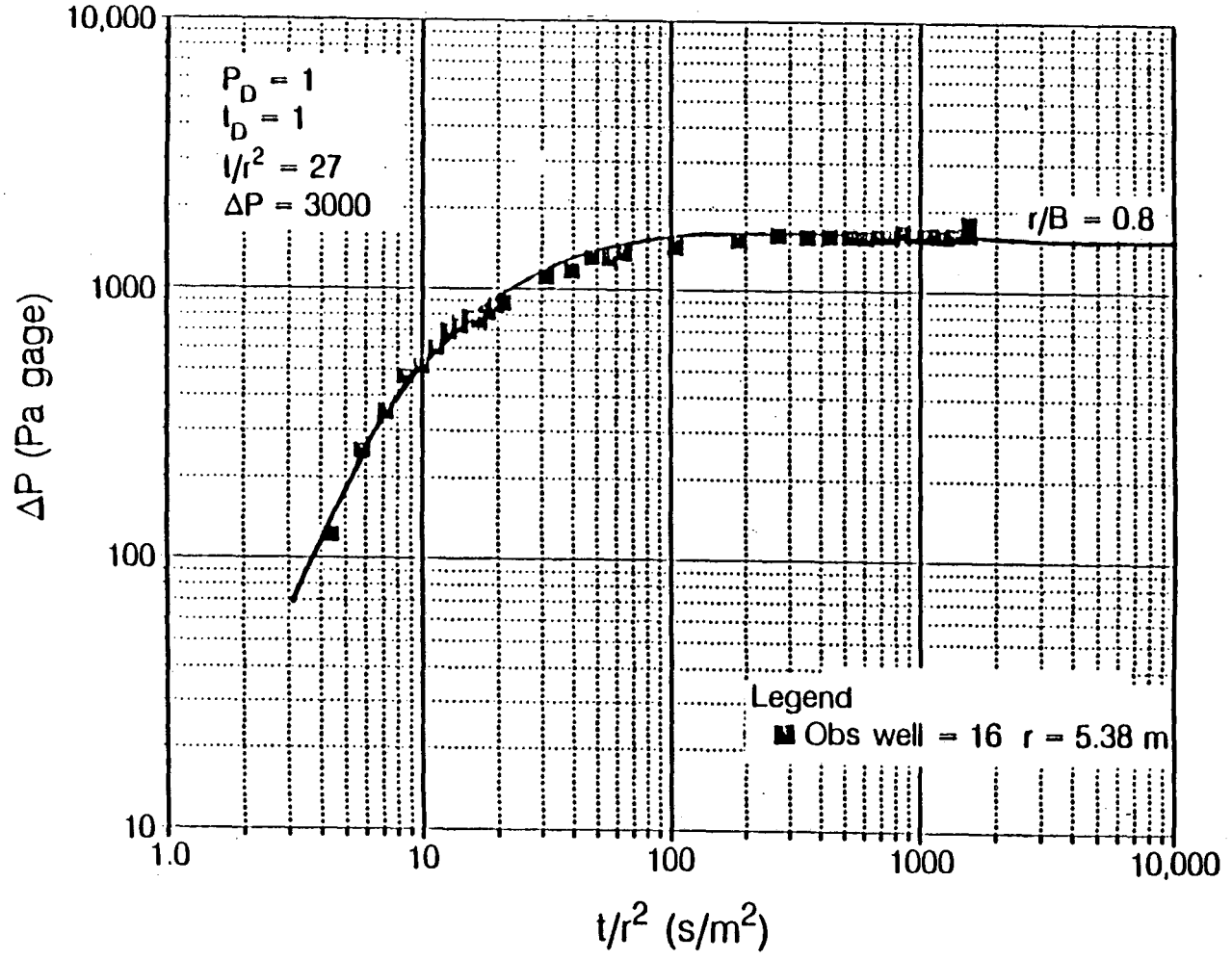
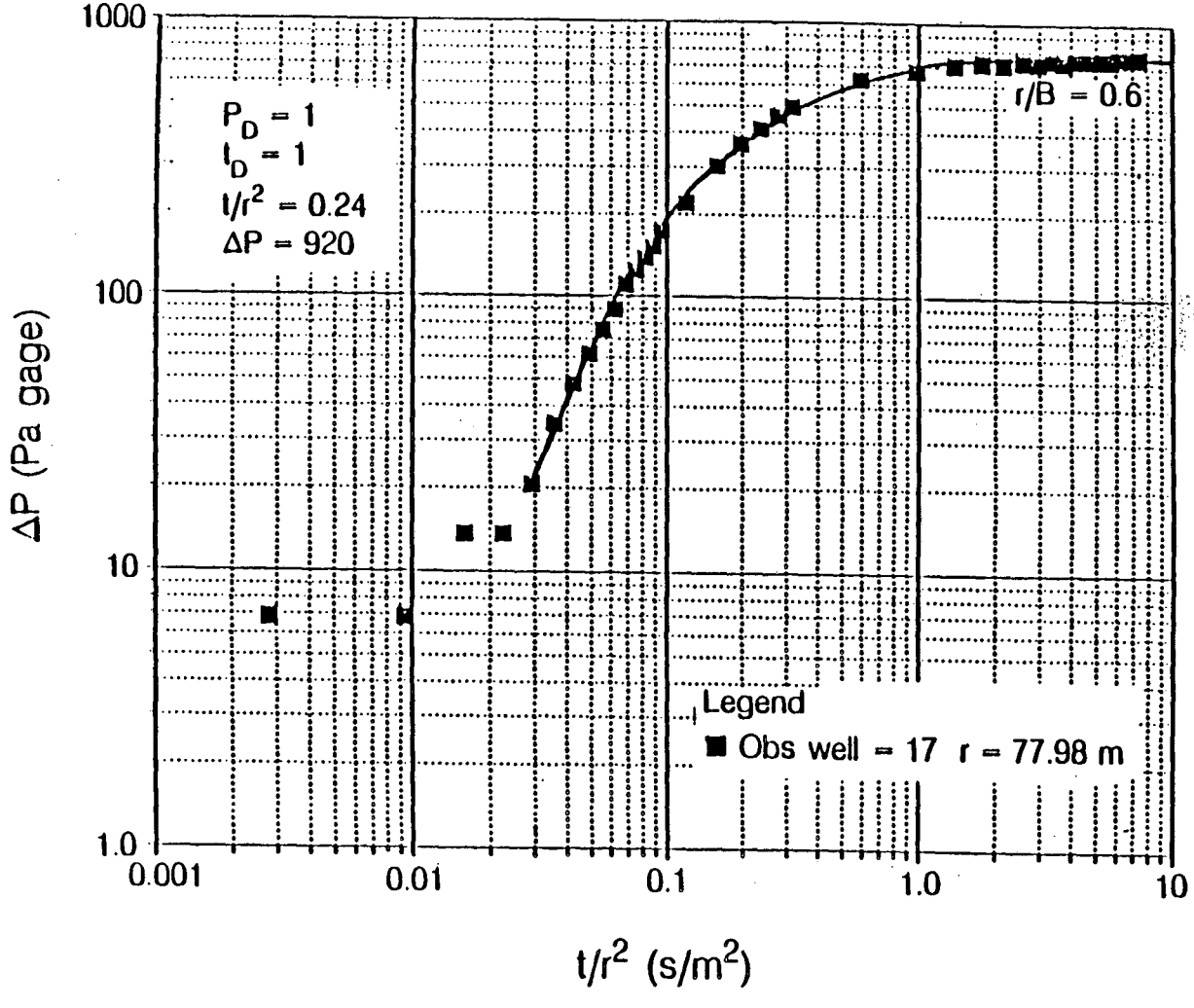


Figure 7.11 Match of Interference Test 3 field data from Observation Well I6 to leaky aquifer type-curve showing "match points" P_D, t_D, ΔP, and t/r^2.

XBL 8812-10583



XBL 8812-10590

Figure 7.12 Match of Interference Test 3 field data from Observation Well I7 to leaky aquifer type-curve showing "match points" P_D, t_D, ΔP, and t/r^2.

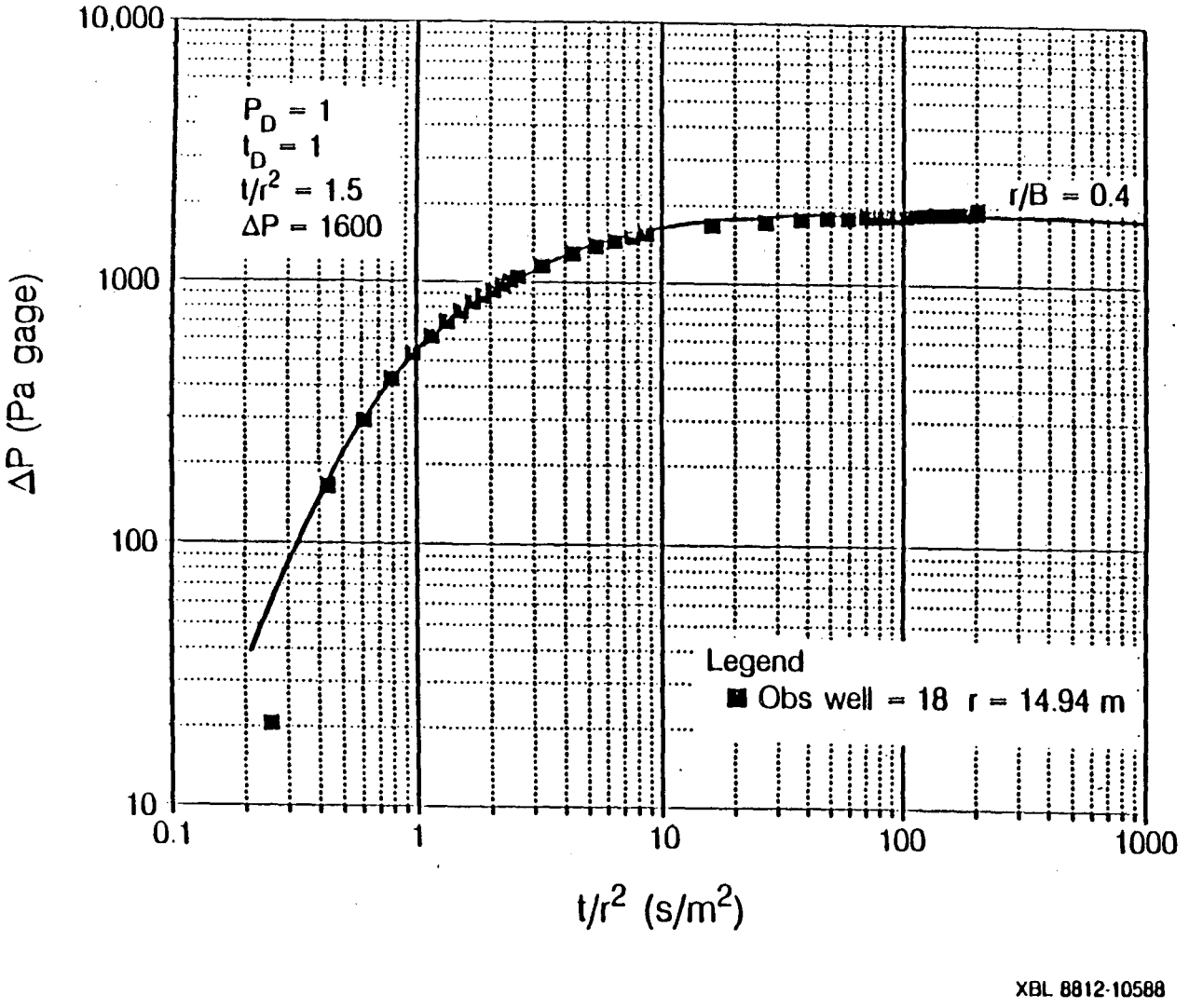
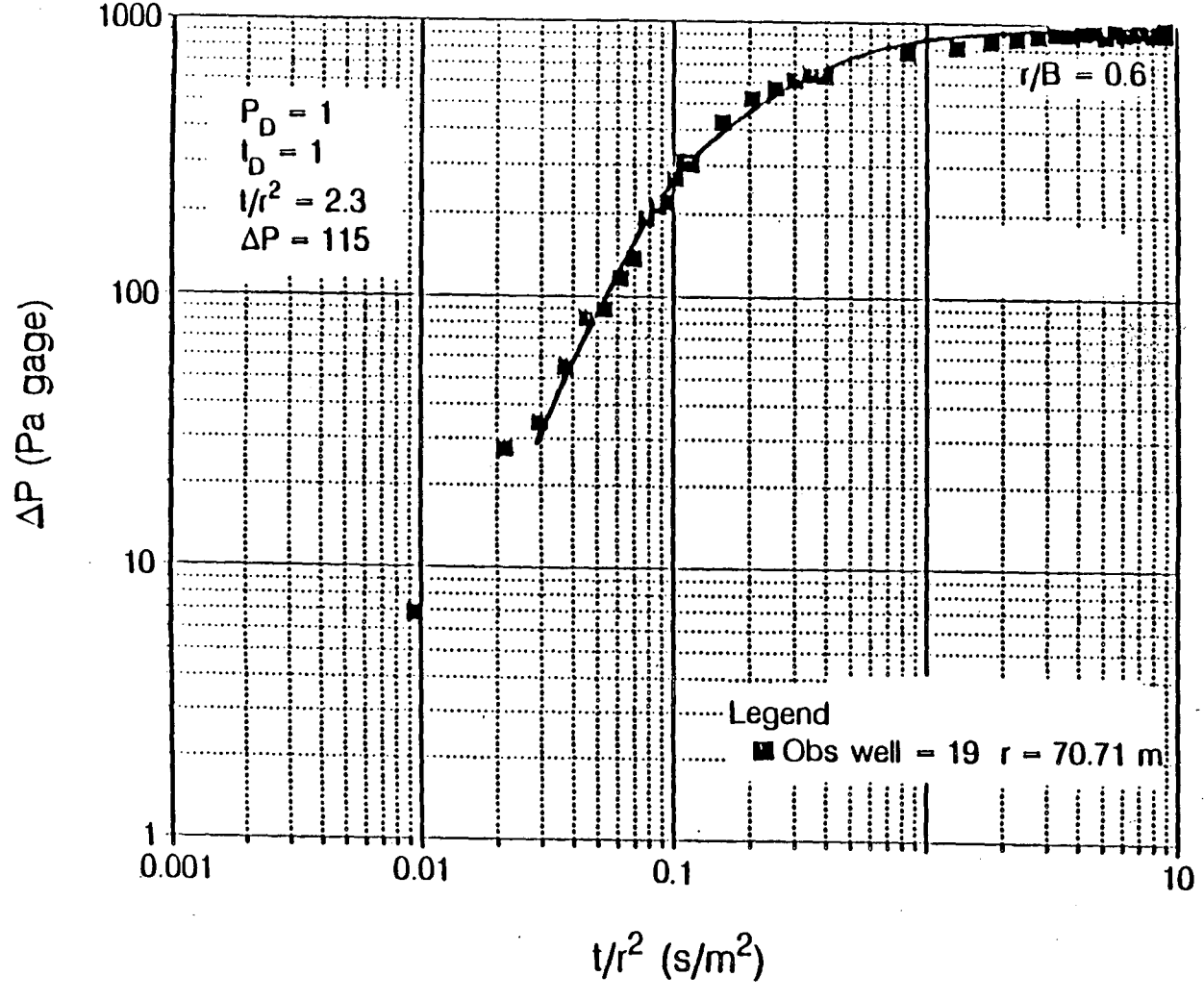


Figure 7.13 Match of Interference Test 3 field data from Observation Well I8 to leaky aquifer type-curve showing "match points" P_D, t_D, ΔP, and t/r^2.



XBL 8812-10589

Figure 7.14 Match of Interference Test 3 field data from Observation Well I9 to leaky aquifer type-curve showing "match points" P_D, t_D, ΔP, and t/r^2.

7.1.2 Pulse Tests Results

The analytical method used in analyzing the pulse test data was explained in Chapter 5, Section 5.2.3. The permeability k and the specific storage S_s of the aquifer is solved for by using Eqs. 5.16 and 5.17:

$$k = \frac{Q\mu}{4\pi H \Delta P_{max}} \left[W\left[\frac{r^2}{4\eta(t_p + t_{lag})}\right] - W\left[\frac{r^2}{4\eta t_{lag}}\right] \right] \qquad (5.16)$$

$$S = \frac{T}{\eta} = \frac{k\rho g H}{\mu\eta} \qquad S_s = \frac{k\rho g}{\mu\eta} \qquad (5.17)$$

Unlike the numerical method of analyzing sets of pulses together, each pulse has to be analyzed individually because of differing values of t_{lag} and ΔP_{max}. 84 pulses were analyzed individually using the analytical method. The results of this analysis are shown in Table 7.3. A series of pulses, obtained from the same observation well, are each analyzed individually and then the specific storage values and the permeability values are averaged together to obtain the Specific Storage and the Well Average. Tests 1, 2, and 3 were all generated at the same production well, I1, and measured at the same observation well, I2, and, therefore, were all averaged together.

For all eight tests, the inner Region Average is less than that of the outer Region Average. The inner region arithmetic average permeability is 3.28×10^{-11} m^2 (3.53×10^{-10} ft^2) while the outer region arithmetic average permeability is 6.55×10^{-11} m^2 (7.05×10^{-10} ft^2). This permeability zoning is in agreement with the analytical results of the interference tests but disagrees with the numerical results. Compared to the numerical results, this method of analysis overestimates the permeability value of the outer region sediments by more than an order of magnitude.

The specific storage S_s values for Tests 1 through 6 are somewhat consistent but they do not show the same trend as the permeability values of an inner and outer hydrologic region. These specific storage values are slightly smaller than the value used for numerical simulations. The values obtained from Tests 7 and 8 vary widely.

The arithmetic mean permeability of the total aquifer as determined from the analytical analysis of the pulse tests is equal to 4.96×10^{-11} m^2 (5.34×10^{-10} ft^2).

Table 7.3. Analytical permeability results of pulse tests.

Test	Production Well	Observation Well	Number of Pulses	Specific Storage $S_s \times10^{-5}$ (m^{-1})	Well Average $k \times10^{-11}$ (m^2)	Region Average $k \times10^{-11}$ (m^2)	Test Average $k \times10^{-11}$ (m^2)
1,2,3	I1	2	8	2.7	2.53	3.08	5.12
		4	8	5.9	2.89		
		6	8	3.7	3.56		
		8	8	3.2	3.34		
4		3	2	5.3	4.89	7.16	
		5	1	6.5	8.74		
		7	2	8.2	8.55		
		9	2	6.5	6.45		
5	HO60	2	7	4.2	4.07	3.33	4.42
		4	7	--	--		
		6	7	8.1	3.15		
		8	7	8.2	2.78		
6		3	1	4.8	4.44	5.50	
		5	1	--	--		
		7	1	6.4	5.94		
		9	1	5.8	6.12		
7	HO80	2	4	1.6	2.45	3.42	5.21
		4	4	97.0	6.45		
		6	4	330.0	2.45		
		8	4	43.0	2.31		
8		3	1	5.1	3.87	6.99	
		5	1	12.0	13.2		
		7	1	14.0	5.15		
		9	1	11.0	5.73		

7.2 DISCUSSION OF RESULTS

Table 7.4 summarizes the permeability information obtained from all of the pump tests and methods of analysis. The depth interval refers to the interval of aquifer for which information has been obtained. The top confining layer is located from 0-6.1 m (0-20 ft) below ground surface, the aquifer is located from 6.1-24.4 m (20-80 ft) below ground surface, and the bottom confining layer is located at 24.4-30.5 m (80-100 ft) below ground surface. The permeability-thickness product kH of the aquifer for each test is given in the last column.

The analytical analysis of the single-well steady-state tests does not yield any information for the depth interval from 0-6.1 m (0-20 ft), the leaky aquitard, because there wasn't a well available at this depth in which to conduct a test. Information from nine of the wells used for testing indicate that the sediments at a depth of 6.1-12.2 m (20-40 ft) are divided into two permeability regions, a higher-permeable inner radius region and a lower-permeable outer radius region. Table 7.4 presents both these values under the 6.1-12.2 m depth interval heading. The permeabilities of these two regions differ by as much as an order of magnitude. The permeabilities for the next three depth intervals were determined from a single well in each interval, therefore, these permeability results represent a very small portion of the sediments at these depth intervals. More information would be needed before accepting these results as accurate over a larger area.

The analytical analysis of the single-well transient tests yielded higher permeability values for the aquitard than for the aquifer. The calculations for the aquitard's permeability were very sensitive to the r/B value. The pressure response curves were difficult to match to a leaky aquifer type-curve because of a lack of early-time data. Because of this, the results obtained are considered unreliable.

The analytical method of analysis for the interference tests yielded an arithmetic mean permeability of 4.23×10^{-13} m^2 (4.5×10^{-13} ft^2) for the leaky aquitard if the

Table 7.4. Summary of permeability values obtained from pumping tests.

Method of Analysis	Type of Test	$k \times 10^{-11}(m^2)$ Depth Interval (m)					Aquifer $kH \times 10^{-10}$ (m^2)
		0.0-6.1	6.1-12.2	12.2-18.3	18.3-24.4	24.3-30.5	6.1-24.4
Analytical	Single-Well Steady-State	--	4.0/0.53	1.2	1.6	0.073	2.92
	Single-Well Transient	105.9	0.4	0.4	0.4	--	0.81
	Interference	0.042/0.07	3.19	3.19	3.19	--	5.84
	Pulse	--	4.92	4.92	4.92	--	8.99

		0.0-6.1	6.1-12.2	12.2-16.8	16.8-17.4	17.4-19.8	19.8-24.4	24.4-30.5	6.1-24.4
Numerical	Single-Well Transient	0.040	4.4/0.5	3.7	0.007	3.0	2.1	0.073	3.77
	Interference	0.045	4.4/0.5	3.7	0.009	3.0	2.7	0.073	3.99
	Pulse	0.045	4.4/0.5	3.9	0.009	4.0	2.7	0.073	4.43

values from only Test 1 are used and of 6.97×10^{-13} m^2 (7.54×10^{-12} ft^2) if the values from all three tests are used. The value obtained from using only Test 1 compares well with the numerical results. The arithmetic mean for the entire aquifer was determined to be 3.19×10^{-11} m^2 (3.4×10^{-10} ft^2). The Region Average values indicate, in contrast to the numerical results, the presence of an inner low-permeable zone and an outer high-permeable zone. The results from the single-well steady-state pump tests contradict these results, indicating that this trend is an artifact of the analysis procedure. The numerical simulation runs also demonstrated that such a reversal would apparently occur when a high-permeable region was surrounded by lower-permeable sediments.

The analytical analysis of the pulse test data yielded an arithmetic mean permeability of the aquifer of 4.96×10^{-11} m^2 (5.34×10^{-10} ft^2). The permeability zoning results are similar to those obtained from the analysis of the interference tests but are even more evident here. One reason that the pulse tests over-estimate the permeability of the outer region is that they neglect the effects of leakage. For wells far from the production well, as shown on leaky type-curves, leakage is very significant and can result in large over-estimations of the aquifer's hydrological properties.

Difficulties involved in analytical pulse test analysis arose in obtaining the time lag t_{lag} and the maximum pressure change ΔP_{max} from the pressure response data. Noisy data obscured the inflection point of the pulse making the determination of the exact t_{lag} and ΔP_{max} difficult. This method of analyzing the pulse test data involved analyzing each individual pulse separately, whereas, the numerical method allowed pulses with the same production well, observation well, and flow rate to be grouped together for analysis.

The numerical results were obtained by incorporating the results from the single-well steady-state tests into an aquifer model and progressively refining the model until a single set of permeability values were achieved which would fit all of the well data from all of the pump tests. The final aquifer model consisted of eight

sedimentary units with differing permeabilities. Table 7.4 shows the depth intervals of each sedimentary unit and the permeability values of each. The results of the interference tests are probably more representative of the aquifer than the single-well tests or pulse tests since the interference tests achieve a greater radius of influence than the single-well tests and since much better matches were found for the interference tests than the pulse tests.

The single-well steady-state tests took the least amount of preparation. The actual pumping time for one single-well steady-state test was approximately 30 minutes but, since all 12 wells at the LBLI/HO Site needed to be tested individually, the total test time for the Site was approximately 12 hours including 30 minutes between each test to move the pump.

Setting up the instrumentation for the pressure-transient tests (the single-well transient, interference, and pulse tests) involved installing and connecting the pressure transducers, installing the submersible pump, and readying the computer system. The set-up took one day to complete. The single-well transient tests involved measuring pressure responses in a production well while it was being pumped, whereas, interference and pulse tests involved measuring the pressure responses in one or more observation wells while pumping a production well. The single-well transient tests and the interference tests were conducted simultaneously.

Collecting background data for each single-well/interference test took about four hours, the actual pumping time for one test was approximately nine hours, and collecting more background data after a test took about another four hours. The total time to conduct one single-well/interference test at the LBLI/HO Site was approximately two days. However, once all the instrumentation was completed, conducting a second test using a different production well took only one more day.

The same set-up procedure used for the single-well/interference tests was also used for the pulse tests, therefore, the set-up time for the pulse tests was also approximately one day. In contrast to the single-well/interference tests, collecting

background data before the pulse tests was not necessary. The shortest pulses used for these tests were 15 seconds long. The pulses arrived at the observation wells anywhere from 1 second to five minutes after the pulse was generated at the production well. Therefore, an approximate time for collecting background data after the pump was shut-in was 10 minutes. The total time to set-up for and conduct one pulse test would be about one day. However, at the LBLI/HO Site, the pulse tests were conducted a few minutes after the interference tests and set-up was not required. For this case, the pulse tests only took approximately 10-15 minutes to conduct.

Comparing the results from the different methods of analysis demonstrates the non-uniqueness of the permeability values obtained. The results shown in Table 7.5 reveal that the analytical analysis of either the interference or pulse tests would have greatly over-estimated the permeability of the outer radius region and under-estimated the permeability of the inner radius region. The single-well steady-state results seem to slightly under-estimate the permeability-thickness product of the aquifer but, overall, compares the best with the numerical results and were the quickest to conduct and to analyze. If single-well tests had not been conducted, it may never have been possible to arrive at a final aquifer model which can match all the well data from all of the pump tests.

Table 7.5. Permeability results obtained from analytical and numerical methods of analysis showing radial zoning of aquifer.

Method of Analysis	Type of Test	Depth Interval (m^2)	$k \times 10^{-11}$ (m^2)	
			Inner Region	Outer Region
Analytical	Single-Well Steady-State	6.1 - 12.2	4.00	0.53
	Interference	6.1 - 24.4	2.64	3.82
	Pulse	6.1 - 24.4	3.28	6.55
Numerical	Interference	6.1 - 12.2	4.40	0.50
	Pulse	6.1 - 12.2	4.40	0.50

8.0 CONCLUSION

The purpose of this report was to determine the hydrologic properties of the shallow aquifer system at the LBLI/HO Site at Kesterson Reservoir. Secondary points of interest consist of comparing methods of obtaining pump test data (single-well steady-state, single-well transient, interference, and pulse tests) and methods of analyzing the data (analytical and numerical techniques).

The aquifer system is composed of interbedded sands, silts, and clays bounded on the top by a leaky aquitard and on the bottom by an aquiclude. Because of the complex nature of the aquifer system, numerical methods of analysis were used to determine the hydrologic properties of the system and the configuration of the sedimentary units.

Four types of pumping tests were conducted at the site. Single-well steady-state pump tests were conducted in order to obtain approximate initial hydrologic values for use in the numerical simulations. Well pressure-transient response data was then obtained from single-well transient, interference, and pulse pumping tests.

After the well data were collected, an aquifer model representing the aquifer system was created using data from the single-well steady-state pump tests and information about the subsurface geology obtained from lithological and geophysical well-logs. The aquifer model was progressively refined from a simple, purely layered model to a final model which could use a single set of hydrological values to simulate the pressure responses from all the pumping tests. The final model ended up consisting of both a composite and layered system made up of eight different sedimentary units with differing permeabilities.

Two important features of the final aquifer model are the inclusion of inner and outer permeable regions in Layer 2, with a higher-permeable inner region and a lower-permeable outer region, and the addition of a very thin clay layer (0.61 m

thick) that was incorporated into the model at a depth interval of 16.76 m -17.37 m. Layer 2 was divided up into these two permeability regions because of the information obtained from the single-well steady-state pump tests. Equally good pressure response matches could be made with or without the division of Layer 2, however, not with using the same permeability values. The addition of the thin clay layer (Layer 4) was brought about by the inability to match the pressure responses generated by Production Well HO80 (the deepest production well). After double checking lithological well-logs and incorporating this thin clay layer into the aquifer model, matches of well data from pumping HO80 were made satisfactorily.

Analytical analysis of the pump test data were completed in order to compare analytical results with the numerical results and determine the uniqueness of the results. It was found that the analytical analysis of the single-well transient tests were totally unreliable and that the analytical analysis of the interference and pulse tests greatly over-estimated the permeability values of the outer region of Layer 2 and did not reflect the presence of vertical layering of the aquifer since these methods assumed a homogeneous aquifer. One of the main conclusions of this report is that, depending on how many wells are used for a pump test and which method of analysis is used to analyze the pump test data, different hydrological values can be obtained giving very different conceptions of the aquifer system.

The numerical results from the interference tests yielded a kH product for the aquifer of 3.99 $\times 10^{-10}$ m^3 and a permeability value of the leaky aquitard of 4.5 $\times 10^{-13}$ m^2. The inner region of Layer 2 has a permeability value of almost an order of magnitude higher than the outer region. Numerical analysis yielded a relatively comprehensive model of the aquifer properties that would match all of the well data from all of the pump tests. This was not possible with any of the other methods of analysis.

REFERENCES

Benson, S. M., 1986. Computerized data acquisition system for production, injection, and interference tests. LBL-21727, Lawrence Berkeley Laboratory, Berkeley, CA.

Bodvarsson, G. S., 1982. Mathematical modeling of the behavior of geothermal systems under exploitation. Ph.D. thesis, University of California, Berkeley, CA.

Boulton, N. S. and T. D. Streltsova, 1977. Unsteady flow to a pumped well in a fissured water-bearing formation. J. Hydrol., Vol. 35, pp. 257-269.

Brigham, W. E., 1970. Planning and analysis of pulse-tests. J. Pet. Tech., Vol. 22, pp. 618-624.

Brons, F. and V. E. Marting, 1961. The effect of restricted fluid entry on well productivity. J. Pet. Tech., Vol. 13, pp. 172-174.

Croft, M. G., 1972. Subsurface geology of the late Tertiary and Quaternary water-bearing deposits of the southern part of the San Joaquin Valley, California. U. S. Geological Survey Water-Supply Paper 1999-H, 27 pp.

Davis, G. H., Green, J. H., Olmsted, F. H., and D. W. Brown, 1959. Groundwater conditions and storage capacity in the San Joaquin Valley, California. U. S. Geological Survey Water-Supply Paper 1469, 287 pp.

Earlougher, R. C. Jr., 1977. *Advances in Well Test Analysis*. Monograph Series, Vol. 5, Dallas: Society of Petroleum Engineers of AIME, 263 p.

Edwards, A. L., 1972. TRUMP: A computer program for transient and steady state temperature distribution in multidimensional systems, Lawrence Livermore Laboratory, UCRL-14754, Rev. 3, Livermore, CA.

Flexser, S., 1988. Lithologic composition and variability of the sediments underlying Kesterson Reservoir as interpreted from shallow cores. LBL-25586, Lawrence Berkeley Laboratory, Berkeley, CA.

Freeze, R. A. and J. A. Cherry, 1979. *Groundwater*. Prentice-Hall, Englewood Cliffs, NJ.

Goldstein, N. E., Alumbaugh, D., and S. M. Benson, 1988. Ground conductivity measurements adjacent to the Kesterson Ponds 1, 2, and 5. LBL-24657, Lawrence Berkeley Laboratory, Berkeley, CA.

Hantush, M. S., 1964. *Hydraulics of Wells*. In Advances in Hydroscience, Ven Te Chow, ed., Vol. 1, Academic Press, New York, pp. 281-432.

Hantush, M. S., and C. E. Jacob, 1955. Non-steady radial flow in an infinite leaky aquifer. Trans. Am. Geophys. Union, Vol. 36, No. 1, pp. 95-100.

Herd, D. G., 1979. Geologic map of O'Neill Forebay, western Merced County, California. U. S. Geological Survey, Open-File Report 79-359.

Hoots, H. W., Bear, T. L., and W. W. Kleinpell, 1954. Geological summary of the San Joaquin Valley, California. Geology of Southern California, Division of Mines, Bulletin No. 170.

Hotchkiss, W. R. and G. O. Balding, 1971. Geology, hydrology, and water quality of the Tracy-Dos Palos area, San Joaquin Valley, California. U. S. Geological Survey Open-File Report.

Hubbert, M. K., 1940. The theory of groundwater motion. J. Geol., Vol. 48, pp. 785-944.

Hurst, W., 1953. Establishment of the skin effect and its impediment to fluid flow into a well bore. Pet. Eng., Vol. 25, No. 11, B6-B16.

Johnson, C. R., Greenkorn, R. A., and E. G. Woods, 1966. Pulse-testing: A new method for describing reservoir flow properties between wells. J. Pet. Tech., Vol. 18, pp. 1599-1604.

LBL, 1986. Hydrological, geochemical, and ecological characterization of Kesterson Reservoir. Second Progress Report, LBL-1188, Lawrence Berkeley Laboratory, Berkeley, CA.

LBL, 1987. Hydrological, geochemical, and ecological characterization of Kesterson Reservoir: Annual Report, October 1, 1986-September 30, 1987. LBL-24250, Lawrence Berkeley Laboratory, Berkeley, CA.

LBL, 1988. Hydrological, geochemical, and ecological characterization of Kesterson Reservoir. Seventh Progress Report, LBL-1188, Lawrence Berkeley Laboratory, Berkeley, CA.

Lettis, W. R., 1982. Late Cenezoic stratigraphy and structure of the western margin of the central San Joaquin Valley, California. U. S. Geological Survey Open-File Report 82-526, 203 p.

Luthin, J., 1966. Report on expected seepage into Salt Slough and the San Joaquin River from the Kesterson enhancement area, Western Merced County.

Mandle, R. J. and A. L. Kontis, 1986. Directions and rates of groundwater movement in the vicinity of Kesterson Reservoir, San Joaquin Valley, California. U. S. Geological Survey, Water Resources Investigations Report 86-4196.

Manning, J. C., 1972. Resume of ground water hydrology in the Southern San Joaquin Valley. San Joaquin Geol. Soc., Selected Papers, Vol. 4, pp. 26-32

Mitten, H. T., LeBlanc, R. A., and Bertoldi, G. L., 1969. Geology, hydrology, and quality of water in the Madera area, San Joaquin Valley, California. U. S. Geological Survey Open-File Report, 97 p.

Muskat, M., 1949. *Physical Principles of Oil Production*. McGraw-Hill Book Co., New York, NY.

Narasimhan, T. N. and P. A. Witherspoon, 1976. An intergrated finite-difference method for analyzing fluid flow in porous media. Water Resour. Res., Vol. 12, No. 1, pp. 57-64.

Neuman, S. P. and P. A. Witherspoon, 1969. Applicability of current theories of flow in leaky aquifers. Water Resour. Res., Vol. 5, No. 4, pp. 817-829.

Russel, D. G. and M. Prats, 1962. The practical aspects of interlayer crossflow. J. Pet. Tech., June, pp. 589-594.

Smith, M. B., 1964. Map showing distribution and configuration of basement rocks in California. U. S. Geological Survey Oil and Gas Inv., Map OM-215.

State of California, Department of Water Resources, San Joaquin District, 1967. Monthly shallow groundwater elevations - San Joaquin Master Drain Reservoir sites-Gustine-Kesterson and South Dos Palos area, Draft Office Report.

Streltsova, T. D., 1988. *Well Testing in Heterogeneous Formations*. An Exxon monograph, John Wiley and Sons, New York, NY.

Terzaghi, K., 1925. Settlement and consolidation of clay. Engineering News Record, 26 pp.

Theim, G., 1906. *Hydrologische Methoden*. Gebhardt, Leipzig, 56 p.

Theis, C. V., 1935. The relationship between the lowering of the piezometric surface and the rate and duration of discharge of a well using ground-water storage. Trans. Am. Geophys. Union, Vol 16, pp. 519-524.

Todd, D. K., 1959. *Ground Water Hydrology*. John Wiley & Sons, New York, 336 p.

Van Everdingen, A. F., 1953. The skin effect and its influence on the productive capacity of a well. Trans., AIME, Vol. 198, pp. 171-176.

Vela, S. and R. M. McKinley, 1970. How areal heterogeneities affect pulse-test results. Soc. Pet. Eng. J., Vol 10, pp. 181-191.

Wang, H. F. and M. P. Anderson, 1982. *Introduction to Groundwater Modeling: Finite Difference and Finite Element Methods*. W. H. Freeman and Company, University of Wisconsin, Madison, WI.

Weres, O., White, A. F., Wollenberg, H. A., and A. Yee, 1985. Geochemistry of selenium at Kesterson Reservoir: Possible remedial measures. LBL-431, Vol. 8, pp. 1-4, Lawrence Berkeley Laboratory, Berkeley, CA..

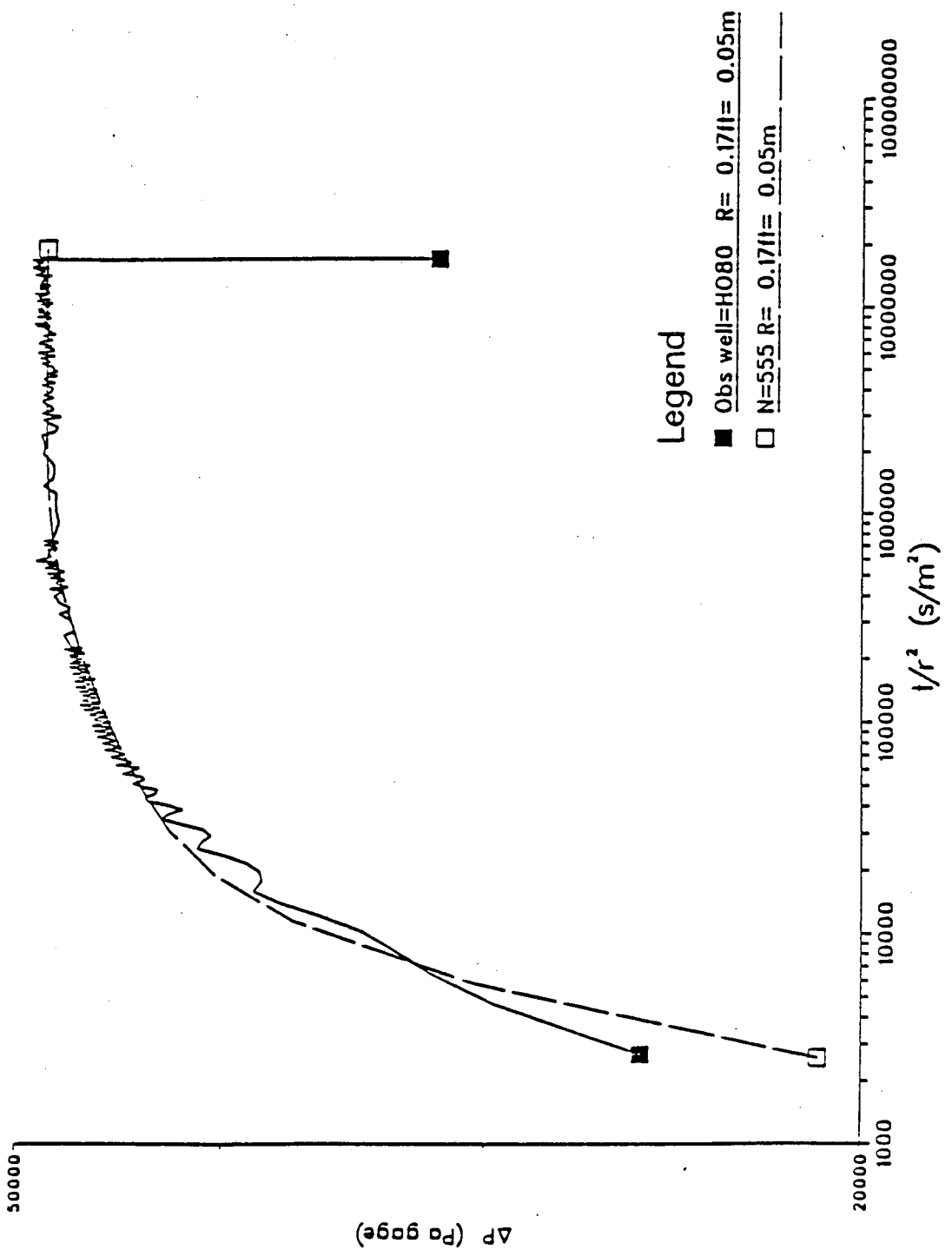
Williamson, A. K., Prudic, D. E., and L. A. Swain, 1985. Groundwater flow in the Central Valley, California. U. S. Geological Survey Open-File Report 85-345.

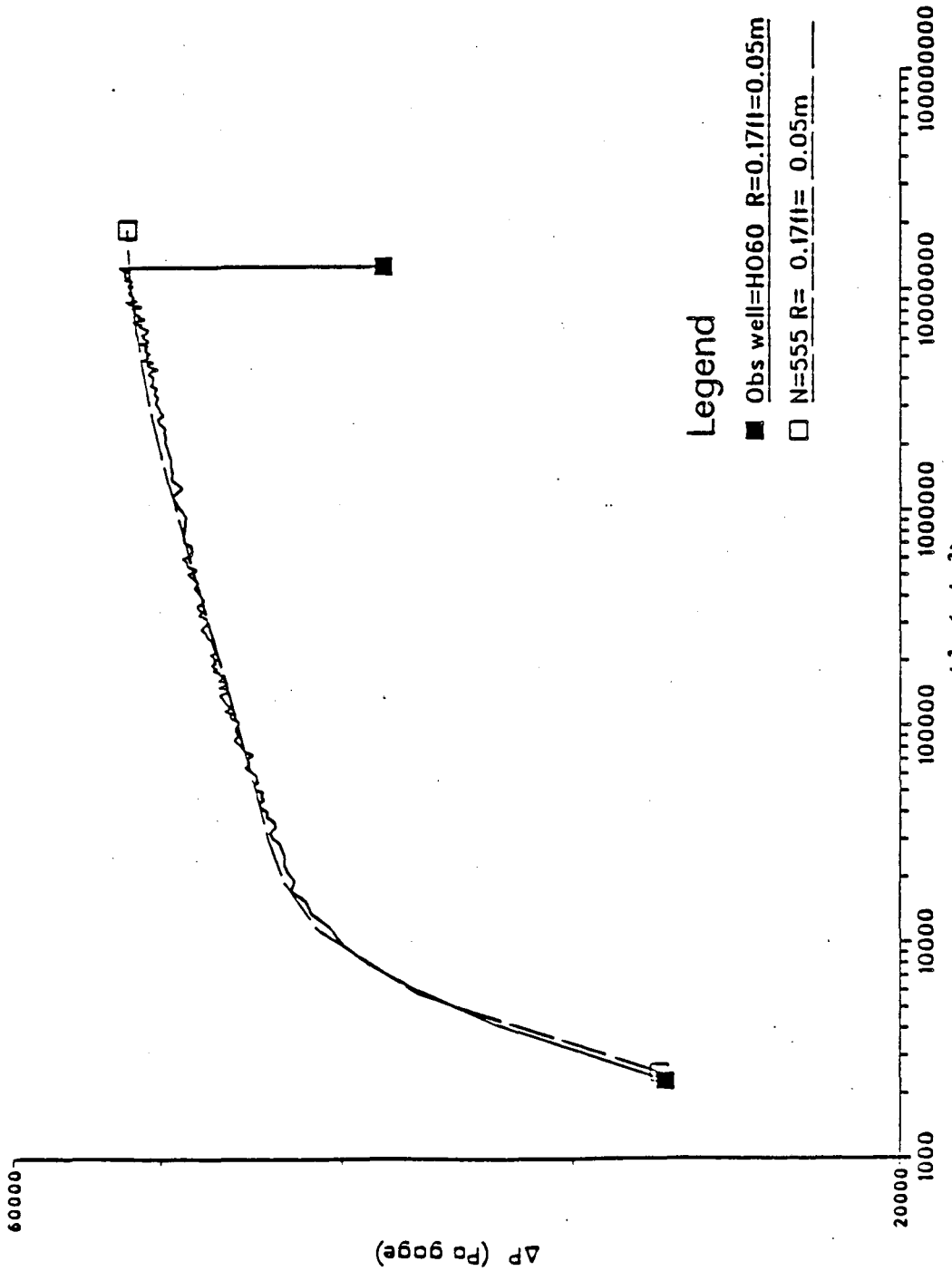
Witherspoon, P. A., Javandel, I., Neuman, S. P., and R. A. Freeze, 1967. Interpretation of aquifer gas storage conditions from water pumping tests. Monograph prepared on Project NS-38 at University of California, Berkeley for the Pipeline Research Committee of the American Gas Assoc., Inc. 273 pp.

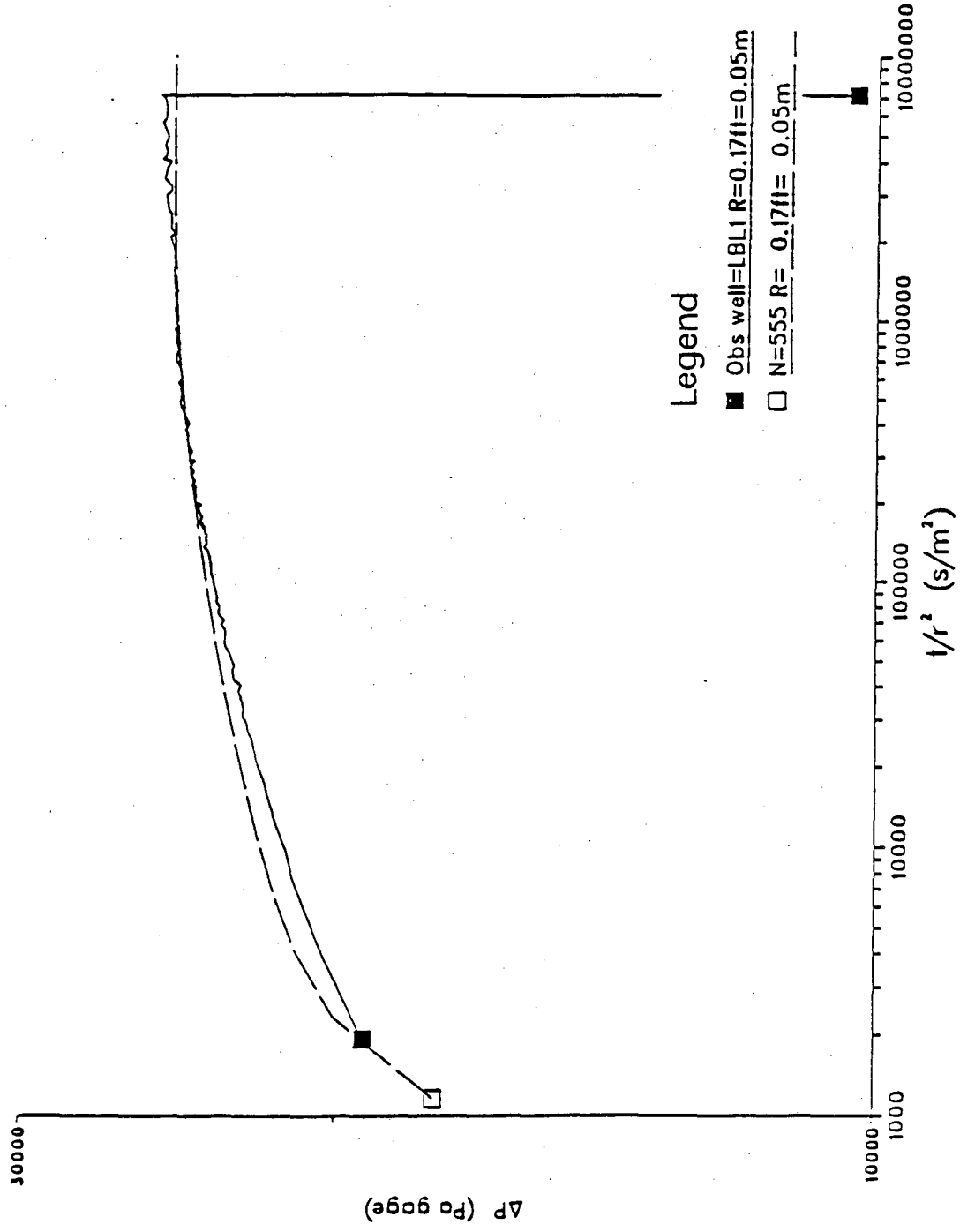
APPENDIX

The final curve matches of the simulated and field pressure responses using the final aquifer model are given in this section. The matches include the single-well transient test data, the interference test data, and the pulse test data.

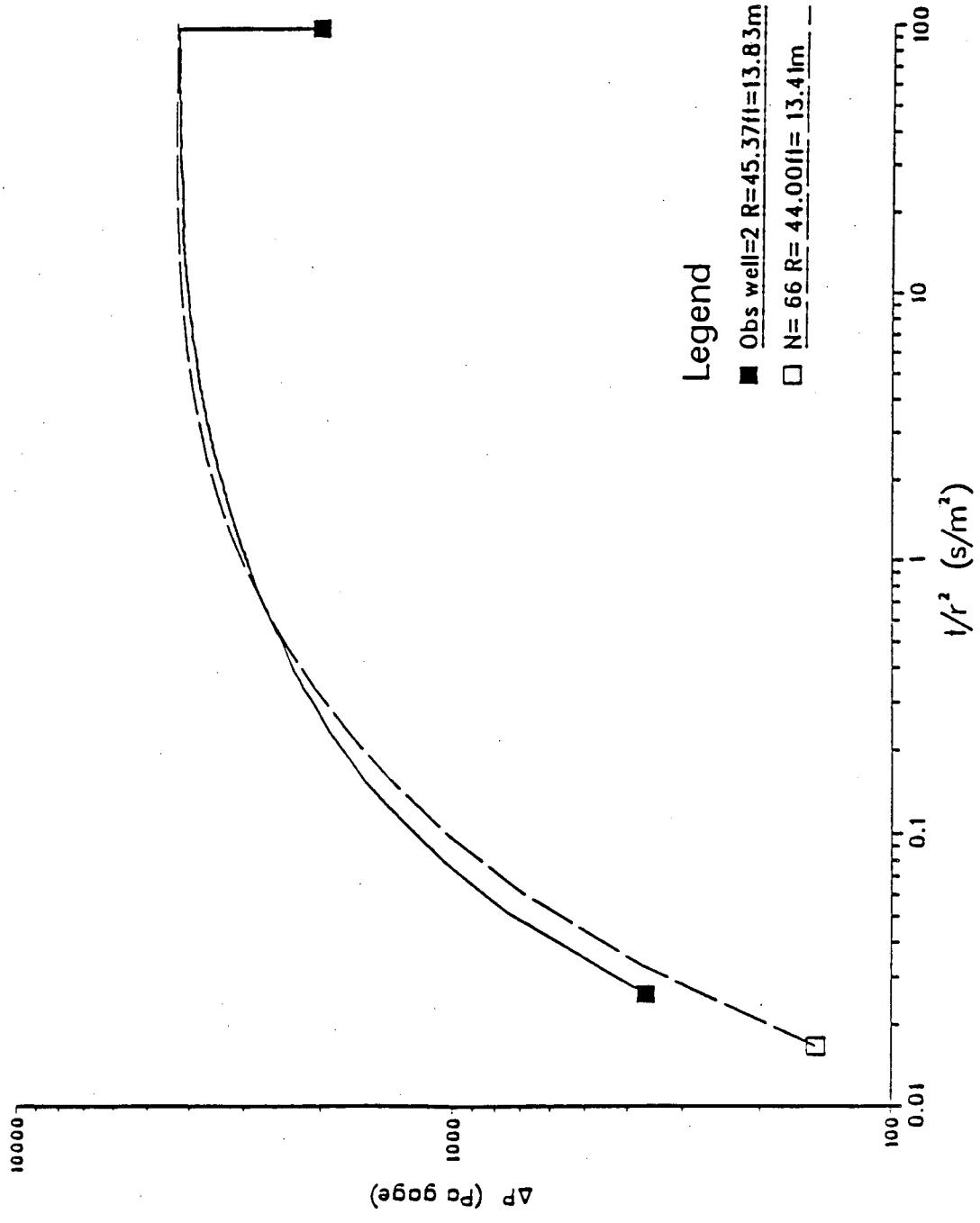
SINGLE-WELL TRANSIENT TESTS 1, 2, AND 3

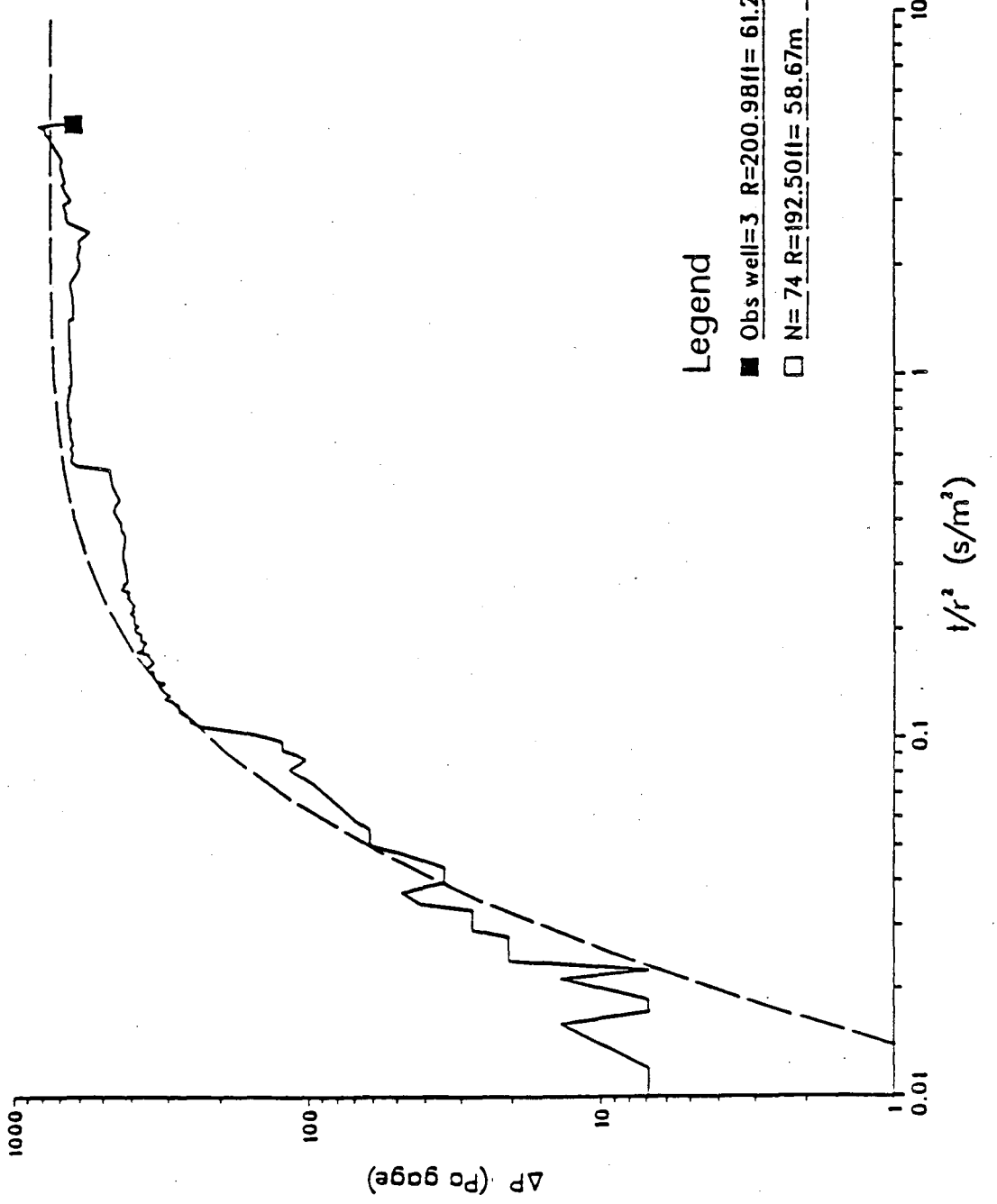

50000
20000
ΔP (Pa gage)
1000
10000
100000
1000000
10000000
100000000
t/r² (s/m²)
Legend
Obs well=HO80 R= 0.171ft= 0.05m
N=555 R= 0.171ft= 0.05m

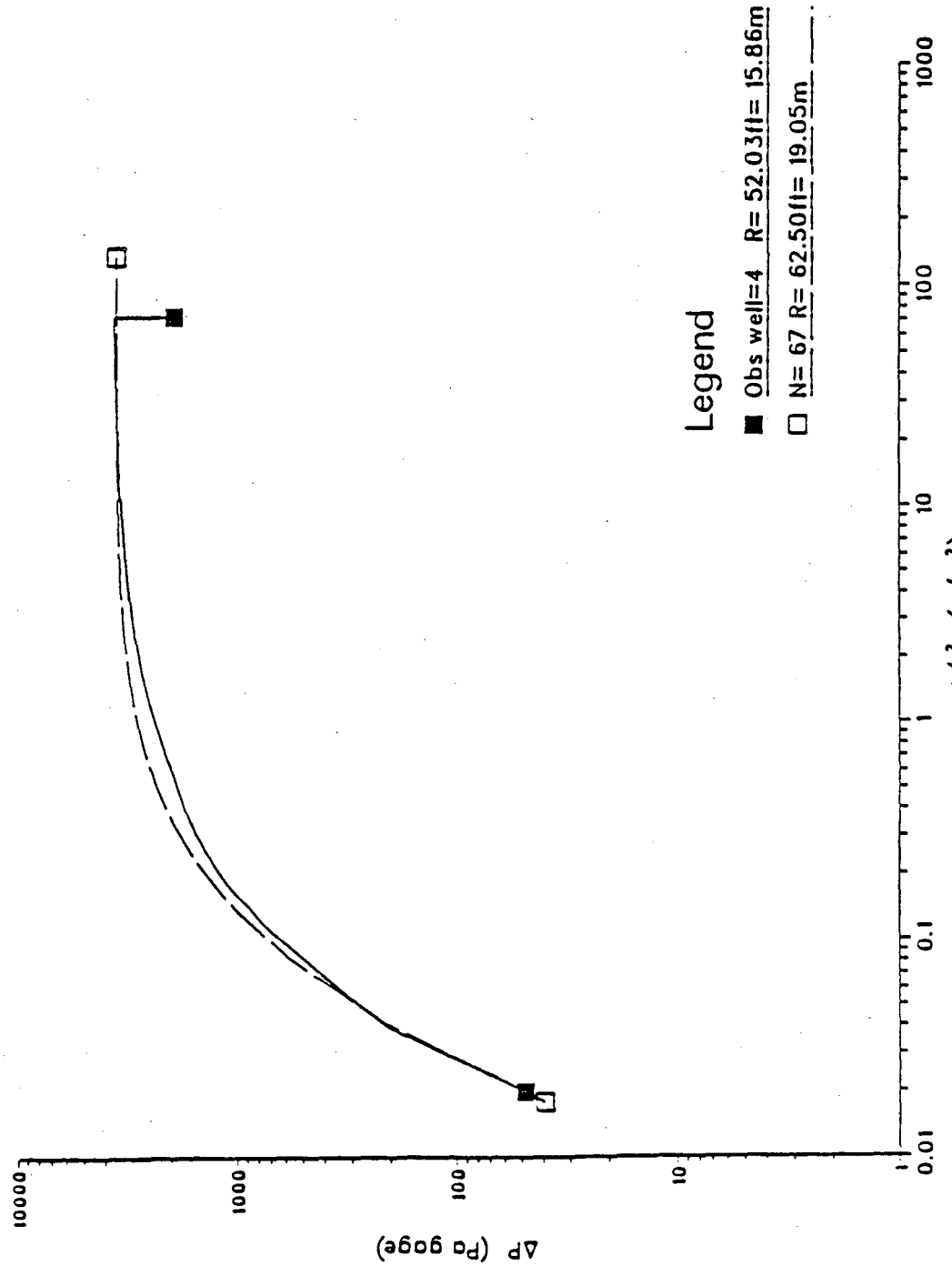

60000
20000
ΔP (Po gage)
1000
10000
100000
1000000
10000000
100000000
t/r² (s/m²)
Legend
Obs well=H060 R=0.1711=0.05m
N=555 R= 0.1711= 0.05m

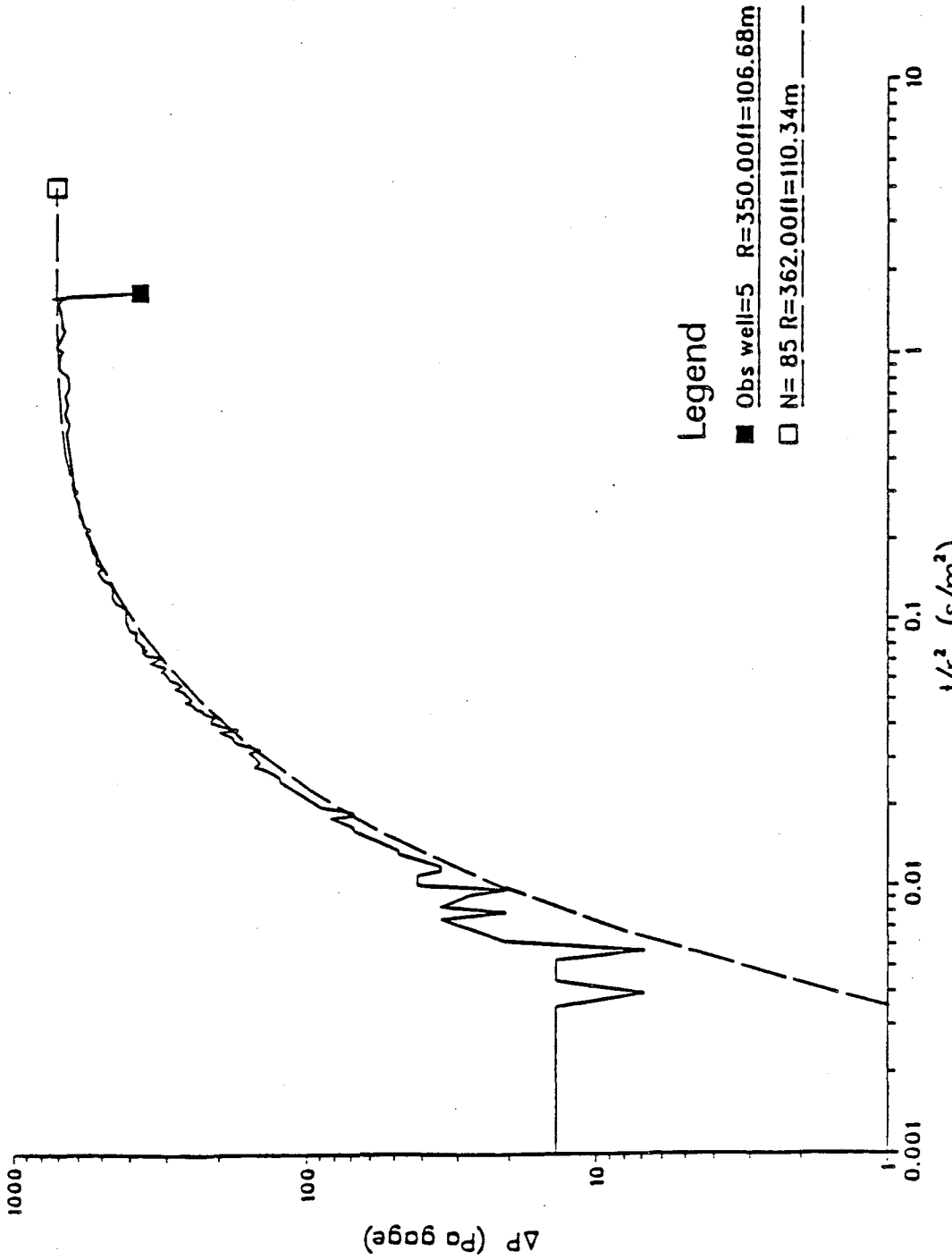

Legend
Obs well=LBL1 R=0.171l=0.05m
N=555 R= 0.171l= 0.05m
ΔP (Pa gage)
1/r² (s/m²)
10000
1000
100000
1000000
10000000

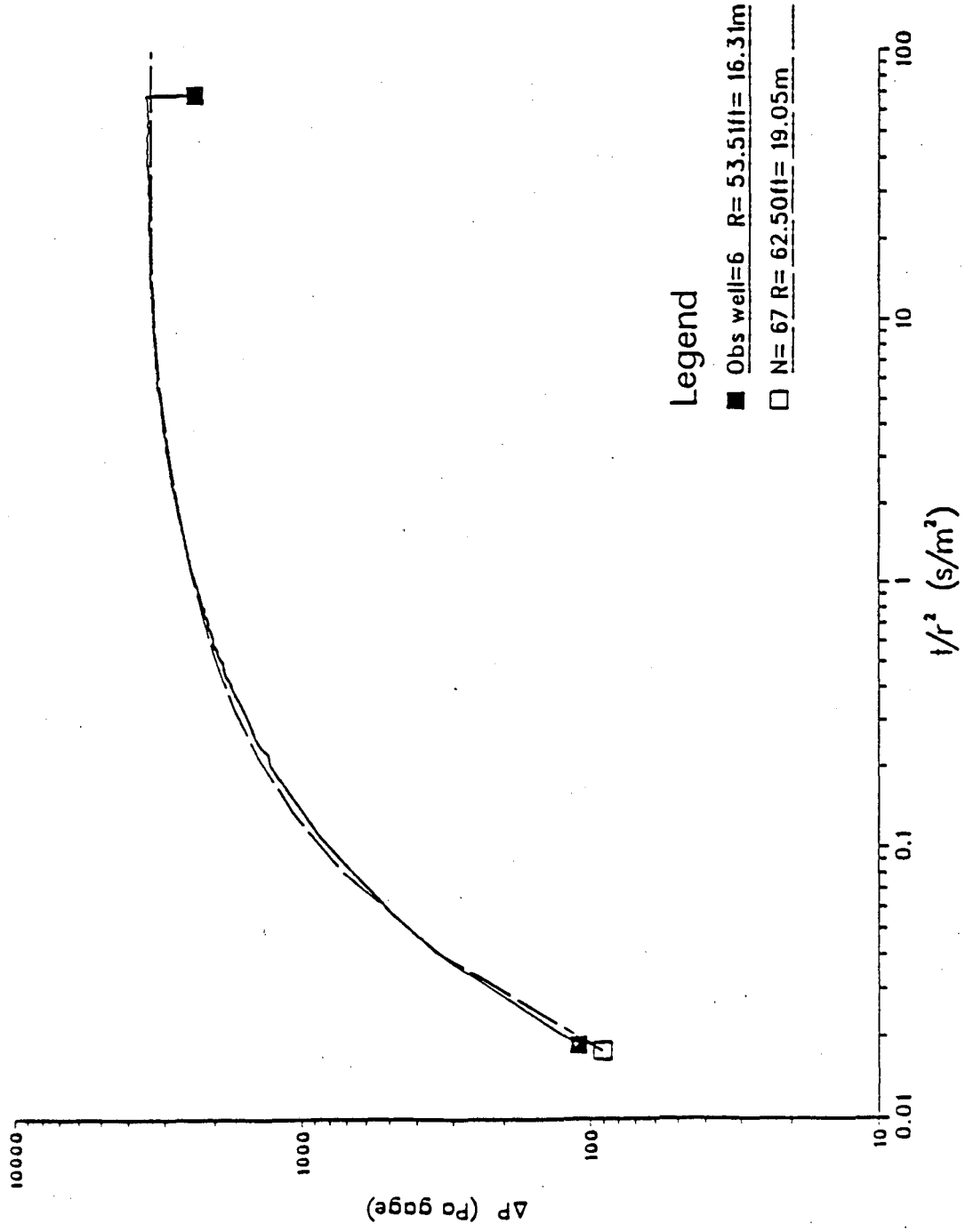
INTERFERENCE TEST 1 - PRODUCING I1

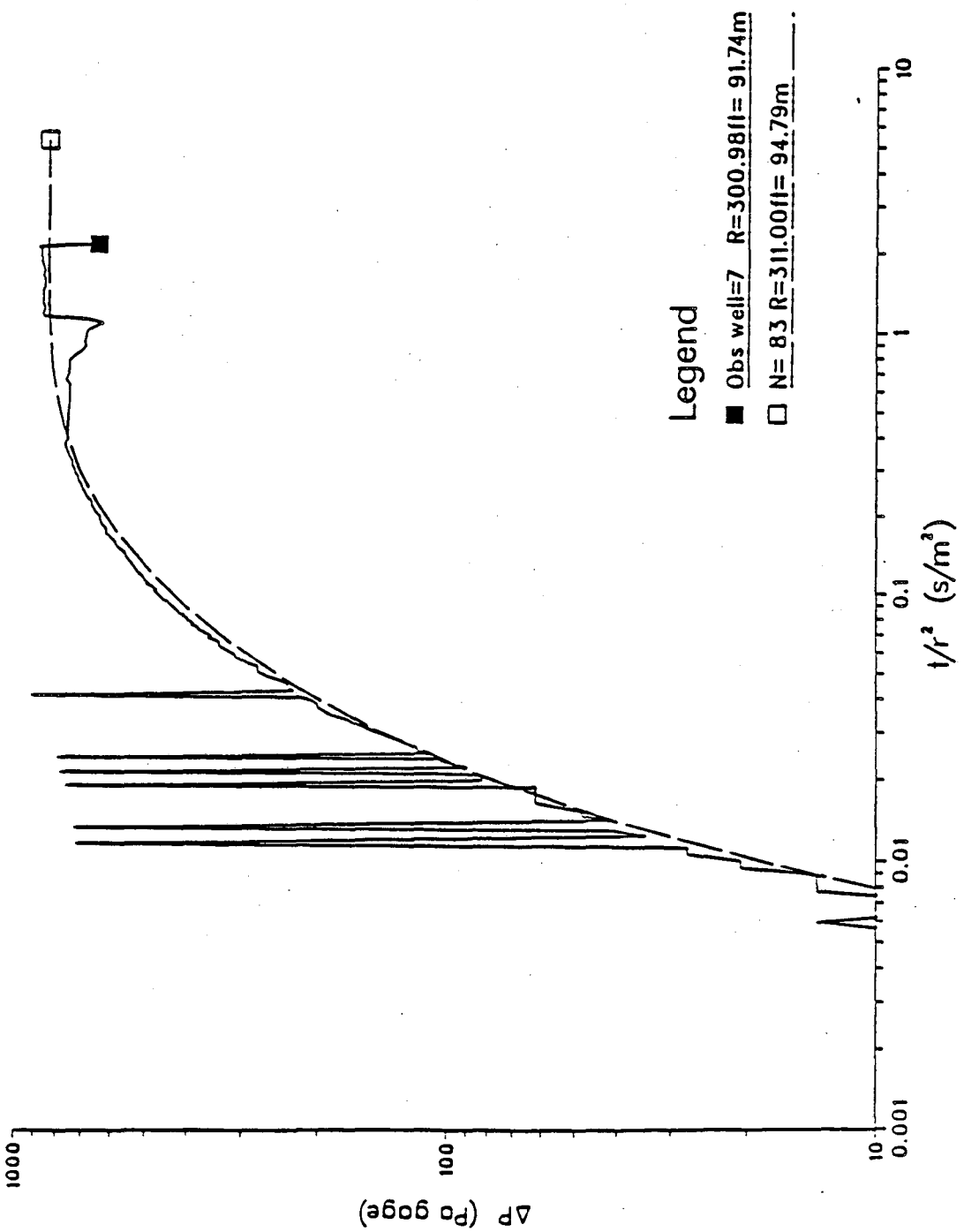

Legend
Obs well=2 R=45.37ft=13.83m
N= 66 R= 44.00ft= 13.41m
ΔP (Pa gage)
10000
1000
100
0.01
0.1
1
10
100
t/r² (s/m²)

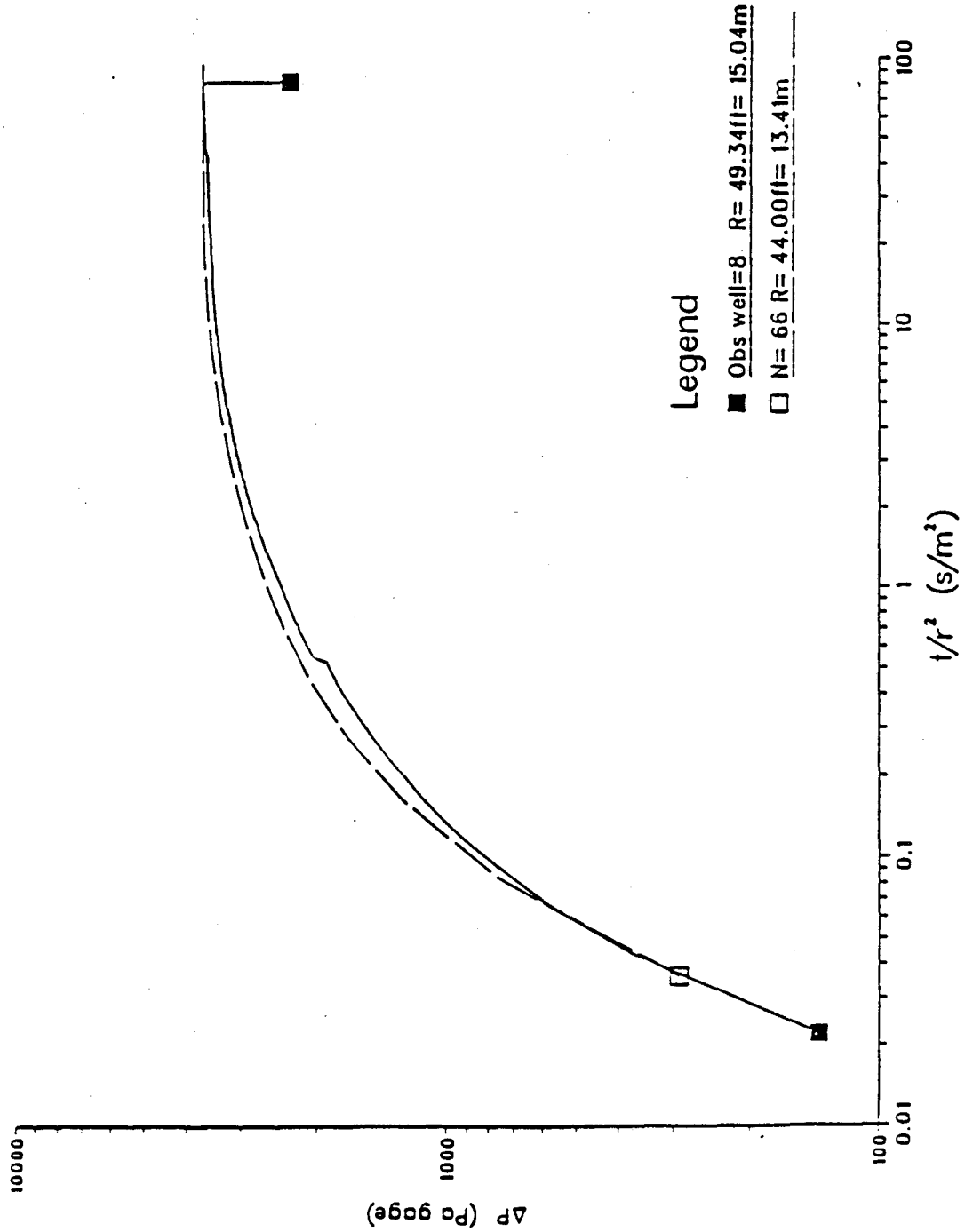

Legend
Obs well=3 R=200.98ft= 61.26m
N= 74 R=192.50ft= 58.67m
ΔP (Po gage)
1000
100
10
1
0.01
0.1
1
10
t/r² (s/m²)

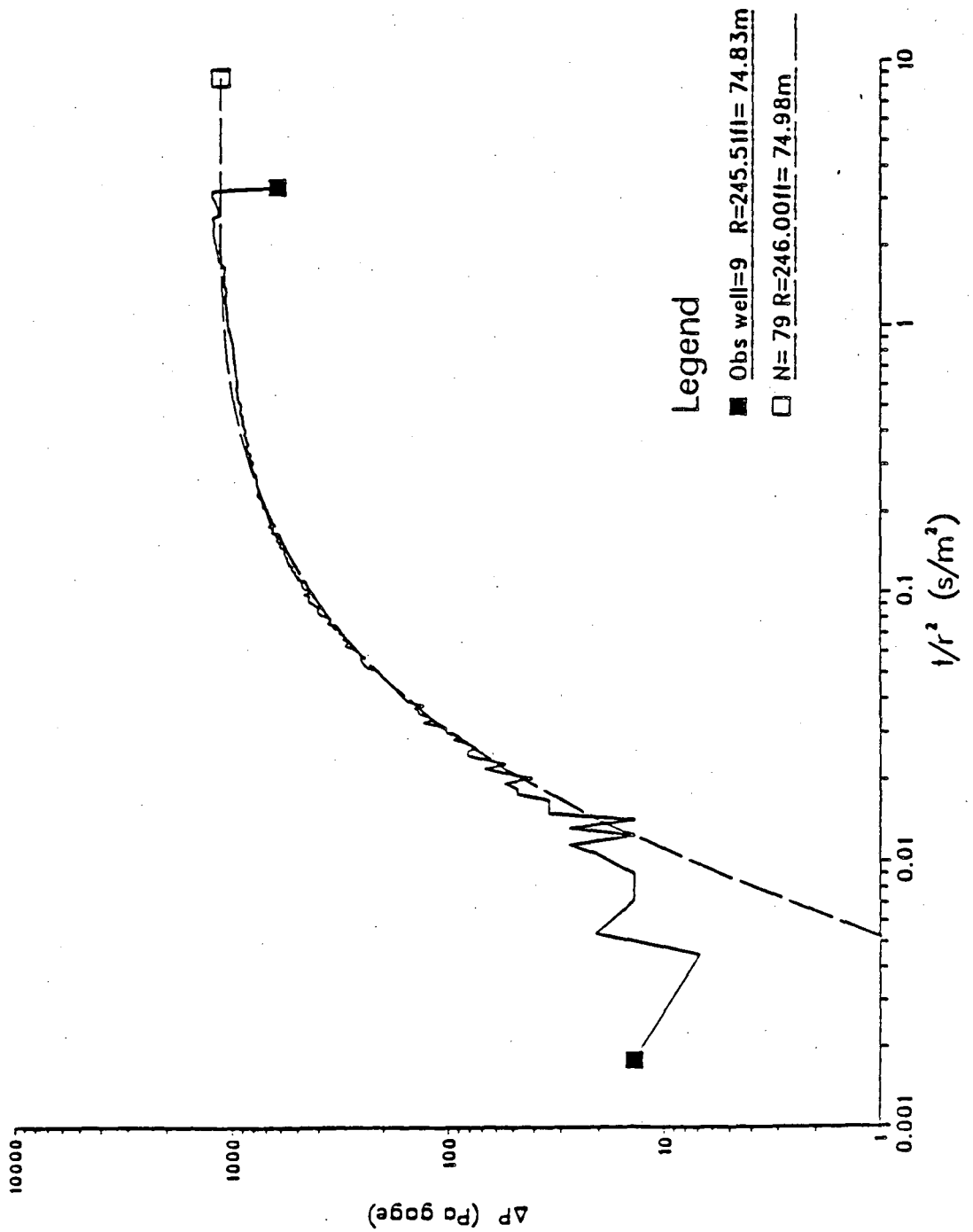

Legend
Obs well=4 R= 52.03ft= 15.86m
N= 67 R= 62.50ft= 19.05m
ΔP (Pa gage)
10000
1000
100
10
1
0.01
0.1
1
10
100
1000
1/r² (s/m²)


Legend
Obs well=5 R=350.00ft=106.68m
N= 85 R=362.00ft=110.34m
ΔP (Po gage)
1000
100
10
1
0.001
0.01
0.1
1
10
t/r² (s/m²)

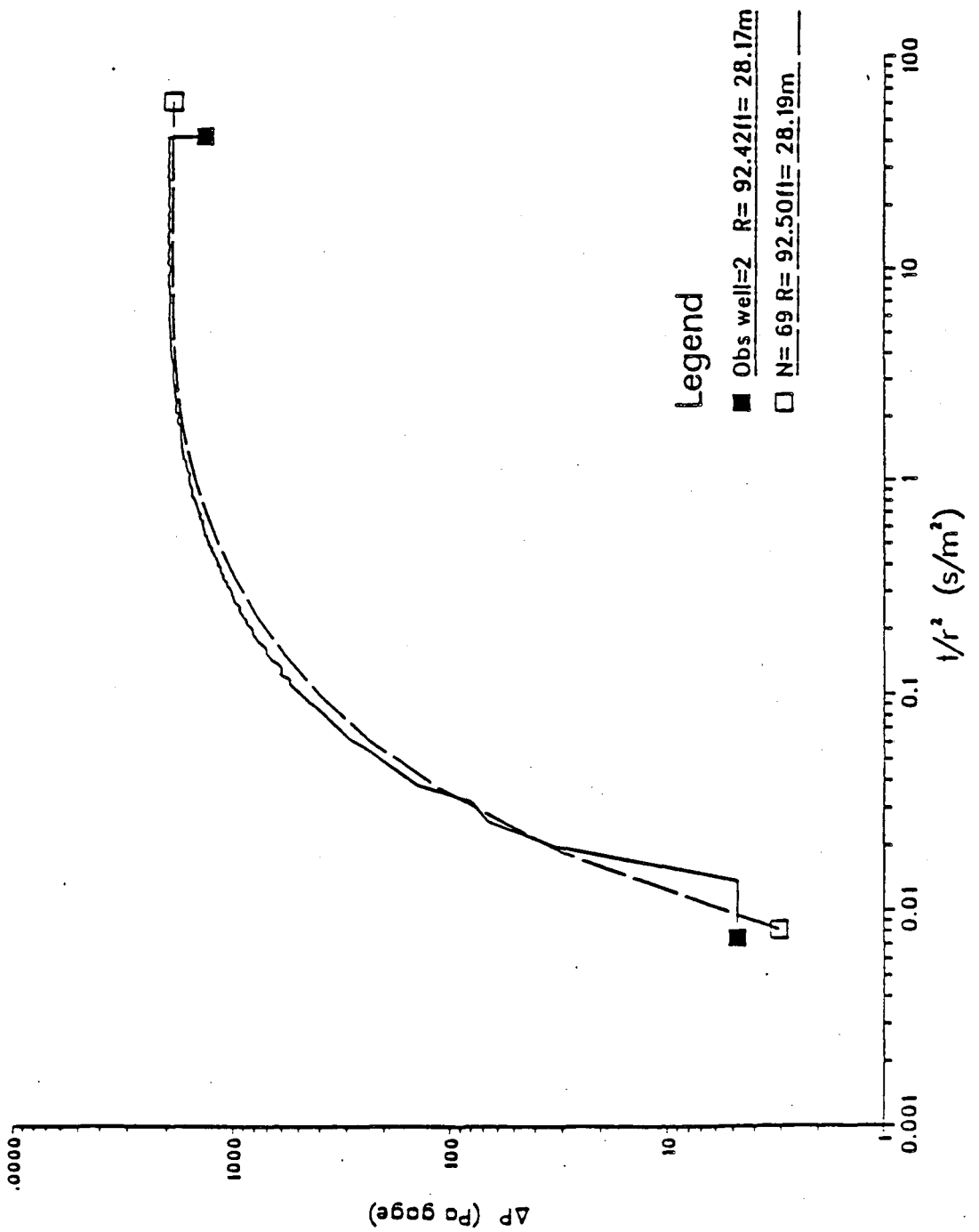

Legend
Obs well=6 R= 53.51ft= 16.31m
N= 67 R= 62.50ft= 19.05m
ΔP (Po gage)
10000
1000
100
10
0.01
0.1
1
10
100
t/r² (s/m²)

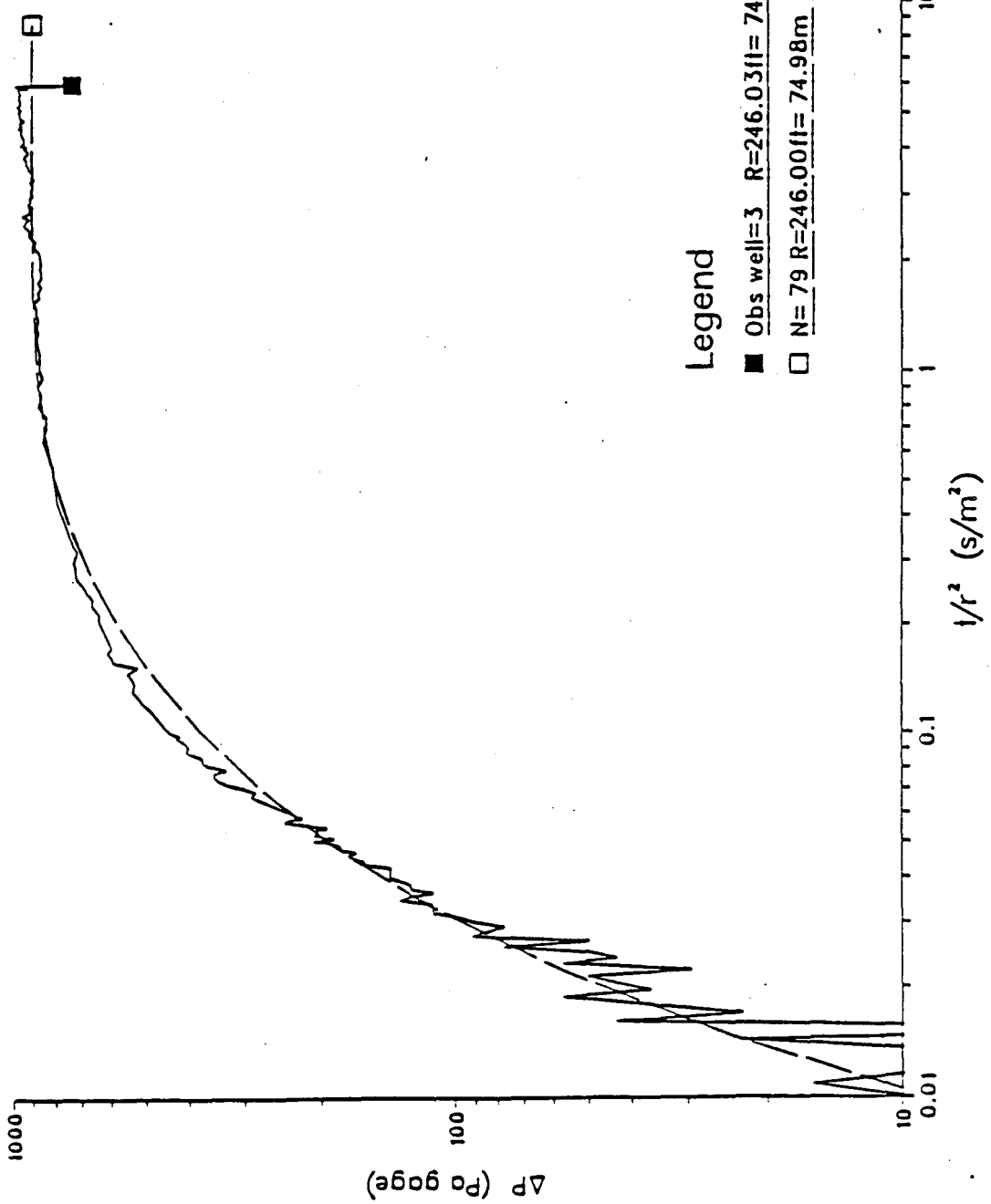

Legend
Obs well=7 R=300.98ft= 91.74m
N= 83 R=311.00ft= 94.79m
ΔP (Po gage)
1000
100
10
0.001
0.01
0.1
1
10
t/r² (s/m²)

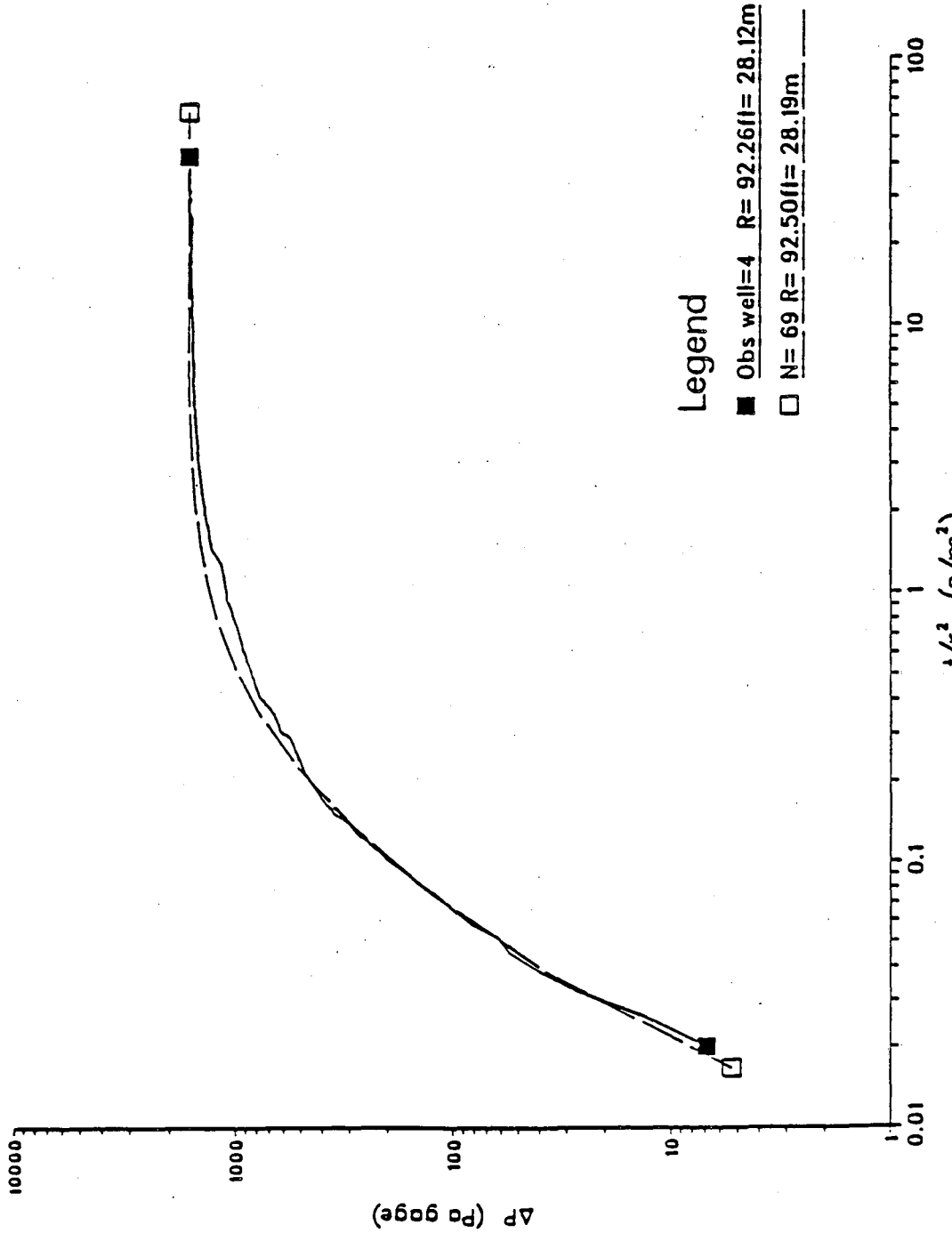

Legend
Obs well=8 R= 49.34ft= 15.04m
N= 66 R= 44.00ft= 13.41m
ΔP (Pa gage)
10000
1000
100
0.01
0.1
1
10
100
t/r² (s/m²)

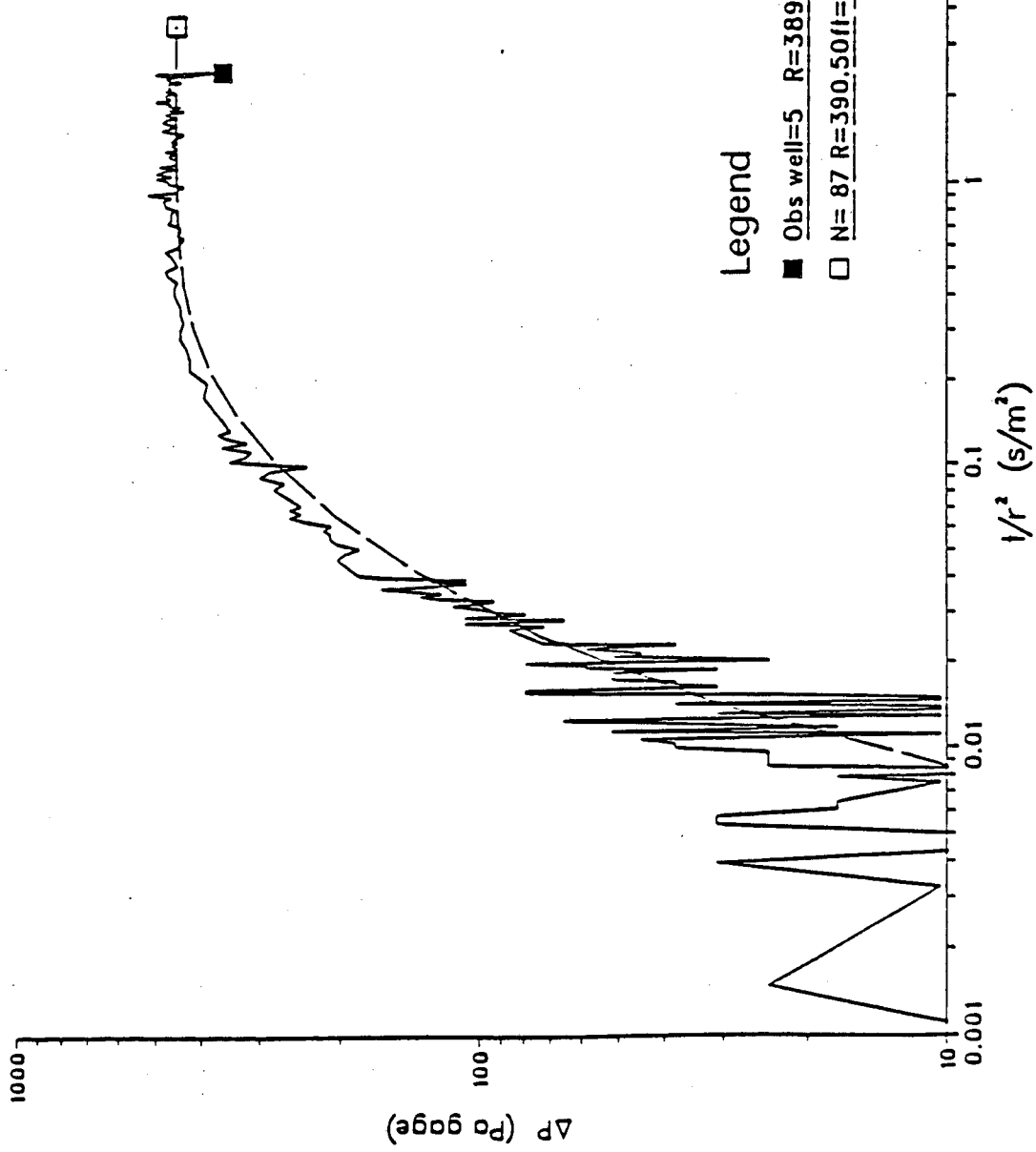

Legend
Obs well=9 R=245.5111= 74.83m
N= 79 R=246.0011= 74.98m
ΔP (Pa gage)
10000
1000
100
10
1
0.001
0.01
0.1
1
10
1/r² (s/m²)

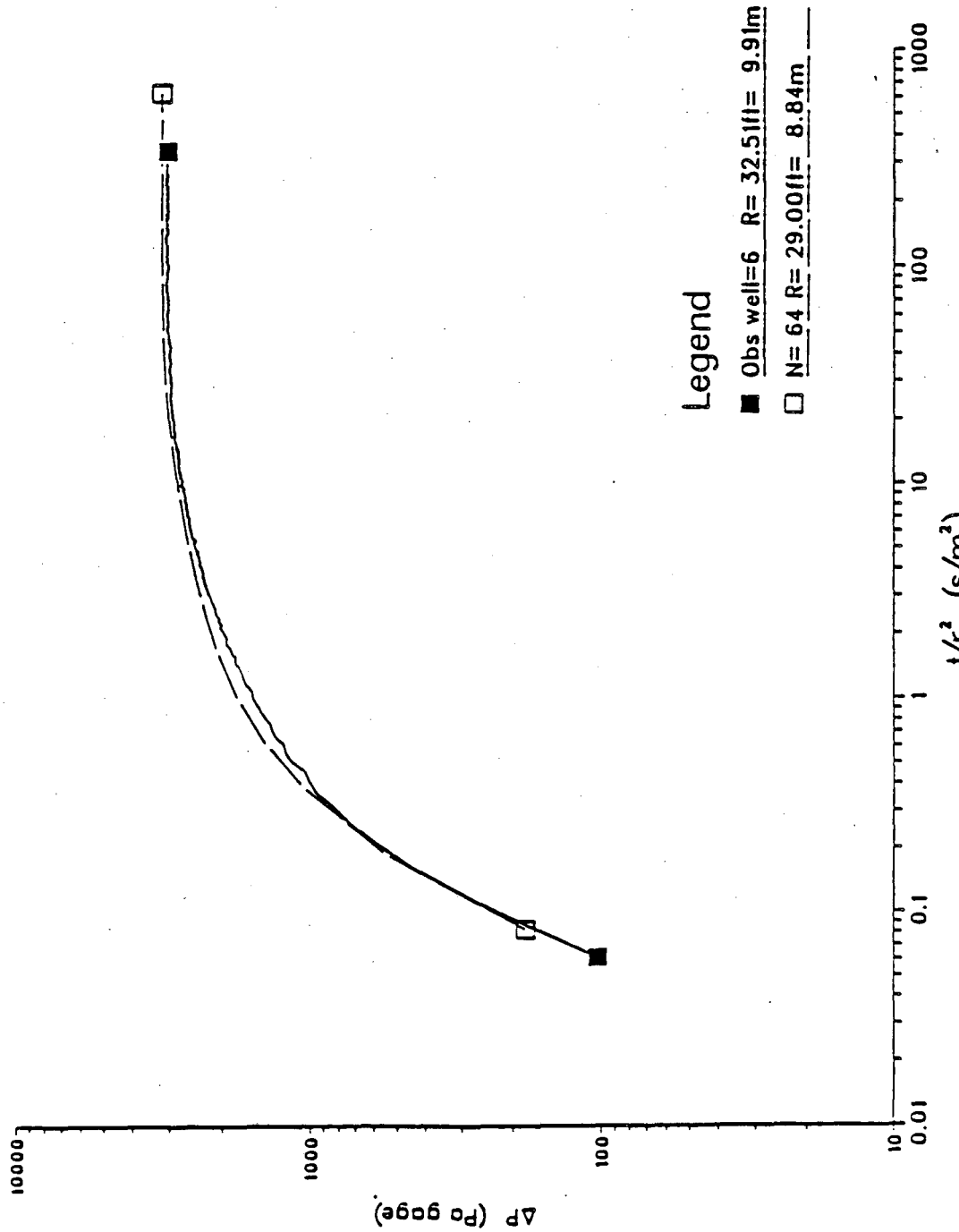
INTERFERENCE TEST 2 - PRODUCING HO60

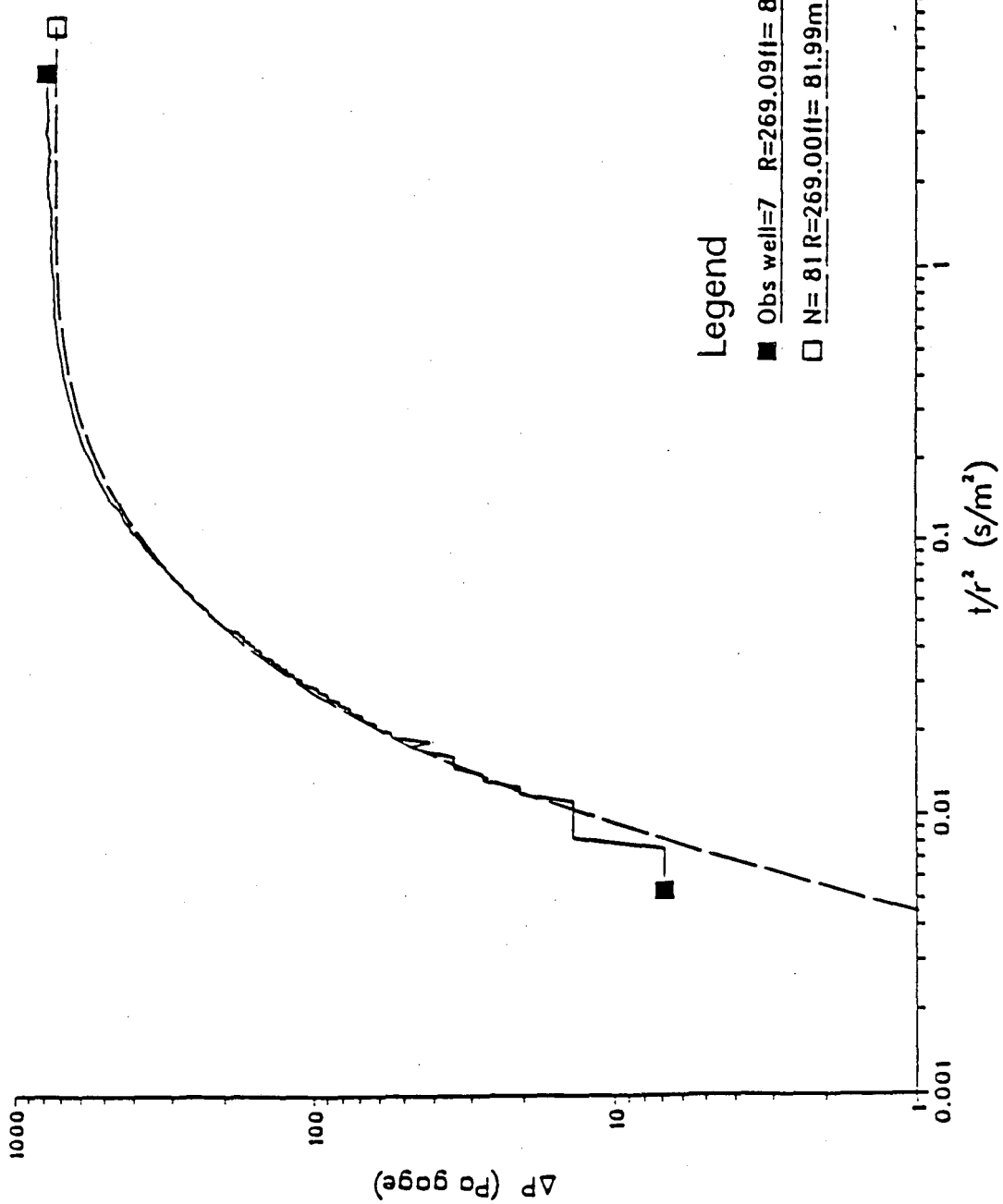

Legend
Obs well=2 R= 92.42ft= 28.17m
N= 69 R= 92.50ft= 28.19m
ΔP (Po gage)
10000
1000
100
10
1
0.001
0.01
0.1
1
10
100
t/r² (s/m²)

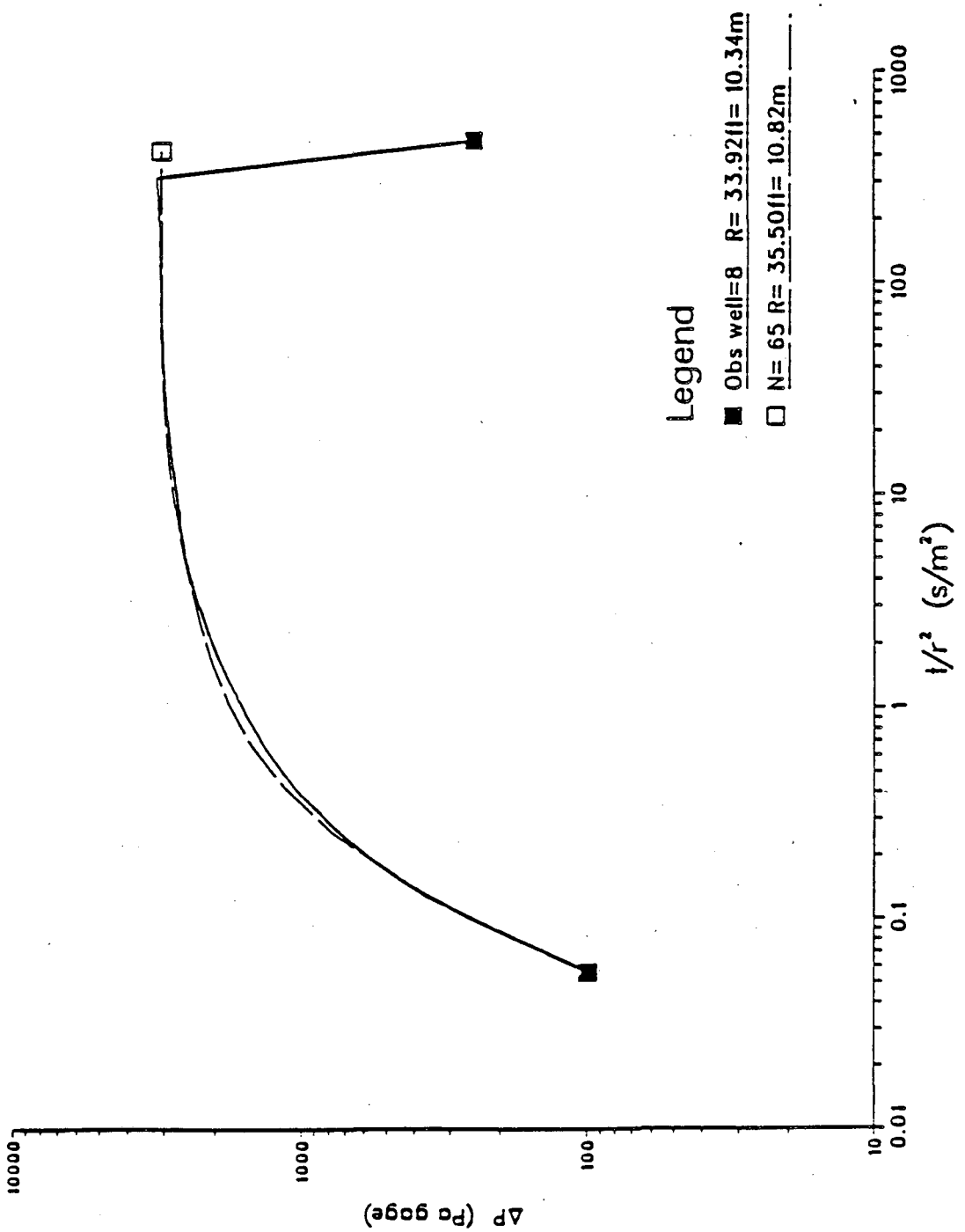

Legend
Obs well=3 R=246.03ft= 74.99m
N= 79 R=246.00ft= 74.98m
ΔP (Po gage)
1000
100
10
0.01
0.1
1
10
1/r² (s/m²)

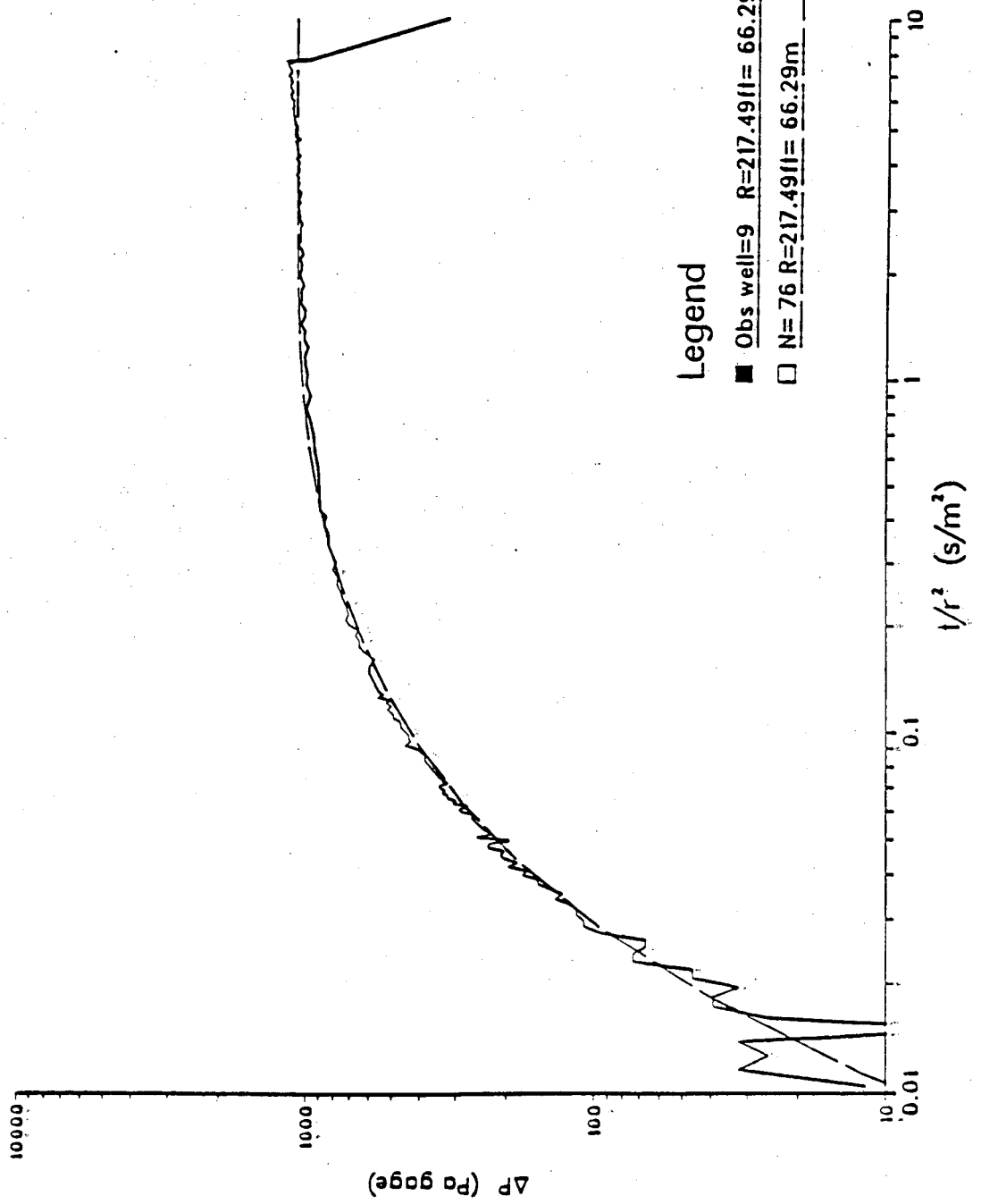

Legend
Obs well=4 R= 92.26ft= 28.12m
N= 69 R= 92.50ft= 28.19m
ΔP (Pa gage)
10000
1000
100
10
1
0.01
0.1
1
10
100
t/r² (s/m²)


Legend
Obs well=5 R=389.99ft=118.87m
N= 87 R=390.50ft=119.02m
ΔP (Po gage)
1000
100
10
0.001
0.01
0.1
1
10
t/r² (s/m²)

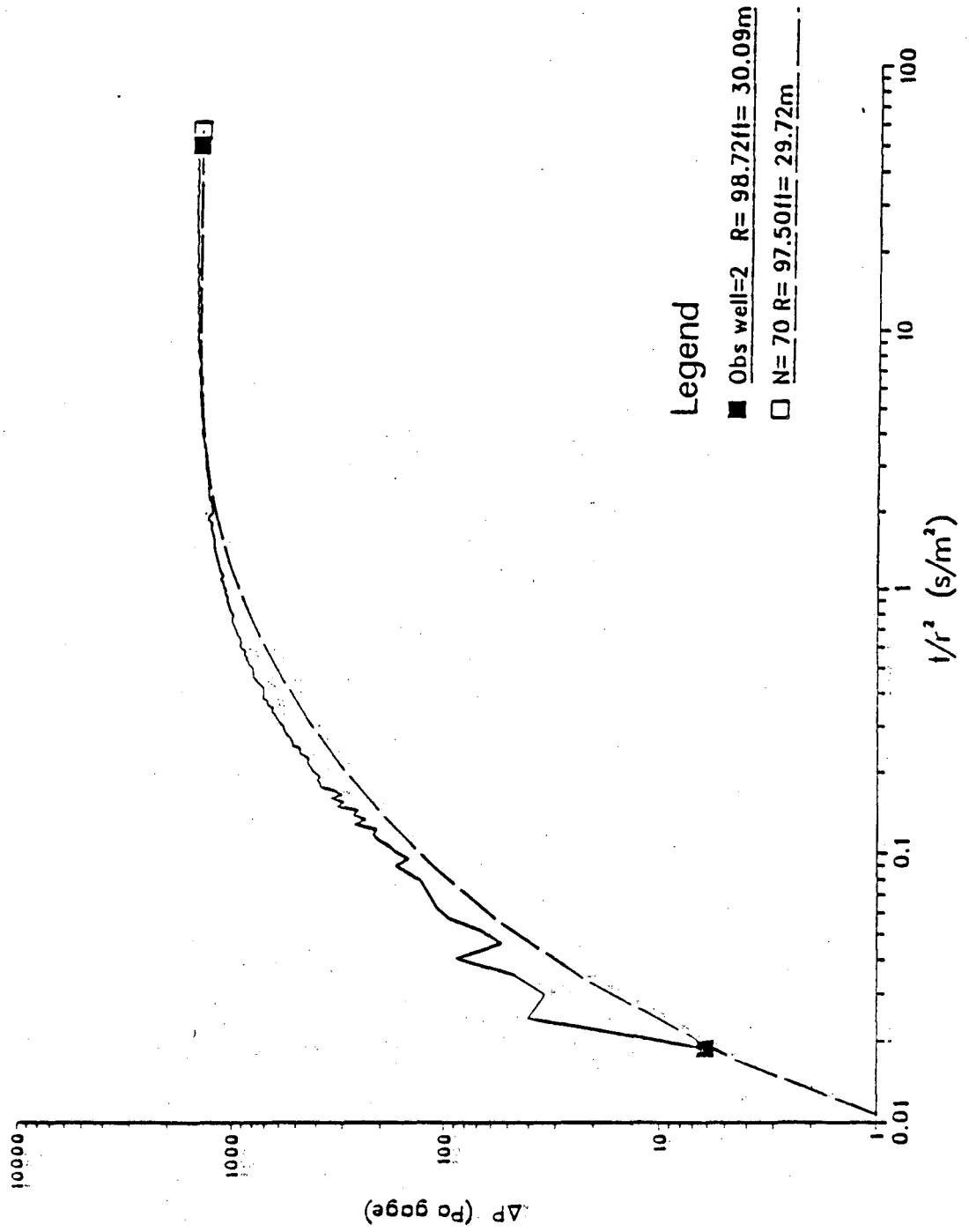

Legend
Obs well=6 R= 32.51ft= 9.91m
N= 64 R= 29.00ft= 8.84m
ΔP (Po gage)
10000
1000
100
10
0.01
0.1
1
10
100
1000
t/r² (s/m²)

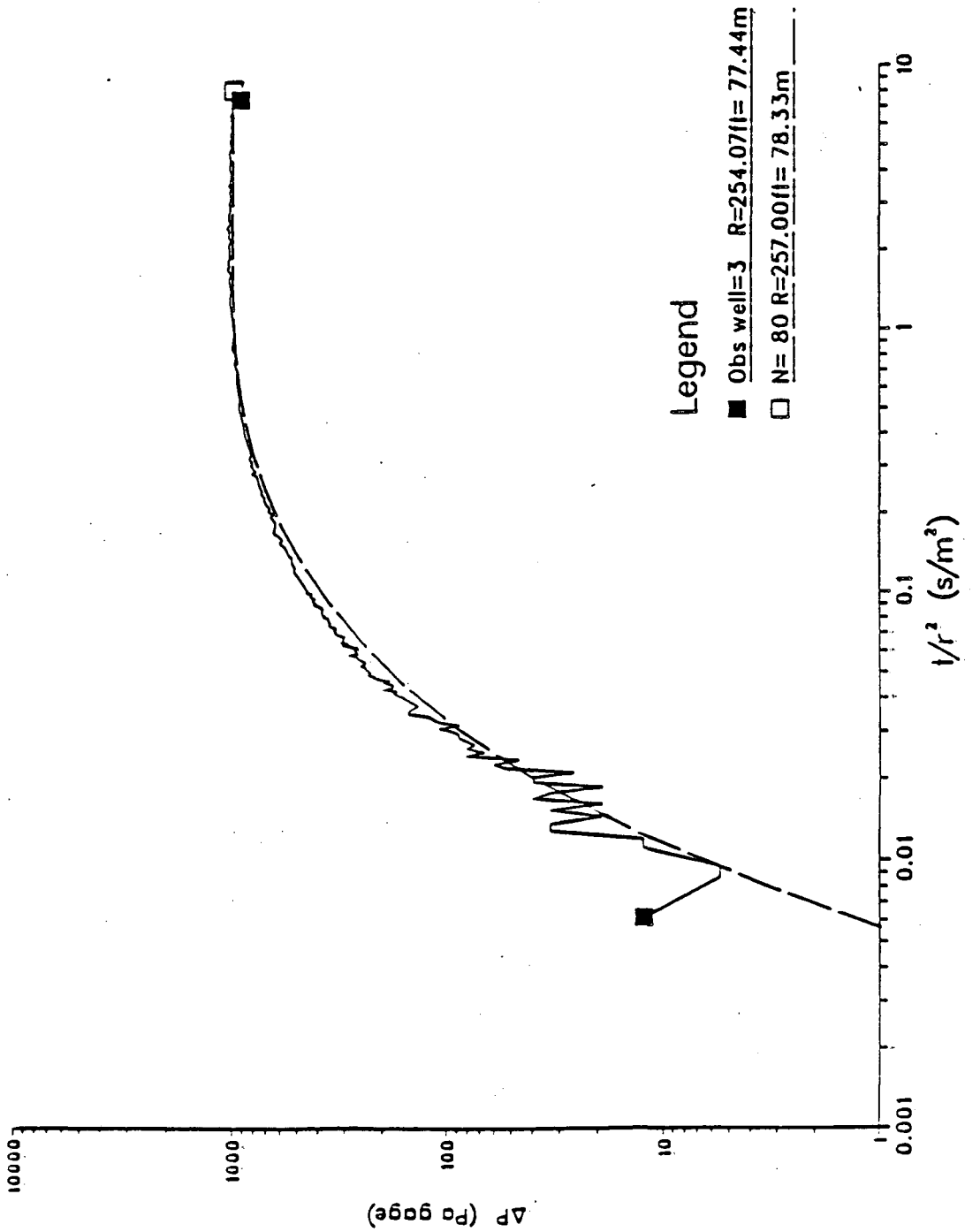

Legend
Obs well=7 R=269.091l= 82.02m
N= 81 R=269.001l= 81.99m
ΔP (Po gage)
1000
100
10
1
0.001
0.01
0.1
1
10
t/r² (s/m²)

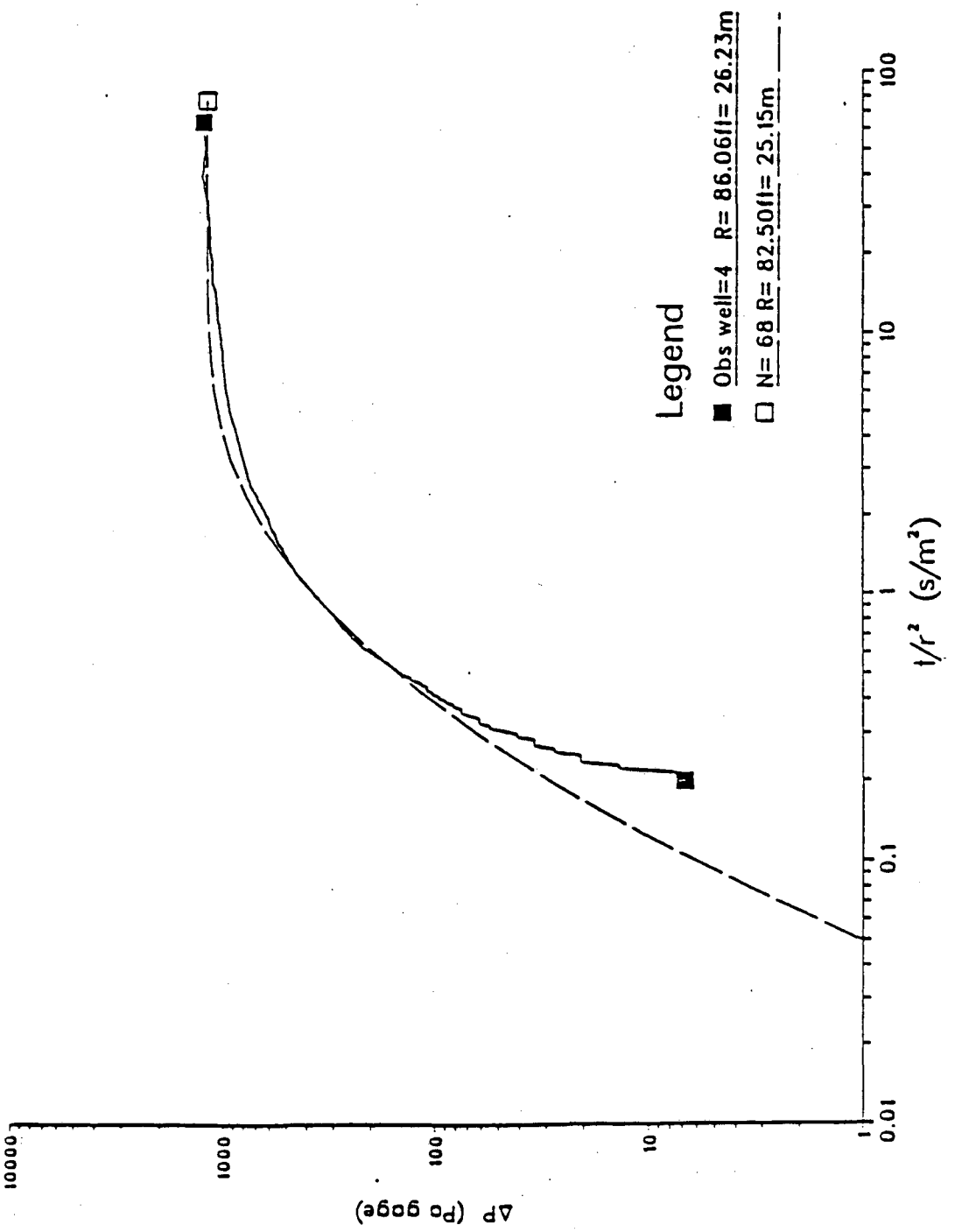

Legend
Obs well=8 R= 33.92ft= 10.34m
N= 65 R= 35.50ft= 10.82m
ΔP (Pa gage)
10000
1000
100
10
0.01
0.1
1
10
100
1000
t/r² (s/m²)

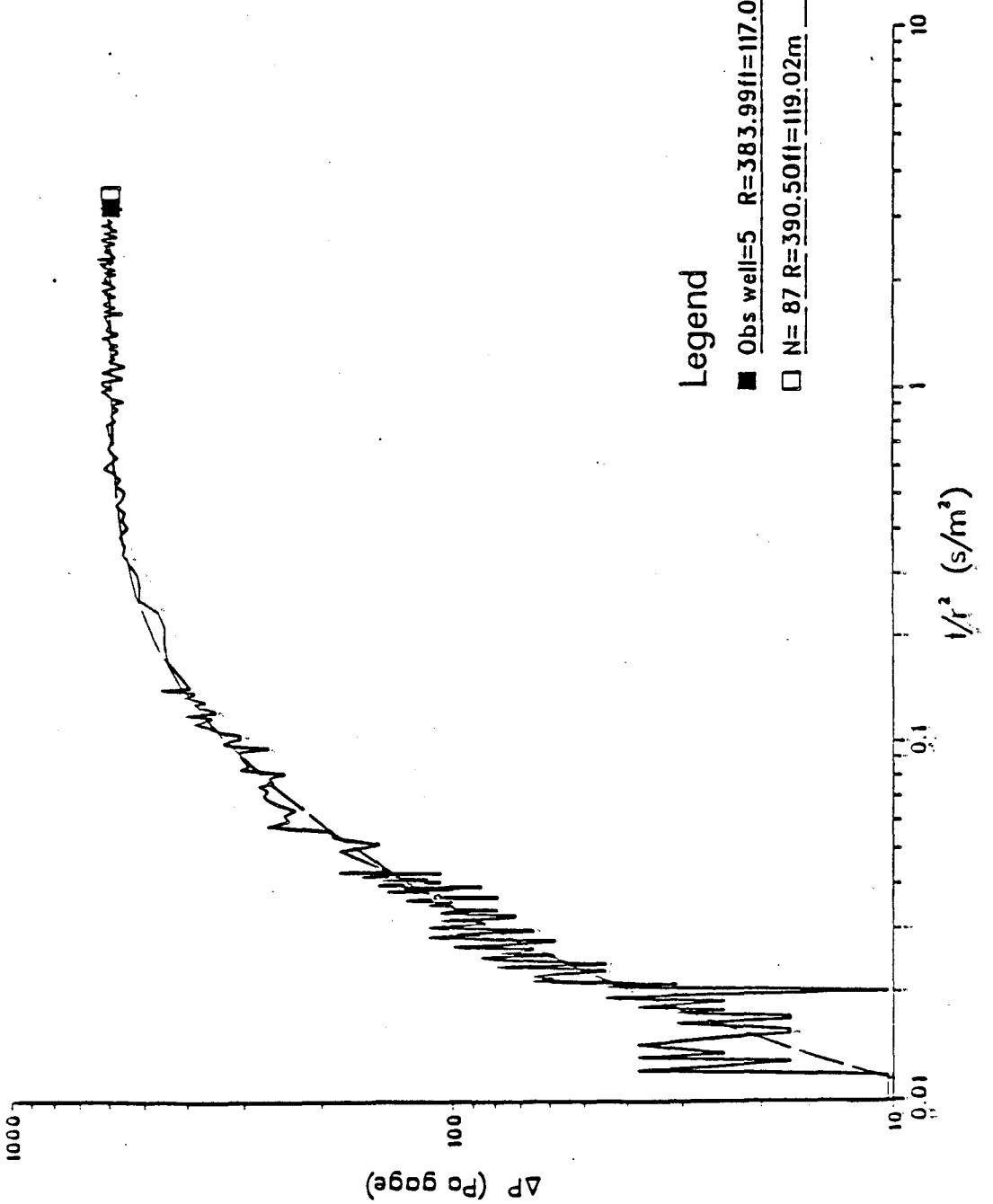

Legend
Obs well=9 R=217.491l= 66.29m
N= 76 R=217.491l= 66.29m
ΔP (Pa gage)
10000
1000
100
10
0.01
0.1
1
10
1/r² (s/m²)

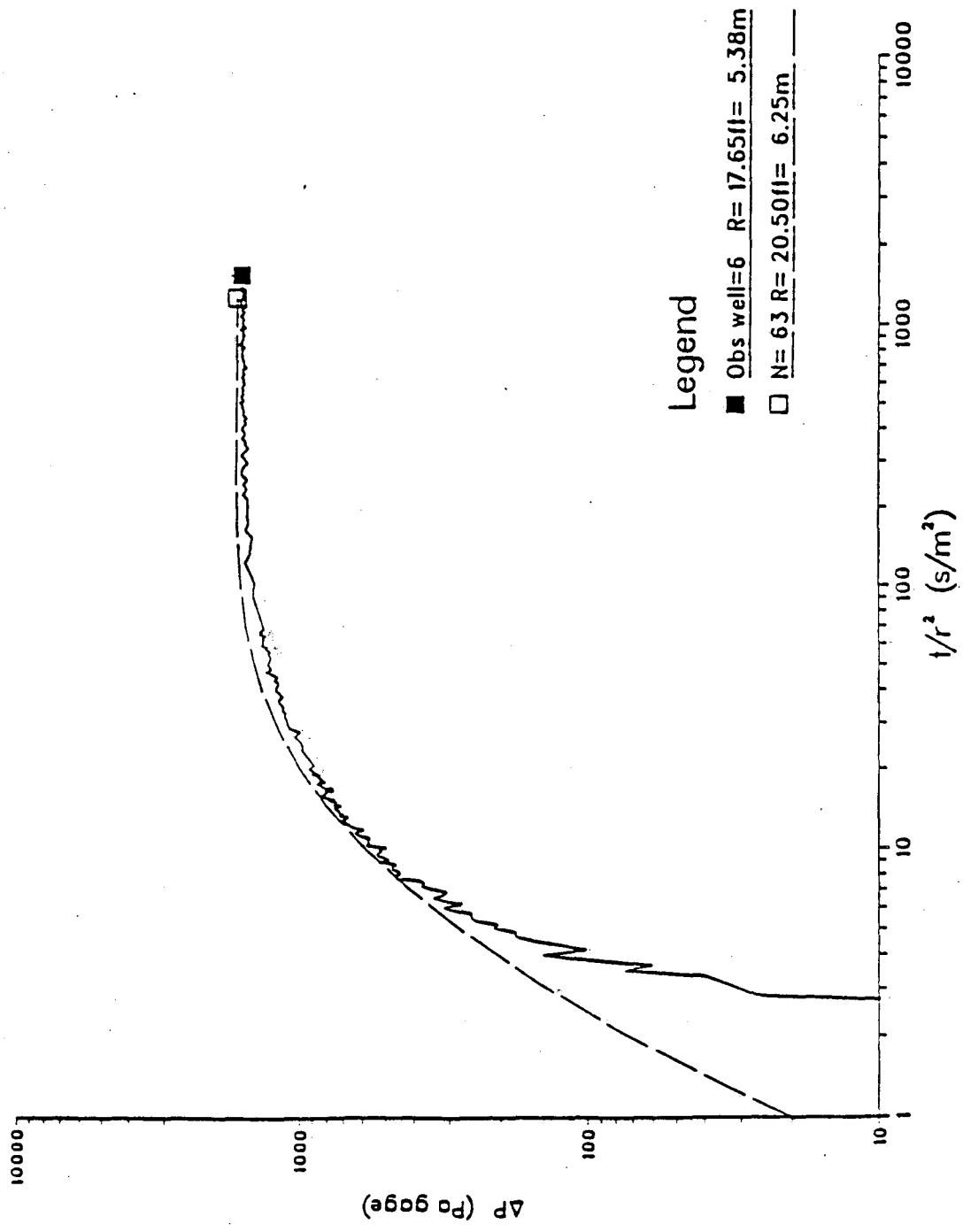
INTERFERENCE TEST 3 - PRODUCING HO80

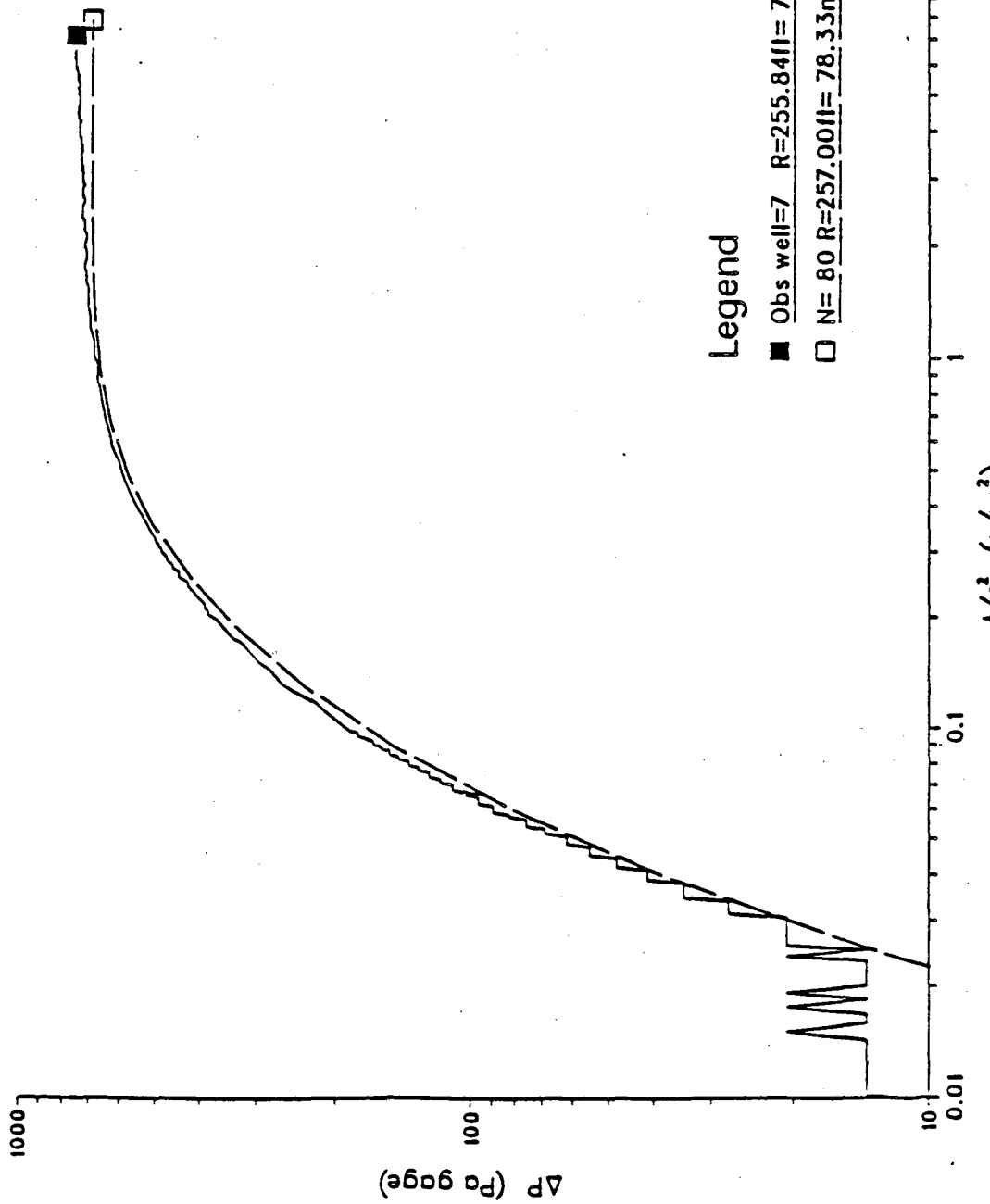

Legend
Obs well=2 R= 98.72ft= 30.09m
N= 70 R= 97.50ft= 29.72m
ΔP (Po gage)
10000
1000
100
10
1
0.01
0.1
1
10
100
t/r² (s/m²)

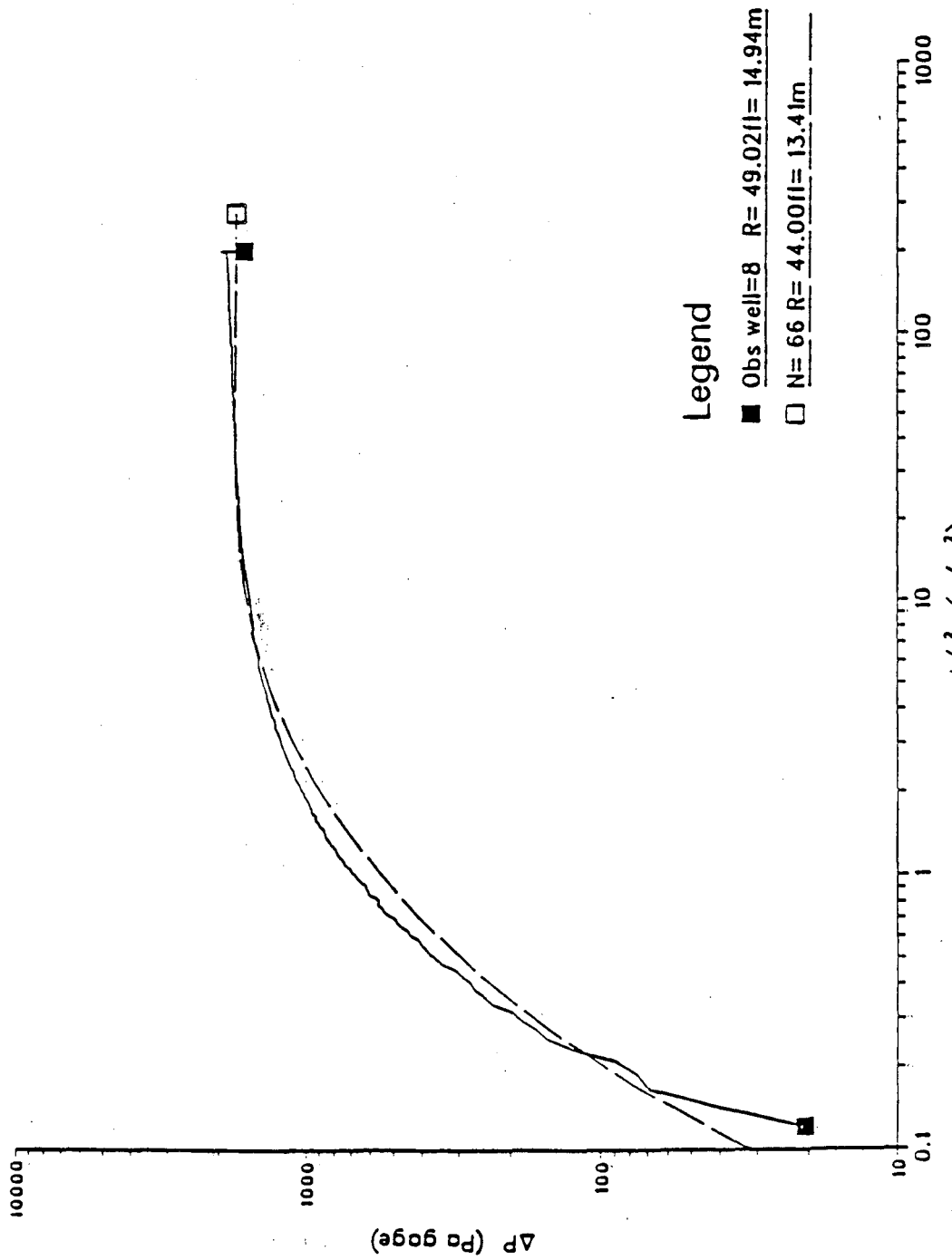

Legend
Obs well=3 R=254.07(l= 77.44m
N= 80 R=257.00(l= 78.33m
ΔP (Pa gage)
10000
1000
100
10
1
0.001
0.01
0.1
1
10
t/r² (s/m²)

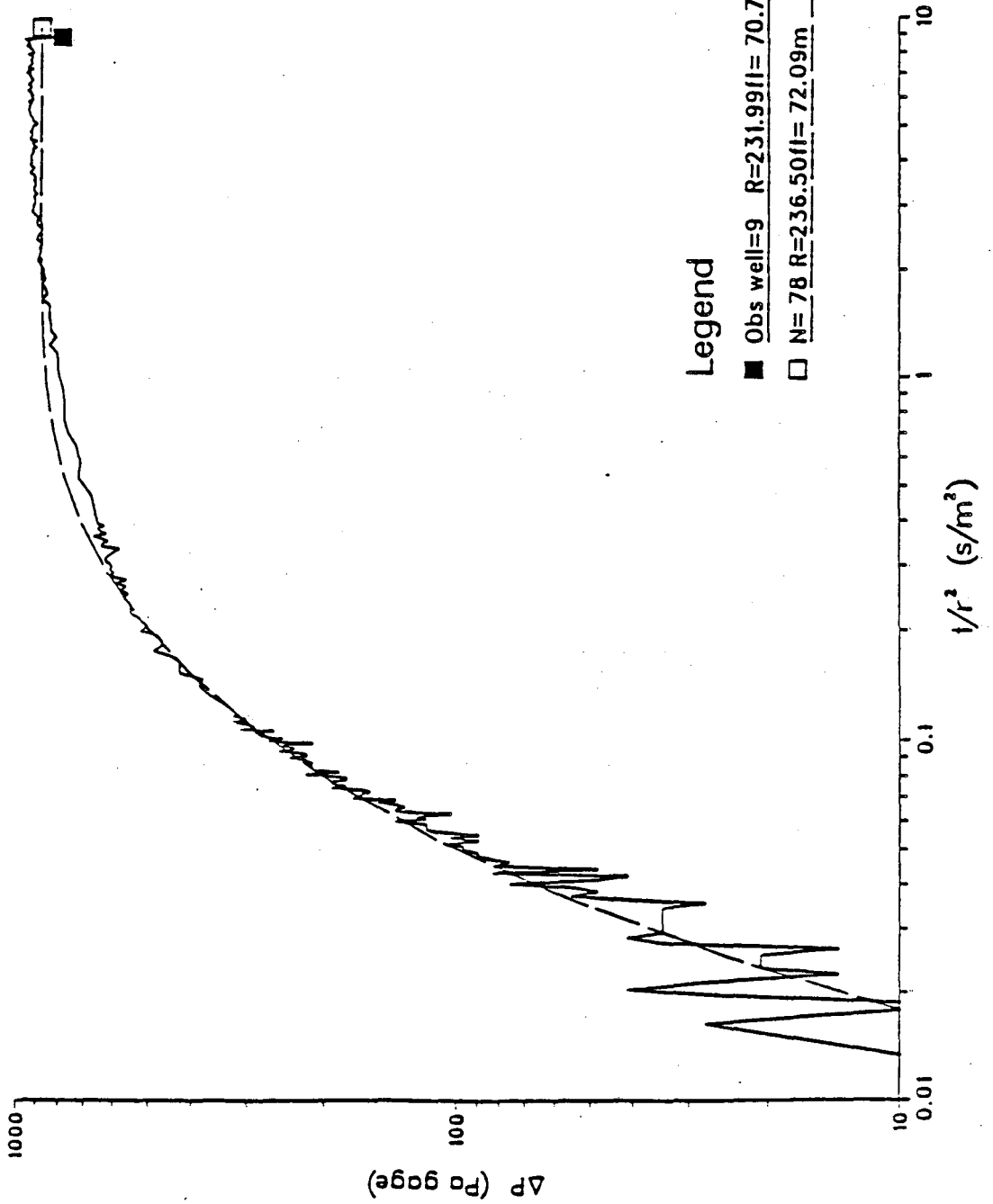

Legend
Obs well=4 R= 86.06ft= 26.23m
N= 68 R= 82.50ft= 25.15m
ΔP (Po gage)
10000
1000
100
10
1
0.01
0.1
1
10
100
t/r² (s/m²)


Legend
Obs well=5 R=383.99ft=117.04m
N= 87 R=390.50ft=119.02m
ΔP (Po gage)
1000
100
10
0.01
0.1
1
10
1/r² (s/m²)

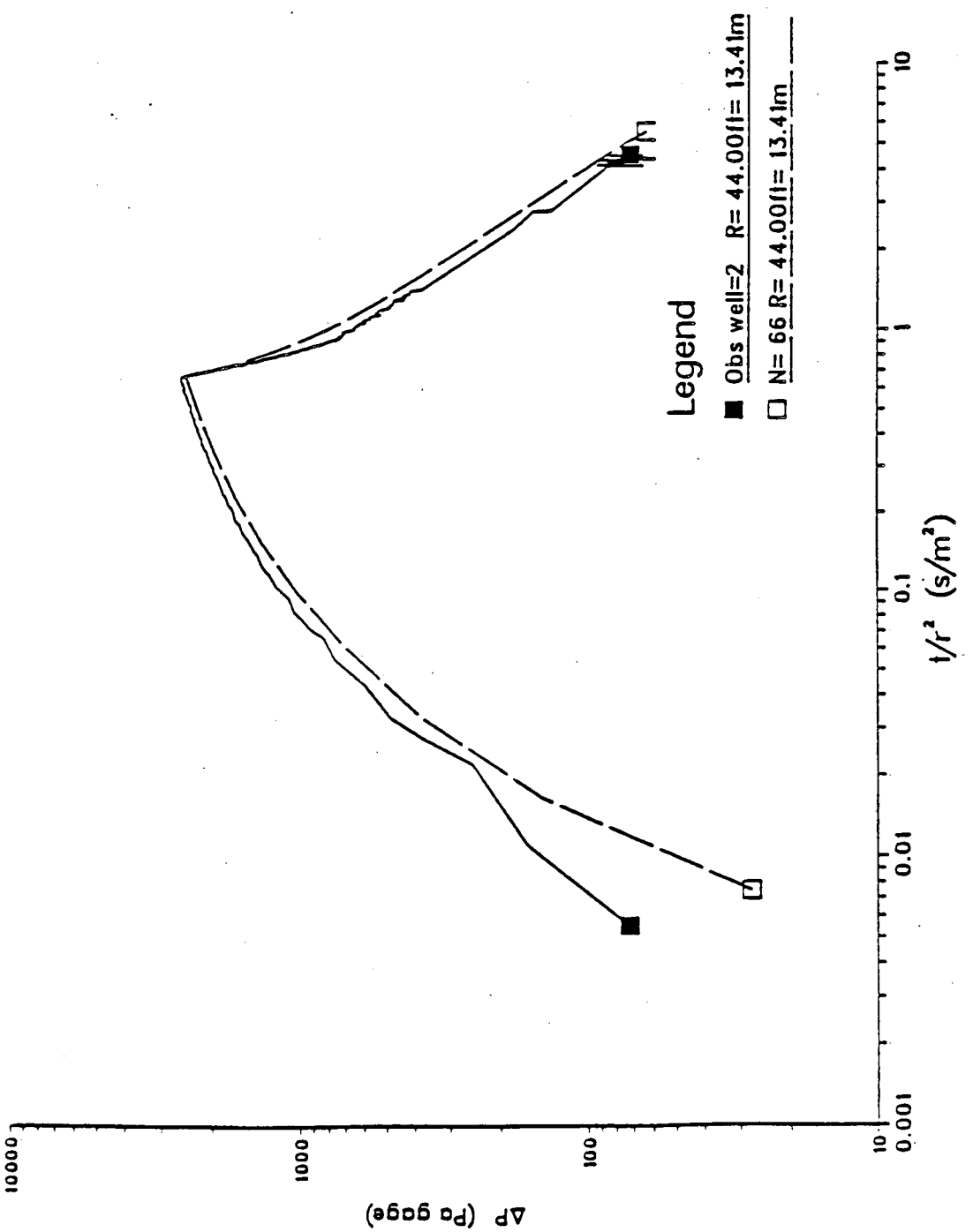

Legend
Obs well=6 R= 17.65ft= 5.38m
N= 63 R= 20.50ft= 6.25m
ΔP (Po gage)
10000
1000
100
10
1
10
100
1000
10000
t/r² (s/m²)

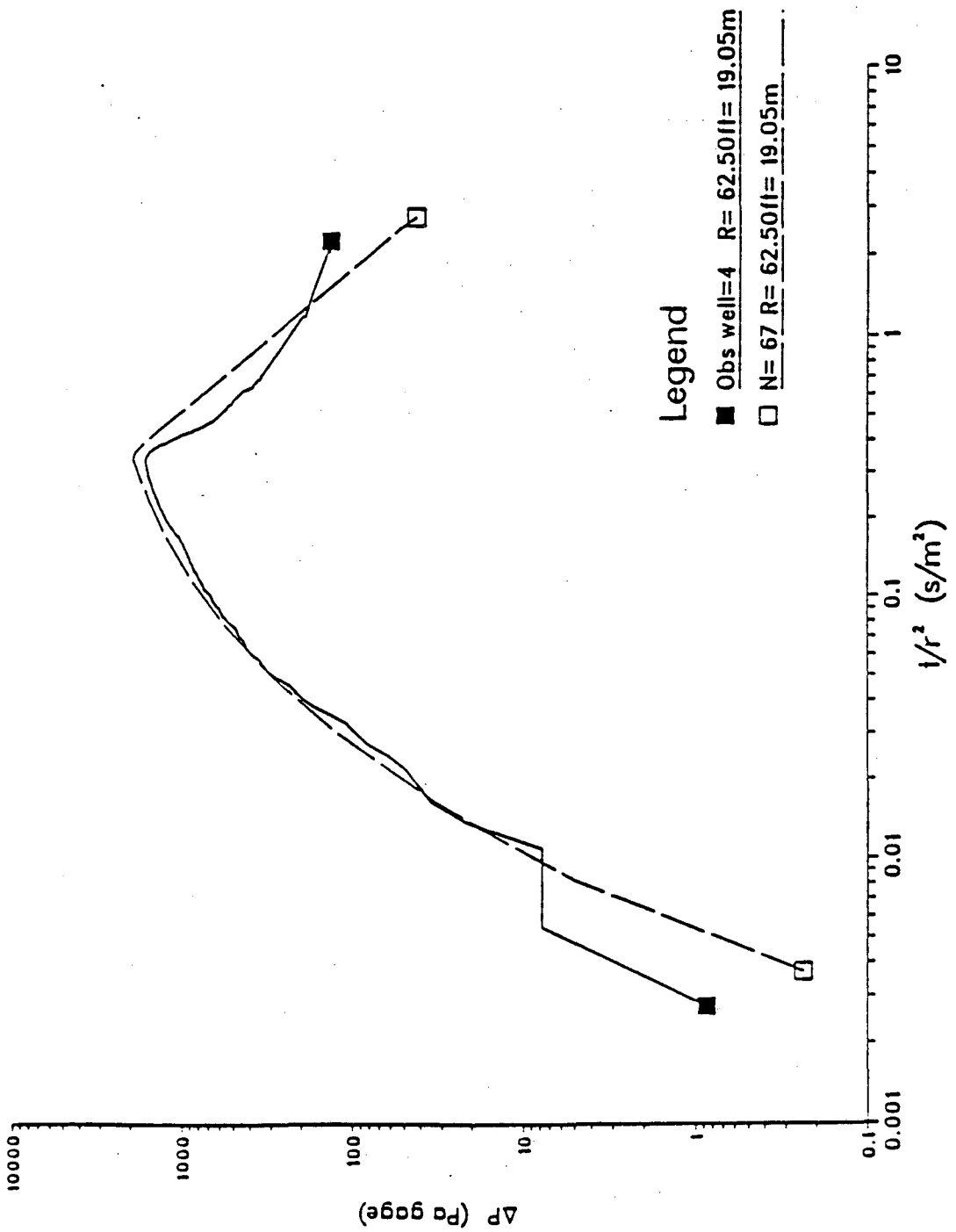

Legend
Obs well=7 R=255.84ll= 77.98m
N= 80 R=257.00ll= 78.33m
ΔP (Pa gage)
1000
100
10
0.01
0.1
1
10
t/r² (s/m²)

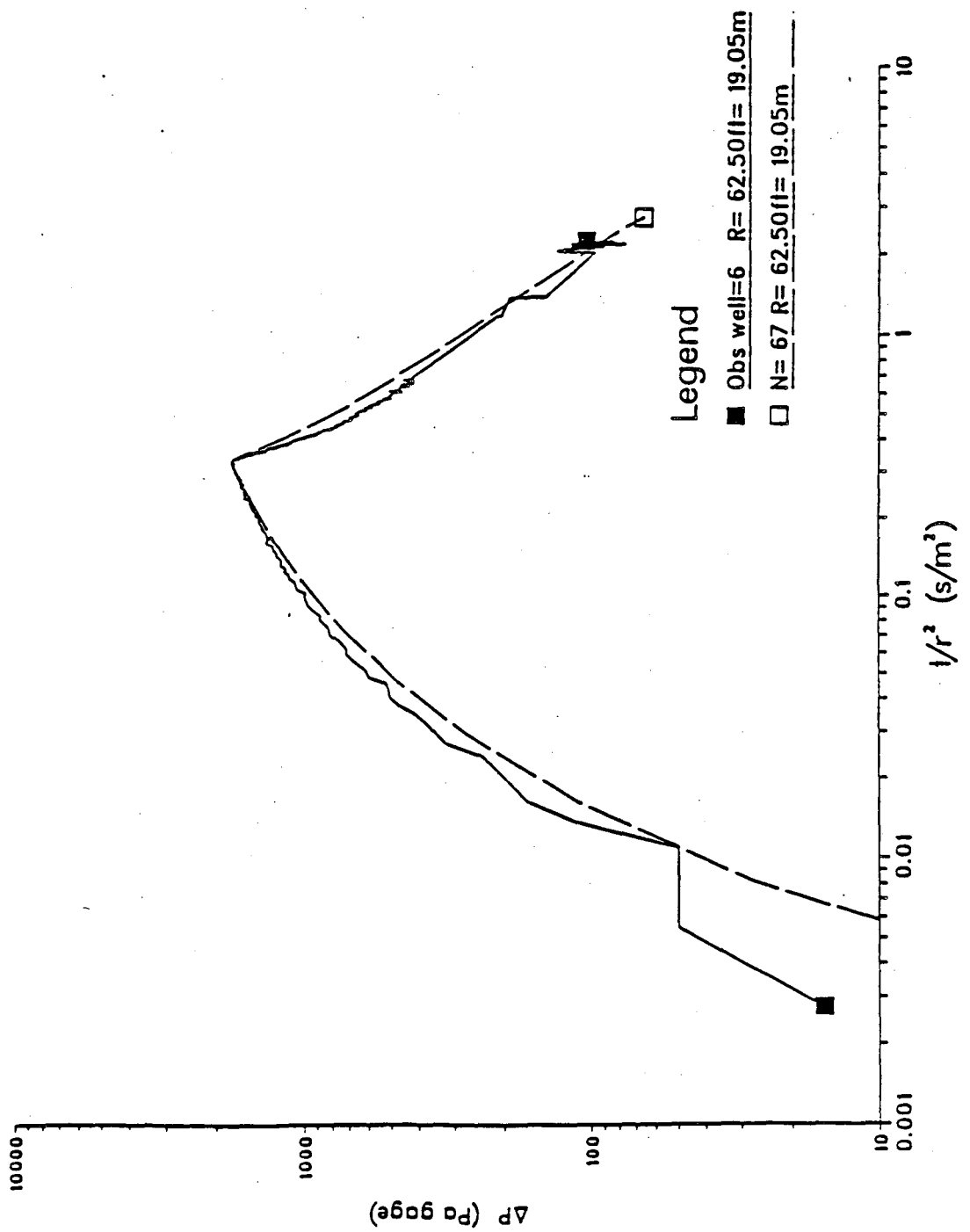

Legend
Obs well=8 R= 49.02ft= 14.94m
N= 66 R= 44.00ft= 13.41m
ΔP (Pa gage)
10000
1000
100
10
0.1
1
10
100
1000
t/r² (s/m²)

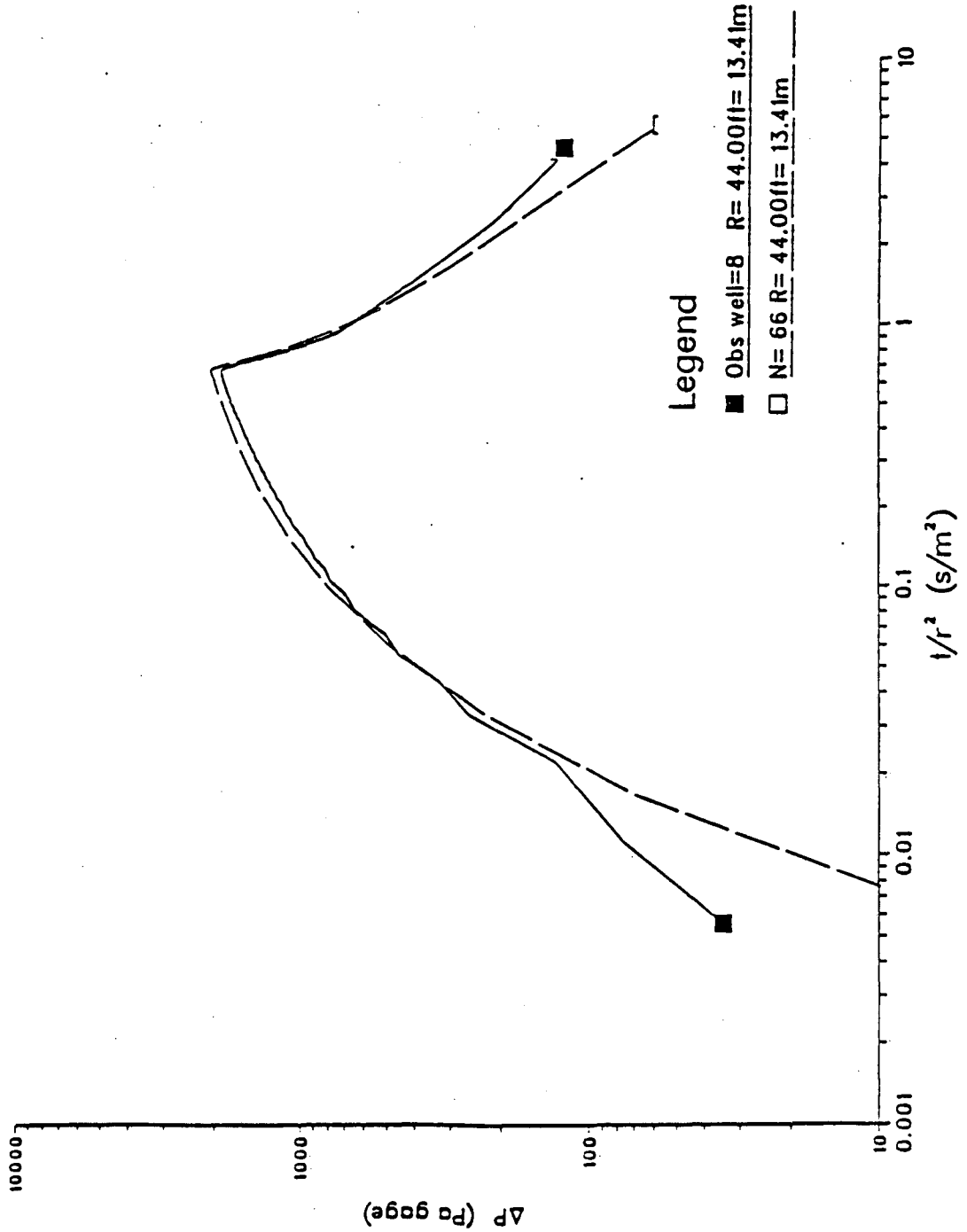

Legend
Obs well=9 R=231.99ft= 70.71m
N= 78 R=236.50ft= 72.09m
ΔP (Po gage)
1000
100
10
0.01
0.1
1
10
t/r² (s/m²)

PULSE TEST 1 - PRODUCING I1

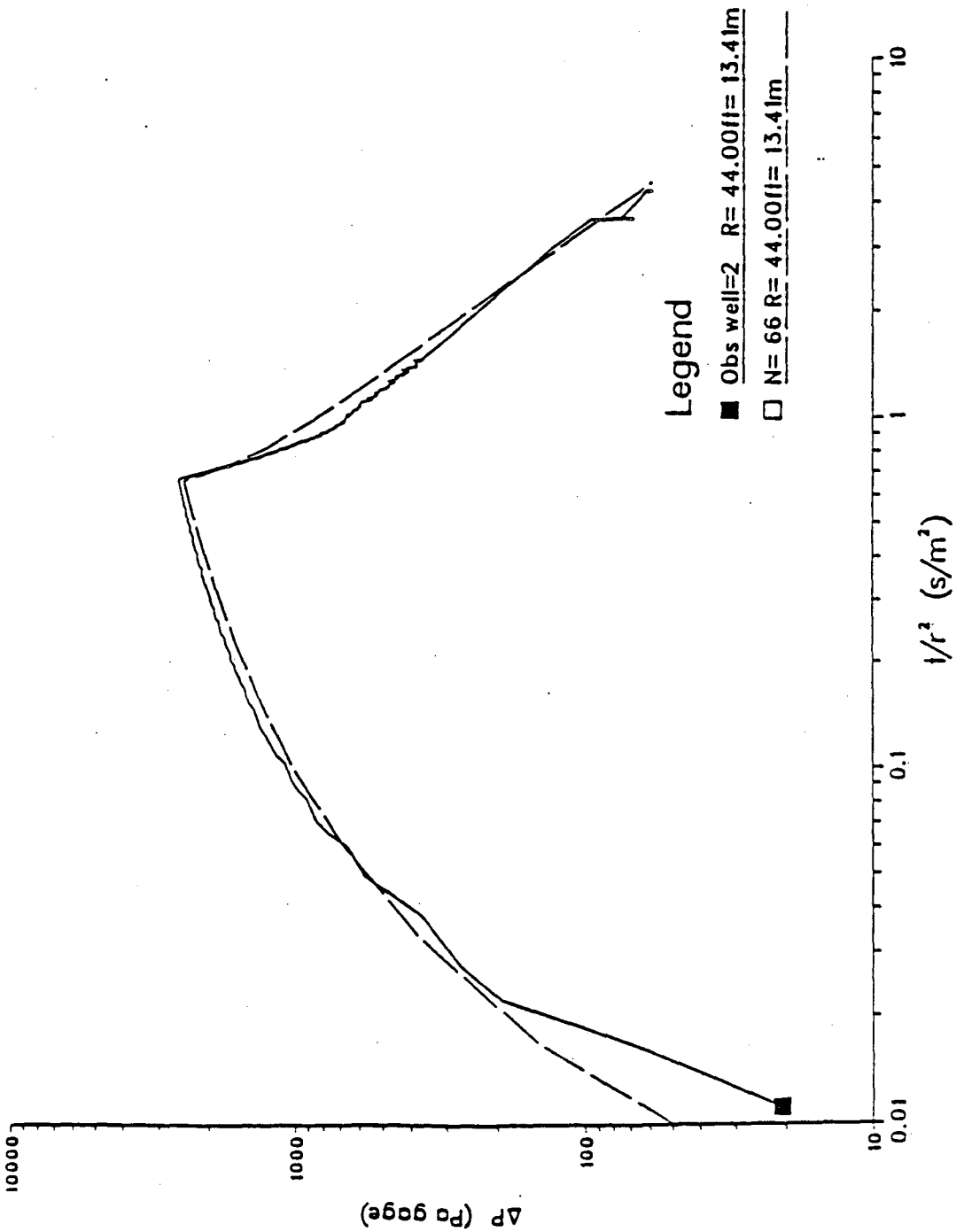

Legend
Obs well=2 R= 44.00ft= 13.41m
N= 66 R= 44.00ft= 13.41m
ΔP (Pa gage)
10000
1000
100
10
0.001
0.01
0.1
1
10
t/r² (s/m²)

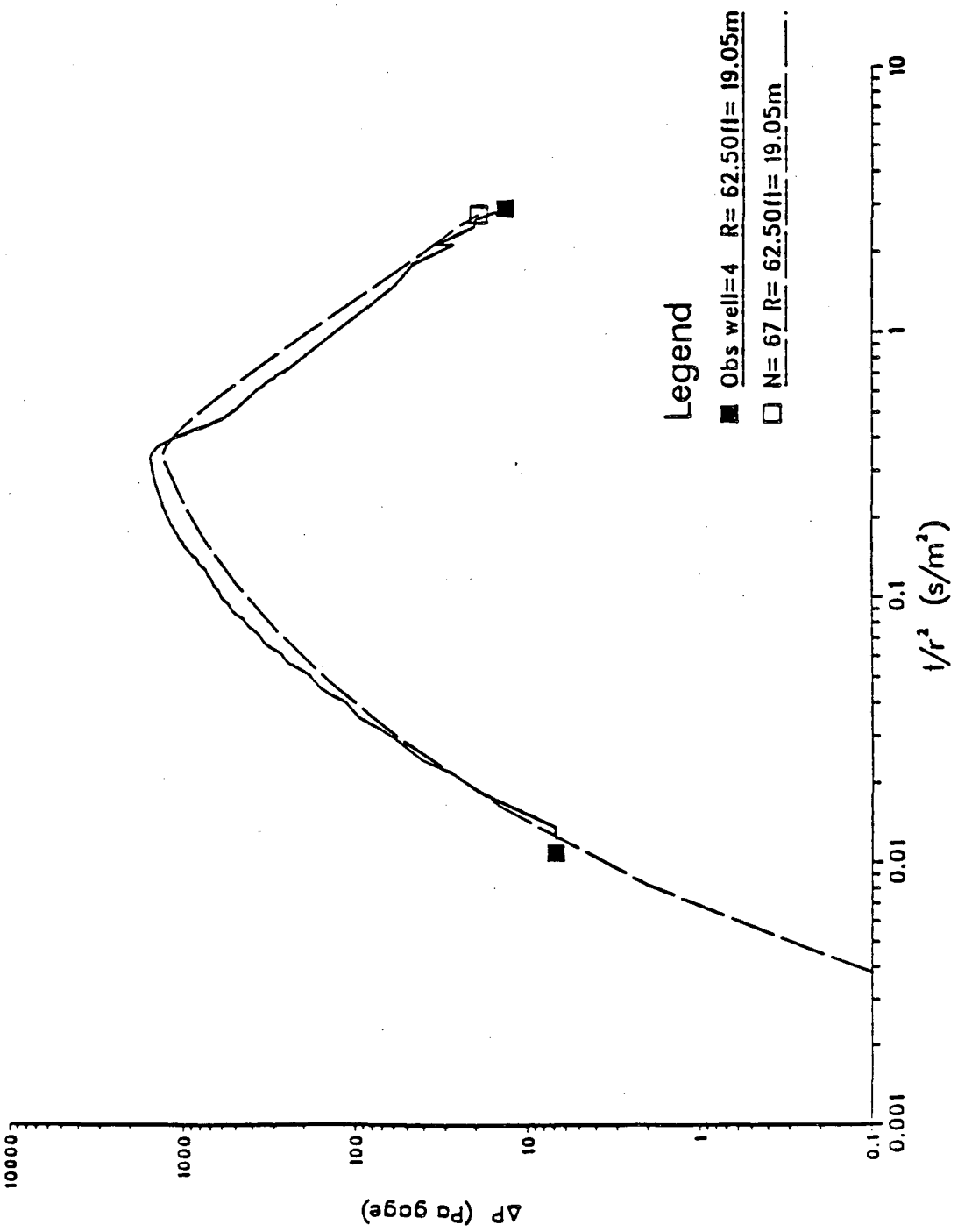

Legend
Obs well=4 R= 62.50ft= 19.05m
N= 67 R= 62.50ft= 19.05m
ΔP (Pa gage)
10000
1000
100
10
1
0.1
0.001
0.01
0.1
1
10
t/r² (s/m²)

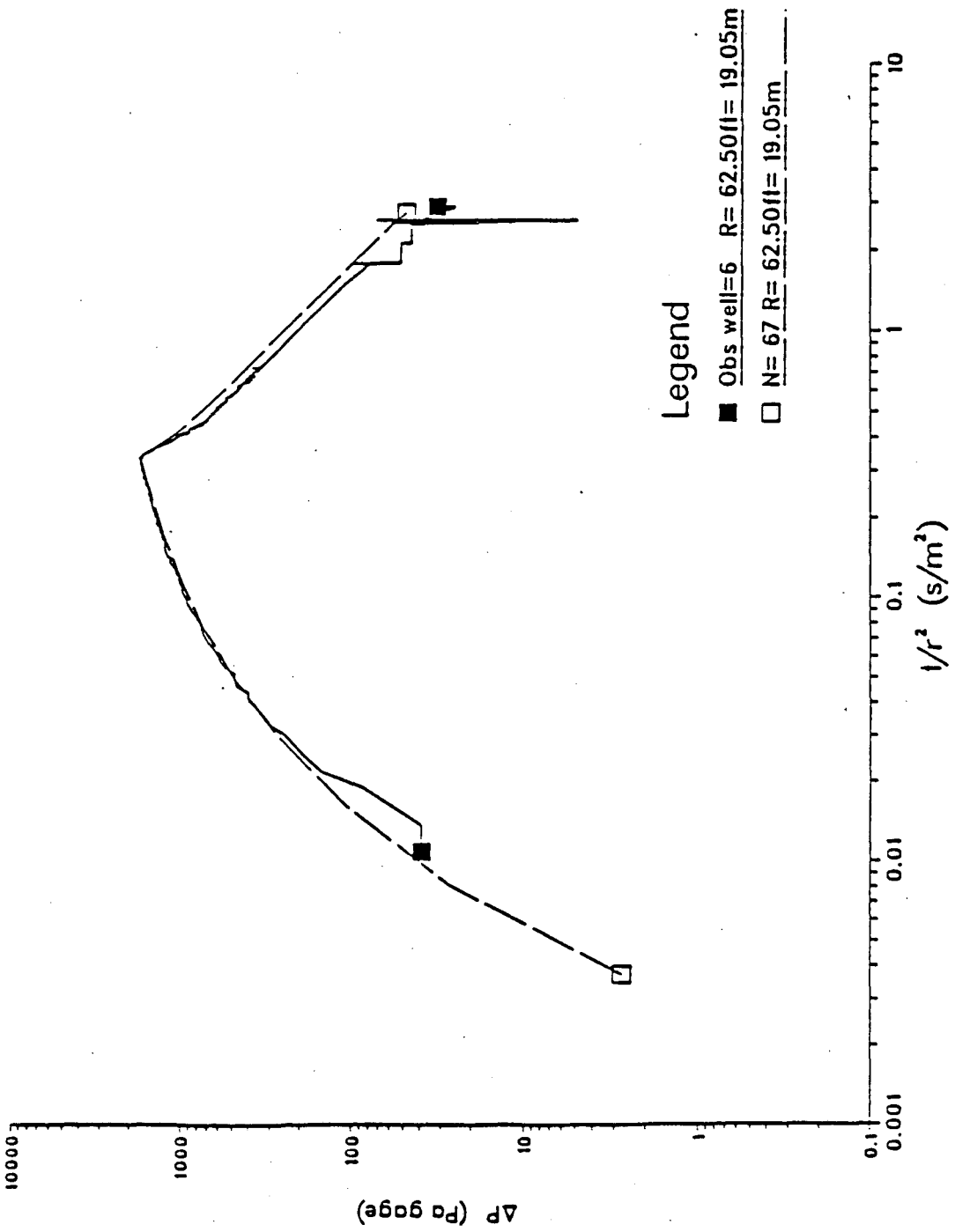

Legend
Obs well=6 R= 62.50ft= 19.05m
N= 67 R= 62.50ft= 19.05m
ΔP (Pa gage)
10000
1000
100
10
0.001
0.01
0.1
1
10
t/r² (s/m²)

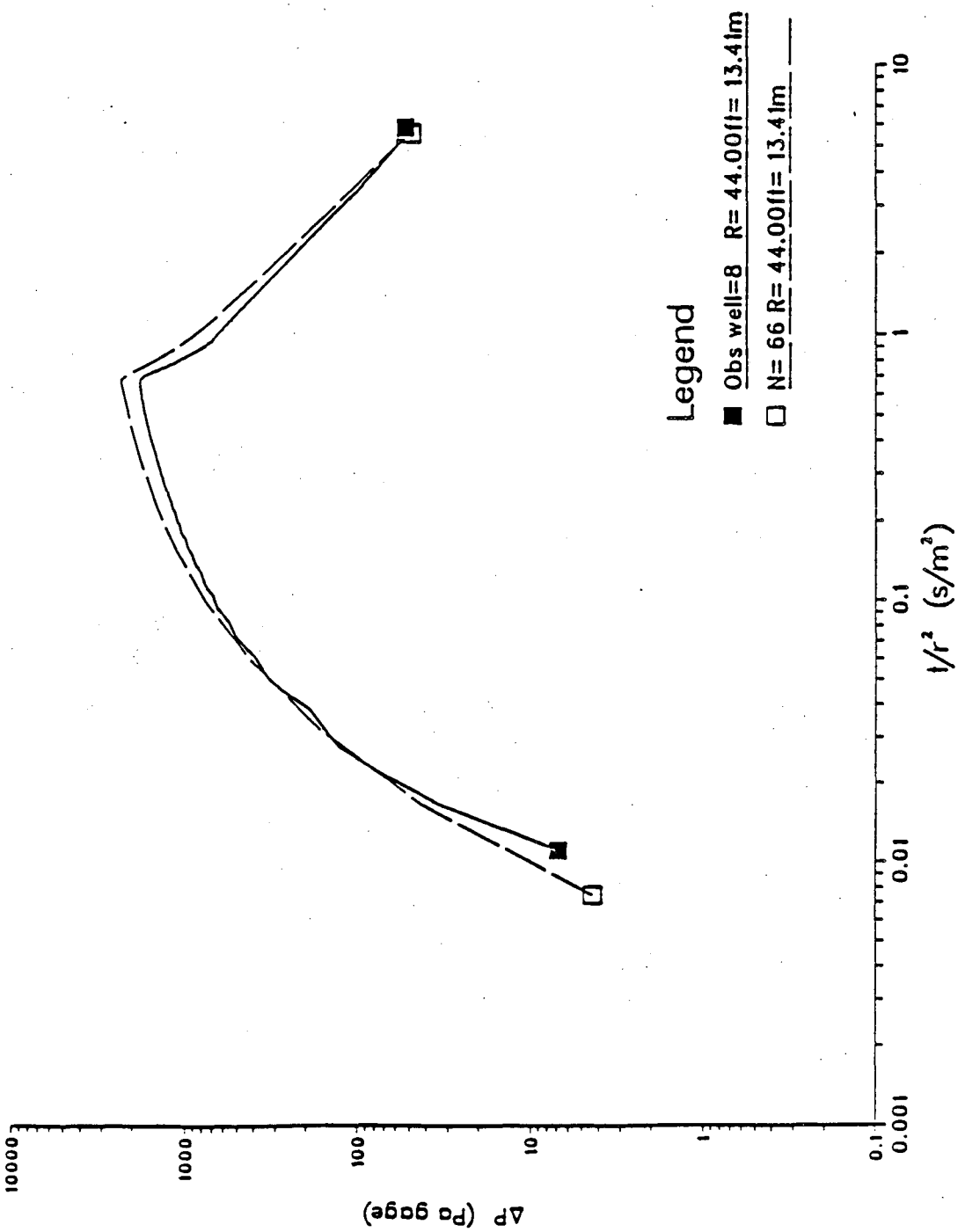

ΔP (Pa gage)
10000
1000
100
10
0.001
0.01
0.1
1
10
t/r² (s/m²)
Legend
Obs well=8 R= 44.00ft= 13.4m
N= 66 R= 44.00ft= 13.4m

PULSE TEST 2 - PRODUCING I1

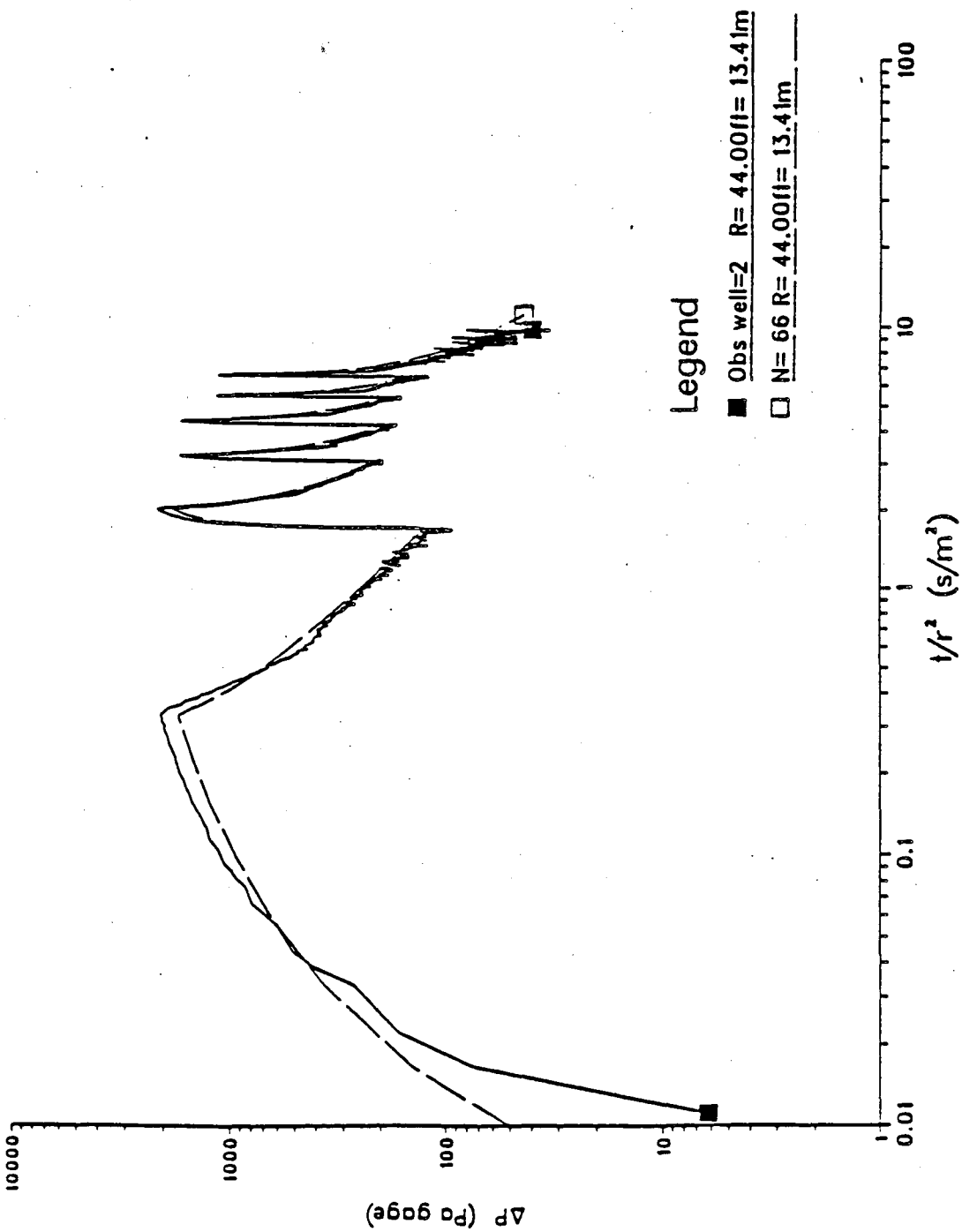

Legend
Obs well=2 R= 44.00ft= 13.4m
N= 66 R= 44.00ft= 13.4m
ΔP (Po gage)
10000
1000
100
10
0.01
0.1
1
10
t/r² (s/m²)

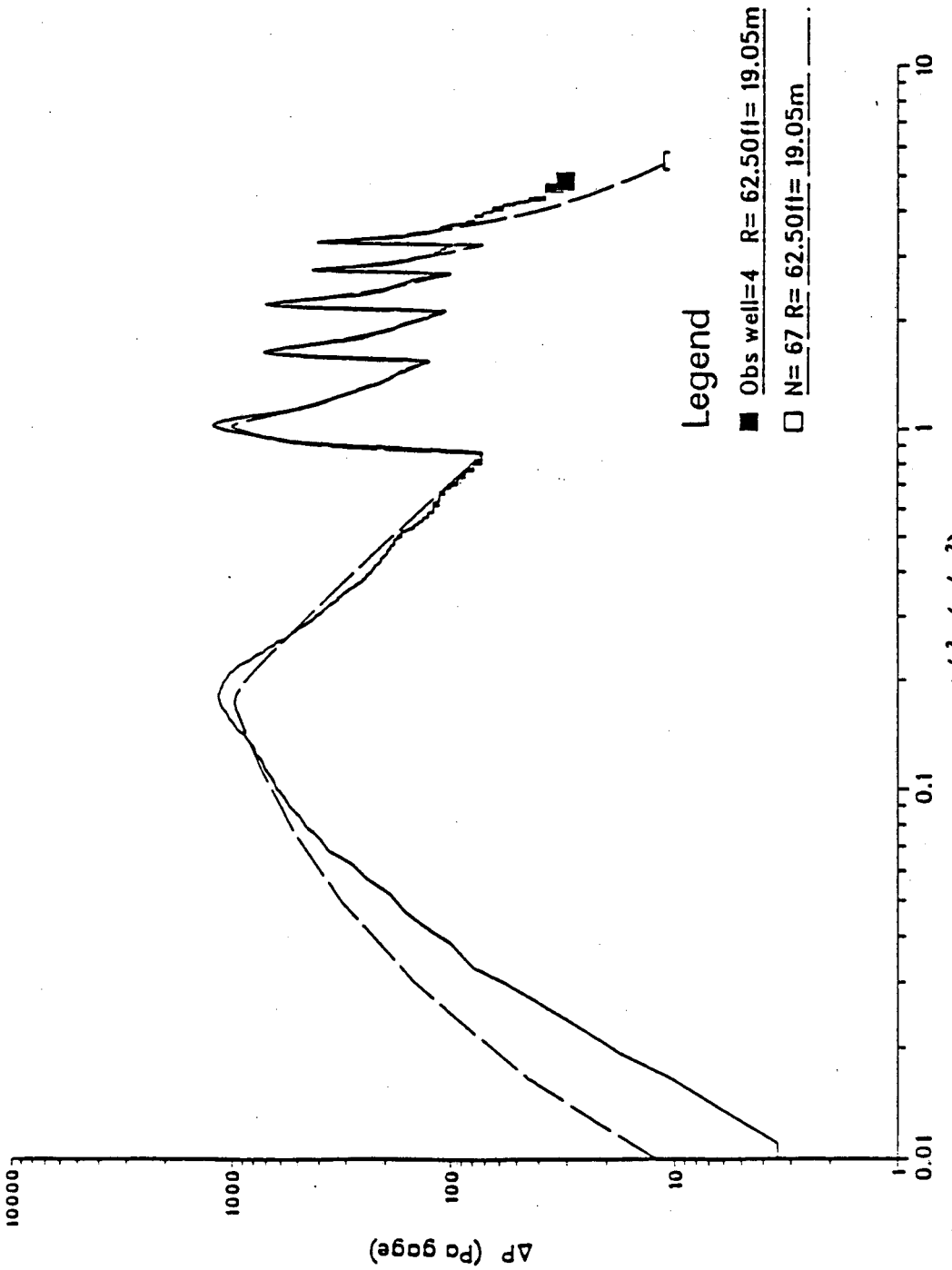

Legend
Obs well=4 R= 62.50ft= 19.05m
N= 67 R= 62.50ft= 19.05m
ΔP (Pa gage)
10000
1000
100
10
1
0.1
0.001
0.01
0.1
1
10
t/r² (s/m²)

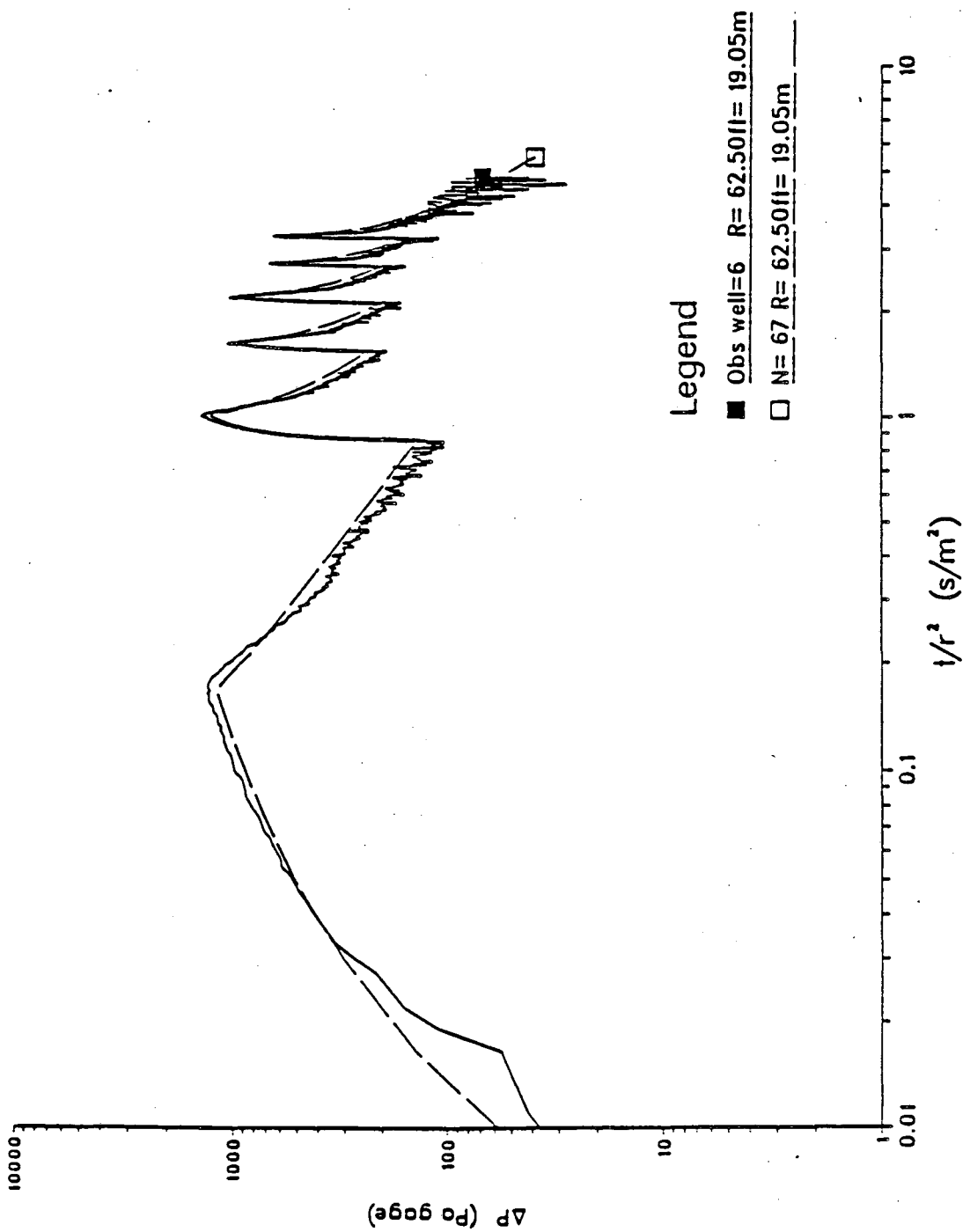

Legend
Obs well=6 R= 62.50ft= 19.05m
N= 67 R= 62.50ft= 19.05m
ΔP (Pa gage)
10000
1000
100
10
1
0.1
0.001
0.01
0.1
1
10
t/r² (s/m²)

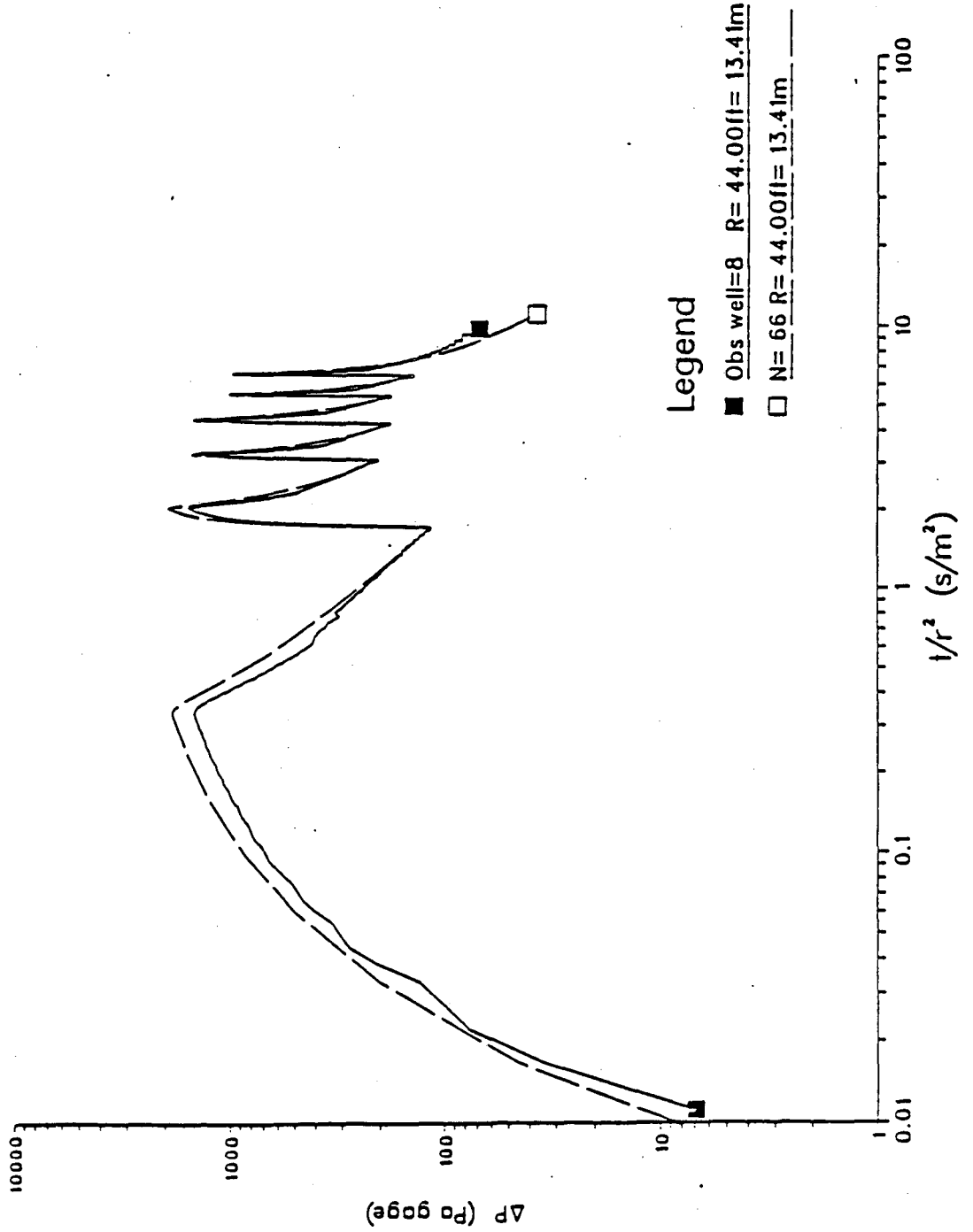

Legend
Obs well=8 R= 44.00ft= 13.4lm
N= 66 R= 44.00ft= 13.4lm
ΔP (Pa gage)
10000
1000
100
10
1
0.1
0.001
0.01
0.1
1
10
t/r² (s/m²)

PULSE TEST 3 - PRODUCING I1

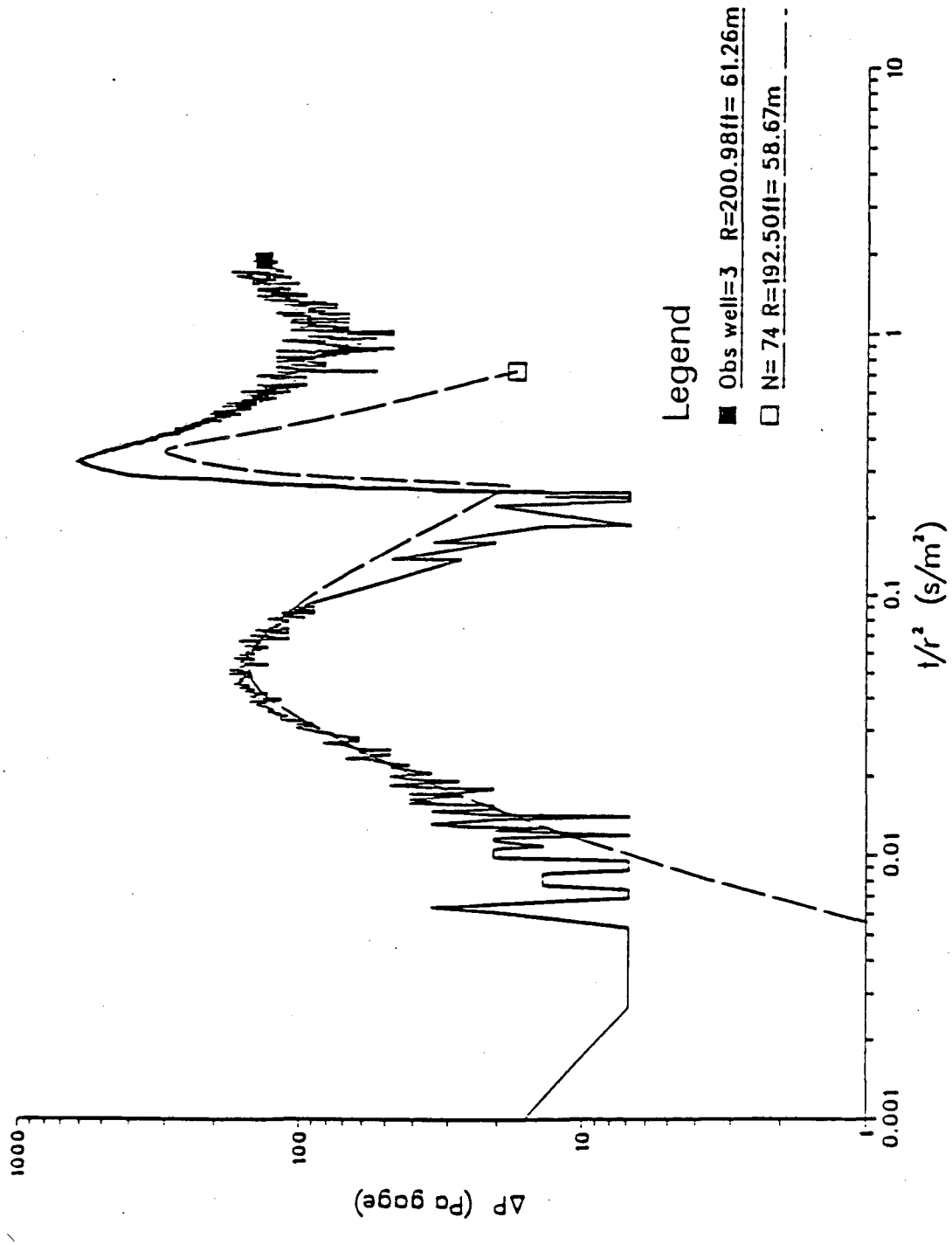

Legend
Obs well=2 R= 44.00ft= 13.41m
N= 66 R= 44.00ft= 13.41m
ΔP (Pa gage)
t/r² (s/m²)
10000
1000
100
10
1
0.01
0.1
1
10
100

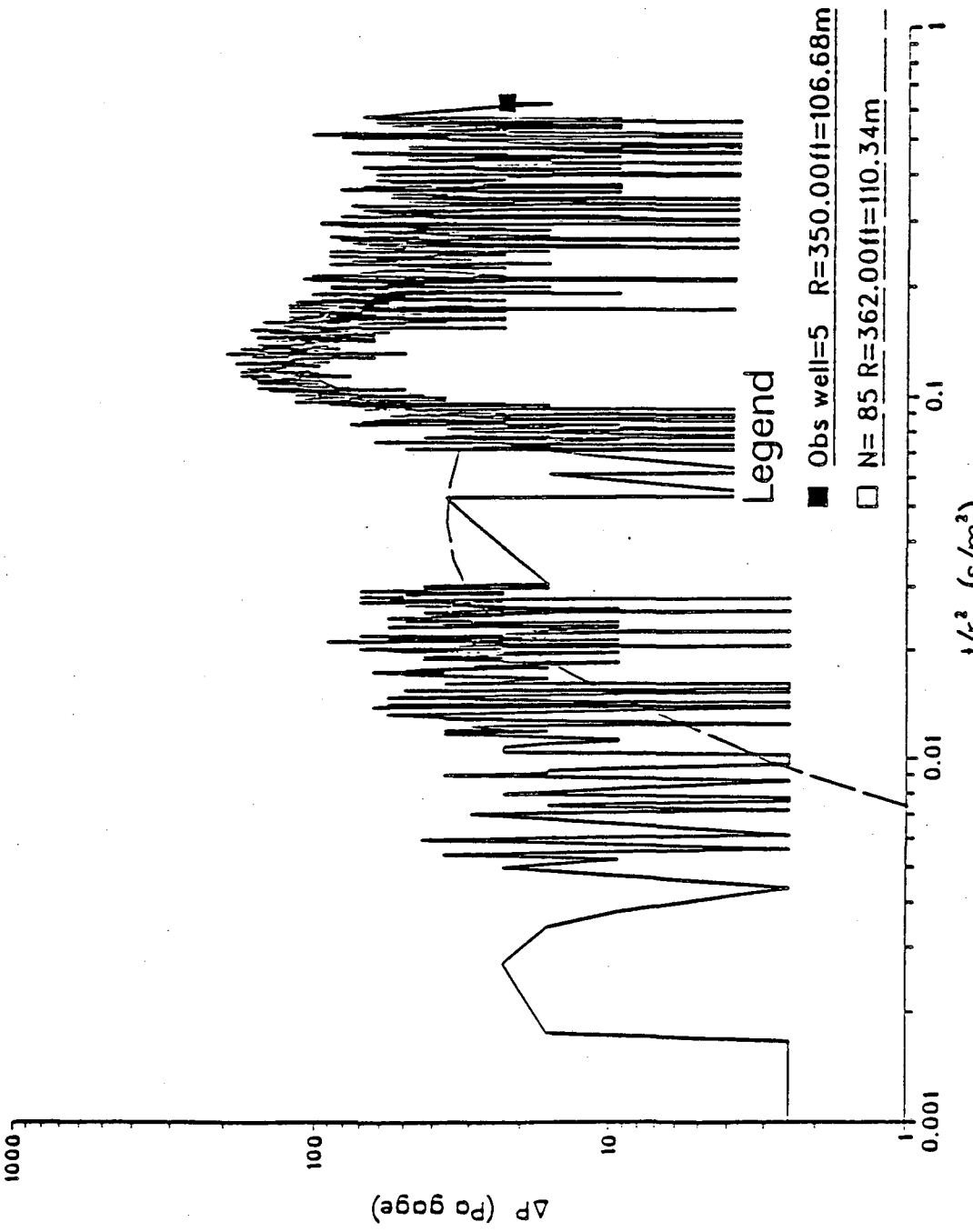

Legend
Obs well=4 R= 62.50ft= 19.05m
N= 67 R= 62.50ft= 19.05m
ΔP (Pa gage)
10000
1000
100
10
1
0.01
0.1
1
10
1/r² (s/m²)

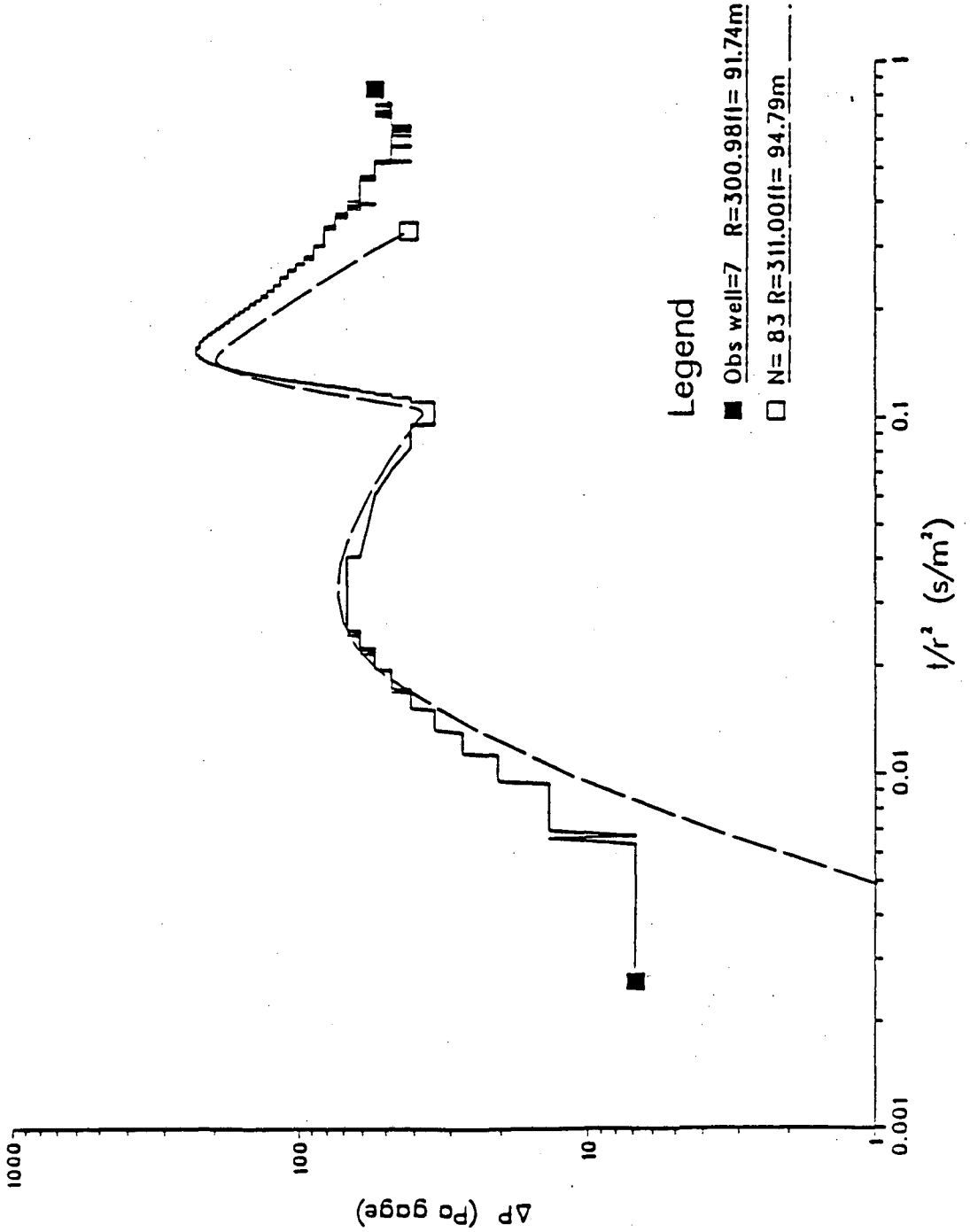

Legend
Obs well=6 R= 62.50ft= 19.05m
N= 67 R= 62.50ft= 19.05m
ΔP (Po gage)
10000
1000
100
10
1
0.01
0.1
1
10
1/r² (s/m²)

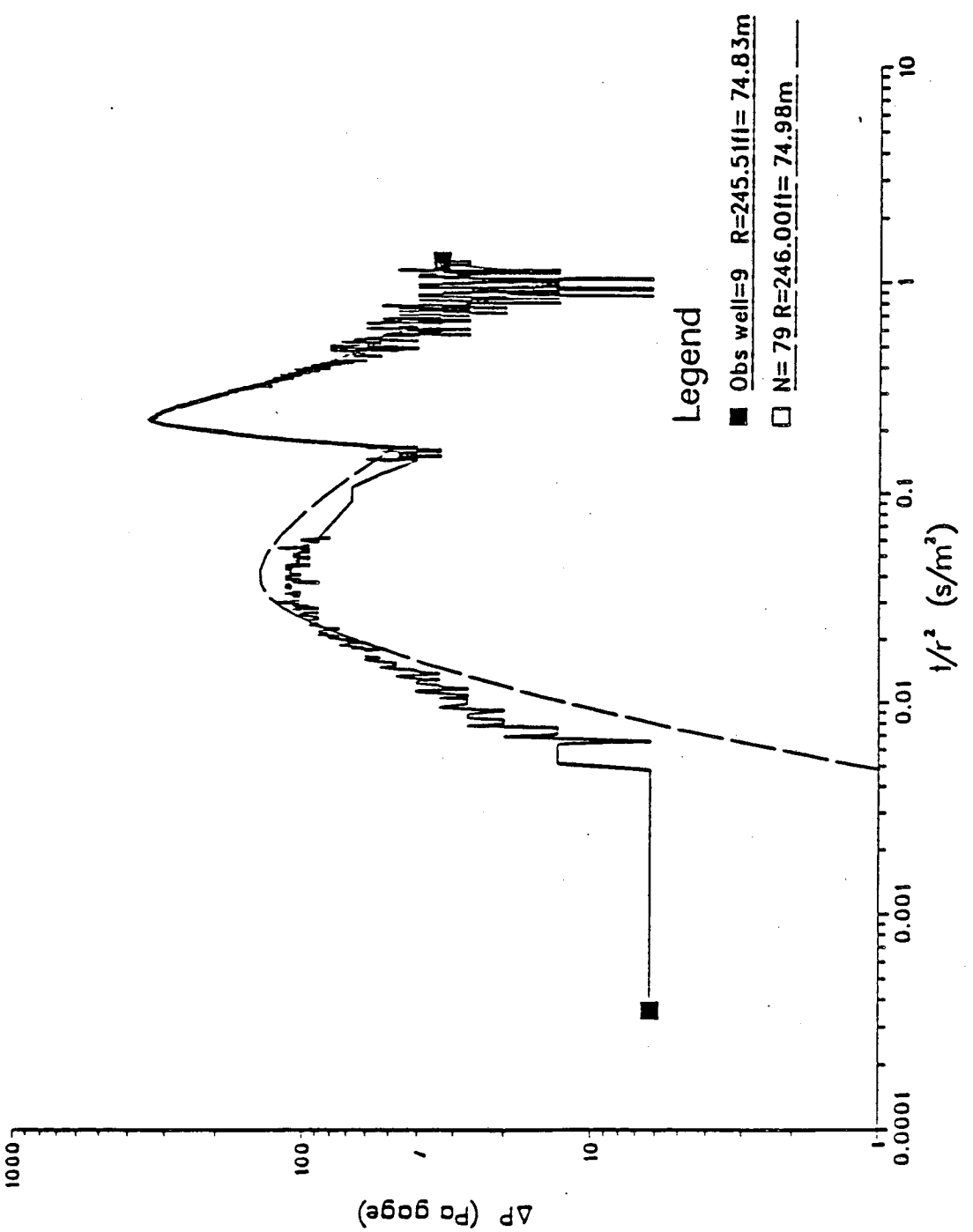

Legend
Obs well=8 R= 44.00ft= 13.41m
N= 66 R= 44.00ft= 13.41m
ΔP (Pa gage)
10000
1000
100
10
1
0.01
0.1
1
10
100
t/r² (s/m²)

PULSE TEST 4 - PRODUCING I1

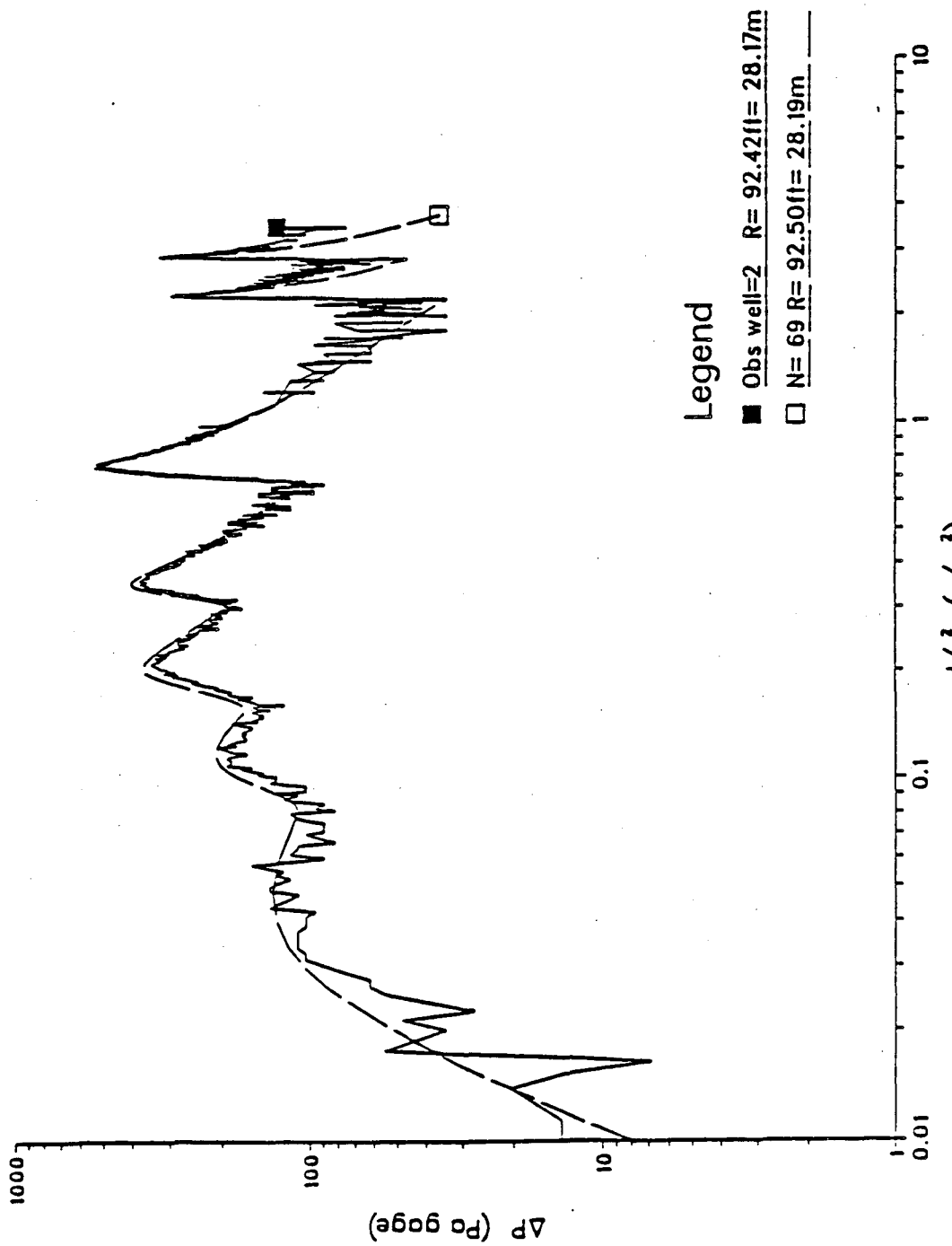

Legend
Obs well=3 R=200.98ft= 61.26m
N= 74 R=192.50ft= 58.67m
ΔP (Po gage)
1000
100
10
1
0.001
0.01
0.1
1
10
t/r² (s/m²)

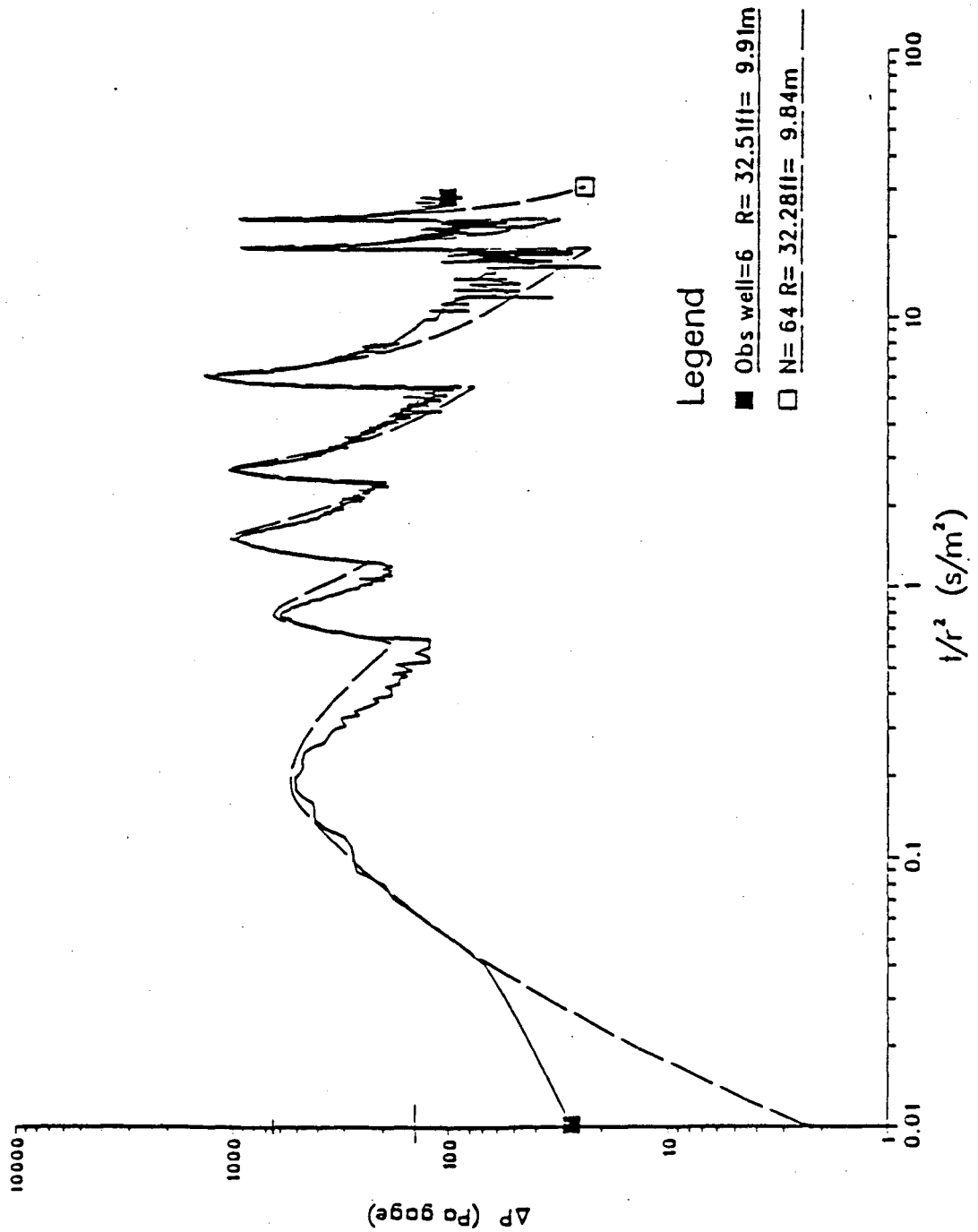

ΔP (Po gage)
1000
100
10
1
0.001
0.01
0.1
1
t/r² (s/m³)
Legend
Obs well=5 R=350.00ft=106.68m
N= 85 R=362.00ft=110.34m

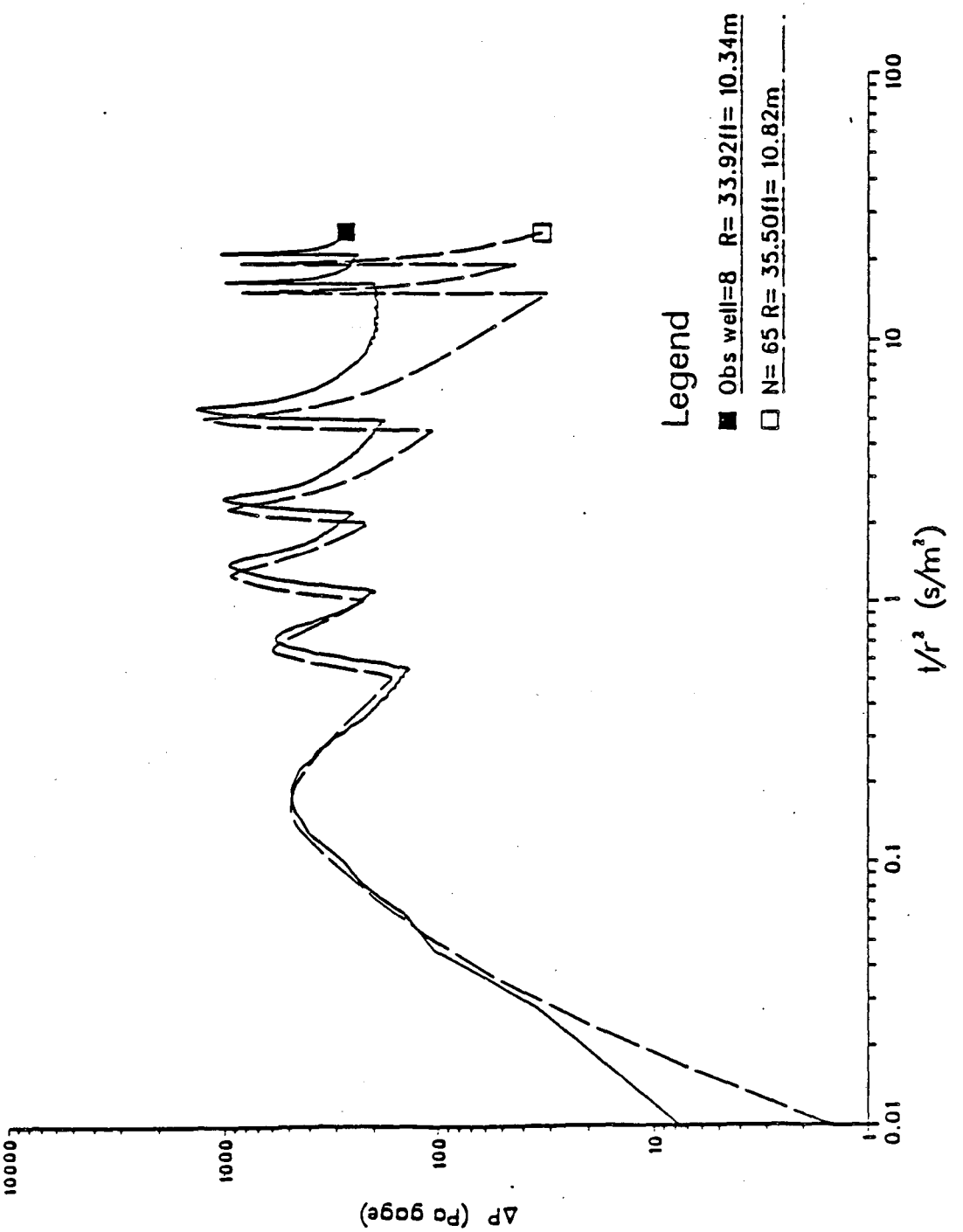

Legend
Obs well=7 R=300.98ft= 91.74m
N= 83 R=311.00ft= 94.79m
ΔP (Po gage)
1000
100
10
1
0.001
0.01
0.1
1
1/r² (s/m²)


Legend
Obs well=9 R=245.51ft= 74.83m
N= 79 R=246.00ft= 74.98m
ΔP (Pa gage)
1000
100
10
1
0.0001
0.001
0.01
0.1
1
10
t/r² (s/m²)

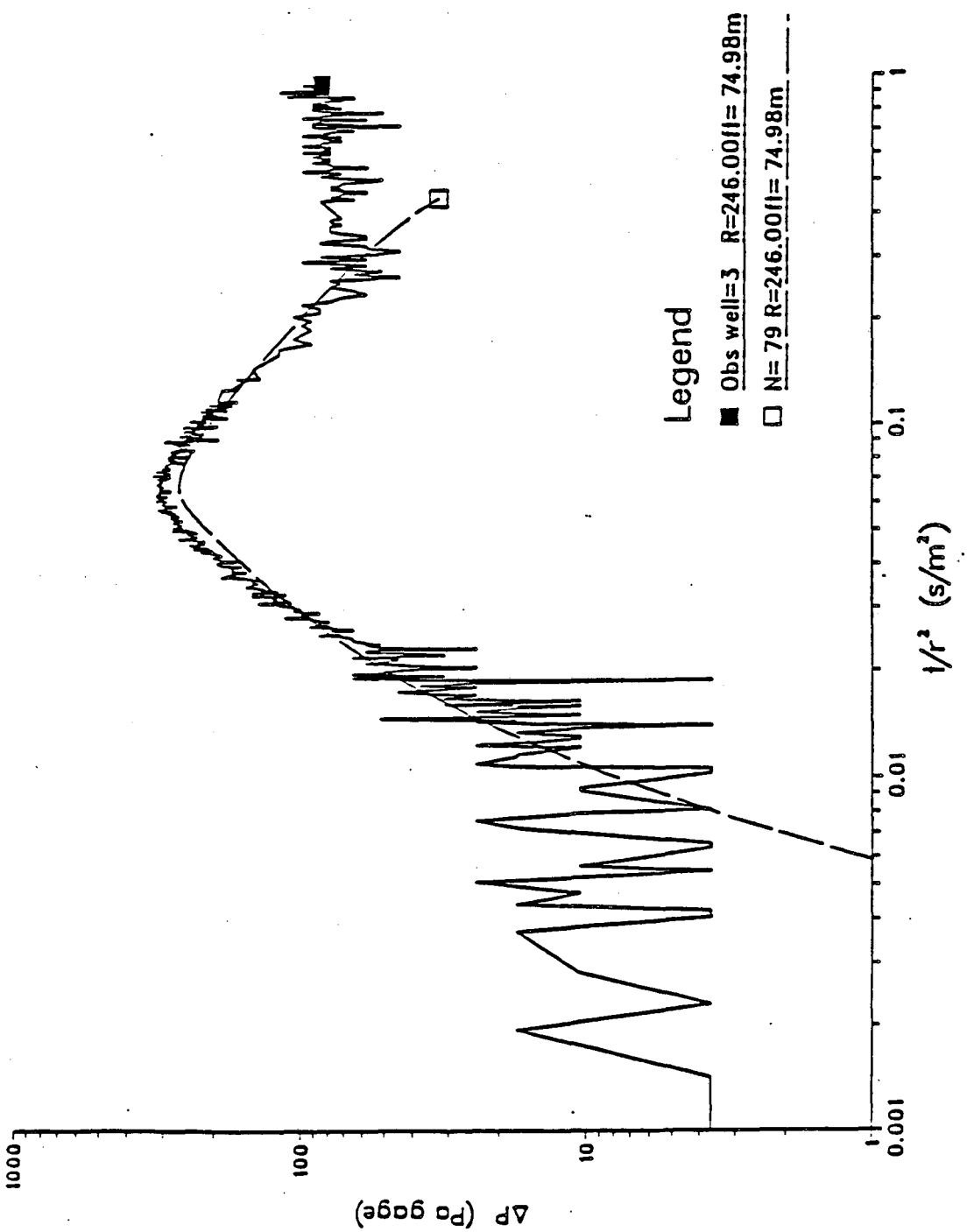
PULSE TEST 5 - PRODUCING HO60

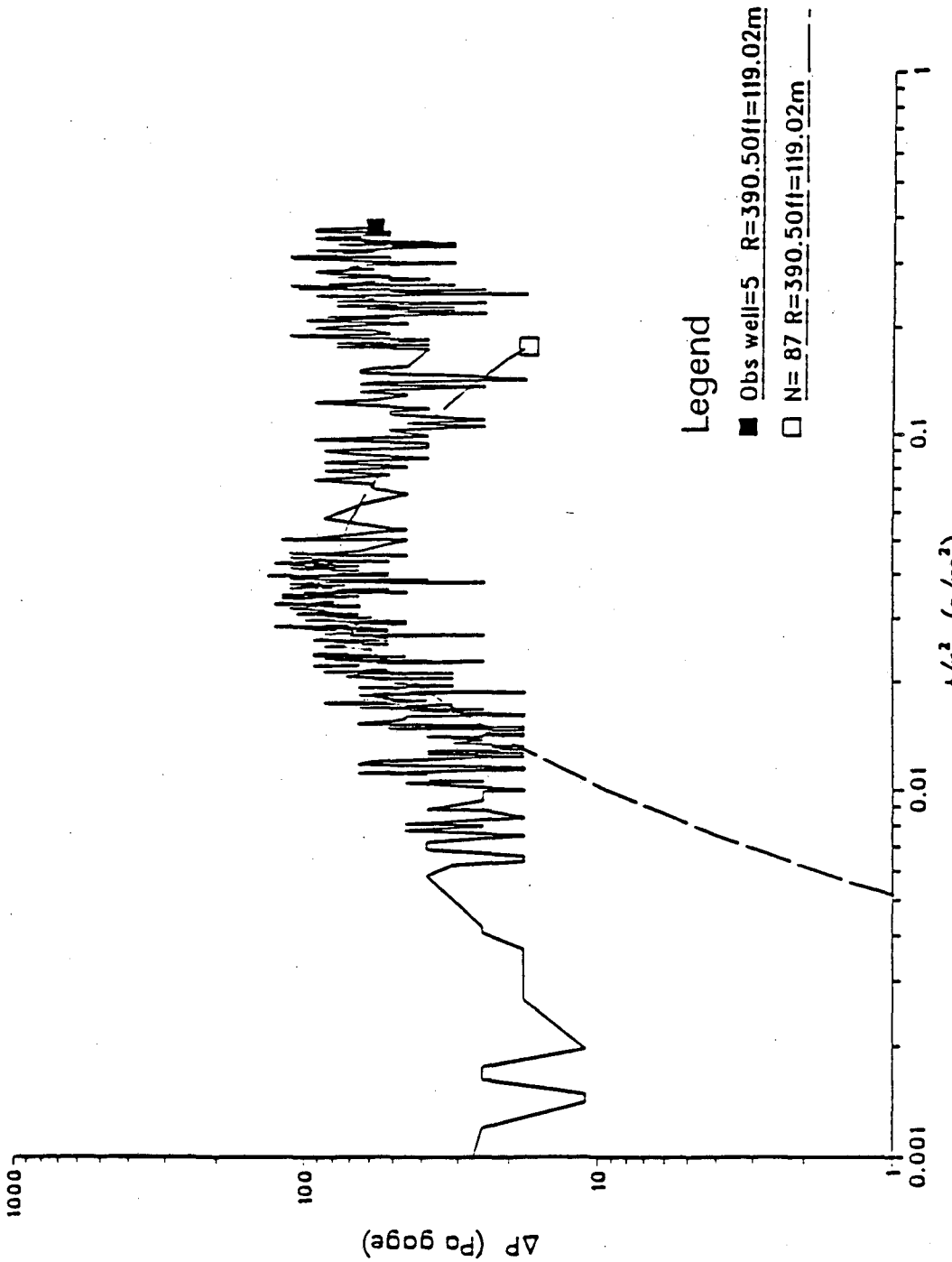

ΔP (Pa gage)
1000
100
10
1
0.01
0.1
1
10
t/r² (s/m²)
Legend
Obs well=2 R= 92.42ft= 28.17m
N= 69 R= 92.50ft= 28.19m

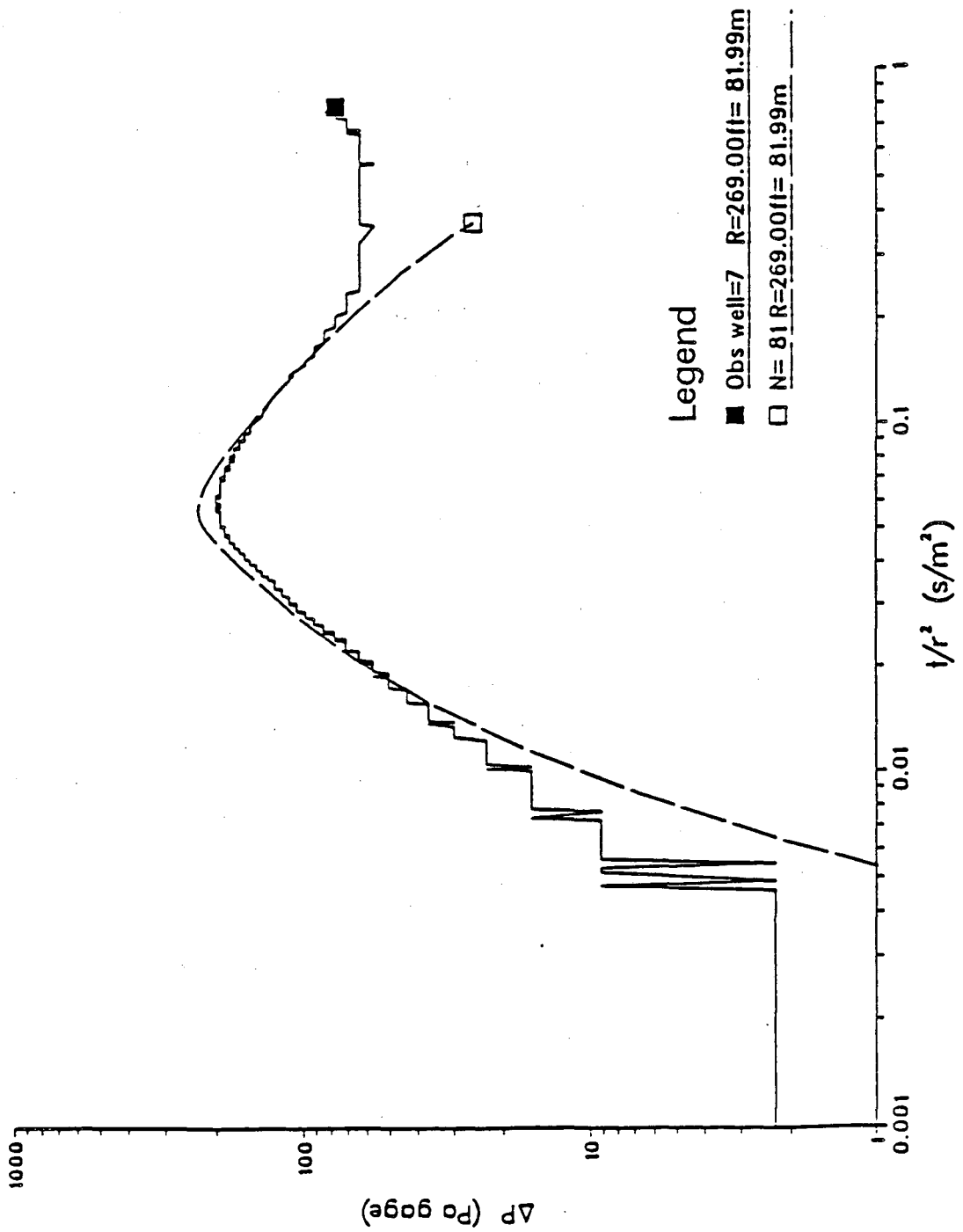

Legend
Obs well=6 R= 32.51ft= 9.91m
N= 64 R= 32.28ft= 9.84m
ΔP (Po gage)
10000
1000
100
10
1
0.01
0.1
1
10
100
t/r² (s/m²)

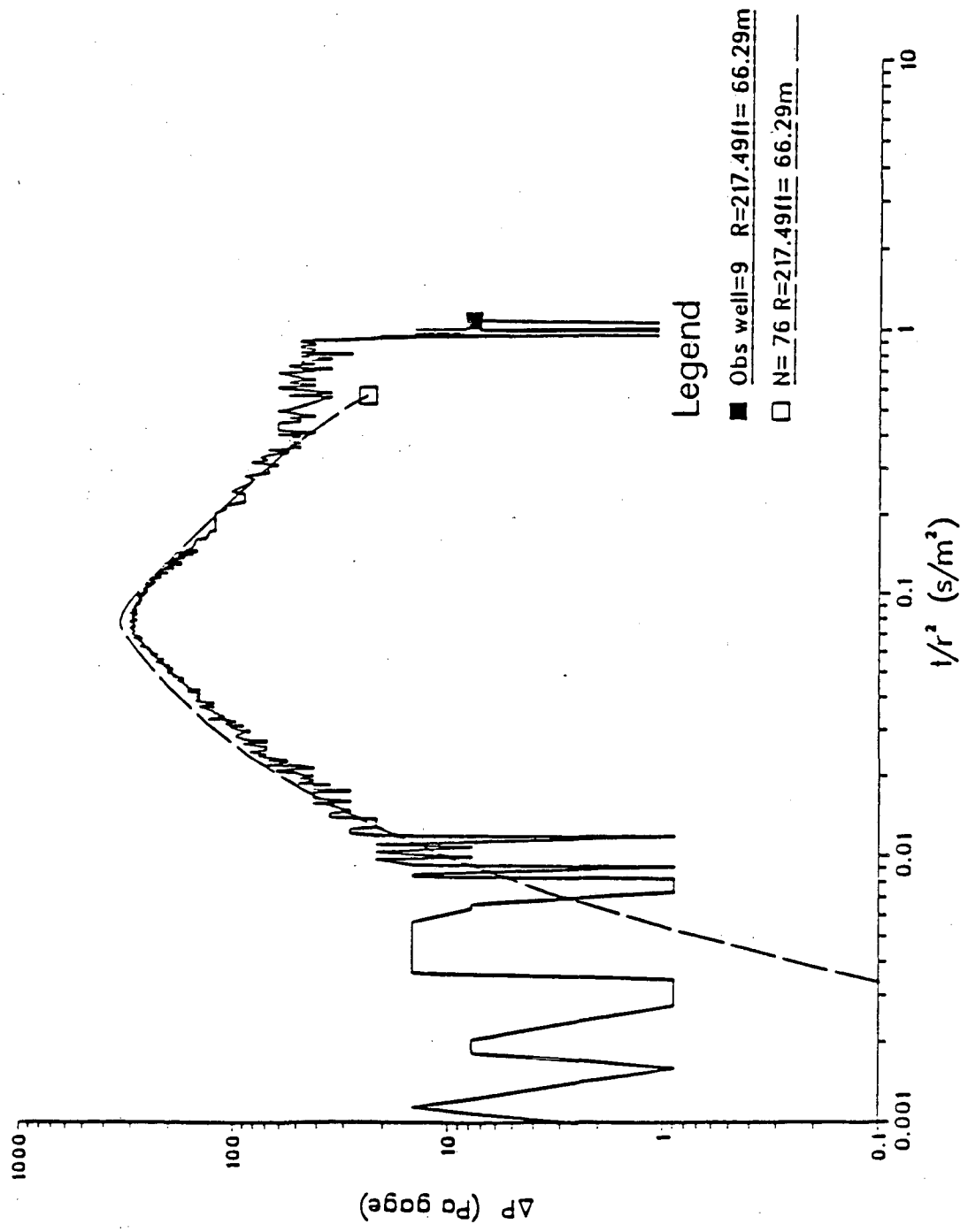

Legend
Obs well=8 R= 33.92ft= 10.34m
N= 65 R= 35.50ft= 10.82m
ΔP (Pa gage)
10000
1000
100
10
1
0.01
0.1
1
10
100
1/r² (s/m³)

PULSE TEST 6 - PRODUCING HO60

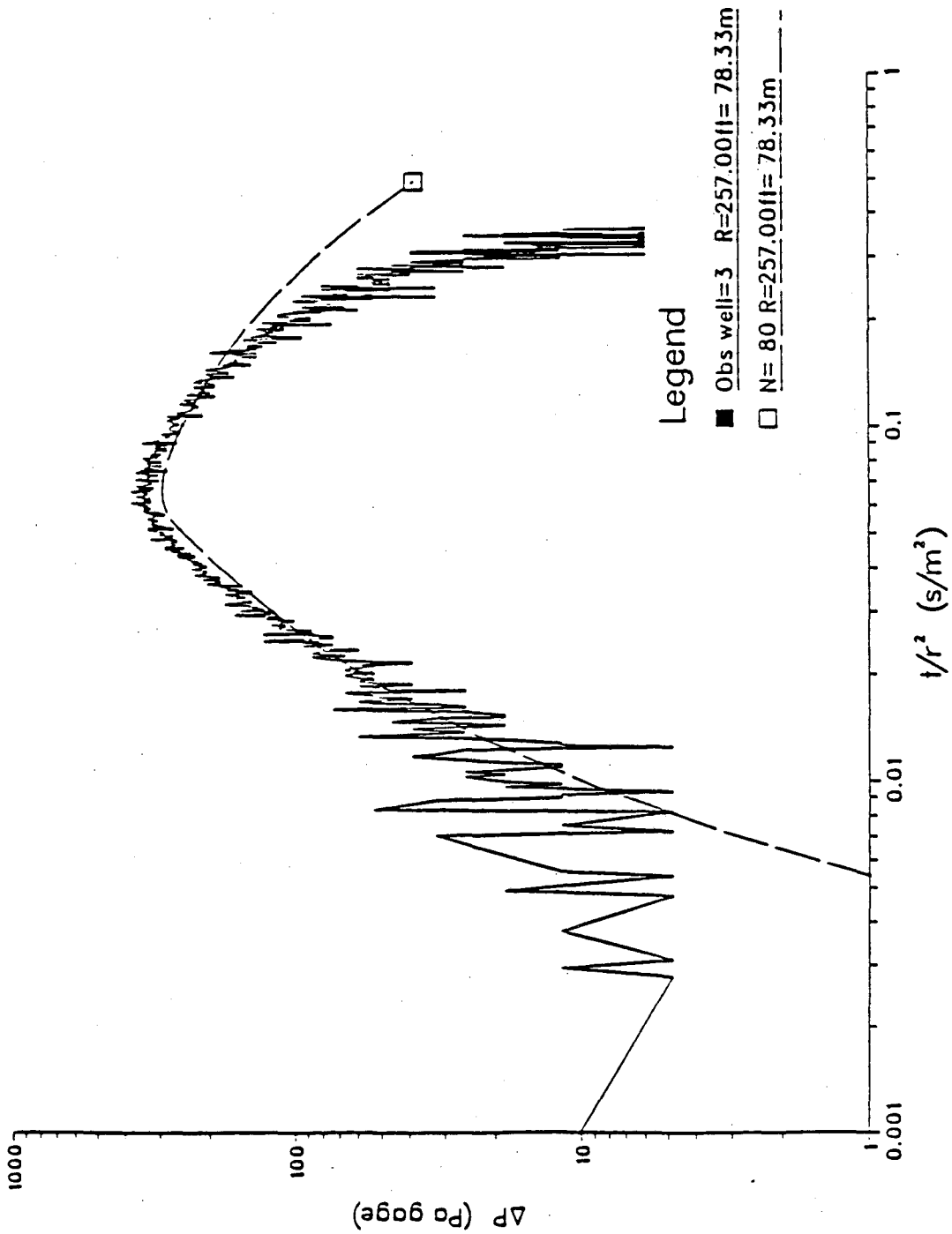

Legend
Obs well=3 R=246.00ft= 74.98m
N= 79 R=246.00ft= 74.98m
ΔP (Po gage)
1000
100
10
1
0.001
0.01
0.1
1
t/r² (s/m²)

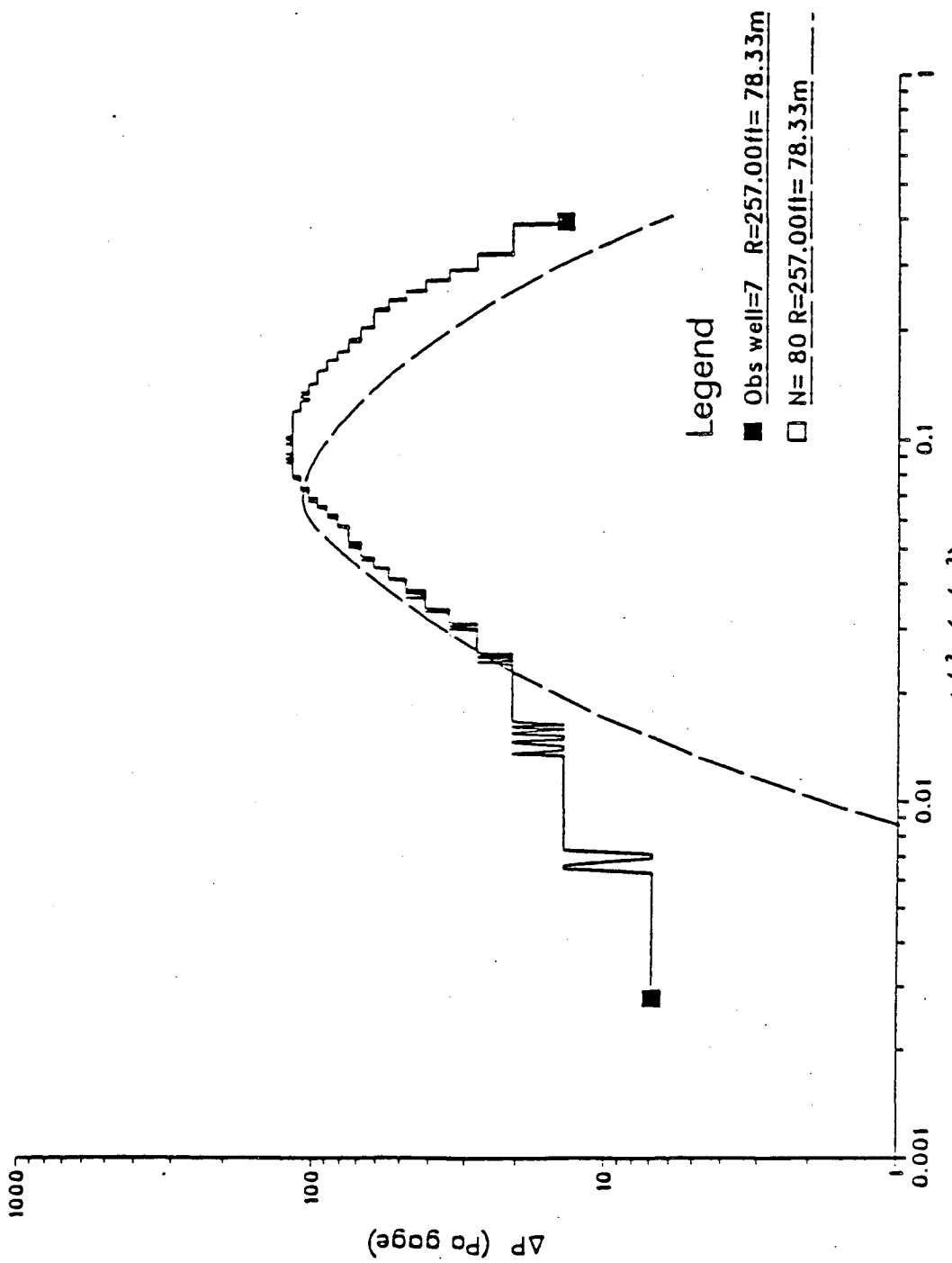

Legend
Obs well=5 R=390.50ft=119.02m
N= 87 R=390.50ft=119.02m
ΔP (Po gage)
1000
100
10
1
0.001
0.01
0.1
1
t/r² (s/m²)


ΔP (Po gage)
1000
100
10
1
0.001
0.01
0.1
1
t/r² (s/m²)
Legend
Obs well=7 R=269.00ft= 81.99m
N= 81 R=269.00ft= 81.99m


ΔP (Pa gage)
1000
100
10
1
0.1
0.001
0.01
0.1
1
10
1/r² (s/m²)
Legend
Obs well=9 R=217.49ft= 66.29m
N= 76 R=217.49ft= 66.29m

PULSE TEST 8 - PRODUCING HO80


ΔP (Po gage)
1000
100
10
1
0.001
0.01
0.1
1
t/r² (s/m²)
Legend
Obs well=3 R=257.0011= 78.33m
N= 80 R=257.0011= 78.33m


ΔP (Po gage)
1000
100
10
1
0.001
0.01
0.1
1
t/r² (s/m²)
Legend
Obs well=7 R=257.00ft= 78.33m
N= 80 R=257.00ft= 78.33m

LAWRENCE BERKELEY LABORATORY
TECHNICAL INFORMATION DEPARTMENT
UNIVERSITY OF CALIFORNIA
BERKELEY, CALIFORNIA 94720